NANOSTRUCTURED TiO_2 BASED MATERIALS FOR THE PHOTOCATALYTIC DEGRADATION OF EMERGING ORGANIC POLLUTANTS FROM AQUEOUS SOLUTION

By

SHEPHERD SUNDAYI SAMBAZA

(201461721)

Thesis in fulfilment of the requirement for the degree

DOCTOR OF PHILOSOPHY(Ph.D.)

in

CHEMISTRY

in the

FACULTY OF SCIENCE

of the

UNIVERSITY OF JOHANNESBURG

Supervisor: **Prof K. Pillay**

Co-supervisor: **Prof A. Maity**

DECLARATION

I hereby declare that this dissertation, which I herewith submit for the research qualification

DOCTOR OF PHILOSOPHY (Ph.D.) DEGREE IN CHEMISTRY

to the University of Johannesburg, Department of Chemistry, is, apart from the recognised assistance of my supervisors, my own work and has not previously been submitted by me to another institution to obtain a research diploma or degree.

_____ on this ____ day of _____

(Candidate)

_____ on this ____ day of _____

(Supervisor)

_____ on this ____ day of _____

(Co-Supervisor)

DEDICATION

This thesis is dedicated to my late father, Sylvester Sambaza, who was a source of encouragement, and inspiration throughout my life. Dad, although you are no longer with us in this world, your memory continues to regulate my life. My mother, Mavis, your love for me knows no bounds. My beautiful and lovely wife Marian Kaledyele, my love for you shall live forever. Thank you for the unconditional love and support throughout my studies. My son, Keith Anthony Sambaza, Thank you for being 'patient' with me in this challenging period for our family.

ACKNOWLEDGEMENTS

I thankfully acknowledge the effort, dedication and financial support of the following people and institutions:

- Prof Kriveshini Pillay and Prof Arjun Maity for the opportunity to do my Ph.D. studies under their supervision.
- The Faculty of Science, University of Johannesburg for funding of this work.
- The University of the Witwatersrand (School of Chemistry) for allowing me to access their LC-MS that was used for analysis of degradation products.
- Eric Ngigi and Tareken Dolla for the assistance with TEM and various aspects of my project.
- I am also grateful to Eric Morifi, for assistance with LC-MS at University of Witwatersrand (School of Chemistry).
- I graciously thank my fellow laboratory colleagues and staff members of Applied Chemistry for their co-operation during my stay at the University of Johannesburg.
- I consider myself fortunate to have Mr. Ephraim Marondedze, Passion and Prosper Chisi as my best friends, forever. I appreciate your presence in every critical phase of my personal life.
- My special gratitude go to my family, Tsitsi, Juliet, Farai Stanley, Gwinyai, Trust, Vimbai, Tanya, Nomsa, James, Qhelani, Huggins, Farai Mark and Ibrahim for their unconditional support and encouragement throughout my entire research study.
- I deeply thank my lovely wife, Marian Kaledyele-Sambaza and my son Keith Anthony Sambaza in Zimbabwe for the unconditional love, perseverance, and encouragement during this challenging period of my life. They have lost a lot of

family time during my stay at the University of Johannesburg. Without their patience and understanding, it would have been impossible for me to finish this work.

- My mother, Mavis Sambaza, for her prayers and unconditional love.
- Finally, I give thanks and praise to God, the Almighty, my Lord for his grace in my life, for the will power and strength to make it this far.

ABSTRACT

Water is regarded as the most vital of natural resources for the sustainability of life, yet freshwater systems are directly threatened by pollution. Among the many pollutants are organic emerging pollutants such as synthetic chemicals and pharmaceuticals. Bisphenol A (BPA) and ibuprofen are examples of such a synthetic organic compounds. Current wastewater treatment technologies such as membrane technology, chemical treatment and biodegradation are not always efficient in removing toxic emerging organic pollutants. This is because they were not specifically designed to remove these contaminants. Photocatalysis on the other hand, has shown great potential to remove toxic emerging pollutants from the environment. Over the years, TiO_2 catalyst has been used widely for water remediation applications.

Surface modification of TiO_2 is necessary to extend its use in the visible region of the solar spectrum and to reduce the inherent fast recombination rate of charges. Polyaniline (PANI)-wrapped TiO_2 nanorods (PANI-TiO_2), obtained through the oxidative polymerization of aniline at the surface of hydrothermally pre-synthesized TiO_2 nanorods, were evaluated as photocatalysts for the degradation of BPA. Fourier-transform infrared spectroscopy (FTIR) analysis revealed the successful incorporation of PANI into TiO_2 by the appearance of peaks at 1577 cm^{-1} and 1502 cm^{-1} that are due to the C=C and C=N stretch of the benzoid and quinoid. Brunauer-Emmett-Teller (BET) analysis revealed the presence of mesoporous material in PANI-TiO_2. Transmission electron microscopy (TEM) analysis showed that TiO_2 nanorods with different diameters were synthesized. The TEM analysis showed that a thin layer of PANI wrapped the TiO_2 nanorods. X-ray diffraction (XRD) and Raman spectroscopy revealed that anatase phase TiO_2 was synthesized with typical Raman

vibration peaks at 637 cm^{-1}, 514 cm^{-1}, 396 cm^{-1}, and 195 cm^{-1}. X-ray Photon Spectroscopy (XPS) survey scan of the PANI-TiO_2 nanocomposite revealed the presence of C, O, Ti, and N. Photocatalytic activity evaluation under UV radiation through the effect of key parameters, including, pH, contact time, dosage and initial concentration of BPA was carried out in batch studies. Within 80 min, 99.7% of 5 ppm BPA was attained using 0.2 g/L PANI-TiO_2 photocatalyst at pH 10. PANI-TiO_2 showed a better performance than as-synthesized TiO_2 with a rate constant of 4.46 x 10^{-2} min^{-1} compared to 2.18 x 10^{-2} min^{-1}. Nitrate ions increased the rate of degradation of BPA whilst humic acid consistently inhibited the degradation of BPA. LC-MS analysis identified degradation products with m/z 213.1, 135.1 and 93.1. The PANI-TiO_2 nanocomposite was reused up to five cycles with a removal of at least 80% in the fifth cycle.

PANI capped WO_3@TiO_2 nanocomposite prepared through a three–stage synthetic route was evaluated for the degradation of ibuprofen under visible light. XRD analysis confirmed the anatase phase of TiO_2 and monoclinic and orthorhombic WO_3 crystalline structures were formed. The XRD analysis confirmed that the phases were not affected by wrapping in PANI.TEM analysis confirmed that TiO_2 nanorods were synthesized with different diameters. TEM analysis showed that a WO_3@TiO_2 heterojunction was formed. A PANI layer was wrapping the heterojunction was observed.

Photoluminescence analysis revealed that pairing TiO_2 and WO_3 resulted in improved charge separation. The charge separation was further improved by wrapping the heterojunction in a PANI matrix. DRS calculations showed that pairing TiO_2 with WO_3 extended the band edge to about 420 nm thus facilitating the use of the nanocomposite in the visible region of the solar spectrum. XPS analysis revealed

the presence of W, C, O, Ti, N, and their corresponding photo electron peaks were found to be W4f, W4d, C1s, O 1s, N1s, and Ti 2p. The degradation of ibuprofen was influenced by pH with maximum degradation observed at pH 9. The degradation conformed to the Langmuir-Hinshelwood kinetic model. The rate constant, K for the degradation of ibuprofen by WO_3@TiO_2 and PANI/WO_3@TiO_2 was 2.59 x 10^{-2} and 3.5 x 10^{-2} respectively that were significantly higher than that of pristine TiO_2, which was 1.92 x10^{-2}.

Bicarbonate/carbonate ions accelerated the degradation of ibuprofen at 0.5 mM to 5 mM concentrations. There was little difference after increasing the concentration to 10 mM HCO_3^-. The presence of persulfate ions accelerated the degradation process of ibuprofen.

PANI supported Ag@TiO_2 nanocomposite was synthesized *via* oxidative polymerization of aniline on Ag@TiO_2. The Ag@TiO_2 nanocomposite was synthesized by the photo-reduction of Ag nanoparticles on hydrothermally synthesized TiO_2 nanofibers. Raman analysis revealed that the anatase phase of TiO_2 was synthesized showing typical peaks at 195 cm^{-1}, 396 cm^{-1}, 514 cm^{-1}, and 637 cm^{-1}. The incorporation of PANI, a carbonaceous material was confirmed by appearance of D-band and G-band in Ag@TiO_2-PANI that were located at 1505 cm^{-1} and 1603 cm^{-1} respectively. XRD analysis confirmed the anatase phase of TiO_2 was synthesized. TEM analysis revealed that TiO_2 nanofibers were synthesized successfully and Ag nanoparticles of different sizes were deposited on their surface. XPS survey scan of the Ag@TiO_2-PANI-nanocomposite revealed that the nanocomposite was made from C, O, Ag, Ti, and N. DRS and Tauc`s plot estimated the band gap of Ag@TiO_2-PANI to be 3.0 ev. A comparative study of the photocatalytic performance of Ag@TiO_2-PANI catalyst showed better degradation

performance under both conditions than pristine TiO_2, and $Ag@TiO_2$ with a degradation of up to 99.7% under visible light irradiation. The degradation experiments showed that the reactive species that were dominant in the degradation of BPA were h^+ and $\cdot O^{2-}$. $Ag@TiO_2$-PANI nanocomposite was re-used to degrade BPA with a removal of at least 90% in the fourth cycle.

TABLE OF CONTENTS

LIST OF FIGURES

LIST OF TABLES

CONFERENCE AND SYMPOSIUM PRESENTATIONS

1. Sambaza SS, Pillay K, and Maity A, TiO_2-based nanocomposite materials for the degradation of Bisphenol A from wastewater, University of Johannesburg Postgraduate symposium, 2016 (**Oral presentation**).

2. Sambaza SS, Pillay K, and Maity A, PANI-TiO_2 nanocomposite for the degradation of Bisphenol A from wastewater, University of Johannesburg Postgraduate symposium, 2017(**Oral presentation**).

3. Sambaza SS, Pillay K, and Maity A, Nanostructured TiO_2-based nanocomposite materials for the degradation of Bisphenol A from wastewater, *International conference on Pure and Applied Chemistry*, **Mauritius** 2-6 July 2018 (**Oral presentation**).

LIST OF PUBLICATIONS

1. **S.S. Sambaza,** H.K. Paumo, A. Maity, and K., Photocatalytic degradation of bisphenol A in water using PANI-wrapped TiO_2 nanorods.'' Journal of Applied Nanoscience (APNA), 2018 (Manuscript under review).

2. **S.S. Sambaza**, A. Maity, and K. Pillay, Recent trends in bisphenol A removal: A review (manuscript under preparation).

3. **S.S. Sambaza**, .A. Maity, and K. Pillay, **"**Visible light photodegradation of ibuprofen by PANI capped WO_3@TiO_2 nanocomposite in water". Journal of Chemical Engineering (manuscript under review).

4. **S.S. Sambaza**, .A. Maity, and K. Pillay, **"**Enhanced degradation of BPA in water by PANI supported Ag/TiO_2 nanocomposite under UV and visible light**."** Manuscript published in the Journal of Environmental Chemical Engineering 2019, 7,102880. DOI:10.1016/jece.2019.102880

LIST OF ABBREVIATIONS

AOP	Advanced oxidation process
AMO	Ammonia monooxygenase
BFRs	Brominated flame retardants
BPA	Bisphenol A
BET	Brunauer-Emmett-Teller
CB	Conduction band
CdS	Cadmium Sulfide
DBP	Dibromophenol
EDS	Energy dispersive spectroscopy
ESI-MS	Electron spray-mass spectroscopy
FL	Fluorescence
FO	Forward osmosis
FR	Flame retardants
FTIR	Fourier transform Infrared
GC	Gas chromatography
GC-MS	Gas chromatography-mass spectroscopy
HA	Humic acid
HCl	Hydrochloric acid
HPLC	High performance liquid chromatography
HUMO	Highest occupied molecular orbital
JCPD	Joint Committee on Powder Diffraction
KI	Potassium iodide
LC-MS/MS	Liquid chromatography-tandem mass spectrometer
LC-ED	Liquid chromatography-electrochemical detection

LDH	Lactate dehydrogenase
L-H	Langmuir-Hinshelwood
LLE	Liquid-liquid extraction
LPME	Liquid-phase micro extraction
LUMO	Lowest unoccupied molecular orbital
MAE	Microwave-assisted extraction
MB	Methylene blue
MBRs	Membrane bioreactors
MeP	Methylparaben
MDEA	Methylenedioxylethylamphetamine
NF	Nanofiltration
NPs	Nanoparticles
PAEs	Phthalate ethers
PANI	Polyaniline
PPCPs	Pharmaceutical personal care products
PAHs	Polycyclic aromatic hydrocarbon
PEG	Polyethylene glycol
PL	Photoluminescence
PLE	Pressurised liquid extraction
PXRD	Powder X-ray diffraction
QqTOF	Quadropole time of flight mass spectroscopy
RO	Reverse osmosis
SE	Soxhlet extraction
SEM	Scanning electron microscope
SDME	Single drip micro extraction

SPE	Solid phase extraction
SPME	Solid phase micro extraction
SWE	Subcritical water extraction
TEM	Transmission electron microscope
TGA	Thermogravimetric analysis
TFC	Thin film composite
TTIP	Titanium isopropoxide
TOF-MS	Time of flight-mass spectroscopy
UNICEF	United nations international children`s emergency fund
USA-EPA	United States of America-environment protection agency
UV-Vis	Ultraviolet and visible spectrophotometer
VB	Valence band
WHO	World health organization
WWTP	Wastewater treatment plant
XPS	X-ray photoelectron spectroscopy

CHAPTER 1:

INTRODUCTION

1.1 BACKGROUND

The rapid expansion of industry and the increase in human population has increased the strain on 'clean' water resources. As the world struggles with the increased demand for clean water, which is also aggravated by unpredictable climate change, the burdens on natural resources are escalating. Water is the most vital of natural resources, yet the quality of freshwater habitats is deteriorating. Safeguarding water quality and safety has become important for governments and water controlling bodies in order to avoid human health problems because clean water is essential for human development and well-being. The World Health Organization (WHO 2017) estimated that 844 million people are at risk of using contaminated water [1]. In addition, millions have been reported to die from severe water borne diseases annually [2]. These numbers are expected to grow significantly in the near future, as water pollution is anticipated due to the increasing rate of discharge of pollutants in water systems. A growing number of pollutants ranging from biological, inorganic and organic contaminants to emerging micropollutants are finding their way to water sources [3, 4]. Their presence in water bodies pose a serious threat to the environment and the health of humans and animals [5, 6].

However, besides the presence of other toxic contaminants in water, emerging pollutants have recently raised a lot of concern [7, 8]. Emerging pollutants are a new class of chemicals without regulatory status and impact on the environment and human health, (USA-EPA). They include drugs of abuse, pesticides, pharmaceuticals, personal care products, flame-retardants, disinfection by-

products, and synthetic industrial chemicals [9-12]. The willful or accidental discharge of these emerging pollutants into the environment has deleterious effects on the quality and aesthetics of water sources [11]. The undoubted threat posed by their presence has prompted research activities towards their removal using different wastewater treatment technologies [12-14].

Therefore, this study focuses on the removal of emerging organic pollutants from water using an adsorptive photodegradation technology, wherein a robust and efficient system was developed using TiO_2-polyaniline based nanocomposites as a new generation of photocatalysts.

1.2 PROBLEM STATEMENT

Recently, emerging pollutants have been identified as a new threat to human, animal and environmental wellness [11, 15]. The detection of emerging pollutants in treated drinking water is testimony that the current conventional wastewater treatment methods are not effective in their removal [16-18]. This is mainly because the conventional techniques were not designed to remove these specific contaminants. Furthermore, treatment methods such as chemical oxidation pose threats to human and animal health [18, 19]. For example, chlorine can be used to disinfectant water but its use can result in mutagenic and carcinogenic disinfection by-products [20]. In addition, the use of chemicals results in generation of sludge that presents challenges in disposal and secondary pollution of water resources [19]. Some of the treatment methods such as reverse osmosis though effective are expensive due to the power demands [21]. Recently adsorption technology, lauded as a cheap and efficient method, suffers from cardinal challenges such as selectivity, sensitivity and secondary pollution threats from the spent adsorbents [22]. In addition, conventional

methods such as reverse osmosis, and biological treatment are operationally, financially and energetically not viable for most developing countries [23]. Therefore, there is a need to develop methodologies that are robust, effective and relatively cheap to address the challenges presented by emerging pollutants.

1.3 JUSTIFICATION

Water pollution has become a critical issue worldwide and the biggest challenge faced by governments and local water regulatory authorities is to provide clean water to all the citizens. Among the challenges they face, is the removal of emerging pollutants from drinking water [11]. The presence of these emerging pollutants has raised concerns due to their potential negative impact to humans, animals and the environment [10, 24]. Therefore, there is a drive to develop technologies that are cheap, robust and sustainable towards wastewater treatment. There are ongoing studies in our research group and in the Department of Applied Chemistry, University of Johannesburg that focus mainly on the synthesis of adsorptive and photodegradation materials for removal of pollutants from water. For example, TiO_2@polypyrrole hybrid nanocomposite was synthesized *via* a sol-gel method and oxidative polymerization reaction. The nanocomposites displayed excellent deflouridation performance on simulated water, with rapid adsorption and a high adsorption capacity of 31.93 mg g^{-1} [25].

Among the treatment methods that have been applied, advanced oxidation processes has been consistently identified as effective methodology for the removal of persistent organic pollutants from aqueous environment [26-28]. Among the advanced oxidation processes, for example, the photodegradation technique, which is based on the ability of semiconductor materials to absorb a photon of energy

equal to or greater than its band gap energy and generate hydroxyl (·OH) and superoxide ($\cdot O_2^-$) radicals has been consistently used to degrade organic contaminants [29]. Photodegradation offers high efficiency, low toxicity, simplicity in design and ease of operation [29-31]. In addition, photocatalysis is highly regarded as an efficient and eco-friendly technique in wastewater treatment especially if it is utilized under visible light irradiation [30, 31]. Photodegradation can be made more efficient by using nanomaterials as they have been shown to have better performance than their bulk counterparts [32, 33]. For example, Fe_2O_3/TiO_2 nanoparticles prepared by sol–gel method showed excellent removal efficiency for methylene blue dye [34]. The authors attributed the removal performance to both adsorption and photodegradation by the Fe_2O_3/TiO_2 nanoparticles.

Amongst the many photocatalysts that have been applied in environmental remediation, titania has consistently shown excellent ability to degrade organic pollutants [35, 36]. This is because of its admirable properties including strong oxidizing power, large surface area, corrosion resistance, non-toxicity, and cost effectiveness [35-37]. However, its application has been hindered by the high recombination rate of the electron-hole pairs and the fact that it is only active under ultraviolet radiation [29]. Recent research developments have shown that TiO_2 can be modified to extend its use in the visible region of the solar spectrum [38, 39]. For example, pairing of TiO_2 with low band gap semiconductors such as $BiVO_4$ has been shown to extend the use of TiO_2 based nanocomposite into the visible region of the spectrum [39]. Surface modification of TiO_2 with metal dopants has also been shown to reduce the recombination rate of charges [40]. The metal centers have been

reported to scavenge electrons resulting in significant reduction of the rate of recombination [40].

Recently, polyaniline (PANI) polymers have gained interest in water remediation as adsorbents or as supports for various metal oxides [41, 42]. This is due to its attractive intrinsic properties such as biocompatibility, facile synthesis, stability, electrical conductivity, and tunable properties [43-45]. In addition, PANI tends to undergo π-π stacking with organics and hence may be utilized to contact organic pollutants and facilitate their degradation by a photocatalyst when the polymer is used as a photocatalyst support [46]. Furthermore, supporting nanometals on PANI eliminates the inherent agglomeration of nanomaterials, allowing full efficiency of systems to be attained.

Based on the above consideration, this work seeks to fabricate photocatalysts that are cheap, efficient, sustainable and can be utilized under ultraviolet and visible radiation towards degrading emerging organic pollutants such as pharmaceuticals and synthetic organic compounds such as ibuprofen. The resultant nanocomposites are expected to have promising potential as photocatalysts for degrading emerging organic pollutants.

1.4 AIM AND OBJECTIVES

1.4.1 Aim

The aim of this project was to synthesize nanostructured TiO_2 photocatalyst and their nanocomposites for the photodegradation of emerging pollutants such as bisphenol A and ibuprofen from wastewater.

1.4.2 Objectives

In order to achieve the aim, the following objectives were fulfilled:

- To synthesize nanostructured TiO_2 photocatalyst using hydrothermal and the microwave synthesis technique.
- To modify the nanostructured TiO_2 with Ag noble metals and WO_3.
- To synthesize polyaniline (PANI) and use it as a support for nanostructured photocatalysts.
- To support nanostructured TiO_2 photocatalyst and their nanocomposites on PANI polymer.
- To characterize modified and unmodified TiO_2 photocatalyst using techniques such as FTIR spectroscopy, scanning electron microscopy (SEM), thermogravimetric analysis (TGA), XRD and BET.
- To investigate the efficiency of the TiO_2-based nanocomposite materials in the degradation of bisphenol A and ibuprofen in simulated wastewater samples using photodegradation studies.
- To study the reusability of the nanocomposite materials.

1.4 STUDY HYPOTHESIS

Modified Titania nanostructures can be synthesized by wet chemical methods. The structural and morphological properties can be varied on the as-prepared nanostructures. These can be applied effectively for environmental applications.

1.5 THESIS OUTLINE

Below is an outline of the thesis. It provides a concise description of the remaining chapters covered in this thesis.

Chapter 2

This chapter outlines a review of the literature relevant to this study. Current analytical techniques that have been used in the detection and quantification of emerging pollutants are highlighted in this chapter. The chapter contextualizes the issues introduced in the problem statement by providing a review of conventional methods for water treatment and highlighting the advantages of advanced oxidation with emphasis on the importance of photodegradation as an advanced treatment method for emerging organic method. The process of photocatalysis is discussed in detail with emphasis on degradation using TiO_2 and its nanocomposites. The problems associated with the practical use of TiO_2 photocatalyst are highlighted. Modification techniques applied thus far to improve the use of TiO_2 and its nanocomposites are discussed in detail.

Chapter 3

This chapter summarizes the various methods and instruments that were used in this work providing the theory behind the operation of the relevant instruments.

Chapter 4: Photocatalytic degradation of bisphenol A in water using PANI-wrapped TiO_2 nanorods

This chapter presents the synthesis of PANI-wrapped TiO_2 nanorods and their subsequent application in degradation of bisphenol A under UV light irradiation. The

kinetic data of the degradation process was fitted into the Langmuir-Hinshelwood model.

Chapter 5: Visible light photodegradation of ibuprofen by PANI capped WO_3@TiO_2 nanocomposite in water

The synthesis of PANI capped WO_3@TiO_2 nanocomposite is outlined in this chapter. Various characterizations of the as-synthesized photocatalysts were carried out and presented in this chapter. The degradation of ibuprofen was influenced by pH with maximum degradation observed at pH 9. The degradation conformed to the Langmuir-Hinshelwood kinetic model.

Chapter 6: Enhanced degradation of BPA in water by PANI supported Ag/TiO_2 nanocomposite under UV and visible light

The synthesis of PANI supported Ag/TiO_2 nanocomposite is presented in this chapter. The characterization techniques and their results were shown in this chapter. The degradation performance of the as-synthesized photocatalyst in degrading bisphenol A under UV and visible light radiation are highlighted.

Chapter 7: Recommendations and conclusion

All the important findings of this study and recommendations drawn from it are discussed in detail in this chapter.

1.6 REFERENCES

[1] WHO and UNICEF. Progress on drinking water, sanitation, and hygiene: 2017 update and SDG baselines. (2017)

[2] P. Gleick. Dirty water: Estimated deaths from water-related diseases.Pacific Institute Research Report, 2000-2020 (2002).

[3] J.G. Speight. Sources and types of inorganic pollutants. in Environmental Inorganic Chemistry for Engineers. J.G. Speight Editor. Butterworth-Heinemann, (2017) 231-282.

[4] L. Schweitzer and J. Noblet. Chapter five: Water contamination and pollution. Green Chemistry, *Elsevier* (2018) 261-290.

[5] M. Elliott. Biological pollutants and biological pollution—an increasing cause for concern. *Marine Pollution Bulletin* 46 (2003) 275-280.

[6] O.M.L. Alharbi, A.A. Basheer, R.A. Khattab, and I. Ali. Health and environmental effects of persistent organic pollutants. *Journal of Molecular Liquids* 263 (2018) 442-453.

[7] R. Reif, S. Suárez, F. Omil, and J. Lema. Fate of pharmaceuticals and cosmetic ingredients during the operation of a MBR treating sewage. *Desalination* 221 (2008) 511-517.

[8] X. Wei, P. Gu, G. Zhang, and J. Huang. Occurrence of emerging and priority pollutants in municipal reverse osmosis concentrates. *Environmental Science Process Impacts* 17 (2015) 488-494.

[9] E. Archer, B. Petrie, B. Kasprzyk-Hordern and G.M. Wolfaardt. The fate of pharmaceuticals and personal care products (PPCPs), endocrine disrupting contaminants (EDCs), metabolites and illicit drugs in a WWTW and environmental waters. *Chemosphere* 174 (2017) 437-446.

[10] D. Lapworth, N. Baran, M. Stuart, and R. Ward. Emerging organic contaminants in groundwater: a review of sources, fate, and occurrence. *Environmental Pollution* 163 (2012) 287-303.

[11] V. Geissen, H. Mol, E. Klumpp, G. Umlauf, M. Nadal, M. van der Ploeg, S.E. van de Zee, and C.J. Ritsema. Emerging pollutants in the environment: a challenge for water resource management. *International Soil and Water Conservation Research* **3** (2015) 57-65.

[12] B.-V. Chang, S.-N. Fan, Y.-C. Tsai, Y.-L. Chung, P.-X. Tu and C.-W. Yang. Removal of emerging contaminants using spent mushroom compost. *Science of the Total Environment* 634 (2018) 922-933.

[13] B. Cojocaru, V. Andrei, M. Tudorache, F. Lin, C. Cadigan, R. Richards, and V.I. Parvulescu. Enhanced photo-degradation of bisphenol pollutants onto gold-modified photocatalysts. *Catalysis Today* 284 (2017) 153-159.

[14] A.M. Paz-Alberto and G.C. Sigua. Phytoremediation: A green technology to remove environmental pollutants. *American Journal of Climate Change 2* (2013) 71.

[15] T. Deblonde, C. Cossu-Leguille, and P. Hartemann. Emerging pollutants in wastewater: A review of the literature. *International Journal of Hygiene and Environmental Health* 214 (2011) 442-448.

[16] C.M. Villanueva, E. Gracia-Lavedan, J. Julvez, L. Santa-Marina, N. Lertxundi, J. Ibarluzea, S. Llop, F. Ballester, A. Fernández-Somoano and A. Tardón. Drinking water disinfection by-products during pregnancy and child neuropsychological development in the INMA Spanish cohort study. *Environment International* 110 (2018) 113-122.

[17] S. Canonica, L. Meunier, and U. von Gunten. Phototransformation of selected pharmaceuticals during UV treatment of drinking water. *Water Research* 42 (2008) 121-128.

[18] X.-F. Li and W.A. Mitch. Drinking water disinfection byproducts (DBPs) and human health effects: Multidisciplinary challenges and opportunities. *Environmental Science and Technology* 52 (2018) 1681-1689.

[19] T. Ahmad, K. Ahmad, and M. Alam. Characterization of water treatment plant's sludge and its safe disposal options. *Procedia Environmental Sciences* 35 (2016) 950-955.

[20] K.E. Furst, B.M. Pecson, B.D. Webber and W.A. Mitch. Tradeoffs between pathogen inactivation and disinfection by-product formation during sequential chlorine and chloramine disinfection for wastewater reuse. *Water Research* 143 (2018) 579-588.

[21] S. Yüksel, N. Kabay, and M. Yüksel. Removal of bisphenol A (BPA) from water by various nanofiltration (NF) and reverse osmosis (RO) membranes, *Journal of Hazardous Materials* 263 (2013) 307-310.

[22] S. Lata, P. Singh, and S. Samadder. Regeneration of adsorbents and recovery of heavy metals: a review. *International Journal of Environmental Science and Technology* 12 (2015) 1461-1478.

[23] M.M. Pendergast and E.M. Hoek. A review of water treatment membrane nanotechnologies, *Energy and Environmental Science 4* (2011) S1946-1971.

[24] M. Lorenzo, J. Campo, and Y. Picó. Analytical challenges to determine emerging persistent organic pollutants in aquatic ecosystems. *TrAC Trends in Analytical Chemistry* 103 (2018) 137-155.

[25] K. Parashar, N. Ballav, S. Debnath, K. Pillay, and A. Maity. Hydrous TiO_2@ polypyrrole hybrid nanocomposite as an efficient selective scavenger for the defluoridation of drinking water. *The Royal Society of Chemistry Advances* 6 (2016) 99482-99495.

[26] Y. Deng and R. Zhao. Advanced oxidation processes (AOPs) in wastewater treatment. *Current Pollution Reports* 1 (2015) 167-176.

[27] M.A. Quiroz, E.R. Bandala and C.A. Martínez-Huitle. Advanced oxidation processes (AOPs) for removal of pesticides from aqueous media in pesticides-formulations, effects, fate. *InTech*, (2011)

[28] D. Kanakaraju, B.D. Glass and M. Oelgemöller. Advanced oxidation process-mediated removal of pharmaceuticals from water: A review. *Journal of Environmental Management* 219 (2018) 189-207.

[29] M. Wang, J. Ioccozia, L. Sun, C. Lin and Z. Lin. Inorganic-modified semiconductor TiO_2 nanotube arrays for photocatalysis. *Energy Environmental Science* 7 (2014) 2182-2202.

[30] P.A. Zapata, F.M. Rabagliati, I. Lieberwirth, F. Catalina and T. Corrales. Study of the photodegradation of nanocomposites containing TiO_2 nanoparticles dispersed in polyethylene and in poly(ethylene-co-octadecene). *Polymer Degradation and Stability* 109 (2014) 106-114.

[31] K. Kalyanasundaram, Photochemical applications of solar energy: photocatalysis and photodecomposition of water in photochemistry. *The Royal Society of Chemistry*, 41 (2013) 182-265.

[32] R. Das, C.D. Vecitis, A. Schulze, B. Cao, A.F. Ismail, X. Lu, J. Chen, and S. Ramakrishna. Recent advances in nanomaterials for water protection and monitoring. *Chemical Society Reviews* 46 (2017) 6946-7020.

[33] M.M. Khin, A.S. Nair, V.J. Babu, R. Murugan, and S. Ramakrishna. A review on nanomaterials for environmental remediation. *Energy and Environmental Science* 5 (2012) 8075-8109.

[34] M.A. Ahmed, E.E. El-Katori and Z.H. Gharni. Photocatalytic degradation of methylene blue dye using Fe_2O_3/TiO_2 nanoparticles prepared by sol–gel method. *Journal of Alloys and Compounds* 553 (2013) 19-29.

[35] W.J. Ong, L.L. Tan, S.P. Chai, S.T. Yong and A.R. Mohamed. Highly reactive {001} facets of TiO_2-based composites: synthesis, formation mechanism and characterization. *Nanoscale* 6 (2014) 1946-2008.

[36] Y.K. Abdel-Maksoud, E. Imam and A.R. Ramadan. Sand supported TiO_2 photocatalyst in a tray photo-reactor for the removal of emerging contaminants in wastewater. *Catalysis Today*, 313 (2017) 55-62.

[37] S.N. Habisreutinger, L. Schmidt-Mende, and J.K. Stolarczyk. Photocatalytic reduction of CO_2 on TiO_2 and other semiconductors. *Angewandte Chemie International Edition* 52 (2013) 7372-7408.

[38] S.A. Bakar and C. Ribeiro. Rapid and morphology controlled synthesis of anionic S-doped TiO_2 photocatalysts for the visible-light-driven photodegradation of organic pollutants. *The Royal Society of Chemistry Advances* 6 (2016) 36516-36527.

[39] Y. Hu, W. Chen, J. Fu, M. Ba, F. Sun, P. Zhang and J. Zou. Hydrothermal synthesis of $BiVO_4/TiO_2$ composites and their application for degradation of gaseous benzene under visible light irradiation. *Applied Surface Science* 436 (2018) 319-326.

[40] A.T. Kuvarega, R.W. Krause and B.B. Mamba. Nitrogen/palladium-codoped TiO_2 for efficient visible light photocatalytic dye degradation. *The Journal of Physical Chemistry C* 115 (2011) 22110-22120.

[41] M. Omaish Ansari, M.M. Khan, S. Ansari, K. Raju, J. Lee, and M.H. Cho. Enhanced thermal stability under DC electrical conductivity retention and visible light activity of Ag/TiO_2@polyaniline nanocomposite film. *American Chemical Society Applied Materials and Interface* 11 (2014) 8124-8133.

[42] E. Subramanian, S. Subbulakshmi and C. Murugan. Inter-relationship between nanostructures of conducting polyaniline and the photocatalytic methylene blue dye degradation efficiencies of its hybrid composites with anatase TiO_2. *Materials Research Bulletin* 51 (2014) 128-135.

[43] N. Chandrakanthi and M.A. Careem. Thermal stability of polyaniline, *Polymer Bulletin* 44 (2000) 101-108.

[44] J. Kavil, S. Ullattil, A. Alshahrie, and P. Periyat. Polyaniline as photocatalytic promoter in black anatase TiO_2. *Solar Energy* 158 (2017) 792-796.

[45] A. Mostafaei and A. Zolriasatein. Synthesis and characterization of conducting polyaniline nanocomposites containing ZnO nanorods. Progress in Natural Science: *Materials International* 22 (2012) 273-280.

[46] X. Tan, J. Wang, X. Pang, L. Liu, Q. Sun, Q. You, F. Tan and N. Li. Indocyanine green-loaded silver nanoparticle@polyaniline core/shell theranostic nanocomposites for photoacoustic/near-infrared fluorescence imaging-guided and single-light-triggered photothermal and photodynamic therapy. *American Chemistry Society Applied Materials and Interfaces* 8 (2016) 34991-35003.

CHAPTER 2:

TIO_2 BASED NANOCOMPOSITES FOR PHOTODEGRADATION OF EMERGING POLLUTANTS: A REVIEW

(Manuscript under preparation)

2.1 INTRODUCTION

The modern world is faced with an increase in industrialisation, population, and urbanisation, which has led to a strain on clean water attracting attention worldwide [1]. The increase in discharged pollutants into the natural water cycle has been reported to have an impact on the availability of clean and potable water [1-4]. In recent years, emerging organic pollutants have been detected in water sources. Their presence has raised concerns across the world. This chapter presents a review of the current analytical techniques that have made their detection and quantification in the environment possible. A brief explanation on the methods used to remove these emerging organic pollutants is highlighted. Thus, some emphasis is placed on photocatalysis and specifically on the use of TiO_2. The challenges faced in its use also highlighted.

2.2 Pollutants

Water pollution can be due to natural events or anthropogenic sources [1]. The pollution of water habitats by toxic molecules of biological, inorganic and organic nature is currently the world's principal concern [2]. For example, biological pollution makes water unusable and often results in deleterious effects to humans [3]. The presence of excess concentrations of pathogenic organisms in water sources renders the water unsuitable for drinking and recreational purposes [4]. Curiously,

most biological pollutants emanate from human and animal waste [4]. For example, coliform bacteria is mostly released in water bodies through faeces from humans and animals. *Escherichia coli* (E.coli) is an example of such coliform that is released through human and animal faeces [5]. In many developing countries across the world, wastewater treatment systems are not effective and drinking water is mostly contaminated with invasive species [6]. Invasive species such as viruses, parasites, and bacteria have been reported to breed uncontrollably in human waste [4, 6]. These pathogenic microbes are mainly introduced into water habitats through sewage discharge and wastewater from industries [6]. They cause epidemic or sporadic cases of diseases that exhibit a wide range of symptoms. Examples include Hepatitis A, Plasmodium and Vibrio cholera.

Hepatitis A is a virus that causes hepatitis A, a liver disease that is mainly transmitted fecal-orally [7, 8]. In most developed countries, there are fewer cases of hepatitis A than in developing countries due to improved sanitation. Likewise, Plasmodium, a common protozoan parasite that causes malaria is prevalent in developing countries that have poor drainage systems, which provide breeding areas for mosquitoes. Another invasive species that is prevalent in water habitants is Vibrio cholerae, bacteria that causes cholera [9]. Cholera epidemics are common in developing countries due to poor sanitation and social economic conditions [10]. If not treated quickly, cholera can quickly lead to severe dehydration and death [9, 10]. Likewise, dysentery a bacterial disease caused by *Shigella dysenteriae* can be fatal if it is not treated quickly [11]. It is also common in developing countries with poor sewage handling systems.

On the other hand, inorganic contaminants are present in water in high quantities because of anthropogenic and naturogenic actions in addition to human activities

[11]. Due to the high concentrations of these inorganic pollutants, the quality of water has declined to disturbing levels [12]. This is mainly because they are persistent and non-biodegradable [2]. Inorganic contaminants include sulphates, nitrates, mineral acids, inorganic salts, trace elements, complexes of metals with organic compounds and heavy metals [13]. A high concentration of inorganic contaminants such as nitrogen and phosphates in water systems result in overgrowth of plants and algae [14]. When these plants die, they lead to reduction in oxygen due to eutrophication [14].

A substantial number of chemical elements are crucial for human and animal life but at high concentration levels, some of them result in negative impacts to humans and animals. For example, most heavy metals cause detrimental effects to humans at high concentration [15]. They act by changing enzyme specificity [16]. For example, Cu, Zn, and Fe are essential metals for humans and animals but are harmful to the health of living organisms at higher concentrations [17]. Likewise, a higher concentration of fluoride in the body causes deleterious effect to humans [12, 15]. It is recommended to have optimum fluoride concentrations in the range of 1.0-1.5 mg/L in drinking water in order to improve dental and bone health to prevent dental caries and osteoporosis [12]. However, consumption above the recommended concentration may result in fluorosis. The fluoride ion, being highly electronegative readily binds with positively charged calcium ions present in the teeth [18]. Excessive dental fluorosis appears as white patches on teeth [18].

In recent years, organic pollutants continuously degrade the quality of limited fresh water resources, seriously affecting humans and animals. These include dyes, chlorinated organic compounds, polycyclic aromatic hydrocarbons (PAHs), phthalates, phthalate esters (PAEs), pharmaceutical personal care products

(PPCPs), and herbicides [19-22]. For example, organic dyes in wastewater from industries such as textiles, pharmaceuticals, papers, and plastics are well known for their carcinogenic and mutagenic nature [23]. Their uncontrolled discharge in water sources causes severe environmental challenges such as reduction in light absorption, which in turn results in the inhibition of photosynthesis in aquatic vegetation [20].

Other organic pollutants of concern are products that were synthesized for use in industry but end up as pollutants in the environment. For example, phthalates are produced for use as plasticizers in the manufacturing of bottles, toys and personal care products but have since raised concerns due to their carcinogenic potential [24]. Consequently, these synthetic organic compounds present a new challenge to humans because of a lack of knowledge of their effect on long-term exposure to the compounds [25]. Synthetic organic compounds are part of a new class of contaminants of concern known as “emerging pollutants”.

2.3 Emerging pollutants

Emerging pollutants are a new class of chemicals without regulatory status and impact on the environment and human health, (USA-EPA). They include disinfection products, flame-retardants, pesticides, drugs of abuse, personal care products, pharmaceuticals in addition to industrial products and by-products [26-28]. Recently, anthropogenic pollution has presented serious environmental issues worldwide and is increasingly posing problems to water management companies and governments due to the potential harmful effects to humans and animals [29]. Emerging pollutants are increasingly detected in the environment [22]. For example, bromodichloromethane, a by-product of the disinfection process of water is well

known to be carcinogenic [30]. It is formed when chlorine reacts with organic compounds in water. The exposure to bromodichloromethane arises by ingestion, inhalation or skin contact while drinking, showering or bathing [31]. Due to the numerous routes involved and the potential negative consequences, bromodichloromethane represents an environmental pollutant of concern [31, 32].

In recent years, brominated flame-retardants (BFRs) have been extensively applied to decrease the flammability of many products such as construction materials electrical equipment, electronics, textiles, furniture, buildings and coatings [33, 34]. The commonly used ones such as polybrominated biphenyl ethers (PBDEs) were banned in Europe due to concerns over their potential toxicity and persistence in the environment [34]. The ban led to the substitution of reactive flame-retardants (FRs) with brominated and chlorinated flame-retardants additive flame-retardants. However, due to the resemblance in the chemical makeup of these alternatives, there is a high chance of them behaving the same way in an aqueous environment [33]. In addition, these additive flame-retardants have been reported to easily escape the finished products by leaching out more easily than reactive flame-retardants [35].

Subsequently, flame retardants such as 2,6-dibromophenol (2,6-DBP) has raised a lot of concern due to their persistence and bioaccumulation in water sources [36]. 2,6-DBP can enter the aquatic environment through the disposal of industrial products where it can be ingested by animals, fish, and humans. Due to its ability to bioaccumulate, 2,6-DBP has been consistently detected in fish, raising concerns [36, 37]. For example, Hirayama et al reported concerns that 2,6-DBP resulted in the bad taste of fish. PBDEs are suspected to cause a spectrum of protracted cognitive disorder diseases as well as hormonal and liver malfunction [35].

Therefore, their presence in water sources continue to trouble water treatment organizations and scientists.

In years, pesticides have been synthesized and applied to control and kill pesticides. Pesticides can be classified as organophosphates, organochlorines, carbamates, and pyrethrins depending on their chemical structure [38]. Due to their stability, pesticides can bioaccumulate in the environment. Recent studies have confirmed their presence in water habitats [39]. Due to their design, pesticides, bioaccumulate in living organisms and in humans and animals they have been recently associated with a plethora of negative effects. Recently, organophosphates and carbamates have been shown to affect the nervous system in some cases resulting in deaths [40]. Furthermore, prenatal exposure to these pesticides poses a range of other hazards. For example, in a study, atrazine was reported to destroy embryos and greatly reduced their chances to progress to form blastocysts [41]. In addition, pesticides have also been reported to cause birth deformities [40]. The main source of exposure is through run off, agricultural products such as fruits, vegetables as well as animal products such as meat and milk. In addition to morbidity, exposure to pesticides is associated with birth defects and cancers [27, 40].

Remarkably, synthetic organic compounds such as pharmaceutical products continue to be detected in water habitats and there is a growing concern about their potential effects to humans and aquatic life [42]. Some of them are released by industry such as pharmaceutical, personal care, production, and food preservation during manufacturing into the water habitats. For example, pharmaceutical products such as analgesic drugs, (ibuprofen, aspirin, paracetamol) and antibiotics (triclosan and sulfamethoxazole) have been reported to be persistent in water sources [29]. Researchers have reported observable changes in sex ratio of crustacea, on

exposure to pharmaceutical drugs such as sulfamethoxazole, trimethoprim, and triclosan [43]. In addition, diclofenac a pharmaceutical drug that is administered as an anti-inflammatory treatment was reported to be responsible for the enormous decline in populations of vulture species in Asia [27]. Thus, the presence of these pharmaceuticals in water habitats can seriously harm the environment, animals, and humans by causing genetic exchange. In addition to concerns of their negative effects to the fauna and flora, they may activate drug resistance in bacteria [43].

Pharmaceuticals drugs are usually excreted in their original forms or as metabolites after metabolizing in humans and animals [44]. These organic molecules enter the environment via faeces or urine after their consumption by humans and animals, or via disposal in refuse bins.

These pharmaceutical compounds, tend to persist and some of them are only incompletely degraded during wastewater treatment or evade treatment altogether via sewage overflows [45]. This significantly adds to their load in receiving waters, many of which are used for recreational and drinking purposes.

In recent years, researchers have reported the presence of drugs of abuse in water sources including drinking water [46]. These drugs are mostly detected at trace levels (ng/L) and this has raised concerns due to the associated deleterious impacts on the environment and health [47]. Examples of drugs of abuse and some of their metabolites that have been detected in drinking water include methamphetamine, methylenedioxyethylamphetamine (MDEA), cocainics, cannabinoids, benzodiazepines, cyclohexanones, xanthines, 3.4-methylenedioxymethamphetamine (MDMA)] and 3,4-methylenedioxyamphetamine (MDA) [46, 47]. Their presence in wastewater, groundwater and surface water

presents a potential risk for indirect human exposure to them via drinking water supplies [46]. For example, in a study carried out in drinking water sources in Spain, cocainics were detected in three out of the four sampling points [46].

Most emerging organic pollutants are notoriously persistent in the environment. This is because of their ability to resist natural (chemical, biological and photolytic) reactions [48]. As a result, these emerging organic pollutants bioaccumulate in humans and animals causing various diseases and conditions [49]. For example, bisphenol A (BPA), a synthetic organic compound that is widely used in food packaging, manufacture of flame-retardants, plastic products, toys, medical equipment, and tubing has been widely reported to act as an endocrine disruptor when released in water habitats [50-53]. BPA enters water bodies through leaching and as an effluent from manufacturing plants. This persistent organic pollutant acts by binding to an estrogen receptor and influences the function of cells [51, 54].

Despite its occurrence at low concentrations, researchers have highlighted that BPA may cause, obesity, lung cancer, stunted growth and other ecotoxicological effects that may manifest in humans and animals. Currently, there is growing interest in BPA research by many scientists due to its extensive use in several products, as well as its toxicity and persistency in water sources.

The increasing detection of emerging pollutants in water sources is owed to the continuous development of analytical instruments and methods that can accurately, detect and quantify these trace compounds in the environment.

2.4 Methods for detection and quantitation of emerging pollutants

Over the years, the release of “emerging” pollutants into the environment frequently has occurred for quite some time, but methods for their detection have only recently become available [55]. Detection of emerging trace pollutants presented challenges due to the low detection limits required, diverse physico-chemical properties, and challenges in separating these complexes from interference [55]. Their detection has been credited to improvements in analytical instruments and methodologies that afford the necessary sensitivity and specificity to ensure accurate measurement. This has necessitated the analysis of analytes even in the most complex of environmental matrices, leaving negligible uncertainty as to the occurrence of emerging pollutants in the environment [22, 55]. The accurate quantification of the amount of pollutants in food, water, and other sources is of great importance in coming up with a reliable and accurate health risk assessment and recommendation for safe exposure concentration by regulatory bodies.

Analytical techniques such as High performance liquid chromatography (HPLC), Gas chromatography (GC), Liquid Chromatography–Electrochemical Detection (LC-ED), and Gas Chromatography-Mass spectrometry (GC–MS) have been applied to analyze emerging organic pollutants in different matrices [56-58]. HPLC is mainly used for the qualitative and quantitative analysis of non-volatile ionic molecules [44]. It is mainly coupled with ultraviolet (UV), fluorescence (FL), diode array and or MS [59].

Most of these analytical processes involve a pre-concentration before the detection step. For example, the GC detection technique requires derivatization using moderately polar solvents prior to detection of organic pollutants in most aqueous

sample matrices. This derivatization stage makes the use of GC based techniques to be tedious, as it may take long to complete before analysis [60, 61]. However, derivatization of samples is a necessary step with most analytes as it improves detection efficiency. For example, derivatization of bisphenols in protein samples have been shown to significantly improve the signal-to-noise ratios compared with the underivatized samples in analysis done using high-resolution mass spectrometry [61, 62]. Chemical derivatization is commonly utilized for poorly ionizable analytes to improve the detection efficiency using electron spray ionization–mass spectrometry (ESI-MS) [62]. However, the use of chemical reagents results in chemical pollution and there is a call to use techniques that don`t need sample pre-concentration [59]. Although there are calls to eliminate the use of chemicals in derivatization and pre-concentration steps, their elimination implies an increase in problems affecting analyte detection [59].

New methods of analysis continue to be developed to detect as well as project the fate of emerging pollutants in the environment [44]. Hyphenated techniques are gaining popularity for multiple analytes as they deliver reliable results within a short duration with low quantification limits. Hyphenated techniques are especially important in the analysis of emerging pollutants because they are sensitive techniques that also offer selectivity and have low limits of detection [55]. Pairing of LC and GC with mass spectrometry has proved to be one of the best techniques in analytical chemistry as MS gives information on the compound's molecular structure in addition to its high sensitivity and selectivity [44]. Recently, more advanced hybrid mass spectrometry has been developed. For example, TOF-MS, QqToF, quadrupole linear ion-trap-mass spectrometry (QqLIT-MS), and the hybrid linear ion trap FT Orbitrap mass spectrometry (LTQ FT Orbitrap MS) [44]. Hyphenated

techniques are especially helpful in identification and quantification of emerging pollutants that are mostly found in trace amounts in the environment especially in water habitats. For example, the LC–MS/MS methods are popularly applied to analyze pharmaceuticals such as antibiotics and their transformation products [63].

In order to determine emerging organic pollutants quantitatively, in matrices, sample preparation steps are carried out. Sample preparation of emerging pollutants often involves an extraction step to separate the molecules of interest from a complex aqueous matrix [44]. In addition, this critical step concentrates the target molecules improving the sensitivity of the analysis. Emerging organic pollutants are easily extracted using the normal solvent extraction techniques [64]. Extraction solvents that are applied for organic analytes include ethanol, methanol, and acetonitrile [64]. The choice of solvents is important depending on the functional groups of the compounds as well as the pH. For example, most antibiotics often have a non-polar core and polar functional groups, so their dissociation or protonation is depended on the pH [63]. Hence, polar or non-polar phases can lead to incomplete extraction, leading to challenges in analysis.

Researchers use various extraction procedures including solid phase extraction (SPE), Soxhlet extraction (SE), liquid-liquid extraction (LLE), solid-phase micro extraction (SPME) and microwave-assisted extraction (MAE) [65, 66]. SPE and SE have a disadvantage of requiring large volumes of solvents with SE having an additional drawback of requiring longer times compared to most of the extraction techniques. Among the extraction techniques, SPME has gained acceptance due to its suitability in concentrating analytes in complex matrix such as biological samples, food and forensic samples [59]. In addition, the use of small sample volumes also gives it an advantage over other sample pre-concentration techniques. SPME has

been applied to concentrate emerging organic pollutants such as organophosphorus pesticides [59]. On the other hand, MAE is gaining popularity as it is considered environmentally friendly because small solvent volumes are used. In addition, the extraction process is also significantly shorter than the other methods, making it a more efficient method than the other options [65]. LLE is a technique that relies on the partition of dissolved analytes between an organic solvent and an aqueous phase according to their partition coefficients [44]. The major disadvantage of LLE is that it requires the use of large volumes of solvents and it is less efficient than the other techniques although it has an advantage of producing clean extracts [66].

In order to reduce the use of solvents in sample preparation, researchers are encouraged to use techniques that use small amounts such as: SPME, pressurized liquid extraction (PLE), supercritical fluid extraction (SFE), subcritical water extraction (SWE), dispersive liquid–liquid stir bar sorptive extraction (SBSE), liquid-phase microextraction (LPME), microextraction (DLLME); and single-drop microextraction (SDME) [59, 67].

The presence of emerging pollutants in water systems has raised concerns regarding the long-term health effects and therefore there is an urgent need to remove them.

2.5 Methods used to remove emerging pollutants from the environment

In order to meet the undisputable need for clean water, various wastewater treatment processes are carried out involving a variety of physical, chemical and biological technologies [45]. The process of primary treatment involves the removal of solids through processes such as coagulation, flocculation, and sedimentation [68, 69]. However, despite the necessity of the primary treatment of wastewater, the

removal efficiency of emerging organic pollutants such as pharmaceuticals is very low [45, 68, 69]. The organic load of the wastewater is greatly reduced during secondary treatment via techniques such as activated sludge and membrane bioreactors (MBRs). In the secondary treatment of wastewater, most organic pollutants are removed from wastewater. However, the process often leads to production of transformation products that remain in the water after treatment. After primary and secondary treatment, some pollutants remain in the water and therefore further treatment is required. In this chapter, all these treatment processes carried out after primary and secondary treatment fall under tertiary wastewater treatment. These "polishing" steps used for the removal of emerging organic pollutants include techniques such as chemical oxidation, membrane filtration, adsorption, and advanced oxidation processes [70-72].

2.5.1 Chemical oxidation

This treatment approach utilizes strong oxidants to chemically change emerging organic pollutants into less toxic by-products [68, 73, 74]. Chemical oxidation methods have been widely applied in wastewater treatment processes. The oxidants that are currently in use include ozone (O_3), ferrate [Fe (VI)], chlorine, chlorine dioxide, hydrogen peroxide, and permanganate [Mn (VI)] [39, 75].

In water, ozone decays to produce ($OH^{\cdot}$) radicals that will target organic compounds and break them down to small molecules or carbon dioxide and water. Another chemical oxidant, ferrate has the ability to oxidize organic pollutants because of its high electron potential of 2.2 V [76]. It reduces to ferric hydroxide, which can be applied as a coagulation and flocculation agent [76]. For example, Sailo et al used ferrate to degrade BPA over a pH range of 7-12 and concentrations of BPA (0.03–

0.5 mmol/L) were studied at a constant concentration of 0.1 mmol/L ferrate (VI) [77]. The authors found out that, decreasing the pH from 12 to 7, resulted in an increase is percentage degradation of BPA from 23 to 87% [77].

Other oxidants such as permanganate [Mn (VI)] have also been utilized in degrading organic pollutants because in addition to being relatively cheap they are also stable compared to other oxidants. For example, Zhang et al degraded BPA using $KMnO_4$ and noted that the degradation was also dependent on pH and temperature [78]. In a separate study, Jian Jiang et al. demonstrated that $KMnO_4$ was effective in oxidizing triclosan and carbamazepine, pharmaceutical drugs [79].

Although chemical treatment of wastewater remains one of the most used treatment methods by wastewater treatment companies, there is a clear attempt to move to more environmentally friendly methods [80]. Chemical treatment at large scale results in the use of a large amount of chemicals which results in the generation of sludge [65]. The sludge requires further treatment and creates a challenge in disposing [81]. This adds to the expense in application of a method that is also not environmentally friendly.

2.5.2 Membrane technology

To meet the increasing demand for water, membrane technology has been widely applied to treat wastewater [82]. This technique is based on selectively moving materials across a semi-permeable membrane resulting in separation based on, size/steric exclusion, electrostatic repulsion, and hydrophobic adsorption [83]. Emerging pollutants have been reported to be removed from wastewater using, forward osmosis (FO), microfiltration (MF), ultrafiltration (UF), nanofiltration (NF) membranes and reverse osmosis (RO) [84-86].

Zielienska et al utilized ceramic based MF and NF membranes to remove BPA in simulated wastewater samples [71]. Their ceramic membranes completely removed BPA concentration of 0.3 ± 0.14 mg/L from contaminated water. However, they reported a lower removal efficiency by the membranes when they used a concentration of 0.7 mg/L BPA [71]. They attributed the decrease in efficiency to fouling and concluded that the BPA was adsorbed onto particulate matter that had accumulated on the surface of the membrane [71]. In a separate study, Jin et al. removed four pharmaceutical compounds (carbamazepine, naproxen, ibuprofen, and diclofenac) using FO [86]. Their thin film composite (TFC) polyamide based membranes performed well, with high water flux, excellent pH stability with a rejection of >94% for all the pharmaceutical compounds.

Membrane separation has been widely is widely regarded as the most efficient of the treatment methods obtaining efficiencies of up to 90% by nanofiltration and 100% by reverse osmosis [70]. However, the drawback for the use of reverse osmosis treatment is the high-pressure requirements, which makes the method expensive to use especially in developing countries [87]. In addition, the short life span of membranes, due to fouling results in continuous costs for replacement of membranes.

2.5.3 Biodegradation technology

Biodegradation processes use natural microorganisms to degrade organic molecules [88, 89]. In this process, carbon is utilized as source of energy to make new microbial cells [88, 89]. Currently, the biodegradation technique is the most common treatment method for organic pollutants [90]. The biodegradation technique is especially favorable when compared to other treatment methods because of its

relatively low cost and high efficiency in large-scale applications. Few bacterial stains have been found to be effective in degrading emerging organic pollutants such as *Enterobacter gergoviae* strain BYK-7 and *Aeromonas hydrophilia* [91, 92]. For example, in a study Cydzik-Kwiatkowska and co-workers, degraded 12 mg/L BPA solution using aerobic granular sludge, achieving a removal efficiency of up to 97% [92]. They did not detect any BPA metabolites after treatment suggesting complete degradation. The authors attribute the removal mechanism to be due to biodegradation and co-metabolism. In the co-metabolism process, they suggest that hydroxyl radicals ($OH^{\cdot}$) were produced after the ammonium oxidizing bacteria made ammonia monooxygenase (AMO). BPA molecules were then degraded by the $OH^{\cdot}$ radicals produced [93]. In another study, Ji et al showed that BPA has also been successfully removed from wastewater using activated sludge containing an adapted bacterial consortium [89].

Many reported biodegradation studies have mainly been carried out under aerobic conditions, as these processes are believed to be more efficient than the anaerobic degradation [94]. However, some organic pollutants have been reported to be more efficiently degraded under anaerobic conditions, For example, halogenated organic compounds have been shown to be easily degraded under anaerobic conditions [94]. In a separate study, ciprofloxacin was efficiently biodegraded under both nitrate and sulfate-reducing conditions with a removal efficiency of up to 80%. In another study, Jia et al. conducted a study to degrade sulfamethoxazole using a sulfate reducing bacteria sludge systems under anaerobic conditions in a batch reactor [95]. The removal of sulfamethoxazole followed the pseudo-zero-order kinetic model with a specific removal rate of 13.2 ± 0.1 mg/L/d at initial sulfamethoxazole concentration of 100 mg/L.

The conversion of organic molecules is based on the presence of microorganisms with catalytic activities that can specifically target certain functional groups in the molecules [71, 94]. The biodegradation technique can be utilized in batch reactors. This allows for optimizing different parameters that influences the efficiency of the technique [90, 96]. Different parameters such as pH, temperature, concentration as well volume of inoculants can be varied, to optimize the removal efficiency of the system.

While biodegradation has shown outstanding performances in removing emerging organic pollutants, its utilization faces challenges such as the large space that is required as well as limited flexibility in design and operation [97].

Despite the success of membrane technology and biodegradation technology, there have been challenges in implementing them at industrial scale due to the high cost in the case of membrane technology and the limited flexibility in design and operation for biodegradation. Adsorption technology has the potential to solve those challenges.

2.5.4 Adsorption

Adsorption is a promising technique for the removal of emerging contaminants due to its low initial cost for operation, high efficiency and simple operational design [98, 99]. The process of adsorption is a surface phenomenon where an adsorbate attaches to the surface of the adsorbent necessitated by the reduction in the surface tension between the liquid/ gaseous phase of the adsorbate and the solid phase of the adsorbent [100, 101]. Adsorption occurs as either, physisorption or chemisorption. Physisorption is based on weak attractions between the adsorbate and the adsorbent [102]. The forces holding the adsorbent and adsorbate at the

interface are usually Van der Waals forces. On the other hand, chemisorption involves chemical interaction between the adsorbate and the adsorbent where strong bonds are formed [103].

In years, different adsorbents have been applied to remove emerging pollutants by taking advantage of the interactions between the surface functional groups of the adsorbents and the emerging pollutants molecules [104]. These adsorbents include clays, zeolites, chitosan, carbon based adsorbents, nanomaterials, and various composite materials [89, 105-108]. For example, Kumar et al used a composite of graphene oxide and β-cyclodextrin to remove BPA (100 mg/L) from aqueous media achieving an adsorption capacity of 373.4 mg/g. In another study, a composite of goethite and activated carbon was applied to remove BPA in the presence of natural organic matter through adsorption [72]. The presence of natural organic matter was found to increase the adsorption capacity of the adsorbent due to its interaction with a new molecule formed by a reaction of BPA and natural organic molecules [72]. In another study, Zhu et al. demonstrated the ability of graphene oxide to adsorb metformin in the presence of NaCl [109]. They suggested that the adsorption mechanism was due to π-π interactions and hydrogen bonding between graphene oxide and metformin.

Recently, various nanomaterials have been applied as effective adsorbents for the adsorption of emerging organic contaminants from the environment. For example, graphene and it`s composites have gained popularity in environmental remediation especially in adsorbing organic pollutants. Its ability to interact with organic molecules via hydrogen bonding and π-π interactions have been suggested to be accountable for the adsorption of emerging organic pollutants [110]. In years, other carbon materials that have been applied include activated carbon and carbon

nanotubes. Activated carbon has been noted for its high efficiency but despite, the high efficiency its high operating costs as well as challenges in regeneration present challenges in application [111]. On the other hand, the recovery of carbon nanotubes after application present serious challenges in its industrial application for water remediation [112].

Low cost adsorbents have also been developed from waste materials such as orange peels and used tires [113, 114]. However, despite the relatively low cost, simplicity in design and high efficiency of adsorption as a technique, there is a challenge of secondary pollution when discarding the spent adsorbent.

Advanced oxidation processes have the potential to effectively replace the conventional methods of treatment for emerging pollutants.

2.5.5 Advanced oxidation processes

Amongst the various treatment methods that have been used in the removal of emerging pollutants, advanced oxidation processes (AOPs) have shown a good potential to be used for environmental remediation. AOPs rely on the continuous production of OH radicals, which is a strong oxidizing agent and can break down organic pollutants [115]. AOPs technologies include electrochemical oxidation, photocatalysis under UV or solar radiation, Fenton`s, the photo-Fenton`s reagents in combination with hydrogen peroxide, ferrate reagent, and others [75, 115-117].

Recently, AOPs have gained popularity due to their high efficiency [118]. For example, Nadejde et al used a heterogeneous Fenton nanocatalyst consisting of Fe (II) and Fe (III) ions supported on Fe_3O_4/chitosan surface to degrade BPA [119]. They achieved a removal percentage of up to 99% in 15 mins with a catalyst dosage

of 1 g/L and H_2O_2 concentration of 10 mmol/L [119]. The degradation of BPA was based on the chemical oxidation by ·OH radicals that were created by H_2O_2 in the presence of ferro ions. Other chemicals can be added to the Fenton`s reagent to improve reaction time and stability in different pH environments [118]. The additives improve the Fenton`s reagent leading to more efficiency in degrading stable organic compounds that are difficult to break down with the traditional Fenton`s reagent. The main disadvantage of using the Fenton`s reagent is that it is mostly efficient at low pH, therefore it cannot be used in soils that contain calcium [120]. The other disadvantage is the production of ferrous sludge that gives problems of disposal [120]. Recently, Gandhi et al. degraded pesticides (chlorpyrifos, dimethoate, and phorate) using a UV/H_2O_2 system and achieved a degradation efficiency of up to 96.9% [121].

In years, ozonation has been applied in the degradation of organic pollutants [122, 123]. Ozone gas is directly introduced in wastewater or soil where it will react directly with organics or with ·OH, resulting in the decomposition of ozone. However, the use of the process is limited due to the high cost of operation and the slow reaction time [123]. The ozonation process has been found to be more effective in removing organic pollutants if it is used in combination with other techniques. Amongst the AOPs, photocatalysis has shown great promise in the degradation of emerging organic pollutants such as pharmaceuticals.

2.6 Photocatalysis

Photocatalysis is highly regarded as an efficient and eco-friendly technique in wastewater treatment especially if it is utilized under visible light irradiation [124, 125]. It has an advantage over other AOPs because it uses low energy UV light and

it does not require the addition of other oxidants to initiate or propagate the reaction [87]. In addition, the process can be utilized under ambient conditions [87]. Photocatalysis offers many advantages in its application for environmental remediation, as it is an eco-friendly technology with minimum production of secondary pollution such as sludge [87]. It has low energy requirements and therefore it is a relatively cheap technique.

This technique involves the use of semiconductor materials that can be activated after adsorbing photons of light that is equal to or greater than the semiconductor`s band gap [126]. After excitation, electrons leave the valence band and occupy the conduction band, leaving behind positive holes that are highly oxidizing [126]. The positive holes can oxidize emerging organic pollutants and mineralize them or they can react with the moisture to form hydroxyl radicals that can oxidize organic pollutants to carbon dioxide and water [127]. The mechanism of photocatalysis is shown in Figure 2.1.

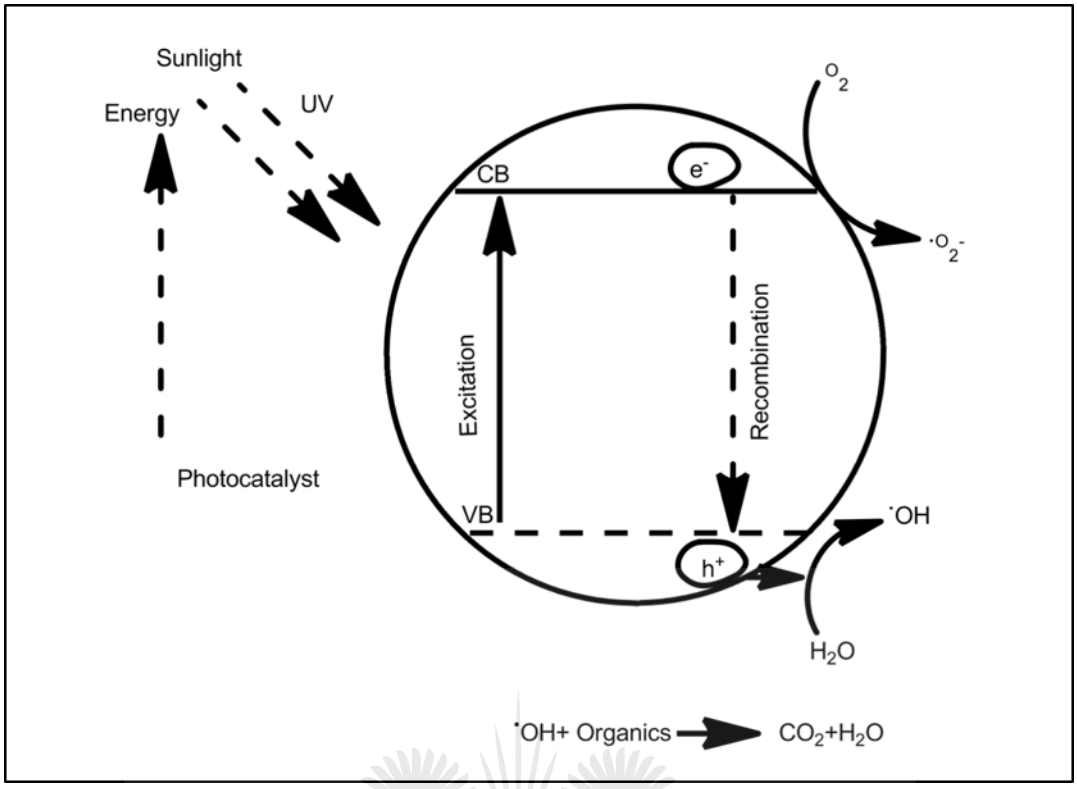

Figure 2.1: Mechanism for photocatalysis under UV-light.

The positive holes can react with water from moisture or with hydroxyl groups to form OH radicals (Equation 2.2) [43, 128]. The electrons can be scavenged by oxygen molecules forming superoxides as shown in Equation 2.3 [128, 129]. Two important processes occur that control the overall efficiency of the photocatalysis process. This includes the recombination of the electron-hole pairs or their separation [110]. When recombination occurs, the excited electron returns to the valence band without reacting with adsorbed species or loses the energy as light or heat [128]. The process of recombination can occur on the surface or in the bulk of the semiconductor material. The recombination rate and process is influenced by various factors including the mobility of charges, defect density and the presence of an interface with secondary material that can interfere with the mobility of charges [130]. The $^{\cdot}OH$ and $^{\cdot}O_2^-$ radicals are highly oxidizing and can be utilized to degrade

organics. In order for the process to be efficient, the recombination rate of the electron-hole pair holes must be reduced [126].

$$TiO_2 + hv \rightarrow hVB^+ + e_{CB}^- \quad 2.1$$

$$H_2O + hVB^+ \rightarrow \cdot OH + H^+ \quad 2.2$$

$$O_2 + e_{CB}^- \rightarrow O_2^{\cdot -} \quad 2.3$$

$$\cdot OH + organic\ pollutant \rightarrow H_2O + CO_2 \quad 2.4$$

The most challenging problem in photocatalysis is developing photocatalysts that can absorb sunlight and produce radicals that can degrade organic pollutants [127]. Solar driven photocatalysts are gaining interest because of the ability of the system to generate active oxidizing species “in situ” [43]. The success of the process of photocatalysis is based on the ability to control or manipulate three important aspects of the process. This involves the excitation of electrons, the dispersion of charges to the surface of the photocatalyst and their transfer [130, 131]. Thus, the chemical composition and the crystallinity of the semiconductors are important factors in the overall performance of the photocatalyst.

2.6.1 Conventional semiconductor photocatalysts

Over the years, semiconductor materials have been proven to be of great importance in environmental remediation due to their ability to generate charges after absorbing the right amount of energy [130]. The charges can be manipulated to degrade pollutants in the environment. Therefore, in order for a semiconductor to

be used to degrade pollutants effectively, it must fulfil the following requirements: [131]

- appropriate band gap
- efficient light absorption
- high charge mobility
- nontoxic and chemically stable

Numerous materials have been under investigation as photocatalysts. These include TiO_2, ZnO, MoO_3, ZnS, CdS, WS_2, ZrO_2, WO_3, CdSe, α-Fe_2O_3, SnO_2, and $SrTiO_3$. Among the wide spectrum of semiconductors, TiO_2 and ZnO are the most popular semiconductors that have been utilized as photocatalysts due to their electronic band structure [128, 131-133]. ZnO exists in three polymorphs: wurtzite, zinc blende, and rock salt. It has a band gap of 3.37 eV [134, 135]. ZnO nanoparticles have been used as an alternative to TiO_2 to degrade emerging organic pollutants. In a study, Bechambi et al degraded BPA, using C-doped ZnO [136]. The authors reported a BPA degradation efficiency of 100% and 70% BPA mineralization within 24 h under UV irradiation [136]. Recently, Roge et al demonstrated the ability of ZnO nanowires to degrade seven organic pollutants under UV light [137]. However, despite its success as a photocatalyst, ZnO suffers from photo corrosion that limits its application [138].

Over the years, tungsten oxide (WO_3) has been utilized as a photocatalyst to degrade organic pollutants. WO_3 consists of four crystal structures: monoclinic, tetragonal, orthorhombic and the cubic [139]. The monoclinic crystal structure is the most popular structure for photodegradation applications [139]. It is an n-type semiconductor with a band gap of 2.8 eV, which can be activated by visible light

[140]. For example, Hunge et al utilized WO_3 thin films to degrade oxalic acid under visible light. The authors reported degradation efficiency of up to 83%.

Another photocatalyst Iron oxide (α-Fe_2O_3) has been widely utilized due to its low band gap of 2.1 eV and its stability in most solutions at pH>3 [131]. Although Fe_2O_3 has good visible light absorption properties, its use has been hampered by the high recombination rate of electron-hole pairs [131]. Several researchers reported the use of this photocatalyst to degrade dyes and other organic pollutants [141, 142].

In years, various kinds of metal oxides such as CuO, CuO_2, CeO_2, V_2O_5, and ZrO_2 have been tested as photocatalysts. There have been challenges that have been reported in their utilization, as most of them are only active under UV radiation. For example, ZrO_2 is only active under UV radiation due to the wide band gap of 3.4 eV [143].

Due to the problems faced in the use of bulky semiconductor materials as photocatalysts, there is a growing trend of using nanomaterials in environmental remediation. For example, in recent years, various nanomaterials have been utilized either to improve existing wastewater treatment methods or to introduce novel treatment methods [133]. Nanomaterials application has gained popularity due to the uniqueness of the materials such as their size and tunable properties [134].

2.6.1.1 Nanostructured photocatalysts

Recently, nanostructured materials are becoming of major significance in energy and environmental applications due to their performance [144]. These novel materials have become popular due to their unique optical, electrical, and magnetic properties compared to their bulky counterparts [80, 145]. The unique properties are

due to their distinctive size, shape, morphology, and surface properties [80]. When designing photocatalysts for environmental remediation, the materials have to be robust, cheap, stable as well as environmentally friendly [80, 145]. Amongst the photocatalyst, TiO_2 and its nanocomposites remain popular in water treatment due to their stability in different pH environments, relative low cost, and availability [146]. In addition, the structural flexibility, light absorption, and charge transfer properties have seen TiO_2 based nanocomposites being applied in making many parts of components such as in fuel cells, capacitors and batteries [107, 147].

The suitability of a semiconductor material for photocatalytic degradation applications is dependent upon the mobility and lifespan of the created charge carriers [148]. In recent years, TiO_2 and its nanocomposites have been continuously designed to optimize their efficiency by reducing the recombination rate and to facilitate the recovery of the catalyst after use [125, 149].

2.6.1.2 TiO_2 photocatalysts for the degradation of emerging pollutants

The presence of emerging contaminants may have an adverse impact on the environment [150]. Amongst the treatment technologies used to remove these emerging pollutants, photocatalysis has consistently been reported to have the potential to alleviate the challenges presented by the presence of emerging pollutants in the environment. TiO_2 is one of the most widely investigated semiconductor materials due to its attractive electronic, surface, and catalytic properties that can be utilized in degrading emerging pollutants [130, 151]. Pure TiO_2 exists as a white powder that has a high surface area and is stable in the environment. TiO_2 has three known crystalline polymorphs: anatase, rutile and brookite [152, 153]. The rutile structure of TiO_2 is the most stable of the three

structures [124]. However, the anatase and brookite phases can be transformed to the thermodynamically stable rutile structure through heat treatment at temperatures exceeding ~ 600°C. The anatase structure is widely reported to have a higher photocatalytic activity compared to the rutile while the brookite form is more active than anatase [154]. Despite, the higher activity of the rutile form of TiO_2, it is difficult to synthesize a pure phase of it. TiO_2 is an n-type semiconductor due to its oxygen deficiency with its crystalline structures having different band gaps: 3.2 eV for anatase, 3.0 eV for rutile, and ~3.2 eV for brookite [155].

Many techniques have been reported to synthesize TiO_2 including hydrothermal, microwave, sol–gel, and solvothermal methods, have been extensively studied [148, 156]. One-dimensional TiO_2 nanostructures in different shapes (wires, rings, rods, and tubes) have attracted attention due to their large surface area to volume ratio and high photoconductivity [151]. They have been widely reported for the degradation of emerging pollutants. For example, Bakar et al. reported a visible-light-driven photodegradation of methyl orange with S-doped TiO_2 nanorods. They reported an improved degradation performance, which they attributed to the large porous channels of nanorods [157].

In another study, Manassero et al. degraded clofibric acid, a pharmaceutical drug with TiO_2-coated glass rings in a fixed bed reactor [158]. In their study, they demonstrated that the catalytic films supported on the glass rings were stable and could be reused up to three times. In a separate study, Elatimani et al. degraded pyrimethanil, a pesticide using a nanocomposite of TiO_2 under UV radiation. They reported total elimination of the pesticides within 5 h of irradiation [159].

Recently, Gomez-Canella et al. reported a study on degradation of 5-Fluorouracil, a pharmaceutical drug used as an antimetabolite using TiO_2 purchased from Aldrich and Degussa P25 [160]. Table 2.1 shows some recently developed forms of TiO_2 for the degradation of emerging pollutants. The results show that TiO_2 can be modified with different dopants and support material to improve its photocatalytic performance.

Table 2.1: Recently developed TiO_2-based photocatalysts and their performance toward emerging pollutants.

Material	**Pollutant(s) degraded**	**Light source**	**Exposure (mins)**	**Dose**	**Conc.**	**% Deg.**	**Ref**
C-TiO_2	Phenol	UV light Visible light	180 420	2.5 g/L	100 mg/L	75 70	[161]
TiO_2/Zeolite	Sulfadiazine	UV light	120	1 g/L	10 mg/L	90	[162]
CdTe/TiO_2	Tetracycline hydrochloride	Visible light	30	0.6 g/L	20 mg/L	78	[163]
N-TiO_2	4-Chlorophenol	Visible light	425	0.5 g/L	500 mg/L	-	[164]
TiO_{2-x}/ rGO	Bisphenol A	Visible light	60	1 g/L	2.5 mg/L	91	[165]
TiO_2/$Ti_3C_2T_x$ (MXene)	Carbamazepine	Sunlight UV light	480 200	1 g/L	5 mg/L	55.8 98.7	[166]

Fe-TiO_2	Pharmaceutical wastewater	UV light	300	1 g/L	-	75	[167]
Sn-Mo-TiO_2 NTs/Ti electrode	Phenol	Eeletrocatalytic	240	-	50 mg/ L	-	[168]
Zr/Ag-TiO_2	Sulphamethoxazole	Visible light	420	0.5 g/L	20 mg/L	90	[169]
SnO_2/TiO_2 and ZnO/TiO_2	Tetracycline	UV light Solar light	35 180	0.5 g/L	35 mg /L	73	[170]
Sand/TiO_2	Phenol	UV light	240	-	25 mg/L	50	[171]
Fe/WO_3/TiO_2	Nitric oxide Acetaldehyde	UV and Visible light	120 240	-	50 mg/L 200 mg/L	88 50	[172]
Al/TiO_2	Propyl paraben	UV light Solar light	90	500 mg/L	420 µg/L	81	[173]
Fe_3O_4@SiO_2@ TiO_2/rGO	Dinitrophenols	UV light	30	0.2 g/L	40 mg/L	88.8	[174]
In,S-TiO_2@rGO	Atrazine	Visible light	20	1 g/L	20 mg/L	95.5	[175]

GO-TiO_2	Perfluorooctanoic acid	UV light	150	-	2.42 µmol/L	83	[176]
rGO/TiO_2/ZnO	Bisphenol-A,	UV light	180	0.5 g/L	200 mg/L	99.7	[177]
TiO_2-metallic form support	Pyrimethanil	UV light	500	50 mg/L	100 mg/L	100	[159]
Degussa P25	5-Fluorouracil	UV light	240	-	10 mg/L	-	[160]
TiO_2-coated glass rings	Clofibric acid, 4-Chlorophenol	UV light	660	150 g/L	20 mg/L	-	[158]
TiO_2@WO_3/Au	Rhodamine B Trimesic acid	Visible light	80	30 mg/L	50 mg/L	94 95	[178]
TiO_2/WO_3	Acetaldehyde	UV light	40	0.05 g/ 0.25 cm^2	200 ppmv	-	[179]
TiO_2	Bisphenol A	UV light	420	1 mg/L	0.1 mg/L	90	[180]
Au/TiO_2	Bisphenol A	UV light	1440	1 g/L	10 mg/L	87.6	[181]

2.6.1.3 Limitation of TiO_2

Over the years, TiO_2 has shown great potential as a photocatalyst. However, there have been challenges in utilizing TiO_2 at an industrial scale due to challenges in its optical properties as well as the high recombination rate of the electrons and holes [126]. TiO_2 photocatalysts are only active in the ultraviolet range of the solar spectrum, which is only 4-5% of the solar spectrum [182]. This limits its application

under visible radiation [156]. In addition, there is a challenge to recover TiO_2 nanoparticles from treated liquid after use as well as agglomeration of the photocatalyst [183]. To overcome these limitations, researchers have suggested many solutions to the potential realization of the application of TiO_2 photocatalyst. This include doping the TiO_2 with metals such as Ag and Au [184] Most recently TiO_2 has been doped using metal ions such as Au and Pt [184]. In a study, Cojocaru et al doped TiO_2 with Au nanoparticles and studied the photocatalytic activity of the photocatalyst according to the loading of Au. The authors reported that the loading of Au significantly improved the performance of the catalyst in the UV radiation photodegradation of BPA [181]. They concluded that the Au nanoparticle provided centers for trapping electrons resulting in reduced electron–hole recombination [181]. In addition, a loading of 0.3-0.7% Au nanoparticles on the TiO_2 also resulted in an improvement in the visible range photocatalysis of BPA resulting 80-83% degradation efficiency [181]. However, they also reported a marked decrease in photodegradation efficiency when they increased the loading of the Au nanoparticles to 1%.

Incorporation of main group elements in TiO_2 based photocatalysts will result in the modification of the surface of the electronic properties of the TiO_2 [185]. This results in introduction of a band state near either the valence band or the conduction band inducing visible light absorption at those sub-band gap energies [185]. In addition, metals have an ability to scavenge electrons from surfaces of semiconductor materials and therefore lead to charge separation and hence improved efficiency.

In recent studies, researchers have been exploring the pairing of TiO_2 with other metal oxides especially with lower band gaps than the 3.2 eV of TiO_2 forming heterojunctions. Various metal oxides such as WO_3, ZnS, ZnO, CeO_2, Fe_2O_3 etc.

have been paired with TiO_2 to form heterojunction material [186]. Research studies have shown that physically linking two semiconductors produces a heterojunction material with higher efficiency than the individual semi-conductors forming it. For example, Makama et al coupled TiO_2 with CdS on an eggshell matrix in a study, to photodegrade methylene blue solution under visible light irradiation. In another study, a heterojunction of Ag/ZnO was synthesized and applied for the degradation of methyl orange [187]. The authors reported a higher degradation efficiency in the heterojunction compared to the individual semiconductors. Improvements in the efficiency of photocatalysts can also be done by doping heterojunction materials with metals and nonmetals. The mechanism is highlighted in Figure 2.2.

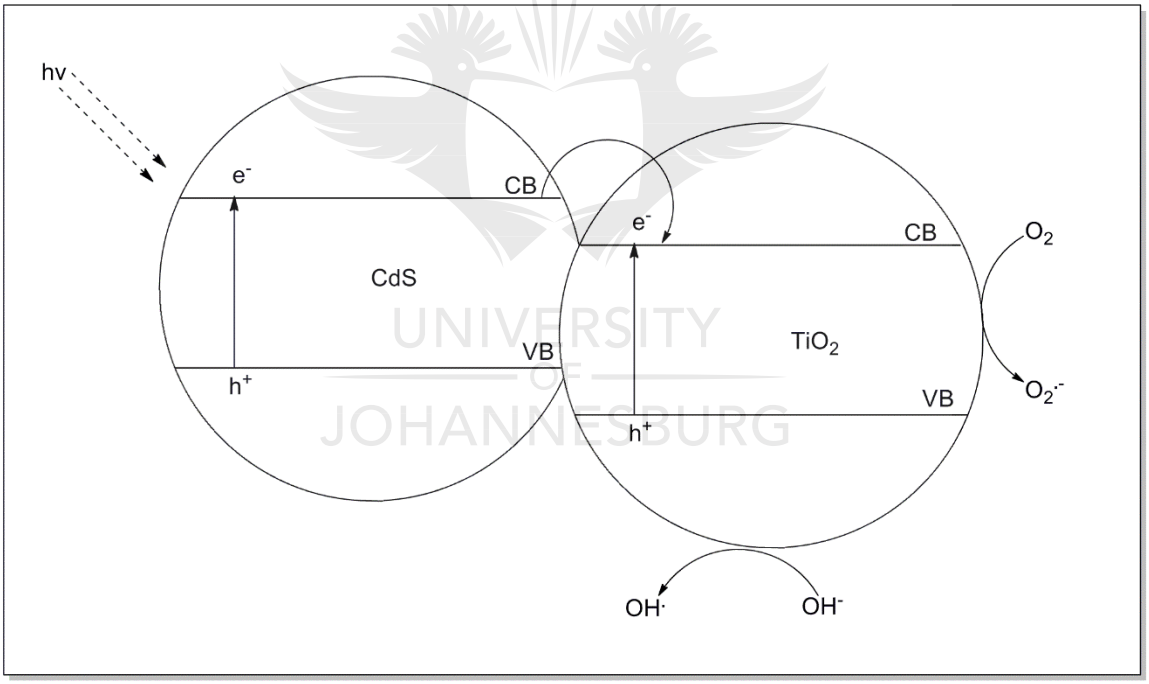

Figure 2.2: Proposed mechanism for photocatalysis using CdS-TiO_2 nanocomposite.

Electrons generated after Cd, with a lower band gap energy (2.4 eV.) will migrate to the conduction of TiO_2 allowing for charge separation and hence higher efficiency. The photo activity of the nanocomposite is enhanced the inter-charge transfer

between the lower band gap semiconductor and TiO_2 resulting in a reduction in the recombination rate [128].

In order to ensure photocatalytic efficiency, there is need to separate the charges. This can be achieved by scavenging of photogenerated electrons or holes in order to limit the recombination rate. Some researchers have utilized dissolved molecular oxygen to scavenge electrons in most photocatalysis reactions. The addition of external oxidant/electron acceptors into photocatalytic degradation reactions has been reported to improve the efficiency of the systems [188]. The additives help to minimize recombination rate, increase the hydroxyl radical concentration and therefore improve the oxidation of organic molecules and their intermediates. In addition, they initiate the generation of more radicals. The most common electron acceptors that have been utilized by researchers include hydrogen peroxide (H_2O_2) and potassium persulfate ($K_2S_2O_8$) [116].

2.6.2 Modification of TiO_2 photocatalysts

In order to improve the electronic and optical properties of TiO_2 photocatalyst, innovative efforts have been made in extending the use of TiO_2 based system under visible light radiation [189]. This includes incorporation of dopants into TiO_2, development of heterojunction photocatalysts, dye sensitization and incorporating support materials. The dopants work by increasing the surface area, crystallinity as well as stability. In addition, some of the dopants reduce the recombination rate of charges. For example, Kuvarega et al. reported an improvement in the TiO_2 nanocomposite after co-doping with nitrogen and palladium [190]. They reported that the palladium metal scavenged electrons delaying recombination rate.

2.6.2.1 Metal doping

Metal doping has been widely reported to improve the photocatalytic activity of TiO_2 based photocatalysts by hindering the rapid recombination of charges *i.e.* electron-hole pairs [191] This is done by the creation of defect states in the band gap of TiO_2 that will absorb visible light [190]. Transition metal ions, noble metals, and non-metal ions are the most used categories of dopants for TiO_2 photocatalysts [184]. Figure 2.3 shows the proposed mechanism for the degradation of emerging organic pollutant by a metal-doped TiO_2 nanocomposite.

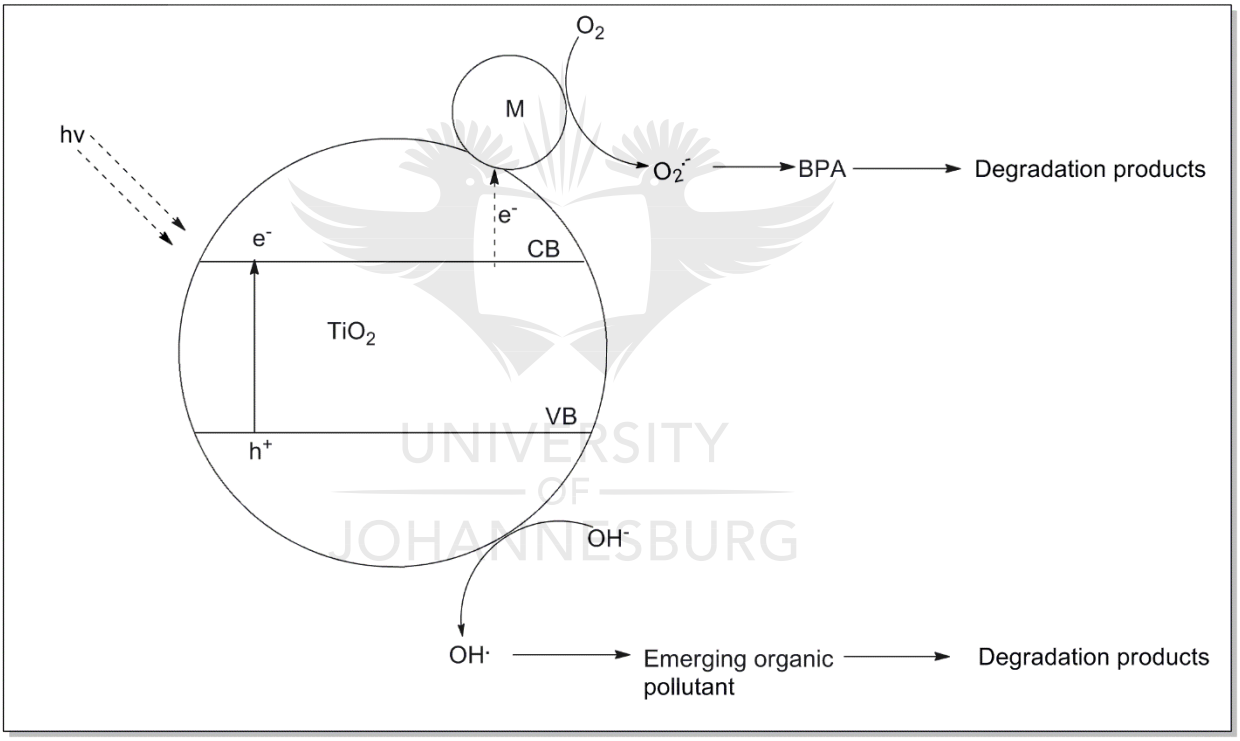

Figure 2.3: Proposed metal doped-TiO_2 nanocomposite degradation mechanism for emerging organic pollutant.

Metal ions such Ni^{2+}, Co^{2+}, $Zn^{2+,}$ and Cu^{2+} have been used as dopants for TiO_2 [192]. The resultant nanocomposite photocatalyst showed improved photocatalytic performances. For example, Blanco-Vega et al doped TiO_2 with Ni and applied the nanocomposite photocatalyst to degrade BPA using Ni-TiO_2 catalysts with different

Ni contents (0.5 and 1.0 wt%) [126]. The authors reported an inhibition in recombination of the electron/hole pairs that was caused by the incorporation of nickel. In a separate study, He et al. developed a Au@TiO_2 core/shell photocatalyst for the degradation of salicylic acid under visible light [193]. They suggested that the improvement in the efficiency of the Au@TiO_2 core/shell photocatalyst compared to the TiO_2 was due to electrons being scavenged by Au and therefore delayed the recombination of charges.

Other metal dopants that have been shown to be effective in improving the photocatalytic activity of TiO_2 include Au, Ag, and Pt. Over the years, many researchers have come up with many innovative methods of depositing metal nanoparticles on TiO_2 photocatalyst including impregnation, photodeposition, and deposition–precipitation [184, 194]. It is important to consider optimum loading of nanometals on the TiO_2 photocatalyst as overloading it may create recombination centers for electron-holes thereby negatively affecting the efficiency of the photocatalytic system [184].

2.6.2.2 Doping with non-metals

Researchers also suggested the doping of the TiO_2 photocatalyst with nonmetals such as nitrogen and sulfur [189]. The non-metal ions replaces some oxygen vacancies in the TiO_2 lattice to form $TiO_{2-x}A_x$ (where A is a non-metal ion, N, S, P, and F) [151]. Many researchers proposed that these nonmetals would result in the reduction of the band gap of the TiO_2 and therefore allow for its use under solar radiation. The reduction in the band gap has been attributed to contribution from p orbitals of elements such as 2p in N, 2p in C and 3p in S to the 2p O and 3d Ti states in the valence band of TiO_2 [191]. Research investigations show that localized states

are formed in the band gap of the material after incorporation of nonmetals leading to absorption of photons of light in the visible range.

Recently, nitrogen doping of TiO_2 has gained popularity [188, 189]. This is mainly because of the ease at which nitrogen can be incorporated in the TiO_2 structure. It is relatively easy to introduce due to its comparable atomic size with oxygen, small ionization energy, and high stability. Many researchers have reported on nitrogen doped TiO_2 with many data reported on the structural, electronic and optical properties of N-doped TiO_2 [189]. For example, Lian et al synthesized a N-TiO_2/fungal hyphae composite for adsorption and photocatalytic degradation of tannin [195]. The authors reported that photocatalytic performance of TiO_2 under visible light was poor, but it greatly improved after doping TiO_2 with nitrogen [195].

Other nonmetal dopants that have been applied with success include carbon, sulphur, phosphorus, and fluorine [189]. They effectively narrowed the band gap of TiO_2 from 3.2 eV and therefore extending its application into the visible range of the solar spectrum. Anionic species are believed to form potentially new impurity levels near the valence and the conduction band of TiO_2 thereby lowering the band gap and moving the band edge into the visible region of the solar spectrum [190]. Although the incorporation of sulphur into the TiO_2 lattice has been carried out successfully, it has presented more challenges than has been the case with nitrogen doping due to its larger ionic radius [157].

2.6.2.3 Pairing of TiO_2 with other photocatalysts

Recently, much effort has been made in designing and synthesizing solar-light-driven photocatalysts. TiO_2 can be paired with other nanometal oxides such as ZnO, ZnS, MoO_3, Cu_2O, and CdS etc. to form heterojunctions that can be used under

visible light irradiation [189]. The synergistic effect of the two semiconductors may result in the inhibition of recombination of electron-hole pairs [196]. For example, ZnO and TiO_2 heterojunction has been shown to have low recombination rate [177]. Many researchers who have reported an improvement in the photodegradation efficiency of TiO_2 based photocatalyst. TiO_2-ZnO nanocomposites have also been explored as catalysts. The band gap of these nanocomposites were reduced due to the influence of ZnO resulting in the nanocomposite being active in the visible light [197].

Another technique that has been applied in improving TiO_2 photocatalyst is co-doping with double metal or double non-metal dopants or double metal/non-metal dopants [191]. This technique leads to shifting of the wavelength absorption of TiO_2 from the ultraviolet to the visible light region. For example, in a study, Wang et al synthesized hollow $CaTiO_3$ cubes modified by La/Cr co-doping via a facile template-free hydrothermal method for photocatalytic hydrogen production [198]. The results from the study show that co-doping resulted in the shifting of the absorption of light into the visible region of the solar spectrum. Although TiO_2 activity can be improved by doping, at an optimal doping level. Doping beyond this level results in a decrease in the TiO_2 activity [191].

2.6.2.4 Dye sensitization

In a bid to develop solar-driven use of TiO_2 based photocatalysts, dye sensitization, has been explored as a viable method to modify the photocatalysts [107]. The mechanism of dye sensitized photodegradation of organic pollutants is the same in principal to coupling two semiconductors except that this process occurs when the highest occupied molecular orbital (HOMO) of a dye absorbs light and excite

electrons to the lowest unoccupied molecular orbital (LUMO) [107, 197]. The excited dye molecule thereafter transfers electrons from its conduction band into the conduction band of TiO_2 [199]. The dye molecule will be converted into its cationic radical [128]. The migrated electrons move to the surface of TiO_2 where they are scavenged by molecular oxygen to form the superoxide radical $\cdot O_2^-$ [128]. These superoxide radicals can oxidize organic pollutants into less harmful by-products or they can completely mineralize them to carbon dioxide and water.

2.6.2.5 Addition of chemical oxidants

In an attempt to eliminate or reduce the recombination of electron-hole pairs, researchers add chemical oxidants to the reactor. The added chemicals work by:

- Increasing the production of ·OH radicals [127].
- Trapping electrons and thereby reducing the recombination rate.
- Optimizing the rate of oxidation of the intermediate products [74].

In order to achieve the target of decontaminating water, the chemical additive must not form toxic intermediates when added to the reactor. In the view of this fact, researchers have used chemicals such as hydrogen peroxide and persulphate [74]. The addition of H_2O_2 can modify the surface of TiO_2 by scavenging the positive holes thereby avoiding recombination (Equation 2.5). The H_2O_2 also reacts with OH radicals (Equation 6).

$$H_2O_2 + 2h_{vb}^+ \rightarrow O_2 + 2\,H^+ \qquad 2.5$$

$$H_2O_2 + HO\cdot \rightarrow H_2O + HO\cdot \qquad 2.6$$

Antonopoullou et al. reported that persulfate ions and hydrogen peroxide act as electron scavengers and enhanced the removal efficiency of N, N-Diethyl-meta-toluamide (DEET) under simulated solar irradiation [200].

2.6.2.6 Incorporation of conducting photocatalyst supports

To enhance the performance of TiO_2 and its nanocomposites towards photocatalytic efficiency, researchers have experimented with the incorporation of carbonaceous materials. In recent years, graphene oxide has been widely utilized in that regard; where researchers take advantage of charge transfer ability to provide charge separation effectively in the nanocomposites [147, 201]. Jo et al. synthesized a magnetic TiO_2-GO nanocomposite for the photocatalysis of methylene blue dye [201]. The authors reported an improved charge separation due to the incorporation of graphene oxide. In addition, carbonaceous materials offer high surface area and mechanical strength to the nanocomposite [202]. Graphene oxide and other carbonaceous materials provide support for the TiO_2 nanocomposite and prevents the inherent agglomeration of the nanoparticles [190].

2.6.2.7 Control of morphology

Tailoring the morphology and surface engineering of TiO_2 has been explored in order to reduce the high recombination rate of charges [151]. Recently, the design and morphological control of TiO_2 crystal facets has been suggested as a way to improve the photocatalytic efficiency of TiO_2 photocatalyst. It is well known that the physical and chemical properties of materials, such as shape, texture, particle size, porosity, crystallinity, functional groups directly affect the photocatalytic performance of materials [131]. The control of such parameters in semiconductor materials, particularly shape and surface structural properties can be closely related

to the reactivity and the selectivity of the material [155, 188]. The most commonly used morphology of TiO_2 is the monodispersed spherical nanoparticles due to their high surface-to-volume ratio that provide abundant surface active sites [148]. However, due to the small size of the spherical particles, they suffer from a high recombination rate reducing its efficiency as a catalyst [126]. On the other hand, TiO_2 nanotubes have been reported to have a large surface area and are more tuned for degradation applications [151].

2.6.2.8 Synthesis techniques for TiO_2 nanostructures

The synthesis of TiO_2 has been reported in literature covering various synthesis methods, such as the hydrothermal method, anodization method, sol-gel method, and the template-assisted method [148]. Synthesis techniques such as the microwave synthesis technique have been employed in order to control the diameter and dispersion of the nanoparticles. Microwave synthesis allows for control of particles sizes and their dispersion in addition, to a shorter synthesis time. It is known to be a greener synthesis technique [203]. The hydrothermal synthesis technique has been utilized to fabricate different TiO_2 nanostructures including, nanorods, nanotubes, nanowires, and nanobelts.

The advantage of using the hydrothermal synthesis technique is the ability to tailor the morphology and porosity of the photocatalysts [153]. For example, Byranvand et al. reported that TiO_2 nanotubes with a diameter of 8 –10 nm were obtained following a hydrothermal synthesis method at a temperature of 110°C after approximately 20 h [204]. Furthermore, data obtained from the research investigation show that the hydrothermal method improves the surface area of materials when compared to other synthesis methods [205]. In addition, the

morphology of materials can be controlled by regulating the temperature and the synthesis time. Research investigations have shown that if the polar face of the photocatalyst are exposed this leads to greater photocatalytic activity. For example, OH^- ions could favorably adsorb onto the surface of the semiconductor because of its positive charge [155]. This could lead to a greater production of $^{\cdot}OH$ radicals and hence degradation of organics. Longer nanotubes may also increase photocatalytic activity due to increased surface area in contact with the pollutant. In addition, tailoring the morphology results in lower recombination rate of positive holes and electron pairs.

2.6.3 Factors affecting the performance of TiO_2 and its nanocomposites

Photocatalytic degradation of emerging organic pollutants by TiO_2 and its nanocomposites is affected by other factors such as pH, dosage, and pollutant initial concentration [43].

2.6.3.1 Effect of pH on emerging pollutant photodegradation

Solution pH plays an important role in determining the efficiency of photodegradation process [42]. This is because it affects the adsorption-desorption of the organic molecules on the surface of the photocatalyst [42]. The pH of the aqueous solution also affects that charges on the surface of the TiO_2 photocatalyst in addition to those of the substrate. In addition, pH influences the generation of hydroxyl radicals as well as active oxygen species that occur on the surface of the photocatalyst [206, 207]. At higher pH, the degradation efficiency tends to decrease. The decrease can be due to the formation of carbonate ions that form at pH > 8 and are known to be good scavengers of hydroxyl radicals [208]. This may contribute to the reduction in the efficiency of the photodegradation process. It is generally logical

and economical to work in the pH range of 4 -10 which is the pH of wastewater produced in most industries.

2.6.3.2 Effect of dosage

TiO_2 based photocatalysts are often used as a suspension and an increase in photocatalyst dosage usually results in an increase in the photodegradation efficiency. The increase in dosage increases the number of ·OH radicals, which can take place in the degradation of emerging organic pollutants [43, 127]. However, a high dosage of the photocatalyst may result in a decrease in efficiency due to agglomeration resulting in a reduction in surface area of the photocatalyst. A high dosage of the photocatalyst results in turbidity thereby impeding the penetration of light to the surface of the photocatalyst and therefore reducing the production of ·OH radicals [127]. A number of studies in the literature show different optimum dosages but they are agree on the need to find the optimum dosage for the reaction depending on the reactor and the photocatalyst used. The design of the reactor is an important part of the process because it also influences the dosage due to the path length that will be needed to illuminate the photocatalyst.

2.6.3.3 Effect of initial emerging pollutant concentration

The initial concentration of pollutant in solution has been shown to influence the degradation efficiency [127]. Many researchers report that the rate of photodegradation of organic pollutants using TiO_2 based photocatalyst fit the Langmuir-Hinshelwood (L-H) kinetic model. The L-H model (Equation 7) relates the degradation rate (r) and the reactant concentration at time t, (C) which is expressed as follows: [208]

$$r = \frac{dC}{dt} = \frac{k_r K_{ad}}{1 + K_{ad} C} \quad 2.7$$

where K_r is the rate constant. When the adsorption is relatively weak or the concentration is low, Equation 8 can be simplified to the pseudo-first order kinetics with an apparent first order rate constant $K_{app.}$ The rate constant expression is given as follows: [208]

$$\ln\left(\frac{C_o}{C}\right) = K_r K_{ad} t = K_{app} \quad 2.8$$

where C_o is the initial concentration.

In TiO_2 based photocatalytic degradation reactions, the amount of substrate covering the photocatalyst is expected to reduce with time and therefore the rate of degradation is expected to reduce to ~ zero and hence decrease in photocatalytic rate with increasing illumination time [127]. Many authors have highlighted that the effect of the initial concentration of substrates on the photocatalyst becomes steady due to saturation of the substrate on the surface of the photocatalyst with increase in concentration. Most studies have shown that the time for complete degradation of pollutants increase with increase in the concentration of the pollutant. This can be ascribed to the increase in the pollutant molecules that were adsorbed on the surface of the photocatalyst [197]. This may result in a reduction in the photons that are able to reach the surface of the photocatalyst surface and therefore less hydroxyl radicals will be generated resulting in reduced photodegradation efficiency [209].

2.6.4 TiO_2 photocatalysts recovery

The recovery of the photocatalyst after treatment is an important process that influences the overall costs of a treatment process. There is growing concern about the recovery of TiO_2 based nanocomposite photocatalysts. In most batch

photocatalytic reactors, the photocatalyst is mostly removed through filtration or centrifugation processes [125]. However, the separation techniques applied for laboratory batch processes are not suitable for large-scale industrial applications [210]. This is a difficult process due to the small size of the photocatalyst. In a system that uses a powdered photocatalyst, the efficiency may be reduced due to agglomeration of the photocatalyst that leads to a reduction in the surface area.

Consequently, the design and development of magnetic photocatalysts is gaining momentum in order to solve the issue of photocatalyst recovery [210]. For example, Alvarez et al prepared magnetic TiO_2/Fe_3O_4 and $TiO_2/SiO_2/Fe_3O_4$ nanoparticles by an ultrasonic-assisted sol–gel method for the photodegradation of pharmaceutical pollutants and BPA [210]. The performance of the photocatalyst was comparable to the commercial Degussa P25 TiO_2 photocatalyst. In addition, the catalyst was recoverable by a magnet. In a separate study, Liu et al synthesized a multifunctional hybrid photocatalyst/magnetic material, $Sr–TiO_2/Ni_{0.6}Zn_{0.4}Fe_2O_4$ for the degradation of emerging organic pollutants under both UV and visible radiation [149]. The authors reported a degradation efficiency of up to 90-100%. The photocatalyst was also recoverable by the use of a magnet.

Recently, polymer supports for TiO_2 and other catalysts have been utilized in order to assist with the recovery of TiO_2 based photocatalyst, many researchers incorporate the photocatalyst in polymers such as polyaniline and polyethyleneimine [211]. The use of polymers to incorporate the photocatalyst is especially attractive because it improves the efficiency of photocatalysts using synergistic effect of both the semiconductor and the polymer [212]. Conducting polymers such as PANI improve the charge separation of the photocatalyst and therefore improve the performance of the photocatalytic system [213]. For example, Sandhya incorporated

TiO_2 nanoparticles in a conducting polymer PANI for the degradation of dyes under visible radiation [213]. The authors reported an improvement in the performance of the photocatalyst after incorporating it in PANI.

Over the years, researchers have immobilized TiO_2 on inert supports such as ceramic, quarts, and glass [213]. This has provided them with advantages and disadvantages in application. The main advantages was the ability to recover the photocatalyst that enables re-usage and an overall reduction in the overall cost of the operation. However, there is loss of photocatalytic activity due to difficulty in mass transfer of the substrate to the surface of the photocatalyst. Fixation of the photocatalyst reduces the accessibility of the surface of the photocatalyst and therefore results in the reduction of the rate of degradation.

2.6.5 CONCLUSION

The presence of emerging organic pollutants in the environment has been confirmed through many research investigations, thanks to advances in analytical techniques. These emerging organic pollutants have the potential to disrupt the normal function of the hormones in humans. Photodegradation has the potential to remove emerging organic pollutants from the environment. In order to achieve an efficient photodegradation system, there is need to design a photocatalyst that has a high photonic efficiency.

The incorporation of nanotechnology in photocatalysis offers a great potential for design of robust and effective technologies for water and environmental remediation. The use of adsorptive support materials has a great potential to improve the overall performance of nanostructured photocatalysts as they will anchor the catalysts and adsorb pollutants and facilitating the degradation process.

The use of these photocatalysts under solar irradiation makes this process to be cheap and affordable to developing countries, many of which cannot afford expensive treatment methods. In summary, there is need to develop robust, cheap photocatalysts that can be applied in water remediation and to explore their performance in large-scale applications.

2.6.6 REFERENCES

[1] S. Muhammad, M.T. Shah, S. Khan, Health risk assessment of heavy metals and their source apportionment in drinking water of Kohistan region, northern Pakistan, *Microchemical Journal*, 98 (2011) 334-343.

[2] M. Masheane, L. Nthunya, S. Sambaza, S. Malinga, E. Nxumalo, B. Mamba, S. Mhlanga, Chitosan-based nanocomposite beads for drinking water production, IOP Conference Series. *Materials Science and Engineering, IOP Publishing*,195 (2017), pp. 012004.

[3] M. Elliott, Biological pollutants and biological pollution – an increasing cause for concern*, Marine Pollution Bulletin* 46 (2003) 275-280.

[4] F. Lugoli, M. Leopizzi, F. Bagordo, T. Grassi, M. Guido, A. De Donno, Widespread microbiological groundwater contamination in the South-eastern Salento (Puglia-Italy). *Journal of Environmental Monitoring* 13 (2011) 192-200.

[5] L.M. Sassoubre, S.P. Walters, T.L. Russell, A.B. Boehm, Sources and fate of Salmonella and fecal indicator bacteria in an urban creek, *Journal of Environmental Monitoring* 13 (2011) 2206-2212.

[6] J.M. Kayembe, F. Thevenon, A. Laffite, P. Sivalingam, P. Ngelinkoto, C.K. Mulaji, J.P. Otamonga, J.I. Mubedi, J. Pote, High levels of faecal contamination in drinking groundwater and recreational water due to poor sanitation, in the sub-rural

neighbourhoods of Kinshasa, Democratic Republic of the Congo, *International Journal of Hygiene and Environmental Health* 221 (2018) 400-408.

[7] M. Hellmér, N. Paxéus, L. Magnius, L. Enache, B. Arnholm, A. Johansson, T. Bergström, H. Norder, Detection of pathogenic viruses in sewage gave early warning on hepatitis A and norovirus outbreaks. *Applied and Environmental Microbiology* 265 (2014). 01914-01981.

[8] G. Tjon, C. Wijkmans, R. Coutinho, A. Koek, J. van den Hoek, A. Leenders, P. Schneeberger, S. Bruisten, Molecular epidemiology of hepatitis A in Noord-Brabant, Netherlands. *Journal of Clinical Virology* 32 (2005) 128-136.

[9] J.D. Clemens, G.B. Nair, T. Ahmed, F. Qadri, J. Holmgren, Cholera, The Lancet, 390 (2017) 1539-1549.

[10] S. Mandal, M.D. Mandal, N.K. Pal, Cholera: a great global concern, Asian Pacific. *Journal of Tropical Medicine*, 4 (2011) 573-580.

[11] L. Schweitzer, J. Noblet, Water contamination and pollution, *Green Chemistry, Elsevier* 1 (2017) 261-290.

[12] K. Parashar, N. Ballav, S. Debnath, K. Pillay, A. Maity, Hydrous TiO_2@ polypyrrole hybrid nanocomposite as an efficient selective scavenger for the defluoridation of drinking water, *The Royal Society of Chemistry Advances*, 6 (2016) 99482-99495.

[13] J.G. Speight, Sources and types of inorganic pollutants, in J.G. Speight (Ed.) Environmental Inorganic Chemistry for Engineers, Butterworth-Heinemann (2017), pp. 231-282.

[14] A. Menesguen, G. Lacroix, Modelling the marine eutrophication: A review, *Science Total Environment* 636 (2018) 339-354.

[15] W. Maret, The metals in the biological periodic system of the elements: concepts and conjectures. *International Journal of Molecular Sciences*, 17 (2016) 66.

[16] S. Majumder, S. Gupta, S. Raghuvanshi, Removal of dissolved metals by bioremediation. *The Royal Society of Chemistry* (2014) pp 44-56.

[17] M. Ugarte, N.N. Osborne, L.A. Brown, P.N. Bishop, Iron, zinc, and copper in retinal physiology and disease, Survey of Ophthalmology, 58 (2013) 585-609.

[18] D. Sun, C. Wang, W. Zhang, L. Zhao, Chapter 13: Fluoride and dietary calcium on bone, Fluorine: Chemistry, Analysis, Function and Effects. *The Royal Society of Chemistry* (2015) 217-235.

[19] F. Peng, W. Ji, F. Zhu, D. Peng, M. Yang, R. Liu, Y. Pu, L. Yin, A study on phthalate metabolites, bisphenol A and nonylphenol in the urine of Chinese women with unexplained recurrent spontaneous abortion, *Environmental Research,* 150 (2016) 622-628.

[20] B. de Campos Ventura-Camargo, M.A. Marin-Morales, Azo dyes: Characterization and toxicity–a review, *Textiles, and Light Industrial Science and Technology* 2 (2013) 85-103.

[21] R. Reif, S. Suárez, F. Omil, J. Lema, Fate of pharmaceuticals and cosmetic ingredients during the operation of a MBR treating sewage, *Desalination*, 221 (2008) 511-517.

[22] X. Wei, P. Gu, G. Zhang, J. Huang, Occurrence of emerging and priority pollutants in municipal reverse osmosis concentrates, *Environmental Science Process Impacts*, 17 (2015) 488-494.

[23] A. Ayati, M.N. Shahrak, B. Tanhaei, M. Sillanpää, Emerging adsorptive removal of azo dye by metal–organic frameworks, *Chemosphere*, 160 (2016) 30-44.

[24] E. Durmaz, P. Erkekoglu, A. Asci, S. Akcurin, I. Bircan, B. Kocer-Gumusel, Urinary phthalate metabolite concentrations in girls with premature thelarche, *Environmental and Toxicological Pharmacology*, 59 (2018) 172-181.

[25] A. Jurado, E. Vàzquez-Suñé, J. Carrera, M.L. de Alda, E. Pujades, D. Barceló, Emerging organic contaminants in groundwater in Spain: a review of sources, recent occurrence, and fate in a European context, *Science of the Total Environment,* 440 (2012) 82-94.

[26] A. Mendoza, B. Zonja, N. Mastroianni, N. Negreira, M. Lopez de Alda, S. Perez, D. Barcelo, A. Gil, Y. Valcarcel, Drugs of abuse, cytostatic drugs, and iodinated contrast media in tap water from the Madrid region (central Spain): A case study to analyse their occurrence and human health risk characterization, *Environment International,* 86 (2016) 107-118.

[27] A.B.A. Boxall, New and emerging water pollutants arising from agriculture, (2012).

[28] A. Pal, K.Y. Gin, A.Y. Lin, M. Reinhard, Impacts of emerging organic contaminants on freshwater resources: review of recent occurrences, sources, fate and effects, *Science of theTotal Environment*, 408 (2010) 6062-6069.

[29] D. Lapworth, N. Baran, M. Stuart, R. Ward, Emerging organic contaminants in groundwater: a review of sources, fate, and occurrence, *Environmental Pollution,* 163 (2012) 287-303.

[30] P.J. Sullivan, J.J.J. Clark, F.J. Agardy, P.F. Rosenfeld, Chapter 9: Toxicity and synthetic chemical mixtures, in P.J. Sullivan, J.J.J. Clark, F.J. Agardy, P.F. Rosenfeld (Eds.) Toxic Legacy, Academic Press, Burlington, 2007, pp. 177-215.

[31] C.M. Villanueva, E. Gracia-Lavedan, J. Julvez, L. Santa-Marina, N. Lertxundi, J. Ibarluzea, S. Llop, F. Ballester, A. Fernández-Somoano, A. Tardón, Drinking

water disinfection by-products during pregnancy and child neuropsychological development in the INMA Spanish cohort study, *Environment International*, 110 (2018) 113-122.

[32] S.M. Barlow, F.M. Sullivan, R.K. Miller, 2.23 - Occupational, industrial and environmental agents, in C. Schaefer, P. Peters, R.K. Miller (Eds.) Drugs During Pregnancy and Lactation (Third Edition), Academic Press, San Diego, 2015, pp. 599-638.

[33] M. Remberger, J. Sternbeck, A. Palm, L. Kaj, K. Strömberg, E. Brorström-Lundén, The environmental occurrence of hexabromocyclododecane in Sweden, *Chemosphere*, 54 (2004) 9-21.

[34] M.A. Siddiqi, R.H. Laessig, K.D. Reed, Polybrominated diphenyl ethers (PBDEs): new pollutants–old diseases, *Clinical Medicine and Research*, 1 (2003) 281-290.

[35] P.O. Darnerud, G.S. Eriksen, T. Jóhannesson, P.B. Larsen, M. Viluksela, Polybrominated diphenyl ethers: occurrence, dietary exposure, and toxicology, *Environmental Health Perspectives*, 109 (2001) 49.

[36] K. Katayama-Hirayama, N. Toda, A. Tauchi, A. Fujioka, T. Akitsu, H. Kaneko, K. Hirayama, Degradation of dibromophenols by UV irradiation, *Journal of Environmental Sciences* 26 (2014) 1284-1288.

[37] F. Whitfield, K. Shaw, D. Walker, The source of 2, 6-dibromophenol: cause of an iodoform taint in Australian prawns, *Water Science and Technology* 25 (1992) 131-138.

[38] F.P. Garcia, S.Y.C. Ascencio, J.C.G. Oyarzun, A.C. Hernandez, P.V. Alavarado, Pesticides: classification, uses, and toxicity. Measures of exposure and

genotoxic risks, *Journal of Research in Environmental Science and Toxicology* 1 (2012) 279-293.

[39] Z. Hasan, S.H. Jhung, Removal of hazardous organics from water using metal-organic frameworks (MOFs): plausible mechanisms for selective adsorptions, *Journal of Hazardous Materials* 283 (2015) 329-339.

[40] A.M. King, C.K. Aaron, Organophosphate and carbamate poisoning, Emergency *Medicine Clinics* 33 (2015) 133-151.

[41] S.S. Kulkarni, D.R. Buchholz, Developmental programs and endocrine disruption in frog metamorphosis: the perspective from microarray analysis, Current topics in developmental biology, *Elsevier* 2013, pp. 329-364.

[42] F.A. Caliman, M. Gavrilescu, Pharmaceuticals, personal care products and endocrine disrupting agents in the environment–a review, *CLEAN–Soil, Air, Water,* 37 (2009) 277-303.

[43] S. Bagheri, A. TermehYousefi, T.-O. Do, Photocatalytic pathway toward degradation of environmental pharmaceutical pollutants: structure, kinetics and mechanism approach, *Catalysis Science and Technology* 7 (2017) 4548-4569.

[44] J. Wu, L. Zhang, Z. Yang, A Review on the analysis of emerging contaminants in aquatic environment, *Critical Reviews in Analytical Chemistry*, 40 (2010) 234-245.

[45] R.L. Oulton, T. Kohn, D.M. Cwiertny, Pharmaceuticals and personal care products in effluent matrices: A survey of transformation and removal during wastewater treatment and implications for wastewater management, *Journal of Environmental Monitoring* 12 (2010) 1956-1978.

[46] A. Mendoza, B. Zonja, N. Mastroianni, N. Negreira, M.L. de Alda, S. Pérez, D. Barceló, A. Gil, Y. Valcárcel, Drugs of abuse, cytostatic drugs, and iodinated contrast media in tap water from the Madrid region (central Spain): A case study to

analyse their occurrence and human health risk characterization, *Environment International*, 86 (2016) 107-118.

[47] Y. Peng, S. Hall, L. Gautam, Drugs of abuse in drinking water – a review of current detection methods, occurrence, elimination and health risks, *TrAC Trends in Analytical Chemistry,* 85 (2016) 232-240.

[48] M. Lorenzo, J. Campo, Y. Picó, Analytical challenges to determine emerging persistent organic pollutants in aquatic ecosystems, *TrAC Trends in Analytical Chemistry*, 103 (2018) 137-155.

[49] L. Schweitzer, J. Noblet, Chapter five: Water contamination and pollution, *Green Chemistry Elsevier* (2018) pp 261-290.

[50] N. Milic, D. Cetojevic-Simin, M. Milanovic, J. Sudji, N. Milosevic, N. Curic, L. Abenavoli, M. Medic-Stojanoska, Estimation of in vivo and in vitro exposure to bisphenol A as food contaminant, *Food Chemical Toxicology*, 83 (2015) 268-274.

[51] C.A. Richter, L.S. Birnbaum, F. Farabollini, R.R. Newbold, B.S. Rubin, C.E. Talsness, J.G. Vandenbergh, D.R. Walser-Kuntz, F.S. vom Saal, In vivo effects of bisphenol A in laboratory rodent studies, *Reproduction Toxicology,* 24 (2007) 199-224.

[52] J. Rajasärkkä, M. Pernica, J. Kuta, J. Lašňák, Z. Šimek, L. Bláha, Drinking water contaminants from epoxy resin-coated pipes: A field study, *Water Research*, 103 (2016) 133-140.

[53] C. Erler, J. Novak, Bisphenol A exposure: human risk and health policy, *Journal of Pediatric Nursing*, 25 (2010) 400-407.

[54] R.K. Bhandari, S.L. Deem, D.K. Holliday, C.M. Jandegian, C.D. Kassotis, S.C. Nagel, D.E. Tillitt, F.S. Vom Saal, C.S. Rosenfeld, Effects of the environmental estrogenic contaminants bisphenol A and 17 alpha-ethinyl estradiol on sexual

development and adult behaviors in aquatic wildlife species, *General and Comparative Endocrinology,* 214 (2015) 195-219.

[55] D.D. Snow, S.L. Bartelt-Hunt, S. Devivo, S. Saunders, D.A. Cassada, Detection, occurrence, and fate of emerging contaminants in agricultural environments, *Water Environment Research,* 81 (2009) 941-958.

[56] C. Kubwabo, I. Kosarac, B. Stewart, B. Gauthier, K. Lalonde, P. Lalonde, Migration of bisphenol A from plastic baby bottles, baby bottle liners and reusable polycarbonate drinking bottles, *Food Additives and Contaminants*, 26 (2009) 928-937.

[57] C. Menale, D.G. Mita, N. Diano, S. Diano, Adverse effects of bisphenol A exposure on glucose metabolism regulation, *The Open Biotechnology Journal* 10 (2016) 122-130.

[58] T.F.T. Omar, A.Z. Aris, F.M. Yusoff, S. Mustafa, An improved SPE-LC-MS/MS method for multiclass endocrine disrupting compound determination in tropical estuarine sediments, *Talanta* 173 (2017) 51-59.

[59] M. Farré, S. Pérez, C. Gonçalves, M. Alpendurada, D. Barceló, Green analytical chemistry in the determination of organic pollutants in the aquatic environment, *TrAC Trends in Analytical Chemistry* 29 (2010) 1347-1362.

[60] R.N. Mead, P.J. Seaton, GC–MS quantitation and identification of bisphenol-A isolated from water, *Journal of Chemical Education* 88 (2011) 1130-1132.

[61] Y. Sun, M. Irie, N. Kishikawa, M. Wada, N. Kuroda, K. Nakashima, Determination of bisphenol A in human breast milk by HPLC with column-switching and fluorescence detection, *Biomedical Chromatograph*, 18 (2004) 501-507.

[62] J. Regueiro, A. Breidbach, T. Wenzl, Derivatization of bisphenol A and its analogues with pyridine-3-sulfonyl chloride: multivariate optimization and

fragmentation patterns by liquid chromatography/orbitrap mass spectrometry, *Rapid Communication Mass Spectrum,* 29 (2015) 1473-1484.

[63] N. Milić, M. Milanović, N.G. Letić, M.T. Sekulić, J. Radonić, I. Mihajlović, M.V. Miloradov, Occurrence of antibiotics as emerging contaminant substances in aquatic environment, *International Journal of Environmental Health Research*, 23 (2013) 296-310.

[64] M.K. Bjornsdotter, J. de Boer, A. Ballesteros-Gomez, Bisphenol A and replacements in thermal paper: A review, *Chemosphere,* 182 (2017) 691-706.

[65] N. Dorival-García, A. Zafra-Gómez, A. Navalón, J. Vílchez, Analysis of bisphenol A and its chlorinated derivatives in sewage sludge samples. Comparison of the efficiency of three extraction techniques, *Journal of Chromatography A*, 1253 (2012) 1-10.

[66] M.N.H. Rozaini, N. Yahaya, B. Saad, S. Kamaruzaman, N.S.M. Hanapi, Rapid ultrasound assisted emulsification micro-solid phase extraction based on molecularly imprinted polymer for HPLC-DAD determination of bisphenol A in aqueous matrices, *Talanta,* 171 (2017) 242-249.

[67] C. De Monte, S. Carradori, A. Granese, G.B. Di Pierro, C. Leonardo, C. De Nunzio, Modern extraction techniques and their impact on the pharmacological profile of Serenoa repens extracts for the treatment of lower urinary tract symptoms, *BMC urology*, 14 (2014) 63.

[68] H. Farajnezhad, P. Gharbani, Coagulation treatment of wastewater in petroleum industry using poly aluminum chloride and ferric chloride*, International Journal of Recent Research and Applied Studies* (13), 1 (2012) 306-310.

[69] O. Sahu, P. Chaudhari, Review on chemical treatment of industrial waste water, *Journal of Applied Sciences and Environmental Management*, 17 (2013) 241-257.

[70] S. Yüksel, N. Kabay, M. Yüksel, Removal of bisphenol A (BPA) from water by various nanofiltration (NF) and reverse osmosis (RO) membranes, *Journal of Hazardous Materials*, 263 (2013) 307-310.

[71] M. Zielińska, K. Bułkowska, A. Cydzik-Kwiatkowska, K. Bernat, I. Wojnowska-Baryła, Removal of bisphenol A (BPA) from biologically treated wastewater by microfiltration and nanofiltration, *International Journal of Environmental Science and Technology,* 13 (2016) 2239-2248.

[72] J.R. Koduru, L.P. Lingamdinne, J. Singh, K.-H. Choo, Effective removal of bisphenol A (BPA) from water using a goethite/activated carbon composite, *Process Safety and Environmental Protection,* 103 (2016) 87-96.

[73] Q. Han, H. Wang, W. Dong, T. Liu, Y. Yin, H. Fan, Degradation of bisphenol A by ferrate (VI) oxidation: Kinetics, products and toxicity assessment, *Chemical Engineering Journal*, 262 (2015) 34-40.

[74] K.F. Chen, Y.C. Chang, W.T. Chiou, Remediation of diesel-contaminated soil using in situ chemical oxidation (ISCO) and the effects of common oxidants on the indigenous microbial community: a comparison study, *Journal of Chemical Technology and Biotechnology*, 91 (2016) 1877-1888.

[75] J. Rivera-Utrilla, M. Sanchez-Polo, M.A. Ferro-Garcia, G. Prados-Joya, R. Ocampo-Perez, Pharmaceuticals as emerging contaminants and their removal from water. A review, *Chemosphere*, 93 (2013) 1268-1287.

[76] D. Tiwari, J.-K. Yang, S.-M. Lee, Applications of ferrate (VI) in the treatment of wastewaters, *Environmental Engineering Research*, 10 (2005) 269-282.

[77] L. Sailo, D. Tiwari, S.-M. Lee, Degradation of some micro-pollutants from aqueous solutions using ferrate (VI): Physico-chemical studies, *Separation Science and Technology,* 52 (2017) 2756-2766.

[78] J. Zhang, B. Sun, X. Guan, Oxidative removal of bisphenol A by permanganate: Kinetics, pathways, and influences of co-existing chemicals, *Separation and Purification Technology,* 107 (2013) 48-53.

[79] J. Jiang, S.-Y. Pang, J. Ma, Role of ligands in permanganate oxidation of organics, *Environmental Science and Technology*, 44 (2010) 4270-4275.

[80] R. Das, C.D. Vecitis, A. Schulze, B. Cao, A.F. Ismail, X. Lu, J. Chen, S. Ramakrishna, Recent advances in nanomaterials for water protection and monitoring, *Chemical Society Reviews*, 46 (2017) 6946-7020.

[81] D. Mohapatra, S. Brar, R. Tyagi, R. Surampalli, Physico-chemical pre-treatment and biotransformation of wastewater and wastewater sludge–fate of bisphenol A, *Chemosphere,* 78 (2010) 923-941.

[82] R. Allabashi, M. Arkas, G. Hörmann, D. Tsiourvas, Removal of some organic pollutants in water employing ceramic membranes impregnated with cross-linked silylated dendritic and cyclodextrin polymers, *Water Research*, 41 (2007) 476-486.

[83] S. Kim, K.H. Chu, Y.A. Al-Hamadani, C.M. Park, M. Jang, D.-H. Kim, M. Yu, J. Heo, Y. Yoon, Removal of contaminants of emerging concern by membranes in water and wastewater: a review, *Chemical Engineering Journal* 335 (2017) 890-914.

[84] V. Vatanpour, S.S. Madaeni, A.R. Khataee, E. Salehi, S. Zinadini, H.A. Monfared, TiO_2 embedded mixed matrix PES nanocomposite membranes: Influence of different sizes and types of nanoparticles on antifouling and performance, *Desalination,* 292 (2012) 19-29.

[85] M.M. Pendergast, E.M. Hoek, A review of water treatment membrane nanotechnologies, *Energy and Environmental Science*, 4 (2011) S1946-1971.

[86] X. Jin, J. Shan, C. Wang, J. Wei, C.Y. Tang, Rejection of pharmaceuticals by forward osmosis membranes, *Journal of Hazardous Materials*, 227-228 (2012) 55-61.

[87] R. Molinari, C. Lavorato, P. Argurio, Recent progress of photocatalytic membrane reactors in water treatment and in synthesis of organic compounds. A review, *Catalysis Today,* 281 (2017) 144-164.

[88] I.B. Ivshina, M.S. Kuyukina, A.V. Krivoruchko, A.A. Elkin, S.O. Makarov, C.J. Cunningham, T.A. Peshkur, R.M. Atlas, J.C. Philp, Oil spill problems and sustainable response strategies through new technologies, *Environmental Science Process Impacts,* 17 (2015) 1201-1219.

[89] K. Margeta, N.A.Z. Logar, M. Šiljeg, A. Farkas, Natural zeolites in water treatment–how effective is their use, Water Treatment, Chapter 5, *InTech* 2013 pp 81-112

[90] E.J. Eio, M. Kawai, K. Tsuchiya, S. Yamamoto, T. Toda, Biodegradation of bisphenol A by bacterial consortia, *International Biodeterioration and Biodegradation,* 96 (2014) 166-173.

[91] O. Gulnaz, S. Dincer, Biodegradation of bisphenol A by Chlorella vulgaris and Aeromonas Hydrophilia, *Journal of Applied Biological Sciences*, (2009) 79-84.

[92] A. Cydzik-Kwiatkowska, K. Bernat, M. Zielińska, K. Bułkowska, I. Wojnowska-Baryła, Aerobic granular sludge for bisphenol A (BPA) removal from wastewater*, International Biodeterioration and Biodegradation,* 122 (2017) 1-11.

[93] S.W. Chang, M.R. Hyman, K.J. Williamson, Cooxidation of naphthalene and other polycyclic aromatic hydrocarbons by the nitrifying bacterium, *Nitrosomonas Europaea, Biodegradation,* 13 (2002) 373-381.

[94] A.K. Ghattas, F. Fischer, A. Wick, T.A. Ternes, Anaerobic biodegradation of (emerging) organic contaminants in the aquatic environment, *Water Research*, 116 (2017) 268-295.

[95] Y. Jia, S.K. Khanal, H. Zhang, G.H. Chen, H. Lu, Sulfamethoxazole degradation in anaerobic sulfate-reducing bacteria sludge system, *Water Research*, 119 (2017) 12-20.

[96] B. Seyhi, P. Drogui, G. Buelna, A. Azaïs, M. Heran, Contribution of a submerged membrane bioreactor in the treatment of synthetic effluent contaminated by Bisphenol-A: mechanism of BPA removal and membrane fouling, *Environmental Pollution,* 180 (2013) 229-235.

[97] M.-K. Ji, A.N. Kabra, J. Choi, J.-H. Hwang, J.R. Kim, R.A. Abou-Shanab, Y.-K. Oh, B.-H. Jeon, Biodegradation of bisphenol A by the freshwater microalgae Chlamydomonas mexicana and Chlorella vulgaris, *Ecological Engineering*, 73 (2014) 260-269.

[98] M. Ahmaruzzaman, Adsorption of phenolic compounds on low-cost adsorbents: a review, Advances in *Colloid and Interface Science,* 143 (2008) 48-67.

[99] E.C. Lima, Removal of emerging contaminants from the environment by adsorption, Ecotoxicology*. Environmental Safety* 150 (2018) 1-17.

[100] J. Rouquerol, F. Rouquerol, P. Llewellyn, G. Maurin, K.S. Sing, Adsorption by powders and porous solids: principles, methodology, and applications, *Academic Press* Chapter 1 (2014) pp 81-626.

[101] A. Dąbrowski, Adsorption—from theory to practice, *Advances in Colloid and Interface Science*, 93 (2001) 135-224.

[102] K.S. Sing, F. Rouquerol, J. Rouquerol, Classical interpretation of physisorption isotherms at the gas-solid interface, Adsorption by Powders and Porous Solids: Principles, Methodology, and Applications, *Elsevier* 2 (2013) 159-189.

[103] D.M. Saad, E.M. Cukrowska, H. Tutu, Phosphonated cross-linked polyethylenimine for selective removal of uranium ions from aqueous solutions, *Water Science and Technology*, 66 (2012) 122-129.

[104] H. Liu, X. Cai, Y. Wang, J. Chen, Adsorption mechanism-based screening of cyclodextrin polymers for adsorption and separation of pesticides from water, *Water Research,* 45 (2011) 3499-3511.

[105] M. Vakili, M. Rafatullah, B. Salamatinia, A.Z. Abdullah, M.H. Ibrahim, K.B. Tan, Z. Gholami, P. Amouzgar, Application of chitosan and its derivatives as adsorbents for dye removal from water and wastewater: A review, *Carbohydrate Polymers,* 113 (2014) 115-130.

[106] S. Li, G. Zhang, P. Wang, H. Zheng, Y. Zheng, Microwave-enhanced Mn-Fenton process for the removal of BPA in water, *Chemical Engineering Journal*, 294 (2016) 371-379.

[107] M. Minella, F. Sordello, C. Minero, Photocatalytic process in TiO_2/graphene hybrid materials. Evidence of charge separation by electron transfer from reduced graphene oxide to TiO_2, *Catalysis Today*, 281 (2017) 29-37.

[108] Y. Park, Z. Sun, G.A. Ayoko, R.L. Frost, Bisphenol A sorption by organo-montmorillonite: implications for the removal of organic contaminants from water, *Chemosphere,* 107 (2014) 249-256.

[109] S. Zhu, Y.G. Liu, S.B. Liu, G.M. Zeng, L.H. Jiang, X.F. Tan, L. Zhou, W. Zeng, T.T. Li, C.P. Yang, Adsorption of emerging contaminant metformin using graphene oxide, *Chemosphere*, 179 (2017) 20-28.

[110] F. Chen, W. An, L. Liu, Y. Liang, W. Cui, Highly efficient removal of bisphenol A by a three-dimensional graphene hydrogel-AgBr@rGO exhibiting adsorption/photocatalysis synergy, *Applied Catalysis B: Environmental*, 217 (2017) 65-80.

[111] H. Ruiz, M. Zambtrano, L. Giraldo, R. Sierra, J.C. Moreno-Pirajan, Production and characterization of activated carbon from oil-palm shell for carboxylic acid adsorption, *Oriental Journal of Chemistry*, 31 (2015) 753-762.

[112] S. Álvarez-Torrellas, A. Rodríguez, G. Ovejero, J. García, Comparative adsorption performance of ibuprofen and tetracycline from aqueous solution by carbonaceous materials, *Chemical Engineering Journal*, 283 (2016) 936-947.

[113] M. Kebaili, S. Djellali, M. Radjai, N. Drouiche, H. Lounici, Valorization of orange industry residues to form a natural coagulant and adsorbent, *Journal of Industrial and Engineering Chemistry,* 64 (2018) 1-15.

[114] M.T. Islam, R. Saenz-Arana, C. Hernandez, T. Guinto, M.A. Ahsan, D.T. Bragg, H. Wang, B. Alvarado-Tenorio, J.C. Noveron, Conversion of waste tire rubber into a high-capacity adsorbent for the removal of methylene blue, methyl orange, and tetracycline from water, *Journal of Environmental Chemical Engineering*, 6 (2018) 3070-3082.

[115] Y. Deng, R. Zhao, Advanced oxidation processes (AOPs) in wastewater treatment, *Current Pollution Reports*, 1 (2015) 167-176.

[116] S.Y. Oh, D.S. Shin, Degradation of spent caustic by Fenton and persulfate oxidation with zero-valent iron, *Journal of Chemical Technology and Biotechnology*, 88 (2013) 145-152.

[117] M. Molkenthin, T. Olmez-Hanci, M.R. Jekel, I. Arslan-Alaton, Photo-Fenton-like treatment of BPA: effect of UV light source and water matrix on toxicity and transformation products, *Water Research*, 47 (2013) 5052-5064.

[118] E.E. Ebrahiem, M.N. Al-Maghrabi, A.R. Mobarki, Removal of organic pollutants from industrial wastewater by applying photo-Fenton oxidation technology, *Arabian Journal of Chemistry*, 10 (2017) S1674-S1679.

[119] C. Nadejde, M. Neamtu, V.-D. Hodoroaba, R.-J. Schneider, G. Ababei, U. Panne, Hybrid iron-based core–shell magnetic catalysts for fast degradation of bisphenol A in aqueous systems, *Chemical Engineering Journal,* 302 (2016) 587-594.

[120] H. Hansson, F. Kaczala, M. Marques, W. Hogland, Photo-Fenton and Fenton oxidation of recalcitrant industrial wastewater using nanoscale zero-valent iron, *International Journal of Photoenergy*, 2012 (2012) 1-11.

[121] K. Gandhi, S. Lari, D. Tripathi, G. Kanade, Advanced oxidation processes for the treatment of chlorpyrifos, dimethoate, and phorate in aqueous solution, *Journal of Water Reuse and Desalination,* 6 (2016) 195-203.

[122] A. Manivel, G.-J. Lee, C.-Y. Chen, J.-H. Chen, S.-H. Ma, T.-L. Horng, J.J. Wu, Synthesis of MoO_3 nanoparticles for azo dye degradation by catalytic ozonation, *Materials Research Bulletin,* 62 (2015) 184-191.

[123] R. Keykavoos, R. Mankidy, H. Ma, P. Jones, J. Soltan, Mineralization of bisphenol A by catalytic ozonation over alumina, *Separation and Purification Technology,* 107 (2013) 310-317.

[124] K. Kalyanasundaram, Photochemical applications of solar energy: photocatalysis and photodecomposition of water, Photochemistry: Volume 41, *The Royal Society of Chemistry* 2013, pp. 182-265.

[125] M.N. Chong, B. Jin, C.W. Chow, C. Saint, Recent developments in photocatalytic water treatment technology: a review*, Water Research*, 44 (2010) 2997-3027.

[126] M. Blanco-Vega, J. Guzmán-Mar, M. Villanueva-Rodríguez, L. Maya-Treviño, L. Garza-Tovar, A. Hernández-Ramírez, L. Hinojosa-Reyes, Photocatalytic elimination of bisphenol A under visible light using Ni-doped TiO_2 synthesized by microwave assisted sol-gel method, *Materials Science in Semiconductor Processing,* 71 (2017) 275-282.

[127] S. Malato, P. Fernández-Ibáñez, M.I. Maldonado, J. Blanco, W. Gernjak, Decontamination and disinfection of water by solar photocatalysis: Recent overview and trends, *Catalysis Today*, 147 (2009) 1-59.

[128] M.R.D. Khaki, M.S. Shafeeyan, A.A.A. Raman, W.M.A.W. Daud, Application of doped photocatalysts for organic pollutant degradation-A review, *Journal of Environmental Management,* 198 (2017) 78-94.

[129] P.A. Zapata, F.M. Rabagliati, I. Lieberwirth, F. Catalina, T. Corrales, Study of the photodegradation of nanocomposites containing TiO_2 nanoparticles dispersed in polyethylene and in poly(ethylene-co-octadecene), *Polymer Degradation and Stability,* 109 (2014) 106-114.

[130] S.N. Habisreutinger, L. Schmidt-Mende, J.K. Stolarczyk, Photocatalytic reduction of CO_2 on TiO_2 and other semiconductors, *Angewandte Chemie International Edition*, 52 (2013) 7372-7408.

[131] A. Hernández-Ramírez, I. Medina-Ramírez, Semiconducting materials, Photocatalytic Semiconductors, *Springer* 2015, 1-40.

[132] K. Mondal, A. Sharma, Recent advances in the synthesis and application of photocatalytic metal–metal oxide core–shell nanoparticles for environmental

remediation and their recycling process, *The Royal Society of Chemistry Advances*, 6 (2016) 83589-83612.

[133] S. Ikram, Role of nanomaterials and their applications as photo-catalyst and senors: A review, *Archivos de Medicina*, 2 (2016) 10.

[134] P. Vishnukumar, S. Vivekanandhan, M. Misra, A. Mohanty, Recent advances and emerging opportunities in phytochemical synthesis of ZnO nanostructures, *Materials Science in Semiconductor Processing*, 80 (2018) 143-161.

[135] S.G. Kumar, K.K. Rao, Zinc oxide based photocatalysis: tailoring surface-bulk structure and related interfacial charge carrier dynamics for better environmental applications, *The Royal Society of Chemistry Advances*, 5 (2015) 3306-3351.

[136] O. Bechambi, S. Sayadi, W. Najjar, Photocatalytic degradation of bisphenol A in the presence of C-doped ZnO: Effect of operational parameters and photodegradation mechanism, *Journal of Industrial and Engineering Chemistry*, 32 (2015) 201-210.

[137] V. Rogé, C. Guignard, G. Lamblin, F. Laporte, I. Fechete, F. Garin, A. Dinia, D. Lenoble, Photocatalytic degradation behavior of multiple xenobiotics using MOCVD synthesized ZnO nanowires, *Catalysis Today*, 306 (2018) 215-222.

[138] P.V.L. Reddy, K.H. Kim, B. Kavitha, V. Kumar, N. Raza, S. Kalagara, Photocatalytic degradation of bisphenol A in aqueous media: A review, *Journal of Environmental Management,* 213 (2018) 189-205.

[139] C. Ramana, S. Utsunomiya, R. Ewing, C. Julien, U. Becker, Structural stability and phase transitions in WO_3 thin films, *The Journal of Physical Chemistry B*, 110 (2006) 10430-10435.

[140] Y. Hunge, M. Mahadik, A. Moholkar, C. Bhosale, Photoelectrocatalytic degradation of oxalic acid using WO_3 and stratified WO_3/TiO_2 photocatalysts under sunlight illumination, *Ultrasonics Sonochemistry*, 35 (2017) 233-242.

[141] E. Ghasemi, H. Ziyadi, A.M. Afshar, M. Sillanpää, Iron oxide nanofibers: A new magnetic catalyst for azo dyes degradation in aqueous solution, *Chemical Engineering Journal*, 264 (2015) 146-151.

[142] E.M. Bakhsh, S.A. Khan, H.M. Marwani, E.Y. Danish, A.M. Asiri, S.B. Khan, Performance of cellulose acetate-ferric oxide nanocomposite supported metal catalysts toward the reduction of environmental pollutants, *International Journal of Biology and Macromolecules*, 107 (2018) 668-677.

[143] K. Gurushantha, L. Renuka, K. Anantharaju, Y. Vidya, H. Nagaswarupa, S. Prashantha, H. Nagabhushana, Photocatalytic and photoluminescence studies of ZrO_2/ZnO nanocomposite for LED and waste water treatment applications, *Materials Today: Proceedings*, 4 (2017) 11747-11755.

[144] J.D. Rodney, S. Deepapriya, P.A. Vinosha, S. Krishnan, S.J. Priscilla, R. Daniel, S.J. Das, Photo-Fenton degradation of nano-structured La doped CuO nanoparticles synthesized by combustion technique*, Optik,* 161 (2018) 204-216.

[145] M.M. Khin, A.S. Nair, V.J. Babu, R. Murugan, S. Ramakrishna, A review on nanomaterials for environmental remediation, *Energy and Environmental Science,* 5 (2012) 8075-8109.

[146] Y. Ohko, I. Ando, C. Niwa, T. Tatsuma, T. Yamamura, T. Nakashima, Y. Kubota, A. Fujishima, Degradation of bisphenol A in water by TiO_2 photocatalyst, *Environmental Science and Technology,* 35 (2001) 2365-2368.

[147] R. Rajagopal, K.-S. Ryu, Synthesis of rGO-doped Nb_4O_5–TiO_2 nanorods for photocatalytic and electrochemical energy storage applications, *Applied Catalysis B: Environmental*, 236 (2018) 125-139.

[148] W.J. Ong, L.L. Tan, S.P. Chai, S.T. Yong, A.R. Mohamed, Highly reactive {001} facets of TiO_2-based composites: synthesis, formation mechanism and characterization, *Nanoscale,* 6 (2014) 1946-2008.

[149] F. Liu, Y. Xie, C. Yu, X. Liu, Y. Dai, L. Liu, Y. Ling, Novel hybrid Sr-doped TiO_2/magnetic $Ni_{0.6}\ Zn_{0.4}\ Fe_2\ O_4$ for enhanced separation and photodegradation of organics under visible light, *The Royal Society of Chemistry Advances*, 5 (2015) 24056-24063.

[150] V. Geissen, H. Mol, E. Klumpp, G. Umlauf, M. Nadal, M. van der Ploeg, S.E. van de Zee, C.J. Ritsema, Emerging pollutants in the environment: a challenge for water resource management, *International Soil and Water Conservation Research,* 3 (2015) 57-65.

[151] M. Wang, J. Ioccozia, L. Sun, C. Lin, Z. Lin, Inorganic-modified semiconductor TiO_2 nanotube arrays for photocatalysis, *Energy and Environmental Science*, 7 (2014) 2182-2202.

[152] L. Cano-Casanova, A. Amorós-Pérez, M. Ouzzine, M. Lillo-Ródenas, M.C. Román-Martínez, One step hydrothermal synthesis of TiO_2 with variable HCl concentration: Detailed characterization and photocatalytic activity in propene oxidation, *Applied Catalysis B: Environmental*, 220 (2018) 645-653.

[153] P. Dong, X. Cheng, Z. Huang, Y. Chen, Y. Zhang, X. Nie, X. Zhang, In-situ and phase controllable synthesis of nanocrystalline TiO_2 on flexible cellulose fabrics via a simple hydrothermal method*, Materials Research Bulletin*, 97 (2018) 89-95.

[154] Y. Li, L. Liu, M. Guo, M. Zhang, Synthesis of TiO_2 visible light catalysts with controllable crystalline phase and morphology from Ti-bearing electric arc furnace molten slag, *Journal of Environmental Sciences*, 47 (2016) 14-22.

[155] S. Riaz, S. Naseem, Controlled nanostructuring of TiO_2 nanoparticles: a sol–gel approach, *Journal of Sol-Gel Science and Technology,* 74 (2015) 299-309.

[156] A.V. Murugan, V. Samuel, V. Ravi, Synthesis of nanocrystalline anatase TiO_2 by microwave hydrothermal method, *Materials Letters*, 60 (2006) 479-480.

[157] S.A. Bakar, C. Ribeiro, Rapid, and morphology controlled synthesis of anionic S-doped TiO_2 photocatalysts for the visible-light-driven photodegradation of organic pollutants, *The Royal Society of Chemistry Advances*, 6 (2016) 36516-36527.

[158] A. Manassero, M.L. Satuf, O.M. Alfano, Photocatalytic degradation of an emerging pollutant by TiO_2-coated glass rings: a kinetic study, *Environmental Science Pollution Research International,* 24 (2017) 6031-6039.

[159] K. Elatmani, N.B. oujji, G. Plantara, V. Goetz, I.A. ichou, 3D Photocatalytic media for decontamination of water from pesticides, *Materials Research Bulletin*, 101 (2018) 6-11.

[160] C. Gomez-Canela, G. Bolivar-Subirats, R. Tauler, S. Lacorte, Powerful combination of analytical and chemometric methods for the photodegradation of 5-Fluorouracil, *Journal of Pharmaceutical Biomedical Analysis*, 137 (2017) 33-41.

[161] S. Moghaddam, M.M. Zerafat, S. Sabbaghi, Response surface methodology for optimization of phenol photocatalytic degradation using carbon-doped TiO_2 nano-photocatalyst, *International Journal of Nano Dimension*, 9 (2018) 89-103.

[162] X.H. Liu, Y. Liu, S.Y. Lu, W. Guo, B.D. Xi, Performance and mechanism into TiO_2/Zeolite composites for sulfadiazine adsorption and photodegradation, *Chemical Engineering Journal*, 350 (2018) 131-147.

[163] Y.Y. Gong, Y.J. Wu, Y. Xu, L. Li, C. Li, X.J. Liu, L.Y. Niu, All-solid-state Z-scheme CdTe/TiO_2 heterostructure photocatalysts with enhanced visible-light photocatalytic degradation of antibiotic waste water, *Chemical Engineering Journal,* 350 (2018) 257-267.

[164] T. Boningari, S.N.R. Inturi, M. Suidan, P.G. Smirniotis, Novel one-step synthesis of nitrogen-doped TiO_2 by flame aerosol technique for visible-light photocatalysis: Effect of synthesis parameters and secondary nitrogen (N) source, *Chemical Engineering Journal*, 350 (2018) 324-334.

[165] L. Xu, L. Yang, E.M.J. Johansson, Y.H. Wang, P.K. Jin, Photocatalytic activity and mechanism of bisphenol a removal over TiO_2-x/rGO nanocomposite driven by visible light, *Chemical Engineering Journal*, 350 (2018) 1043-1055.

[166] X. Zhang, Y. Liu, S. Dong, Z. Ye, Y. Guo, One-step hydrothermal synthesis of a TiO_2-$Ti_3C_2T_x$ nanocomposite with small sized TiO_2 nanoparticles, *Ceramics International,* 43 (2017) 11065-11070.

[167] P. Bansal, A. Verma, S. Talwar, Detoxification of real pharmaceutical wastewater by integrating photocatalysis and photo-Fenton in fixed-mode, *Chemical Engineering Journal,* 349 (2018) 838-848.

[168] X.Y. Ma, Z.R. Sun, X. Hu, Synthesis of tin and molybdenum co-doped TiO_2 nanotube arrays for the photoelectrocatalytic oxidation of phenol in aqueous solution, *Materials Science in Semiconductor Processing*, 85 (2018) 150-159.

[169] S. Naraginti, Y. Li, G.L. Puma, Photocatalytic mineralization and degradation kinetics of sulphamethoxazole and reactive red 194 over silver-zirconium co-doped titanium dioxide: Reaction mechanisms and phytotoxicity assessment, *Ecotoxicology and Environmental Safety*, 159 (2018) 301-309.

[170] L. Rimoldi, E. Pargoletti, D. Meroni, E. Falletta, G. Cerrato, F. Turco, G. Cappelletti, Concurrent role of metal (Sn, Zn) and N species in enhancing the photocatalytic activity of TiO_2 under solar light, *Catalysis Today* 313 (2017) 40-46.

[171] Y.K. Abdel-Maksoud, E. Imam, A.R. Ramadan, Sand supported TiO_2 photocatalyst in a tray photo-reactor for the removal of emerging contaminants in wastewater, *Catalysis Today*, 313 (2017) 55-62.

[172] N.O. Balayeva, M. Fleisch, D.W. Bahnemann, Surface-grafted WO_3/TiO_2 photocatalysts: Enhanced visible-light activity towards indoor air purification, *Catalysis Today*, 313 (2018) 63-71.

[173] S. Kotzamanidi, Z. Frontistis, V. Binas, G. Kiriakidis, D. Mantzavinos, Solar photocatalytic degradation of propyl paraben in Al-doped TiO_2 suspensions, *Catalysis Today,* 313 (2018) 148-154.

[174] B. MirzaHedayat, M. Noorisepehr, E. Dehghanifard, A. Esrafili, R. Norozi, Evaluation of photocatalytic degradation of 2, 4-Dinitrophenol from synthetic wastewater using Fe_3O_4@ SiO_2@TiO_2/rGO magnetic nanoparticles, *Journal of Molecular Liquids, 264* (2018) 571-578.

[175] A.H.C. Khavar, G. Moussavi, A.R. Mahjoub, M. Satari, P. Abdolmaleki, Synthesis and visible-light photocatalytic activity of In, S-TiO_2@ rGO nanocomposite for degradation and detoxification of pesticide atrazine in water, *Chemical Engineering Journal,* 345 (2018) 300-311.

[176] K. Park, I. Ali, J.-O. Kim, Photodegradation of perfluorooctanoic acid by graphene oxide-deposited TiO_2 nanotube arrays in aqueous phase, *Journal of Environmental Management*, 218 (2018) 333-339.

[177] E. Bilgin Simsek, B. Kilic, M. Asgin, A. Akan, Graphene oxide based heterojunction TiO_2–ZnO catalysts with outstanding photocatalytic performance for

bisphenol-A, ibuprofen and flurbiprofen, *Journal of Industrial and Engineering Chemistry,* 59 (2018) 115-126.

[178] J. Cai, X. Wu, S. Li, F. Zheng, Synthesis of TiO_2@WO_3/Au nanocomposite hollow spheres with controllable sze and high visible-light-driven photocatalytic activity, *ACS Sustainable Chemistry and Engineering*, 4 (2016) 1581-1590.

[179] J. Yang, X. Zhang, H. Liu, C. Wang, S. Liu, P. Sun, L. Wang, Y. Liu, Heterostructured TiO_2/WO_3 porous microspheres: preparation, characterization and photocatalytic properties, *Catalysis Today*, 201 (2013) 195-202.

[180] W. Wu, G. Shan, S. Wang, L. Zhu, L. Yue, Q. Xiang, Y. Zhang, Z. Li, Environmentally relevant impacts of nano-TiO_2 on abiotic degradation of bisphenol A under sunlight irradiation, *Environmental Pollution*, 216 (2016) 166-172.

[181] B. Cojocaru, V. Andrei, M. Tudorache, F. Lin, C. Cadigan, R. Richards, V.I. Parvulescu, Enhanced photo-degradation of bisphenol pollutants onto gold-modified photocatalysts, *Catalysis Today*, 284 (2017) 153-159.

[182] K. Biernat, A. Malinowski, M. Gnat, The possibility of future biofuels production using waste carbon dioxide and solar energy, Biofuels, Environment and Sustainabilty Chapter 5, *Intech* (2013) pp 123-172.

[183] X. Chen, H. Li, H. Wu, Y. Wu, Y. Shang, J. Pan, X. Xiong, Fabrication of TiO_2@PANI nanobelts with the enhanced absorption and photocatalytic performance under visible light, *Materials Letters*, 172 (2016) 52-55.

[184] J. Taing, M.H. Cheng, J.C. Hemminger, Photodeposition of Ag or Pt onto TiO_2 nanoparticles decorated on step edges of HOPG, *American Chemistry Society Nano,* 5 (2011) 6325-6333.

[185] X. Chen, S.S. Mao, Titanium dioxide nanomaterials: synthesis, properties, modifications, and applications, *Chemical Reviews*, 107 (2007) 2891-2959.

[186] Z.R. Hesabi, N.K. Allam, K. Dahmen, H. Garmestani, M.A. El-Sayed, Self-standing crystalline TiO_2 nanotubes/CNTs heterojunction membrane: Synthesis and characterization, *American Chemistry Society Applied Materials and Interfaces,* 3 (2011) 952-955.

[187] T. Chen, Y. Zheng, J.-M. Lin, G. Chen, Study on the photocatalytic degradation of methyl orange in water using Ag/ZnO as catalyst by liquid chromatography electrospray ionization ion-trap mass spectrometry, *Journal of the American Society for Mass Spectrometry*, 19 (2008) 997-1003.

[188] K.L. Lin, F.D. Mai, Y.C. Chan, J.C. Chung, K.M. Lin, C.C. Yu, M.Y. Liao, F.Y. Li, Morphology dependence of photocatalytic activity of TiO_2 nanostructure prepared through microwave hydrothermal process, *Journal of the Chinese Chemical Society,* 59 (2012) 603-613.

[189] S.M. El-Sheikh, T.M. Khedr, A. Hakki, A.A. Ismail, W.A. Badawy, D.W. Bahnemann, Visible light activated carbon and nitrogen co-doped mesoporous TiO_2 as efficient photocatalyst for degradation of ibuprofen, *Separation and Purification Technology,* 173 (2017) 258-268.

[190] A.T. Kuvarega, R.W. Krause, B.B. Mamba, Nitrogen/palladium-codoped TiO_2 for efficient visible light photocatalytic dye degradation, *The Journal of Physical Chemistry C*, 115 (2011) 22110-22120.

[191] M. Pelaez, N.T. Nolan, S.C. Pillai, M.K. Seery, P. Falaras, A.G. Kontos, P.S. Dunlop, J.W. Hamilton, J.A. Byrne, K. O'shea, A review on the visible light active titanium dioxide photocatalysts for environmental applications, *Applied Catalysis B: Environmental*, 125 (2012) 331-349.

[192] H.-Y. Lin, C.-Y. Shih, Efficient one-pot microwave-assisted hydrothermal synthesis of M (M= Cr, Ni, Cu, Nb) and nitrogen co-doped TiO_2 for hydrogen

production by photocatalytic water splitting, *Journal of Molecular Catalysis A: Chemical,* 411 (2016) 128-137.

[193] W. He, J. Cai, X. Jiang, J. Yin, Q. Meng, Generation of reactive oxygen species and charge carriers in plasmonic photocatalytic Au@TiO_2 nanostructures with enhanced activity, *Physical Chemistry Chemical Physics 20*, (2018)16117-16125.

[194] S.D. Mhlanga, K.C. Mondal, R. Carter, M.J. Witcomb, N.J. Coville, The effect of synthesis parameters on the catalytic synthesis of multiwalled carbon nanotubes using Fe-Co/$CaCO_3$ catalysts, *South African Journal of Chemistry*, 62 (2009) 67-76.

[195] X. Bai, X. Li, Z. Gao, Z. Hu, G. Hu, Novel fungal hyphae/Fe_3O_4 and N-TiO_2/NG composite for adsorption and photocatalysis, *The Royal Society of Chemistry Advances,* 7 (2017) 6842-6848.

[196] Y. Wang, H. Li, G. Chen, Z. Wang, Y. Sang, H. Liu, PdO/TiO_2 nanobelt heterostructures with high photocatalytic activities based on an exposed highly active facet on ultrathin TiO_2 nanobelts, *Solar Energy Materials and Solar Cells*, 161 (2017) 297-304.

[197] T.J. Brooms, B. Otieno, M.S. Onyango, A. Ochieng, Photocatalytic degradation of P-cresol using TiO_2/ZnO hybrid surface capped with polyaniline, *Journal of Environmental Science and Health, Part A*, 53 (2018) 99-107.

[198] R. Wang, S. Ni, G. Liu, X. Xu, Hollow $CaTiO_3$ cubes modified by La/Cr co-doping for efficient photocatalytic hydrogen production, *Applied Catalysis B: Environmental,* 225 (2018) 139-147.

[199] E. Bae, W. Choi, Highly enhanced photoreductive degradation of perchlorinated compounds on dye-sensitized metal/TiO_2 under visible light, *Environmental Science and Technology*, 37 (2003) 147-152.

[200] M. Antonopoulou, I. Konstantinou, Effect of oxidants in the photocatalytic degradation of deet under simulated solar irradiation in aqueous TiO_2 suspensions, *Global Nest Journal* 16 (2014) pp 507-515.

[201] W.K. Jo, N.C.S. Selvam, Synthesis of GO supported Fe_2O_3–TiO_2 nanocomposites for enhanced visible-light photocatalytic applications, *Dalton Transactions,* 44 (2015) 16024-16035.

[202] R.K. Upadhyay, N. Soin, S.S. Roy, Role of graphene/metal oxide composites as photocatalysts, adsorbents, and disinfectants in water treatment: a review, *The Royal Society of Chemistry Advances*, 4 (2014) 3823-3851.

[203] S. Joseph, B. Mathew, Microwave-assisted green synthesis of silver nanoparticles and the study on catalytic activity in the degradation of dyes, *Journal of Molecular Liquids*, 204 (2015) 184-191.

[204] M. Malekshahi Byranvand, A. Nemati Kharat, L. Fatholahi, Z. Malekshahi Beiranvand, A review on synthesis of nano-TiO_2 via different methods, *Journal of Nanostructures*, 3 (2013) 1-9.

[205] S.H. Cho, H.H. Nguyen, G. Gyawali, J.-E. Son, T. Sekino, B. Joshi, S.H. Kim, Y.H. Jo, T.H. Kim, S.W. Lee, Effect of microwave-assisted hydrothermal process parameters on formation of different TiO_2 nanostructures, *Catalysis Today*, 266 (2016) 46-52.

[206] S.S. Sambaza, M.L. Masheane, S.P. Malinga, E.N. Nxumalo, S.D. Mhlanga, Polyethyleneimine-carbon nanotube polymeric nanocomposite adsorbents for the removal of Cr^{6+} from water, *Physics and Chemistry of the Earth, Parts A/B/C,* 100 (2017) 236-246.

[207] C. Ravidhas, A.J. Josephine, P. Sudhagar, A. Devadoss, C. Terashima, K. Nakata, A. Fujishima, A.M.E. Raj, C. Sanjeeviraja, Facile synthesis of

nanostructured monoclinic bismuth vanadate by a co-precipitation method: structural, optical and photocatalytic properties, *Materials Science in Semiconductor Processing,* 30 (2015) 343-351.

[208] K.V. Kumar, K. Porkodi, Comments on “Photocatalytic properties of TiO_2 modified with platinum and silver nanoparticles in the degradation of oxalic acid in aqueous solution”: Langmuir Hinshelwood kinetics - A theoretical study, *Applied Catalysis B: Environmental*, 79 (2008) 108-109.

[209] J.C.C. da Silva, J.A. Reis Teodoro, R.J.d.C.F. Afonso, S.F. Aquino, R. Augusti, Photodegradation of bisphenol A in aqueous medium: Monitoring and identification of by-products by liquid chromatography coupled to high-resolution mass spectrometry, *Rapid Communications in Mass Spectrometry*, 28 (2014) 987-994.

[210] P.M. Álvarez, J. Jaramillo, F. López-Piñero, P.K. Plucinski, Preparation and characterization of magnetic TiO_2 nanoparticles and their utilization for the degradation of emerging pollutants in water, *Applied Catalysis B: Environmental,* 100 (2010) 338-345.

[211] X. Li, D. Wang, G. Cheng, Q. Luo, J. An, Y. Wang, Preparation of polyaniline-modified TiO_2 nanoparticles and their photocatalytic activity under visible light illumination, *Applied Catalysis B: Environmental*, 81 (2008) 267-273.

[212] J. Kavil, S. Ullattil, A. Alshahrie, P. Periyat, Polyaniline as photocatalytic promoter in black anatase TiO_2, *Solar Energy* 158 (2017) 792-796..

[213] K.P. Sandhya, S. Haridas, S. Sugunan, Visible light induced photocatalytic activity of polyaniline modified TiO_2 and Clay-TiO_2 composites, *Bulletin of Chemical Reaction Engineering and Catalysis* 8 (2013): 145-159.

CHAPTER 3:

REVIEW OF SYNTHESES, CHARACTERIZATION AND ANALYTICAL TECHNIQUES

3.0.1 INTRODUCTION

This chapter summarizes the experimental and the characterization techniques that were employed for this work. The operative principle for the instruments is also explained in detail.

3.0.1.1 Hydrothermal and solvothermal syntheses

Hydrothermal synthesis is based on chemical interactions of chemicals above the boiling point of water to form new compounds [1]. On the other hand, solvothermal synthesis occurs in non-aqueous solutions at high temperatures [1]. These syntheses techniques are usually carried out in sealed vessels such as autoclaves [2]. These chemical reactions are carried out in aqueous solution or organic solvents at high temperatures of up to 1000°C generating pressures of between 1-100 MPa [1]. In addition to these techniques being carried out in one step, the mild reaction conditions highlight the advantages that they have over other syntheses techniques [3].

Hydrothermal synthesis uses water which is a cheap and environmentally safe solvent. This synthesis technique takes advantage of the ability of water to change its physical properties at high temperature and pressure [4]. For example, viscosity, density, and surface tension of water are lower than at room temperature [4]. On the other hand, the variety of organic solvents that are used in solvothermal synthesis give more room for the synthesis of different materials with different properties [1].

A variety of organic solvents have been utilized in solvothermal synthesis including, propanol, methyl alcohol, ethyl alcohol, butanol and ethylene glycol [1].

Various methods can be incorporated into hydrothermal and solvothermal techniques such as templating, addition of structure directing agents, initiating growth via crystal seeds [3]. In the past decades, different nanomaterials such as $BaTiO_3$, TiO_2, $BiVO_4$, and $LiNbO_3$ have been prepared under hydrothermal conditions [5-8]. These materials were synthesized by dissolving their metal salt precursors in water or organic solvents and mixing with a suitable concentration of catalyst solutions such as NaOH, citric acid, oxalic acid and KOH [5-8]. The resultant mixture is then heated under autoclave conditions.

3.0.2 Microwave assisted syntheses

The microwave utilizes electromagnetic radiation to generate heat that is subsequently utilized to prepare materials [9]. This is based on dipolar rotation and an ionic conduction mechanism [10]. In dipolar rotation, heat is generated when heat energy is lost due to friction and dielectric loss after molecules with the same electrical dipole aligned with oscillating electromagnetic field [11]. While in the ionic conduction mechanism, microwave radiation causes dissolved or dissociated charged particles or ions to oscillate back and forth [11].

Recently, microwave-assisted methods have been extensively applied in the synthesis of nanomaterials [10, 12]. In this method, a suitable metal salt precursor is dissolved or dispersed in a liquid solvent and the solution or mixture is heated in the microwave under stirring. Organic solvents act as solvents and stabilizers in the process and have been reported to influence particle growth and eliminate agglomeration [13]. Recently this method has been receiving favorable attention due

to its high efficiency, uniformity of particle distribution on supports and its environmental friendliness. For example, Hasanpoor demonstrated the efficiency of microwave assisted synthesis of needle shaped ZnO nanomaterials [14]. In another study, Chikan et.al highlighted the influence of microwave radiation in control of the nucleation and particle growth during the synthesis of nanomaterial in comparison to the traditional injection method [15].In all these microwave synthesis methods, temperature was shown to greatly influence reactivity [10].

Microwave synthesis has been reported to greatly reduce the time required to synthesize nanomaterials. In addition, there has been a great improvement in the performance of materials synthesized via this method owing to the admirable control of particle size as well as the uniform dispersion of the particles on supports [12]. A schematic summary of the experimental work carried out in this project is shown in Figure 3.1.

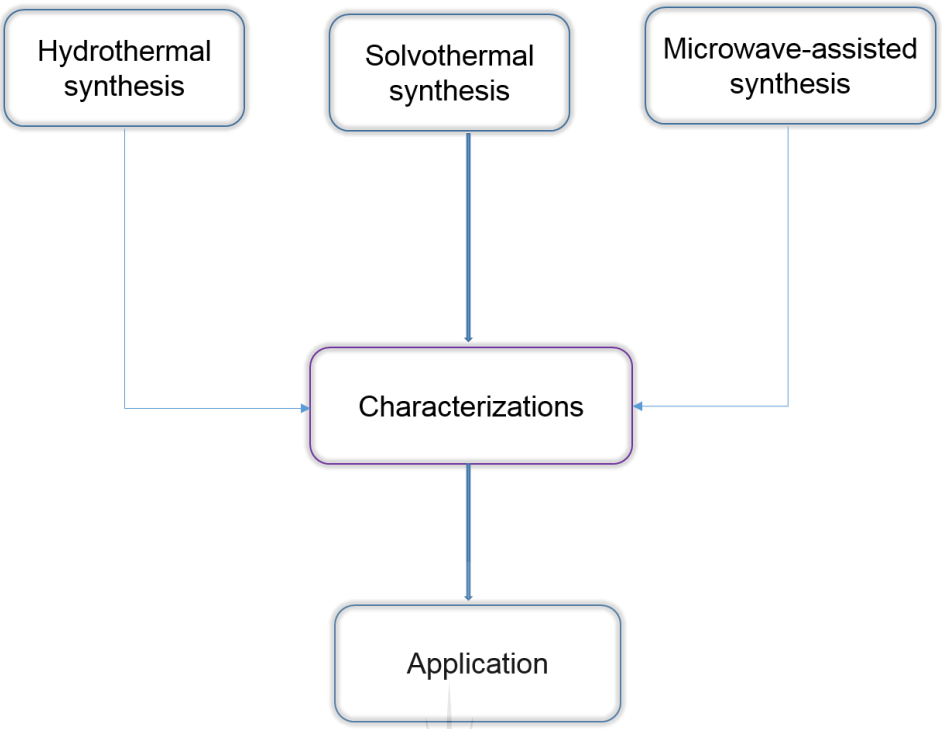

Figure 3. 1: The schematic summary of the experimental work carried out.

In this project, the above mentioned techniques were employed to synthesize the photocatalysts used in this study.

3.1 Characterization techniques

Characterization of the photocatalysts is necessary in order obtain valuable information about the surface, elemental, chemical or molecular properties and other parameters that influence their performance. The materials used in this project were characterized using the following techniques: Fourier infrared spectroscopy (FTIR),UV-vis spectrometry, Raman spectroscopy, X-ray photoelectron spectroscopy (XPS),thermogravimetric analysis (TGA), scanning electron microscopy (SEM), energy dispersive spectroscopy (EDS), transmission electron microscopy (TEM), Brunauer-Emmett-Teller (BET), and X-ray diffraction.

3.1.1 Fourier transform infrared spectroscopy (FTIR)

FTIR is used to identify functional groups in materials [16, 17]. This non-destructive technique can be used for qualitative analysis of inorganic and organic compounds [17]. It involves the use of photons to bring transitions between vibrational states in molecules and functional groups in the infrared region of the solar spectrum [16]. Molecules absorb energy at specific frequencies and this phenomenon can be used to identify the molecules using IR spectra. A molecular finger print is created when infrared radiation has been passed through a sample as a result of some of the infrared radiation being absorbed whilst some of it being transmitted [18]. The signals that make the spectrum result from the vibrational and rotational excitation of molecules and or atoms within a molecule [18]. The spectrum produced is unique and no two unique molecular structures produce identical spectra. This makes the technique suitable for identification of molecules. A typical schematic diagram of modern FTIR spectrometer is shown in Figure 3.2.

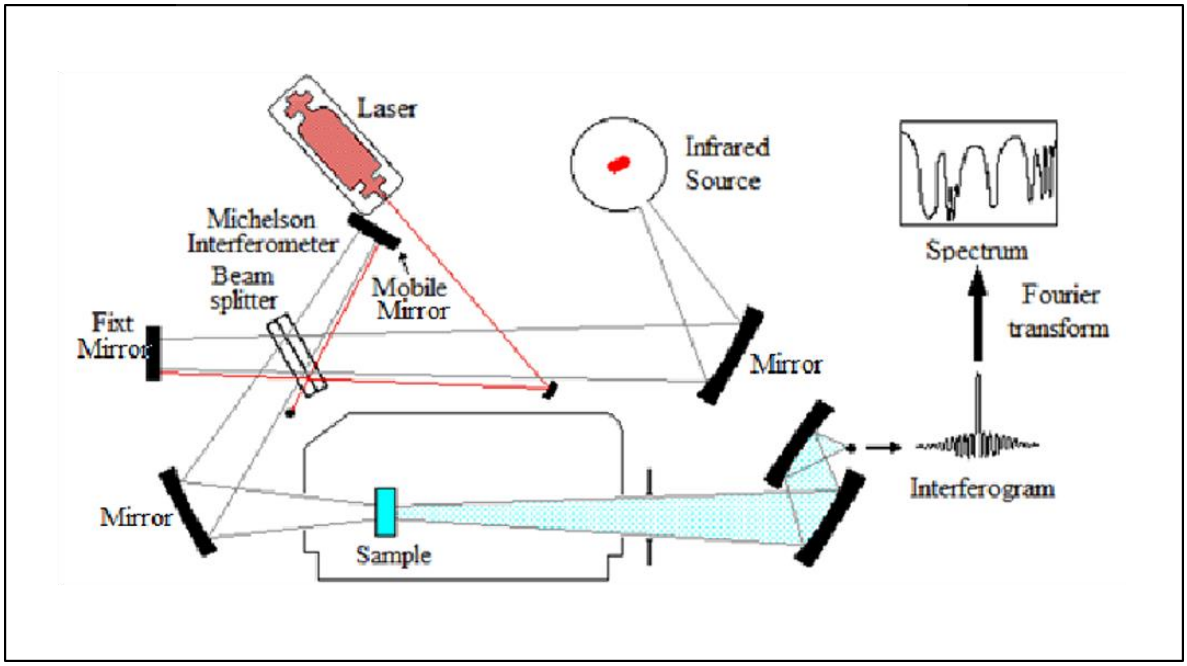

Figure 3.2: Schematic-illustration-of-a-modern-FTIR-Spectrophotometer [19].

The FTIR spectra used in this project were obtained by a Perkin Elmer FTIR 100 spectrophotometer in the range 500-4000 cm^{-1} averaging 32 scans at a spectra resolution of 4 cm^{-1}.

3.1.2 Raman spectroscopy

Raman spectroscopy is a vibrational spectroscopy technique that is used for evaluating molecular motion and identifying compounds [18]. This technique is based on the inelastic scattering of photons after their interaction with vibrating molecules of the sample under analysis [20]. Raman spectroscopy can used for both quantitative and qualitative analysis. Qualitative analysis using Raman spectroscopy can be performed by measuring the frequency of scattered radiations while intensity of scattered radiations can be used for quantitative analysis [20]. During the analysis, a sample is illuminated with a laser beam that is directed by a monochromator, which then interacts with the molecules of sample and creates a scattered light [18].

The scattered light has a different frequency from that of incident light (inelastic scattering) is used to construct a Raman spectrum. Since the vibrational energy spectrum of a sample is influenced by its chemical composition, the Raman spectrum provides a specific chemical fingerprint of the sample. A Raman spectrum is presented as an intensity-versus wavelength shift [20]. A typical schematic diagram of modern Raman spectrometer is shown in Figure 3.3.

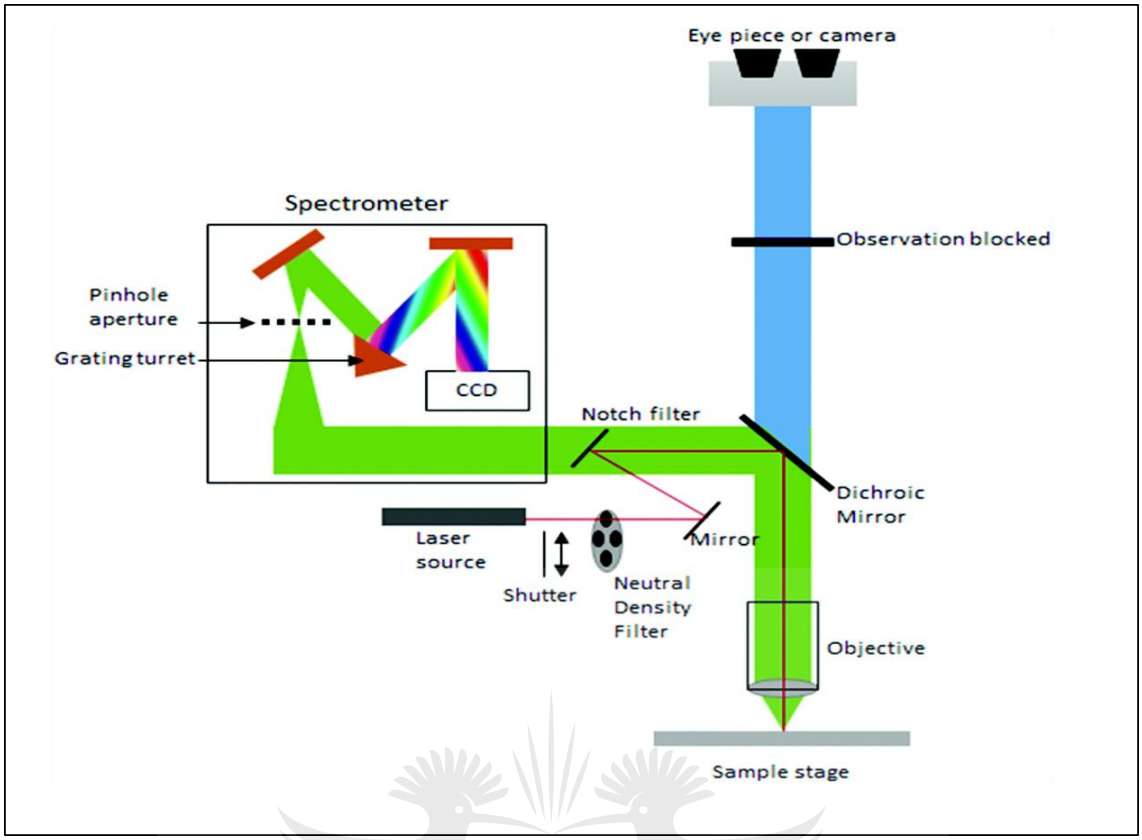

Figure 3.3: Schematic-illustration-of a Raman spectrometer [21].

Raman spectra reported in this study were recorded using WITec Confocal Raman Microscope and a laser beam was focused onto the sample using 50 X magnification lenses. A laser power of 5% was used to avoid possible degradation of the sample. Data was collected and processed using WITec Control scanning and data acquisition software.

3.1.3 X-ray diffraction (XRD)

XRD technique is widely used for phase identification in crystalline materials [22]. The technique can be used to distinguish between amorphous and crystalline materials [23]. The analysis is based on the constructive interference of X-rays and a sample under analysis [24]. The X-rays are generated by a cathode X-ray tube and then directed to a sample by a monochromator. The interaction of the incident

rays with the sample produces constructive inference and diffracted rays when conditions satisfy Bragg's Law ($n\lambda=2d \sin \theta$). The angle of diffraction (θ) is related to the interplanar spacing, d. The angles at which the collimated beam of X-rays are diffracted are measured [25]. In a crystalline solid, atoms are arranged in a periodic ordered manner. The X-ray diffraction patterns generated for a crystalline material provides a unique fingerprint of the crystals present in the sample that are characteristic of the sample. The diffraction patterns at different intensities at specific angles of diffraction produce a specific pattern that is unique to a crystal structure [24]. This periodicity is used to determine the crystallographic structure from an XRD analysis.

In addition, to the determination of crystal structure of these materials, XRD can be utilized to determine crystal sizes, Miller indices, and charge distribution around atoms of crystalline materials such nanomaterials [25]. A typical schematic illustration of an XRD is given in Figure 3.4.

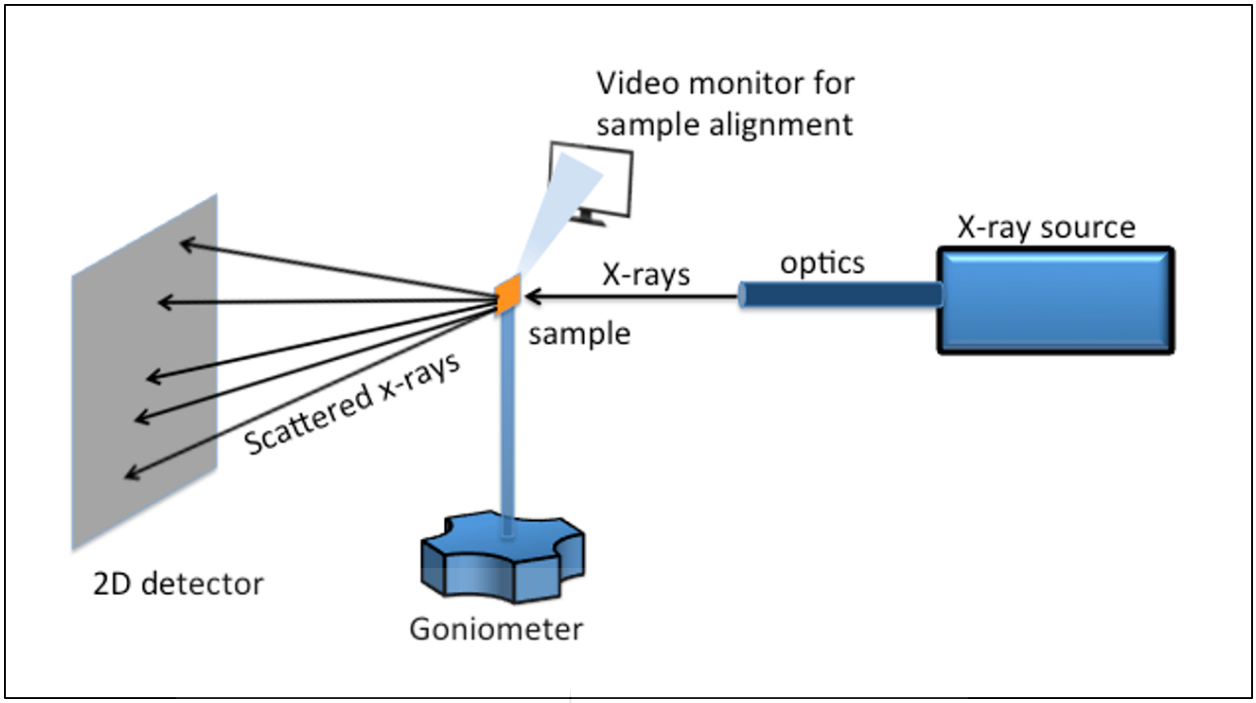

Figure 3. 4: Schematic-illustration-of an X- ray diffractometer [26].

Samples used in this project were analyzed using a Philips, X"Pert PRO MPD X-ray diffractometer that was operated at 40 kV and 40 mA. The instrument uses an X-Ray source of Cu α- radiation beam with an excitation wavelength of 0.15406 nm for the analysis. Data analysis was performed using X"pert Data Collector software.

3.1.1.1 Crystalline phases

The crystalline phases (D) were estimated by using the the Scherrer equation: [27]

$$D = \frac{k\,\lambda}{\beta\,Cos\,\theta} \qquad 3.1$$

Where:

D is the average size in nanometers

k = 0.89

λ = 0.1540 nm (Cu Kα)

β = FWHM x 0.01745 in radians and θ is the peak position.

3.1.4 Ultraviolet–visible (UV) spectroscopy

UV spectroscopy is a technique that can be used for quantitative and qualitative analysis purposes by measuring the absorbance of ultraviolet or visible light by a sample [28]. The UV range covered is from 190-400 nm whilst the visible region is from 400-800 nm [29]. The UV and visible radiation is produced from a light source, which is made up of a combination of tungsten and halogen, or from deuterium lamps. The light is directed onto a diffracting grating, which will split the incoming light into its component colors of different wavelengths. Liquid samples are held in cuvettes or cells, which are optically flat and transparent. Most modern UV spectrometers have two sample holders accommodating a reference solution (blank) and the sample solution.

The intensity of light passing through the reference cell and the sample cell is measured and recorded by a light detector. The absorbance recorded is related to Beer`s law which states that the absorbance (A) is related to the incident intensity (I_o), transmitted light intensity I, concentration of liquid sample (c), path length of the sample (l), absorption coefficient, α and molar absorptivity ε by the Equation 3.2 [30].

$$A = \log\frac{l_o}{l} = -\log T = \alpha C = \varepsilon l C \qquad 3.2$$

where:

T is the transmittance, defined as $I/I_{o,}$ A is the absorbance

l is the optical path length,

C is the concentration in mol dm^{-3}

ε is molar extinction constant.

3.1.4.1 Diffuse reflectance measurement

Diffuse reflectance is a technique for studying the spectral characteristics of opaque solid samples. The principle used for diffuse reflectance is based on the fact that an incident light beam on a powdered sample, is reflected in all directions. Due to the different shapes in powdered samples, it is reflected in different directions. The remaining light is refracted as it penetrates the powders. Due to reflection from the surface of other powders, repeated refraction entry into powders and internal reflections the light is scattered. Some of the scattered light is emitted back in air. The diffuse reflected light becomes weaker if absorption by the powder occurs during reflection or if it passes through the powder. This results in a diffuse reflected spectrum. Figure 3.5 shows a schematic diagram of light scattering from a powdered sample.

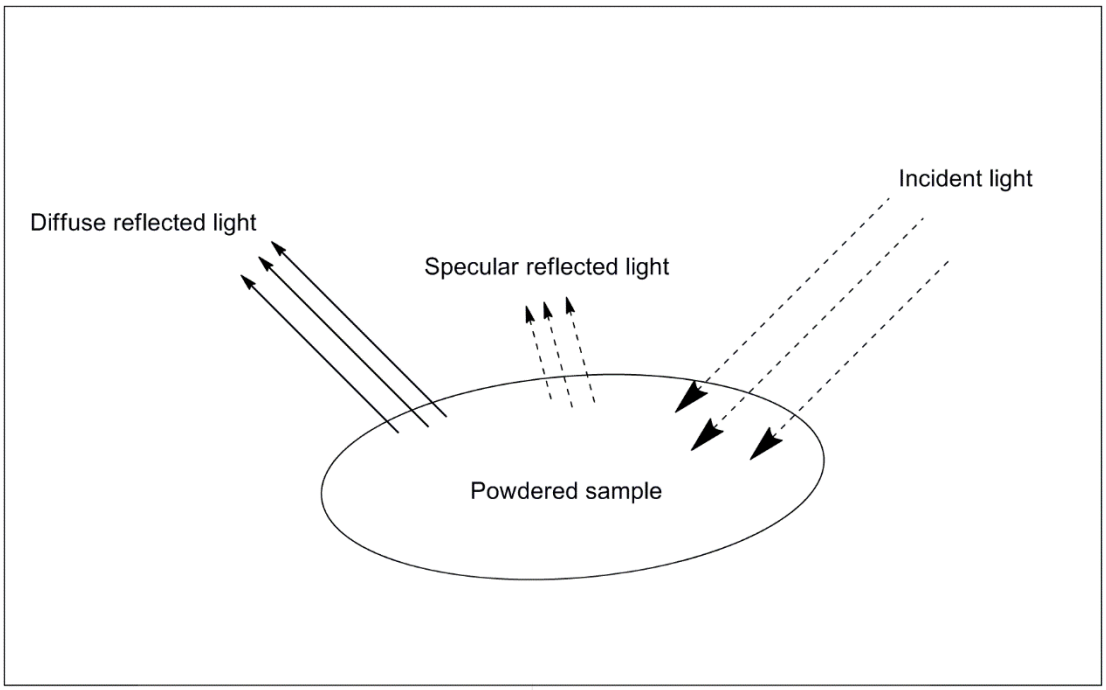

Figure 3. 5: Schematic diagram of light scattering from a powdered sample.

In diffuse reflectance spectroscopy, a sample may be diluted with an alkali halide such as KCl or KBr, therefore, the background spectrum of the used alkali halide should be taken first to remove interference due to it [31].

For finely ground powders, the Kubelka-Munk theory predicts a linear relationship between the absorption coefficient and the value of the factored spectrum [31]. This allows the diffuse reflectance to be used as a quantitative tool [32]. The percentage diffuse reflectance data can be manipulated to Kubelka-Munk units for an infinitely thick layer by using the Kubelka-Munk algorithm according to the Equation 3.3: [32]

$$K = \frac{(1-R)^2}{2R} = F(R) \qquad 3.3$$

where:

K= reflectance transformed according to Kubelka-Munk

R is percentage reflectance

F(R) is the remission or the Kubelka-Munk function.

The band gap E_g and the absorption coefficient, α are expressed in an Equation 3.4 as:[33]

$$\alpha hv = A(hv - E_g)^n \qquad 3.4$$

where:

α is the absorption coefficient

hv is the energy of light

A is a constant

E_g is the band gap and

n is a constant depending on the nature of the band gap transition mode.

The value of n is 2 for indirect allowed transition or $\frac{1}{2}$ for direct allowed transitions [34]. The value of n can be $\frac{3}{2}$ for a direct forbidden transition or 3 for indirect forbidden transition. TiO_2 has an indirect allowed transition, therefore, the value of n is 2 [34]. However due to doping the value of n may vary slightly.

The material band gap can be determined from the absorption coefficient. For crystalline materials Equation, 3.4 can be rearranged as [35]

$$[F(R)hv)]^{1/n} = A(hv - E_g\ )^n \qquad 3.5$$

The band gap of materials can be deduced from the Tauc`s plot, which is a plot of $[F(R)x\ hv]^n$ vs photon energy. The value of n depends on the specific transitions of the material [35].

Optical properties for this project were investigated using a 1800 UV-Vis spectrophotometer (Massachusetts, USA) equipped with a IRS 240A integrating sphere and a $BaSO_4$ was used as a reflectance standard.

3.1.5 Brunauer-Emmett-Teller (BET)

BET analysis provides the specific surface area, pore size distribution and the pore volume of a sample [36]. This information is used to predict the performance of materials in adsorption and catalytic reactions as they are proportional to the surface area [36]. In BET analysis, the samples are dried with nitrogen or by purging in a vacuum at elevated temperatures. The volume of gas adsorbed to the surface of the sample particles is measured at the boiling point of nitrogen (-196°C) [37]. The surface area of the particles is measured by correlating the amount of adsorbed gas to the total surface area of the particles including pores in the surface according to the BET theory [38]. Figure 3.6 shows a typical BET instrument schematic diagram.

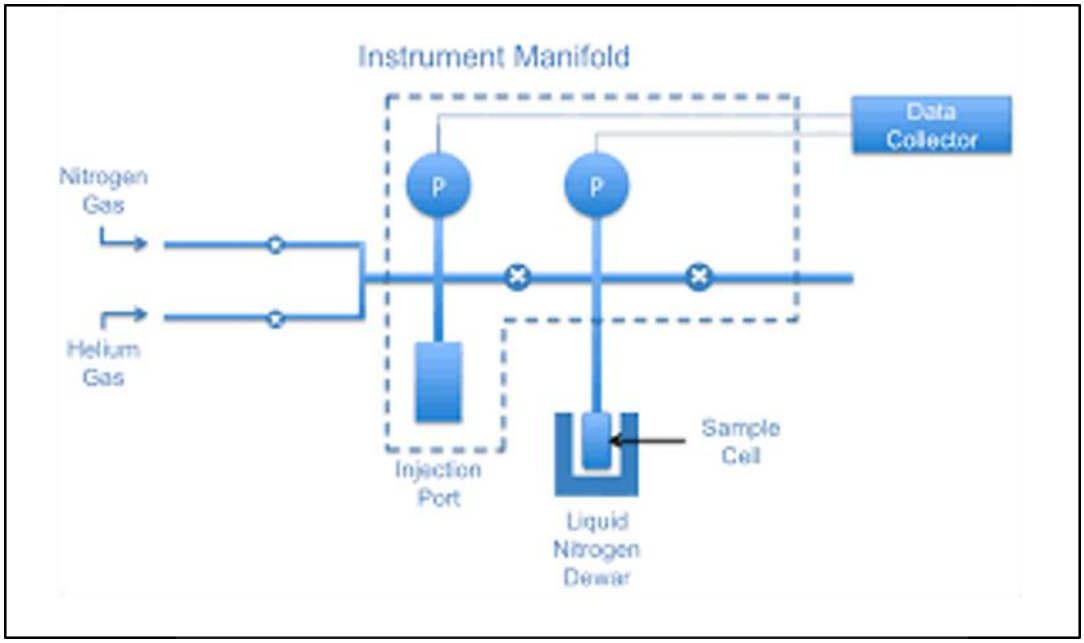

Figure 3. 6: Schematic-illustration-of a BET instrument [39].

The porosity shows the total fraction of void space within a sample. The BET analysis for this project was carried out using a Micromeritics ASAP 2020 surface area and porosity analyzer (Norcross, USA). A sample weight of between 200-300 mg was degassed at 110°C for 6 h under vacuum. Nitrogen gas was used as the probe gas.

3.1.6 Scanning electron microscopy (SEM)

SEM analysis is used to give information about the morphology of a sample. In SEM analysis, an electron beam illuminates a sample and obtains a magnified image of a sample`s surface. The electron beam is produced from a tungsten filament, which produces electrons after application of voltage [40]. This beam of electrons passes through a vacuum and an electromagnetic field. The beam is then focused on a sample by lenses. Once the electrons reach the sample, they lose energy by repeated random scattering and absorption within the interaction volume [25]. The energy interactions between the electron beam and the sample results in reflection

of high-energy electrons by elastic scattering, emission of secondary electrons by inelastic scattering and the emission of electromagnetic radiation [25]. A typical SEM instrument is shown in Figure 3.7.

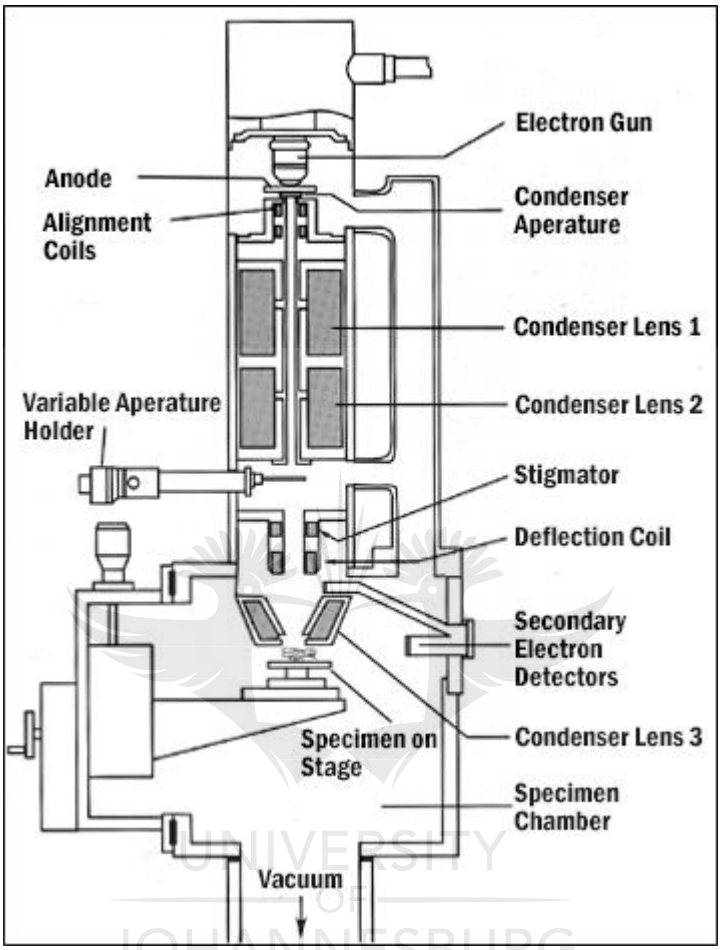

Figure 3. 7: Schematic-illustration-of a SEM instrument.

Source: (https://cmrf.research.uiowa.edu/scanning-electron-microscopy).

These reflections result in signals, which are sent to the detector. Some of the beam of electrons are absorbed by the sample and can be detected by a detector. Some of the beam is scattered. The backscattered, secondary electrons are collected by a detector and converted into a signal that is sent to a screen producing an image [25]. A VEGA3 TESCAN (Bruno, Czech Republic) scanning electron microscope was used for SEM and electron dispersive x-ray spectroscopy analysis.

3.1.6.1 Energy dispersive X-ray spectroscopy (EDS)

SEM analysis can be used in conjunction with detectors such as EDS and wavelength dispersive X-ray spectroscopy (WDS) in order to determine the elemental composition of a sample [25]. The EDS technique can be used for chemical characterization of a sample in conjunction with scanning electron microscopy and transmission electron microscopy. The backscattered electron images in SEM show compositional contrast results from the different elements in the sample and their distribution. EDS allows for the identification of these elements and their relative proportions [25]. A VEGA3 TESCAN (Bruno, Czech Republic) scanning electron microscope was used for SEM and electron dispersive x-ray spectroscopy analysis.

3.1.7 Transmission electron microscopy (TEM)

This is a technique used to obtain in-depth information about the morphology of a sample [41]. In TEM analysis, a collimated beam of electrons is passed through a sample and interacts with it as it passes through it. The high-energy electrons can scatter or backscatter elastically or in-elastically, producing X-rays after their interactions with the sample [42]. The X-ray energy is equal to a difference between two energy levels of the electron cloud of the atom. Since the difference between these energy levels are quantified, the X-ray energy spectrum, which is generated, represents the signature of the atom [42]. An image is formed from the interaction of the electrons transmitted through the sample and then magnified and focused onto an imaging device, and detected by a sensor such as a CCD camera.

In addition, TEM allows for the generation of diffraction patterns of materials, therefore, the crystallography can be determined [43]. Due to the high resolution

power of TEM, the technique can be used to determine materials, particle sizes, shape, growth patterns/ orientation, detection of defects as well as the elemental composition [41, 43]. A generalized schematic illustration of a TEM instrument is shown in Figure 3.8.

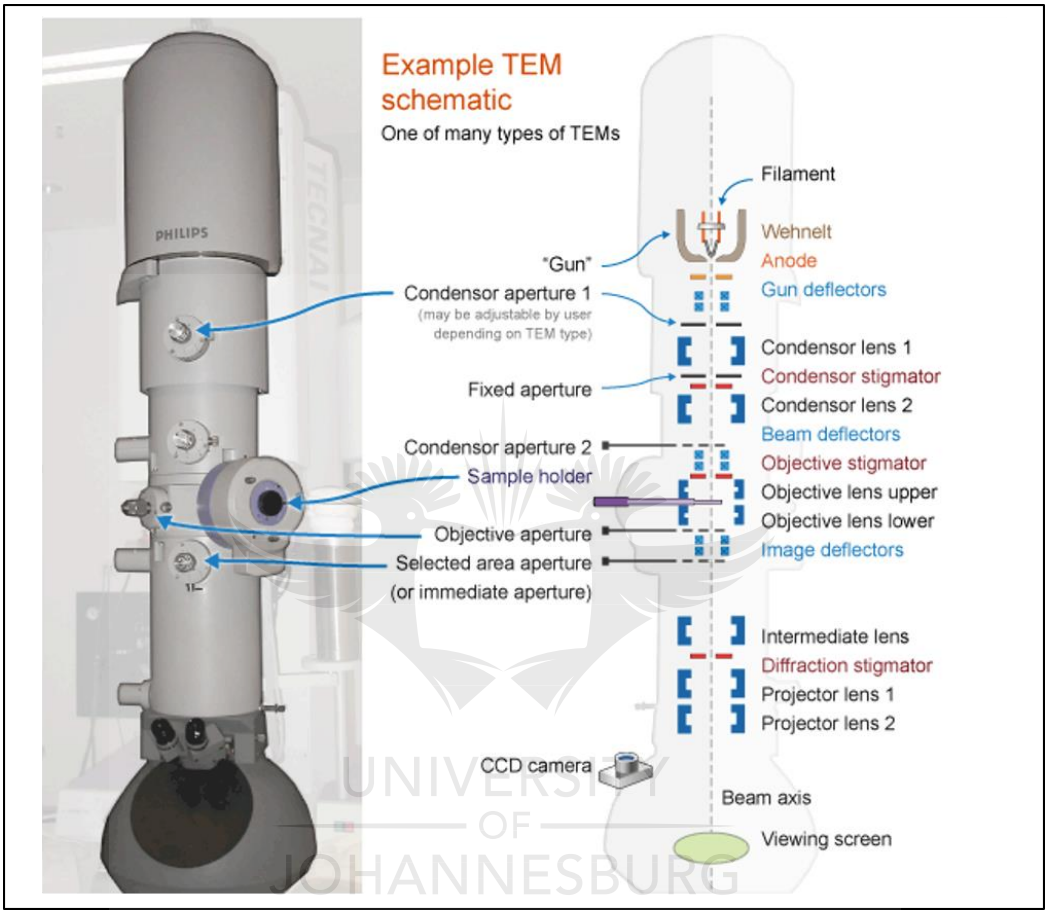

Figure 3. 8: A generalized schematic-illustration-of a TEM instrument.

Source: (https://myscope.training/legacy/tem/introduction/).

A JEOL JEM-2100 TEM electron microscope (Peabody, Massachusetts, USA) was used for in-depth analysis of the morphology of materials. Images were collected on Gaitan Digital Imaging software. The sample were prepared for TEM analysis by sonicating in ethanol for 10 mins and then depositing small drops of the material suspension a coated copper grids. The copper grids were allowed to dry in air before mounting on in the instrument for analysis.

3.1.8 X-ray photoelectron spectroscopy (XPS)

X-ray photoelectron spectroscopy (XPS) is a nondestructive method for studying the electronic structure of atoms, molecules, and solids [44]. XPS involves the irradiation of a sample with monochromatic low energy X-rays detaching electrons from atoms, molecules or solids [45]. The absorption of high energy X-rays results in ionization of an electron level. An electrostatic analyzer is used to determine the energy spectrum of electrons. The momentum and energy of the photoelectrons give direct information on the electronic structure of material, from which they were excited [44]. The binding energy of each core-level electron is unique to the atom and the specific orbital it belongs to [46]. The kinetic energy of a core level photoelectron can be related to its characteristic binding energy since the energy of the incident X-rays will be known [46]. Figure 3.9 shows a typical XPS instrument.

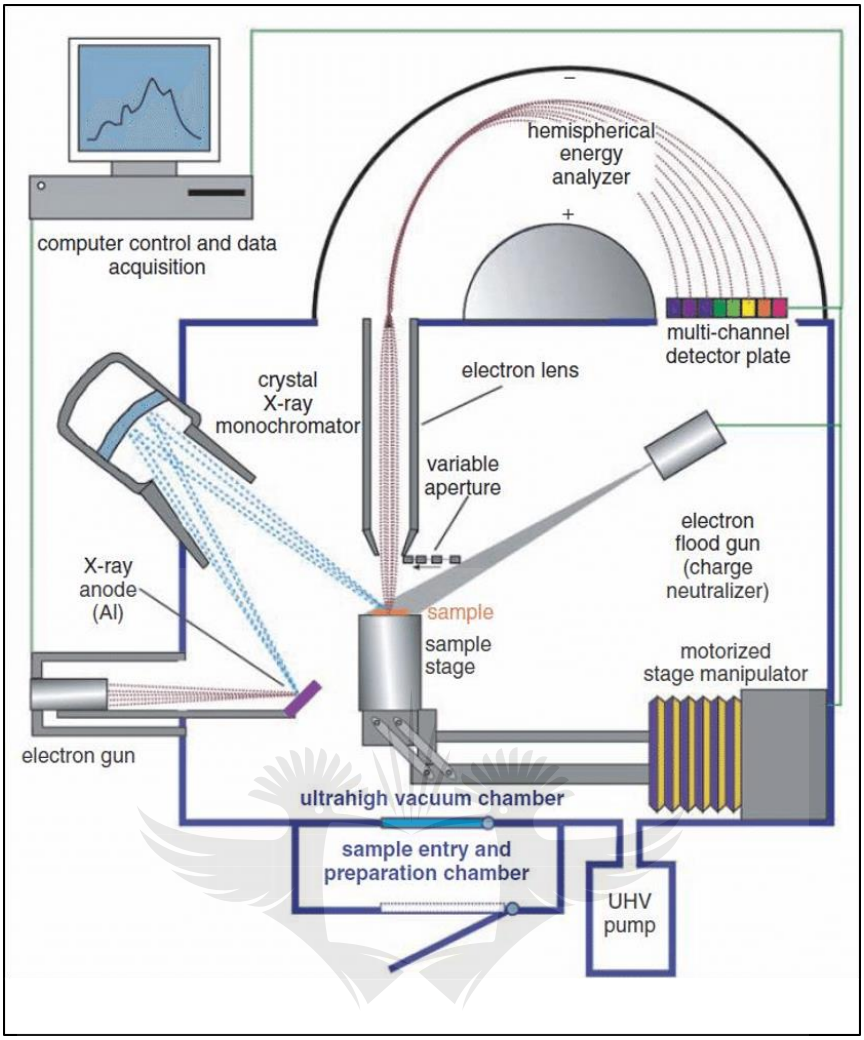

Figure 3. 9: Schematic-illustration-of XPS instrument [47].

XPS is widely used for elemental identification and it provides chemical information about materials. In this project, XPS analysis was performed using a Physical Electronics (PHI) Quantum 200 XPS spectrophotometer with Al Kα as the excitation source.

3.1.9 Thermogravimetric analysis (TGA)

TGA is a thermal characterization technique that measures changes in weight in a sample as a function of temperature (ºC) over time and atmosphere [48]. A TGA instrument comprises of a sample pan that is supported by a precision balance. The

sample pan is accommodated in a furnace and is heated or cooled during the experiment. The mass of the sample is monitored progressively during the analysis [49]. A gas is used to purge the sample pan environment in order to control it. An unreactive or a reactive gas is usually passed over the sample and is purged out through an exhaust. TGA can quantify loss of water, loss of solvent, loss of additives, decomposition, and percentage ash content [48]. Figure 3.10 shows a schematic illustration of a TGA instrument.

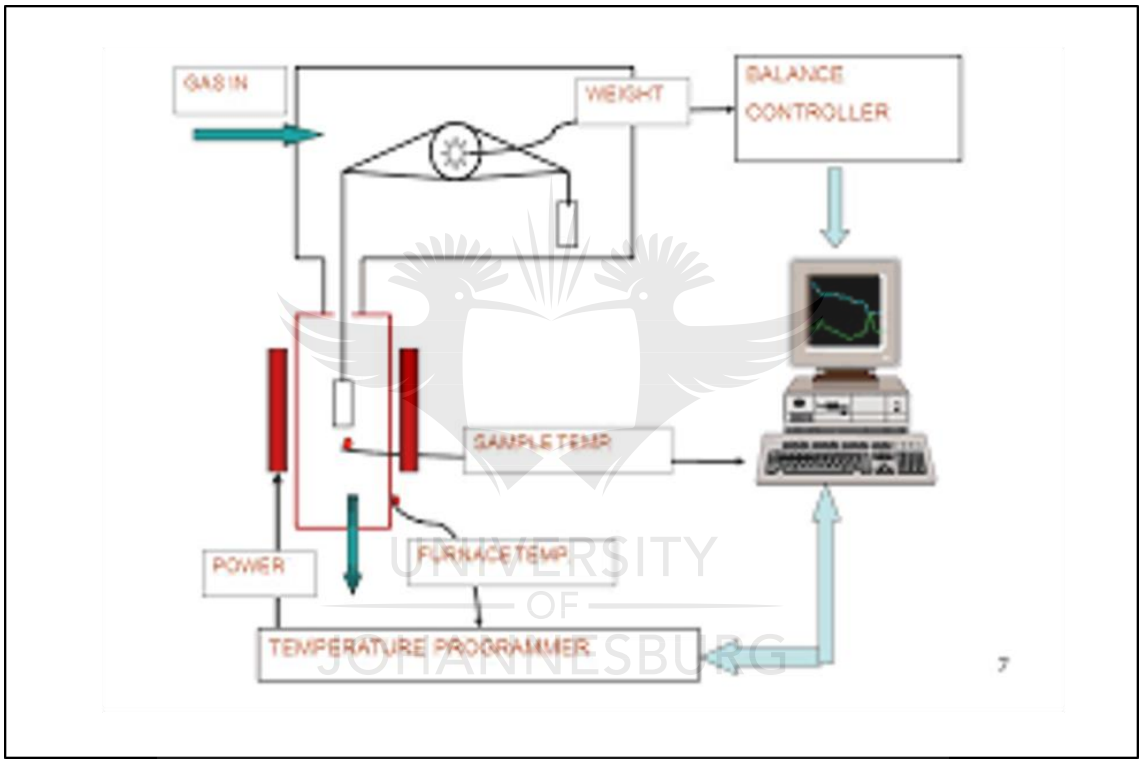

Figure 3. 10: Schematic-illustration-of TGA instrument.

Source: https://slideplayer.com/slide/9234657/

Thermal profiling of materials used in this study was done by a using a STA 7200RV HITACHI thermogravimetric analyzer.

3.1.10 Photoluminescence spectroscopy (PL)

This is a nondestructive technique for probing the electronic structure of materials [50]. In a typical analysis, light is directed onto a sample and the sample absorbs it resulting in the excitation of molecules and atoms of the material in a process called photo-excitation [50]. The absorbed energy is lost over time as emitted light (luminescence) and the process is known as photoluminescence. The amount of the emitted light is related to the relative contribution of the radiative process [50]. Photoluminescence has been reported to be useful in the analysis of alloys to detect inhomogeneity and variations in impurity concentration [51]. Figure 3.11 shows a typical schematic illustration of a PL spectrometer.

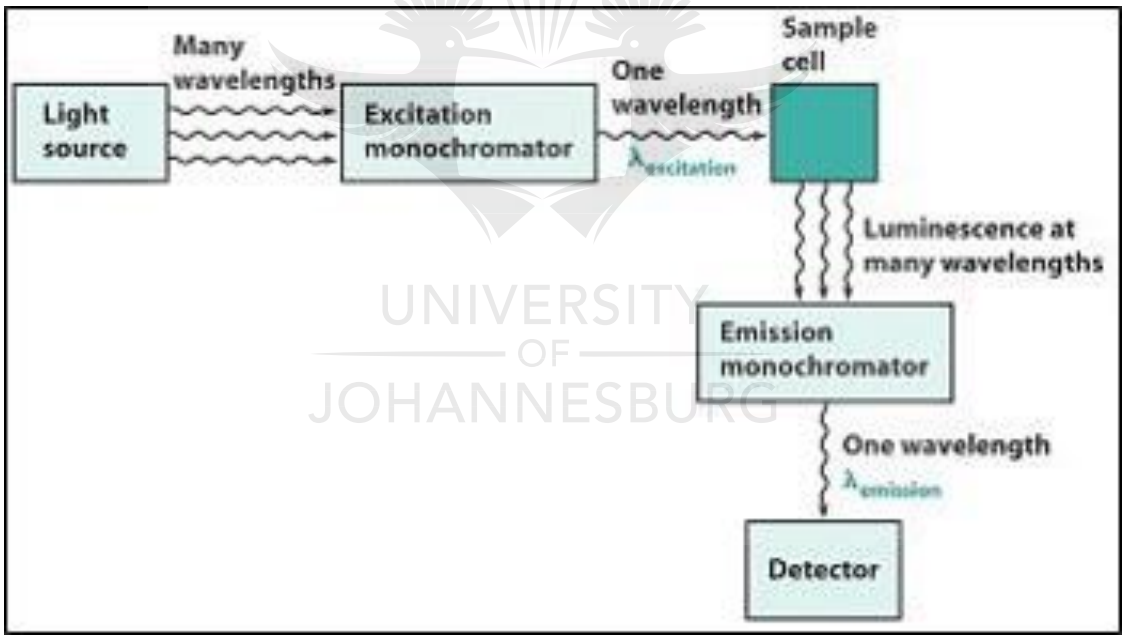

Figure 3. 11: Schematic-illustration-of PL spectrometer [52].

In this study, photoluminescence measurements were performed using a Perkin Elmer LS45 Fluorescence Spectrometer.

3.2 Photodegradation experiments

The photocatalytic experiments were conducted in a reactor under irradiation of either ultra-violet radiation or visible radiation lamp. Two sources of radiation were used; a 150 W tungsten filament lamp and a 500 W Xenon filament lamp. The power output was set at 300 W from the power supply. The photocatalysts were suspended in the analyte solution and the mixture was magnetically stirred continuously during the degradation experiments. Figure 3.12 shows a schematic diagram of the photodegradation experiments used for this work. Quantification of the analytes was performed using an Agilent high-performance liquid chromatography (HPLC) and the degradation products were conducted using a Shimadzu UHPLC-MS/MS 8030 instrument (Tokyo, Japan).

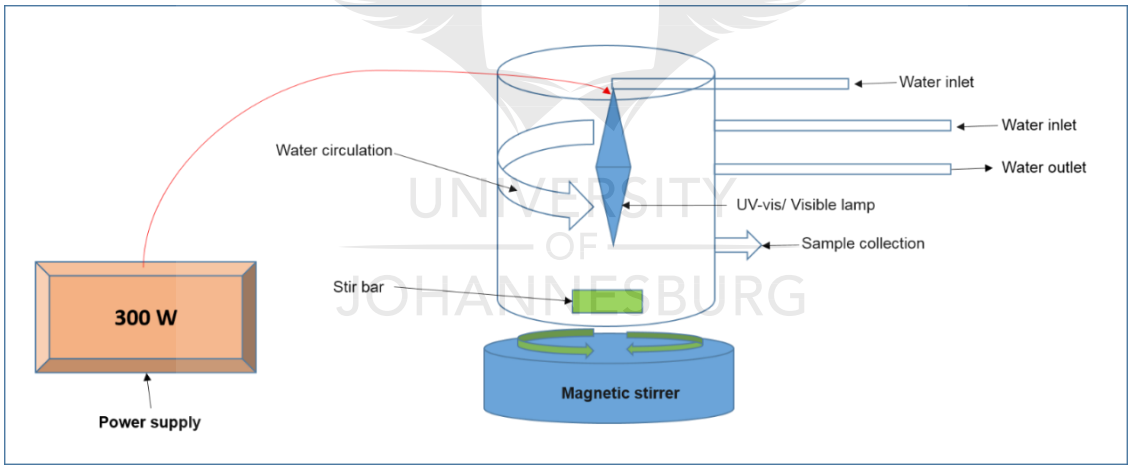

Figure 3. 12: Schematic diagram of photodegradation experiments.

3.2.1 High-performance liquid chromatography (HPLC)

High performance liquid chromatography (HPLC) is a technique used to separate mixtures of substances into individual chemical components based on their molecular structure and molecular composition [53]. Unlike in basic column chromatography, the mobile phase in HPLC technique is forced through the system

at high pressure of up to 400 atmospheres [54, 55]. The mobile phase is forced through a stationary phase and carries the components of the mixture with it. The components are separated according to their interactions with the stationary phase and the mobile phase. Sample components that interact strongly with the stationary phase will move more slowly through the column compared to components with weaker interactions [56, 57]. This difference in the rate of interaction influences the separation of various components.

HPLC can be classified into normal phase, reverse phase, size exclusion and ion exchange depending on the stationary phase [54, 58-60]. In normal phase, HPLC components are separated based on polarity. The stationary phase is made of polar materials such as silica and non-polar mobile phase such as methylene chloride and chloroform. Reverse phase HPLC system uses hydrophobic stationary phases and polar mobile phases such as water, methanol, and acetonitrile [54]. Due to hydrophobic interactions, non-polar components are retained longer in the stationary phase. Size exclusion separates components based on their molecular size [60]. The stationary phase in size exclusion is packed with material having precisely controlled pore sizes. This results in large components washing fast through the column and small components penetrating the pores of the stationary phase and eluting later.

Ion exchange HPLC systems have charged stationary phases, which have an opposite charge to the analyte sample [59]. The stronger the interaction between the analyte and the stationary phase, the longer the analyte is retained in the column. Aqueous buffers are used as mobile phases and both pH and ionic strength are used to control the elution time. HPLC systems commonly use ultraviolet,

fluorescence, mass-spectrometer and electrochemical detectors [61-63]. Figure 3.12 shows a typical schematic illustration of an HPLC instrument.

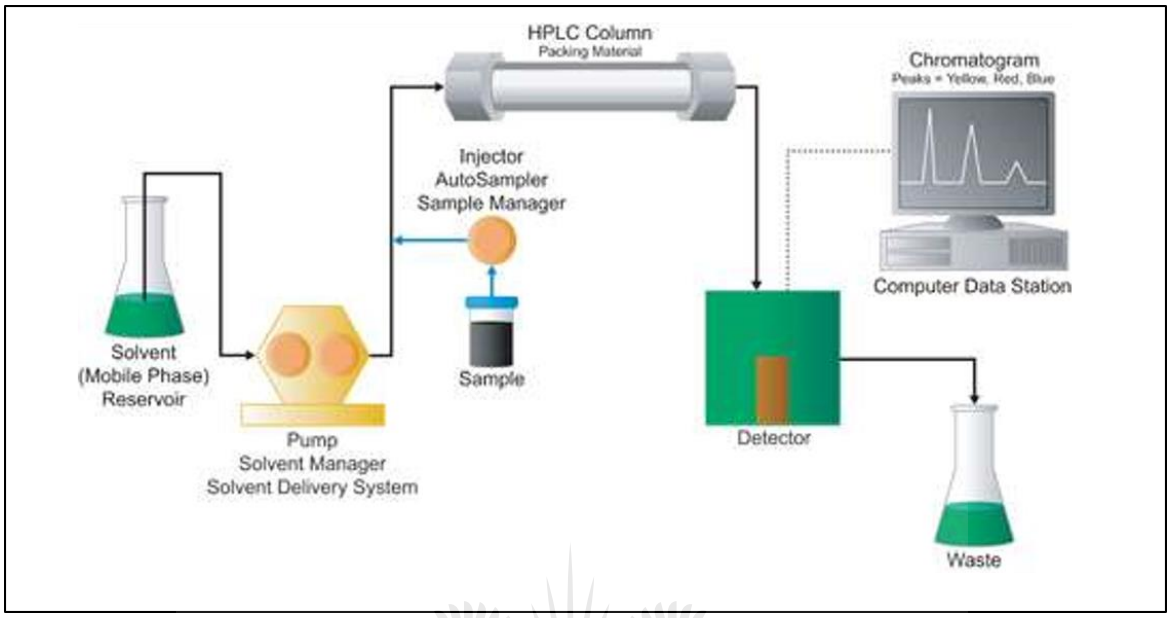

Figure 3. 13: Schematic-illustration-of HPLC instrument.

Source: (http://www.waters.com/waters).

3.2.2 Liquid chromatography-mass spectrometry (LC-MS)

This technique couples liquid chromatography with mass spectrometry. In this technique, individual components of a mixture are first separated by liquid chromatography and channeled into a mass spectrometer where the components are ionized and the ions are separated based on their mass/charge ratio [64]. The separated ions are channeled to a photo or electron multiplier tube detector, which then identifies and quantifies each ion [65]. Different ion sources are used such as Electronspray Ionization (ESI), and Atmospheric Pressure Chemical Ionization (APCI) [64, 66]. The choice of ion source is influenced by the chemical nature of the components i.e. polar or non-polar [66].

3.3 REFERENCES

[1] S. Feng, L. Guanghua, Chapter 4 - Hydrothermal and solvothermal syntheses, in R. Xu, W. Pang, Q. Huo (Eds.) Modern Inorganic Synthetic Chemistry*, Elsevier*, Amsterdam, 2011, pp. 63-95.

[2] G. Gadea, A. Morata, A. Tarancon, Chapter five - Semiconductor nanowires for thermoelectric generation, in S. Mokkapati, C. Jagadish (Eds.), Semiconductors and Semimetals*, Elsevier 2*018, pp. 321-407.

[3] N. Ye, T. Yan, Z. Jiang, W. Wu, T. Fang, A review: Conventional and supercritical hydro/solvothermal synthesis of ultrafine particles as cathode in lithium battery, *Ceramics International,* 44 (2018) 4521-4537.

[4] H. Hayashi, Y. Hakuta, Hydrothermal synthesis of metal oxide nanoparticles in supercritical water, *Journal of Materials*, 3 (2010) 3794-3817.

[5] H. Hayashi, T. Noguchi, N.M. Islam, Y. Hakuta, Y. Imai, N. Ueno, Hydrothermal synthesis of $BaTiO_3$ nanoparticles using a supercritical continuous flow reaction system, *Journal of Crystal Growth*, 312 (2010) 1968-1972.

[6] S. Zanganeh, A. Kajbafvala, N. Zanganeh, R. Molaei, M.R. Bayati, H.R. Zargar, S.K. Sadrnezhaad, Hydrothermal synthesis and characterization of TiO_2 nanostructures using LiOH as a solvent, *Advanced Powder Technology*, 22 (2011) 336-339.

[7] S. Obregón, A. Caballero, G. Colón, Hydrothermal synthesis of $BiVO_4$: Structural and morphological influence on the photocatalytic activity, *Applied Catalysis B: Environmental,* 117-118 (2012) 59-66.

[8] J. Yu, X. Liu, Hydrothermal synthesis and characterization of $LiNbO_3$ crystal, *Materials Letters*, 61 (2007) 355-358.

[9] J.J. Shah, K. Mohanraj, Comparison of conventional and microwave-assisted synthesis of benzotriazole derivatives, *Indian Journal of Pharmaceutical Sciences,* 76 (2014) 46-53.

[10] V. Santagada, F. Frecentese, E. Perissutti, F. Fiorino, B. Severino, G. Caliendo, Microwave assisted synthesis: A new technology in drug discovery, *Mini-Reviews in Medicinal Chemistry*, 9 (2009) 340-358.

[11] J. Anwar, U. Shafique, Z. Waheed uz, R. Rehman, M. Salman, A. Dar, J.M. Anzano, U. Ashraf, S. Ashraf, Microwave chemistry: Effect of ions on dielectric heating in microwave ovens, *Arabian Journal of Chemistry*, 8 (2015) 100-104.

[12] S.C. Motshekga, S.K. Pillai, S. Sinha Ray, K. Jalama, R.W.M. Krause, Recent trends in the microwave-assisted synthesis of metal oxide nanoparticles supported on carbon nanotubes and their applications, *Journal of Nanomaterials,* 2012 (2012) 15.

[13] D. Dallinger, C.O. Kappe, Microwave-assisted synthesis in water as solvent, *Chemical Reviews*, 107 (2007) 2563-2591.

[14] M. Hasanpoor, M. Aliofkhazraei, H. Delavari, Microwave-assisted synthesis of zinc oxide nanoparticles, *Procedia Materials Science*, 11 (2015) 320-325.

[15] V. Chikan, J.E. McLaurin, Rapid nanoparticle synthesis by magnetic and microwave heating, *Nanomaterials*, 6 (2016) 85-94.

[16] A.A. Ismail, F.R. van de Voort, J. Sedman, Chapter 4 Fourier transform infrared spectroscopy: Principles and applications, J.R.J. Paré, J.M.R. Bélanger (Eds.) Techniques and Instrumentation in Analytical Chemistry, *Elsevier* 1997, pp. 93-139.

[17] R.M. Amir, F.M. Anjum, M.I. Khan, M.R. Khan, I. Pasha, M. Nadeem, Application of Fourier transform infrared (FTIR) spectroscopy for the identification of wheat varieties, *Journal of Food Science and Technology,* 50 (2013) 1018-1023.

[18] A.S. Gilbert, Vibrational, rotational and Raman spectrocopy, historical perspective*, in J.C. Lindon (Ed.) Encyclopedia of Spectroscopy and Spectrometry (Second Edition), *Academic Press*, Oxford, 1999, pp. 2938-2948.

[19] T. Theophanides, Introduction to infrared spectroscopy, Chapter 1, Materials Science Engineering, *Intech* (2012) pp 1-10.

[20] G.S. Bumbrah, R.M. Sharma, Raman spectroscopy – Basic principle, instrumentation and selected applications for the characterization of drugs of abuse, *Egyptian Journal of Forensic Sciences*, 6 (2016) 209-215.

[21] R. Smith, K.L. Wright, L. Ashton, Raman spectroscopy: an evolving technique for live cell studies, Analyst, 141 (2016) 3590-3600.

[22] D. Giomi, F.M. Cordero, F. Machetti, Isoxazoles, in A.R. Katritzky, C.A. Ramsden, E.F.V. Scriven, R.J.K. Taylor (Eds.) Comprehensive Heterocyclic Chemistry III, *Elsevier*, Oxford, 2008, pp. 365-485.

[23] T.Y. Inan, Thermoplastic-based nanoblends: Preparation and characterizations, in P.M. Visakh, G. Markovic, D. Pasquini (Eds.) Recent Developments in Polymer Macro, Micro and Nano Blends, Woodhead Publishing 2017, pp. 17-56.

[24] R.E. Dinnebier, S.J.L. Billinge, Chapter 1- Principles of powder diffraction, Powder Diffraction: Theory and Practice, *The Royal Society of Chemistry* 2008, pp. 1-19.

[25] H.C.d. Castillo, D. Strivay*, Chapter 3 X-Ray Methods, Analytical Archaeometry: Selected Topics, *The Royal Society of Chemistry* 2012, pp. 59-113.

[26] B.B. He, U. Preckwinkel, K.L. Smith, Fundamentals of two-dimensional X-ray diffraction (XRD2), *Advances in X-ray Analysis*, 43 (2000) 273-280.

[27] I. Tamura, Y. Yasuda, K.I. Kagota, S. Yoneda, N. Nakada, V. Kumar, Y. Kameda, K. Kimura, N. Tatarazako, H. Yamamoto, Contribution of pharmaceuticals and personal care products (PPCPs) to whole toxicity of water samples collected in effluent-dominated urban streams, *Ecotoxicology and Environmental Safety*, 144 (2017) 338-350.

[28] S. El-Malla, A. Kamal, S. Hammad, A review on UV spectrophotometric methods for simultaneous multicomponent analysis,*European Journal of Pharmaceutical and Medical Research* 3 (2016) 348-360.

[29] J. Yu, H. Wang, J. Zhan, W. Huang, Review of recent UV–Vis and infrared spectroscopy researches on wine detection and discrimination, *Applied Spectroscopy Reviews*, 53 (2018) 65-86.

[30] A.R. Hawkins, H. Schmidt, Handbook of optofluidics, *CRC Press*, First Edition (2010) pp 680 .

[31] H.G. Brittain, S.J. Bogdanowich, D.E. Bugay, J. DeVincentis, G. Lewen, A.W. Newman, Physical Characterization of Pharmaceutical Solids, *Pharmaceutical Research,* 8 (1991) 963-973.

[32] L. Yang, B. Kruse, Revised Kubelka–Munk theory. I. Theory and application, *Journal of the Optical Society of America A,* 21 (2004) 1933-1941.

[33] A. Sáenz-Trevizo, P. Amézaga-Madrid, P. Pizá-Ruiz, W. Antúnez-Flores, M. Miki-Yoshida, Optical band gap estimation of ZnO nanorods*, Materials Research*, 19 (2016) 33-38.

[34] F.A. Mir, Transparent wide band gap crystals follow indirect allowed transition and bipolaron hopping mechanism, *Results in Physics*, 4 (2014) 103-104.

[35] D.A. Zimnyakov, A.V. Sevrugin, S.A. Yuvchenko, F.S. Fedorov, E.V. Tretyachenko, M.A. Vikulova, D.S. Kovaleva, E.Y. Krugova, A.V. Gorokhovsky,

Data on energy-band-gap characteristics of composite nanoparticles obtained by modification of the amorphous potassium polytitanate in aqueous solutions of transition metal salts, *Data in Brief*, 7 (2016) 1383-1388.

[36] S. Lowell, J.E. Shields, M.A. Thomas, M. Thommes, Surface area analysis from the Langmuir and BET theories, in S. Lowell, J.E. Shields, M.A. Thomas, M. Thommes (Eds.) Characterization of Porous Solids and Powders: Surface Area, Pore Size and Density, *Springer*, Netherlands, Dordrecht, 2004, pp. 58-81.

[37] J. Brame, C. Griggs, Surface Area Analysis Using the Brunauer-Emmett-Teller (BET) Method: Standard Operating Procedure Series: SOP-C, *US Army Engineer Research and Development Center-Environmental Laboratory* Vicksburg United States, 2016.

[38] V. Vendange, P. Colomban, Determination of the hydroxyl content in gels and porous “glasses” from alkoxide hydrolysis by combined TGA and BET analysis, *Journal of Porous Materials*, 3 (1996) 193-200.

[39] N. Hwang, A.R. Barron, BET surface area analysis of nanoparticles, The Connexions Project, (2011) 1-11.

[40] W. Nixon, The general principles of scanning electron microscopy, Philosophical Transactions of the Royal Society of London Series B, Biological sviences. *The Royal Society of Chemistry* 261 (1971) 45-50.

[41] Y. Shen, X. Yang, Y. Wang, Y. Zhang, H. Zhu, L. Gao, M. Jia, The states of gold species in CeO_2 supported gold catalyst for formaldehyde oxidation, *Applied Catalysis B: Environmental*, 79 (2008) 142-148.

[42] M. Bobji, A. Hansdah, I.O. Toppo, Material characterisation technique “Transmission Electron Microscope” *Journal of Materials Reviews*14(1999) 2259-2268.

[43] C.J. Kiely, R.C. Pond, G. Kenshole, A. Rockett, A TEM study of the crystallography and defect structures of single crystal and polycrystalline copper indium diselenide, *Philosophical Magazine A*, 63 (1991) 1249-1273.

[44] C.S. Fadley, X-ray photoelectron spectroscopy: Progress and perspectives, *Journal of Electron Spectroscopy and Related Phenomena*, 178-179 (2010) 2-32.

[45] T. Fujikawa, 'Reprint of' new developments in theory of X-ray photoemission from solids, *Journal of Electron Spectroscopy and Related Phenomena*, 178-179 (2010) 33-60.

[46] P.M. Claesson, A. van der Wal, A. Fogden, New techniques for optimization of particulate cleaning, in I. Johansson, P. Somasundaran (Eds.) Handbook for Cleaning/Decontamination of Surfaces, *Elsevier Science B*.V., Amsterdam, 2007, pp. 885-927.

[47] M. Kot, In-operando hard X-ray photoelectron spectroscopy study on the resistive switching physics of HfO_2-based RRAM, Thesis submitted in 2014.

[48] D. Dean, Thermal gravimetric analysis, University of Alabama at Birmingham, report (2016).

[49] E. Lau, Preformulation studies, in S. Ahuja, S. Scypinski (Eds.) Separation Science and Technology, *Academic Press* 2001, pp. 173-233.

[50] R. Ye, A. Barron, Photoluminescence spectroscopy and its applications, Retrieved from the OpenStax-CNX Web site: http://cnx. org/content/m38357/1.2, (2011).

[51] A.M. White, E.W. Williams, P. Porteous, C. Hilsum, Applications of photoluminescence excitation spectroscopy to the study of indium gallium phosphide alloys, *Journal of Physics D: Applied Physics*, 3 (1970) 1322.

[52] A. Mitra, Synthesis and characterization of tungsten disulphide quantum dots and application in bioimaging,Thesis, 2016.

[53] I.H.K. Dias, S.R. Wilson, H. Roberg-Larsen, Chromatography of oxysterols, Biochimie,*Elsevier* 153 (2018) 3-12.

[54] S. Mane, S. Bringans, S. Johnson, V. Pareek, R. Utikar, Reverse phase HPLC method for detection and quantification of lupin seed γ-conglutin, *Journal of Chromatography B*, 1063 (2017) 123-129.

[55] S. Schweiger, S. Hinterberger, A. Jungbauer, Column-to-column packing variation of disposable pre-packed columns for protein chromatography, *Journal of Chromatography A,* 1527 (2017) 70-79.

[56] C.N. Cain, A.V. Forzano, S.C. Rutan, M.M. Collinson, Destructive stationary phase gradients for reversed-phase/hydrophilic interaction liquid chromatography, *Journal of Chromatography A,* (2018).

[57] L.N. Jeong, S.C. Rutan, Simulation of elution profiles in liquid chromatography – III. Stationary phase gradients, *Journal of Chromatography A*, 1564 (2018) 128-136.

[58] A. Mendoza, B. Zonja, N. Mastroianni, N. Negreira, M. Lopez de Alda, S. Perez, D. Barcelo, A. Gil, Y. Valcarcel, Drugs of abuse, cytostatic drugs, and iodinated contrast media in tap water from the Madrid region (central Spain): A case study to analyse their occurrence and human health risk characterization, *Environment International*, 86 (2016) 107-118.

[59] S. Pochet, C. Arnould, P. Debournoux, J. Flament, O. Rolet-Répécaud, E. Beuvier, A simple micro-batch ion-exchange resin extraction method coupled with reverse-phase HPLC (MBRE-HPLC) to quantify lactoferrin in raw and heat-treated bovine milk, *Food Chemistry*, 259 (2018) 36-45.

[60] A. Bodin, X. Framboisier, D. Alonso, I. Marc, R. Kapel, Size-exclusion HPLC as a sensitive and calibrationless method for complex peptide mixtures quantification, *Journal of Chromatography B*, 1006 (2015) 71-79.

[61] A. Petruczynik, K. Wróblewski, M. Szultka-Młyńska, B. Buszewski, H. Karakuła-Juchnowicz, J. Gajewski, J. Morylowska-Topolska, M. Waksmundzka-Hajnos, Determination of some psychotropic drugs in serum and saliva samples by HPLC-DAD and HPLC MS, *Journal of Pharmaceutical and Biomedical Analysis*, 127 (2016) 68-80.

[62] D. Pimentel-Trapero, A. Sonseca-Yepes, S. Moreira-Romero, M. Hernández-Carrasquilla, Determination of macrocyclic lactones in bovine liver using QuEChERS and HPLC with fluorescence detection, *Journal of Chromatography B,* 1015-1016 (2016) 166-172.

[63] P.M. Campos, F.S.G. Praça, M.V.L.B. Bentley, Quantification of lipoic acid from skin samples by HPLC using ultraviolet, electrochemical and evaporative light scattering detectors, *Journal of Chromatography B*, 1019 (2016) 66-71.

[64] J.J. Pitt, Principles and applications of liquid chromatography-mass spectrometry in clinical biochemistry, *The Clinical Biochemist Reviews*, 30 (2009) 19-34.

[65] H. Alrabiah, A.A. Kadi, M.W. Attwa, G.A.E. Mostafa, Development and validation of an HPLC–MS/MS method for the determination of arginine-vasopressin receptor blocker conivaptan in human plasma and rat liver microsomes: application to a metabolic stability study*, Chemistry Central Journal*, 12 (2018) 47.

[66] W. Clarke, Chapter 1 - Mass spectrometry in the clinical laboratory: determining the need and avoiding pitfalls, in H. Nair, W. Clarke (Eds.) Mass Spectrometry for the Clinical Laboratory, *Academic Press*, San Diego, 2017, pp. 1-15.

CHAPTER 4:

PHOTOCATALYTIC DEGRADATION OF BISPHENOL A IN WATER USING PANI-WRAPPED TiO_2 NANORODS

4.0 INTRODUCTION

Water is regarded as the most vital of natural resources worldwide for the sustainability of life, yet freshwater systems are directly threatened by human activities. Currently, the world is facing a serious challenge in saving the few available sources of “clean” water [1]. Rapid industrialization has led to high discharge of organic pollutants into the environment, causing serious damage to aquatic life as well as human well-being [2, 3]. Among these pollutants that are well reported for their negative impact on water quality, are a unique class of compounds referred as emerging organic pollutants. Bisphenol A (BPA) is one of these emerging organic pollutants and is a synthetic organic compound, widely used in the production of food packaging, pesticides, flame retardants, polycarbonate and epoxy resins[4-8]. BPA has been reported to act as an endocrine disruptor [4-8]. It enters the aquatic system during the manufacturing process or through leaching from the products [9-11]. BPA has a high water solubility (120 mg/L at 25°C) and K_{OW} ~3.4 which is considered a moderate potential for bioaccumulation [12]. It acts by binding to the estrogen receptor or membrane-bound estrogen receptor in cellular nucleus and influences cellular activities [10, 11]. In addition, BPA has been shown to affect metabolism through influencing enzyme activity in animal tissues [7].

To date, various methods have been reported for the removal of BPA from wastewater. These include adsorption, biological treatment, chemical oxidation, and

advanced oxidation processes [13-16]. However, some of these methods have proven to be inefficient or are prone to generating large amount of sludge [17, 18]. Advanced oxidation processes, on the other hand, have been consistently identified as effective methodologies for the removal of persistent organic pollutants from an aqueous environment. Among the advanced oxidation processes, the photodegradation technique, which is based on the ability of semiconductor materials to absorb a photon of energy equal to or greater than its band gap energy and generate hydroxyl ($^{\cdot}OH$) and superoxide ($^{\cdot}O_2^-$) radicals has been consistently used to degrade organic contaminants [19]. Photodegradation offers the advantages of high efficiency, low toxicity, simplicity in design and ease of operation [20, 21].

Several catalysts have been reported in the literature for the photodegradation of BPA [22-25]. Taking into consideration TiO_2 properties, including, strong oxidizing power, large surface area, corrosion resistance, non-toxicity, and cost effectiveness, this semiconductor has been widely used as a photocatalyst for the degradation of organic pollutants [26, 27]. However, its application has been hindered by the high recombination rate of the electron-hole pairs [19]. Surface modification of TiO_2 with PANI conducting polymer has been reported to alleviate this challenge by effecting charge separation. For example, commercially available irregularly shaped polyhedra P25 deposited by PANI has been found to exhibit an improved photocatalytic performance towards methylene blue due to electrons being gathered in the conduction band of TiO_2 while holes are trapped in the highest occupied molecular orbital (HOMO) of PANI [28]. On the other hand, spherical black anatase TiO_2 nanoparticles, synthesized *via* a hydrothermal procedure, were deposited onto

a PANI matrix and resulted in improved light absorption for photocatalytic degradation of methyl orange [29].

The conducting polymer PANI has been utilized as a polymer of choice because of its easy synthesis, relatively low cost, non-toxicity, and modifiable surface chemistry [30]. In addition to the stated desirable properties of PANI, we chose it for our study for its added ability to adsorb organic molecules via π-π interactions as well as hydrogen bonding [30]. Furthermore, the incorporation of the TiO_2 photocatalyst into a PANI polymer alleviates the problem of agglomeration that may occur if powders are used [31]. In addition, we envision an improved photodegradation performance of the nanocomposite due to the large surface area offered by nanorods compared to other forms of TiO_2 [32].

Although there have been numerous reports on TiO_2/PANI as photocatalysts, there are no studies reported on PANI wrapped TiO_2 nanorods for the degradation of BPA under UV radiation as per the authors` knowledge [28, 33]. In addition, there are no reports with the experimental data to explain the mechanism of degradation by PANI-supported TiO_2, which were conducted in this study.

Based on the above consideration, in the present work, PANI wrapped TiO_2 nanorods were prepared for the degradation of BPA under UV radiation.

4.1 MATERIALS AND METHODS

4.1.1 Reagents

All chemicals used in present research were of AR grade, except the ones highlighted. Titanium isopropoxide (TTIP), isopropyl alcohol, acetic acid, sodium hydroxide (NaOH), nitric acid (HNO_3), Iron(III) chloride ($FeCl_3$), aniline, bisphenol A

[2,2-bis(4-hydroxyphenyl) propane, BPA], Methanol (HPLC Grade), Acetonitrile (HPLC Grade),benzoquinone, potassium iodide, potassium nitrate, ammonium acetate, humic acid and acetone were acquired from Sigma Aldrich and used without further purification. Ultrapure water was obtained from a Merck water system (MilliQ).

4.1.2 Synthesis of PANI

PANI was synthesized following a method adopted from literature with slight modification [34]. In a typical synthesis, $FeCl_3$ (6 g) was dissolved in 40 mL of distilled water and 0.8 mL of aniline monomer was rapidly added to the oxidant solution under stirring. Distilled water (40 mL) was slowly added to the solution while stirring for about five minutes and then left to stand for 12 hrs. The green product was washed with acetone to stop further polymerization and then further washed with distilled water ~pH 7. The green product was filtered under vacuum and dried in an oven at 60°C.

4.1.3 Synthesis of TiO_2 nanoparticles

TiO_2 nanoparticles were synthesized using a hydrothermal method. Typically, 5 mL of TTIP was dissolved in a mixture of isopropyl alcohol and water (5:3). The solution was poured into a 100 mL beaker and stirred. Concentrated acetic acid (6 mL) was added to the solution whilst stirring. The solution was stirred for 3 h and heated to 180°C in an autoclave for 24 hr. The solution was then cooled at room temperature and washed with excess ethanol to yield a white precipitate. The precipitate was washed with distilled water until ~pH 7. The precipitate was then dried in an oven at 60°C and calcined at 500°C in a muffle furnace in air producing TiO_2.

4.1.4 Synthesis of TiO_2 nanorods

TiO_2 nanoparticles synthesized following the method described in earlier in section 2.4 were then dispersed in 10 M NaOH solution and stirred until homogeneity was achieved. The mixture was placed in a teflon lined autoclave and then heated to 180°C in an autoclave for 48 hr. The solution was then cooled at room temperature and then washed with dilute HNO_3 and then with distilled water until ~ pH 7. The precipitate was then dried in an oven at 60°C and then calcined at 500°C in a muffle furnace in air producing TiO_2 nanorods.

4.1.5 Synthesis of PANI -TiO_2

PANI-TiO_2 nanocomposite was synthesized as follows: varying amounts of TiO_2 nanorods were dispersed in 20 mL of distilled water and stirred continuously. $FeCl_3$ (6 g) was added to the mixture and 0.2 mL of aniline monomer was rapidly added to the oxidant solution under stirring. Distilled water (60 mL) was slowly added to the solution under stirring for about five minutes and then left to stand for 12 h. The green product was washed with acetone to stop further polymerization and then further washed with distilled water ~pH 7. This product was filtered under vacuum and dried in an oven at 60°C.

4.2 CHARACTERIZATION OF THE PHOTOCATALYSTS

The morphology of TiO_2 nanorods and PANI-TiO_2 nanocomposite were analyzed by using VEGA3 TESCAN (Bruno, Czech Republic) Scanning electron microscopy (SEM) and a JEOL JEM-2100 TEM electron microscope (Peabody, Massachusetts, USA) The structural properties were analyzed by X-ray diffraction (XRD) (Philips, X'Pert PRO MPD, mineral powder diffraction) analysis which was carried to

investigate the crystallinity of the nanocomposite. The instrument uses an X-Ray source of Cu α- radiation beam with excitation wavelength of 0.15406 nm for the analysis. The functional groups of the materials were analyzed by Fourier transform infrared (FTIR) spectra were recorded from 400–4000 cm^{-1} using KBr pellets. Raman spectra was recorded using a WITec Confocal Raman Microscope. Data was collected and processed using a WITec Control scanning and data acquisition software.

Surface area and porosity of TiO_2 and PANI-TiO_2 nanocomposite were analyzed using a Brunauer Emmett Teller (BET) surface area analyzer (ASAP 2020, Micromeritics Instruments, USA) using N_2 adsorption and desorption isotherms. Elemental composition, states, and surface characterization was done using a Physical Electronics (PHI) Quantum 200 XPS spectrophotometer with Al Kα as the excitation source. Photoluminescence measurements were performed using a Perkin Elmer LS 45 Fluorescence Spectrometer.

4.3 PHOTOCATALYTIC DEGRADATION STUDIES

The photodegradation studies were carried out in a photocatalytic reactor with a capacity of 1000 mL. A glass column housing of the UV lamp was fixed inside the reactor with tap water circulating around the glass column cooling the solution. The wall of the glass column has a thickness of 3 mm. The reactor was made of Perspex and during reactions, it was placed on a magnetic stirrer to keep the solution under agitation. The mixture of catalyst and BPA solution was left in the dark under magnetic stirring for an hour to until adsorption–desorption equilibrium was established [35]. The mixture was irradiated with a UV lamp light at a predominant wavelength of 365 nm. The photodegradation performance was investigated as a

function of time. In the experiments, the initial solution pH was adjusted to pH 10 from the solution pH of 6.5 with 0.1 M HCl or 0.1 M NaOH for experiments investigating the influence of pH. The suspension was continuously stirred in the dark for 30 min using a magnetic stirrer to ensure the adsorption equilibrium of BPA on the catalyst. Aliquots (10 mL) were removed from the sample at varied time intervals, and filtered through 0.45 µm membranes filter discs for analysis by an Agilent high-performance liquid chromatography (HPLC) using acetonitrile/water (40/60, v/v) as the mobile phase, an elution time of 15 min, and a detector wave-length of 275 nm.

A C18 reversed-phase column (4.6 nm × 150 nm) was used for chromatographic analysis. Reproducibility of the measurements was ensured by performing these three times. The effect of pH on the photodegradation was examined by keeping 0.1 g of the photocatalyst in contact with 500 mL BPA solutions of 5 ppm concentrations, set at pH 4.5, 7 and 10 and at a temperature of 25°C. Similarly, the effect of photocatalyst dosage was investigated for the photodegradation of BPA by varying the mass of the photocatalyst from 10 mg to 250 mg in a 500 mL of 5 ppm BPA solution. The effect of initial BPA concentration was investigated at different initial BPA concentration from 1 ppm to 30 ppm. The presented data points are mean values. The removal efficiency of BPA was calculated using Equation 4.1:

$$\% \, Removal = \frac{C_i - C_f}{C_i} x \, 100 \qquad 4.1$$

where C_i (mg/L) is initial concentration of adsorbate in solution, C_f (mg/L) is the final concentration of adsorbate in the filtrate.

4.3.1 LC/MS conditions

The analysis was conducted using a Shimadzu UHPLC-MS/MS 8030 instrument (Tokyo, Japan). The chromatographic separation was performed using a RAPTOR AR C18, 2.7 µm 100 X 2.1 mm column. The column was previously conditioned with MeCN: (5:95 v/v) at a flow rate of 0.1 mL/min. The column temperature was set at 40°C. BPA solutions were separated following gradient elution program shown in Table 1: To prevent sample carry over, 100% MeOH was used as blank and was injected after every standard and sample injection. A flow rate of 0.2 mL/minute was used for the elution of BPA in UHPLC. For tandem mass spectrometry, the deprotonated molecule $[M+H]^+$ was used as precursor ion. Tandem mass spectrometry spectra were acquired between m/z 30 and m/z 300 in enhanced mass resolution mode Q3. A nebulizing gas flow rate of 3 L/min was used. A drying gas flow rate of 15 L/min was used for the mass spectrometry.

Table 4. 1 LC gradient elution program for BPA

	Time	Module	Command	Value
1	0.01	Pumps	Solvent B conc.	25
2	0.50	Pumps	Solvent B conc.	25
3	3.50	Pumps	Solvent B conc.	95
4	4.00	Pumps	Solvent B conc.	95
5	4.10	Pumps	Solvent B conc.	25
6	10.00	Pumps	Solvent B conc.	25

7	10.10	Controller	Stop

Solvent A: Water.

Solvent B: Acetonitrile.

4.4 RESULTS AND DISCUSSION

4.4.1 FTIR analysis of TiO_2, PANI and PANI-TiO_2

FTIR spectroscopy analysis revealed the incorporation of PANI into a nanocomposite of PANI-TiO_2 as shown by the functional groups of PANI that are present in the PANI-TiO_2 nanocomposite. The main peaks of PANI were all confirmed with peaks appearing at 3662 cm^{-1}, 2955 cm^{-1}, 1577 cm^{-1}, 1502 cm^{-1}, 1301cm^{-1}, 1250 cm^{-1} and 827 cm^{-1} [36-38]. The band at 3662 cm^{-1} corresponds to the N-H stretching mode and the peak around 2955 cm^{-1} correspond to the aromatic C-H vibration [37].

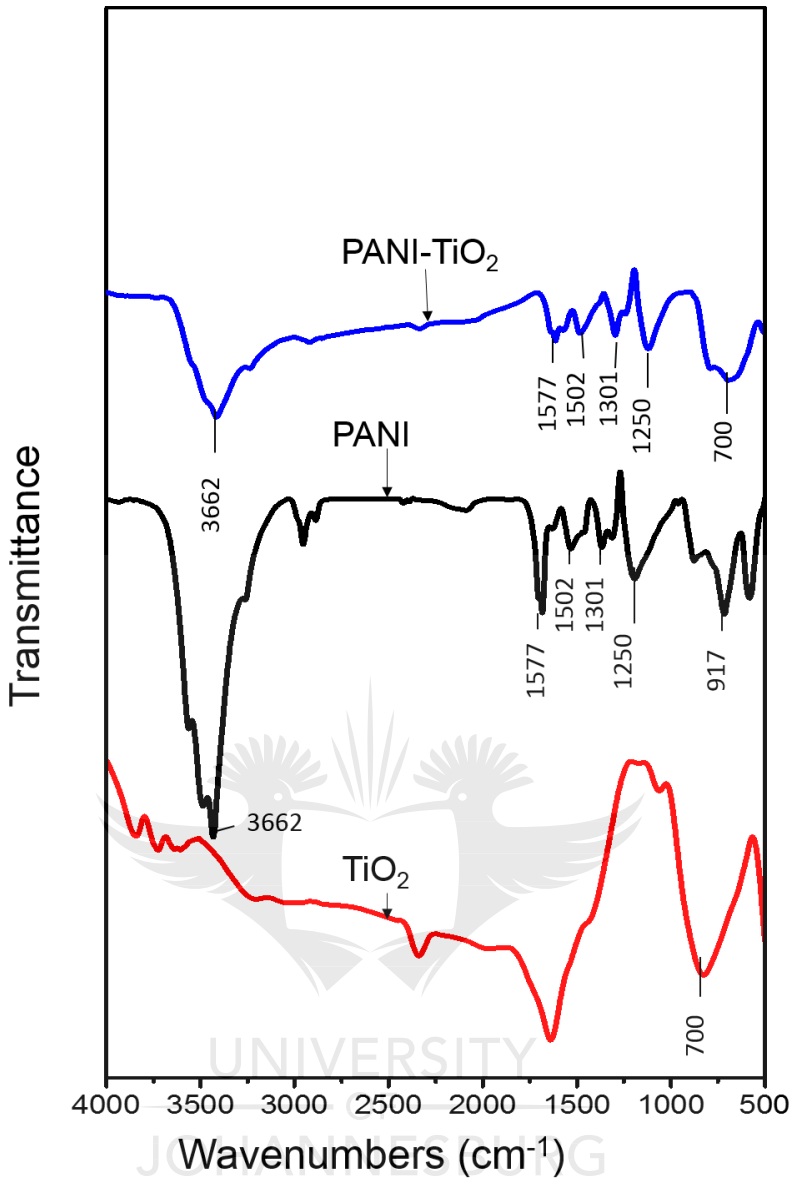

Figure 4. 1: FTIR spectra of pristine TiO_2, pristine PANI and PANI-TiO_2.

The peaks appearing at 1577 cm^{-1} and 1502 cm^{-1} are due to the C=C and C=N stretch of the benzoid and quinoid respectively (Figure 4.1). The peak appearing on 1301

cm^{-1} is due to the C-N vibrations [37]. The peaks due to PANI were clearly observed in PANI-TiO_2 sample. The spectrum displays the major peaks of PANI such as the peak at 3662 cm^{-1} which is due to the N-H stretching and other peaks due to the benzoid and quinoid rings which appear at 1577 cm^{-1} and 1502 cm^{-1}[38].

The new weak peak appearing at 917 cm^{-1} is probably due to the C–H out of plane bending vibration of PANI composite [38]. These bands reveal the existence of PANI in the synthesized PANI-TiO_2 sample. At 700 cm^{-1}, a peak assigned to Ti-O-Ti bridging stretch modes was observed on the TiO_2 spectra [39].

4.4.2 Raman spectroscopy analysis of pristine PANI, pristine TiO_2 and PANI-TiO_2 nanocomposite

Raman spectroscopy confirmed the anatase phase of the TiO_2 nanorods by the appearance of the typical peaks of anatase TiO_2 at 637 cm^{-1}, 514 cm^{-1}, 396 cm^{-1} and 195 cm^{-1} (Figure 4.2) [40]. The Raman spectroscopic analysis showed that the TiO_2 anatase phase was not compromised after the synthesis of PANI-TiO_2 polymer. In addition, it confirmed the incorporation of PANI polymer in the PANI-TiO_2 nanocomposite as evidenced by the appearance of the D band and the G band at 1603 cm^{-1} and 1505 cm^{-1} respectively that are typically associated with carbon based materials [41].

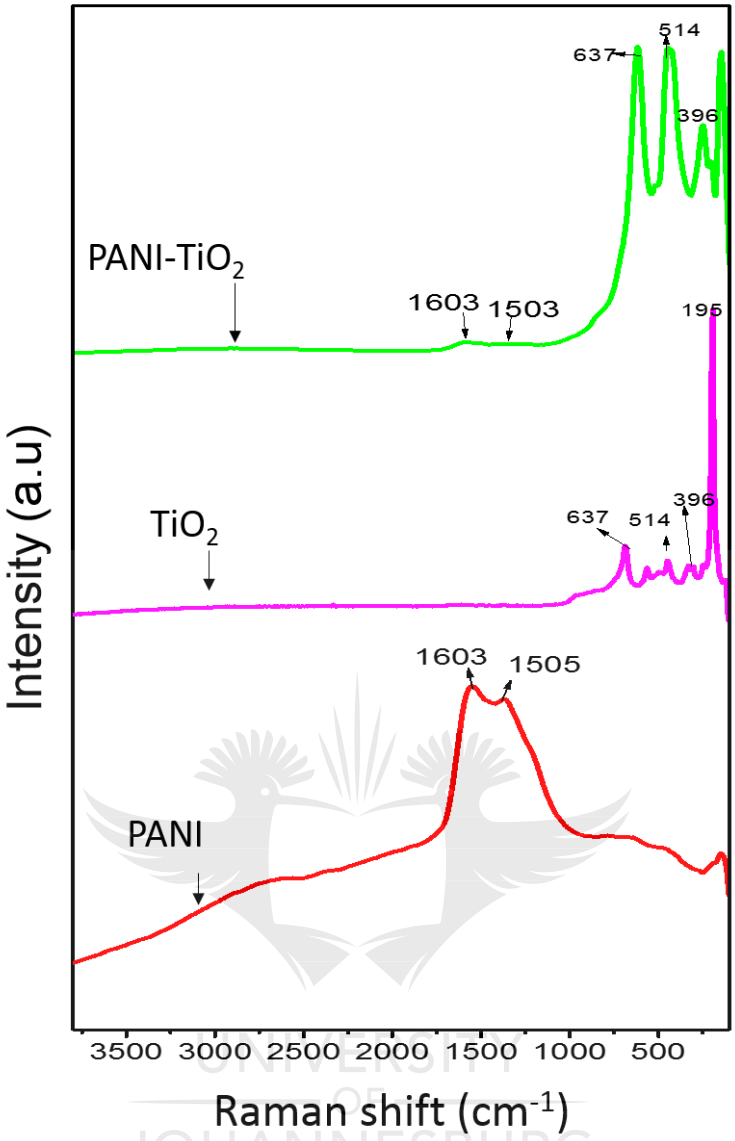

Figure 4. 2: Raman spectra of pristine PANI, pristine TiO_2, and PANI-TiO_2.

The results for Raman analysis are in agreement with FTIR spectroscopy analysis results that were reported earlier. (Figure 4.2).

4.4.3 XRD analysis of pristine PANI, TiO_2, and PANI-TiO_2

The results for XRD analysis are shown in Figure 4.3. XRD analysis of as-synthesized PANI showed two broad peaks at 2θ=20.5° and 25.3°. This suggested an amorphous structure of the PANI and the results are in agreement with results that were obtained by Haldorai et al [42]. The XRD pattern, of as-synthesized TiO_2

nanoparticles, showed peaks at 2θ = 25.30°, 37.90°, 47.99°, 54.2,° 62.72°, 68.84°, 70.28°, 75.12° and 82.79° [26, 37].

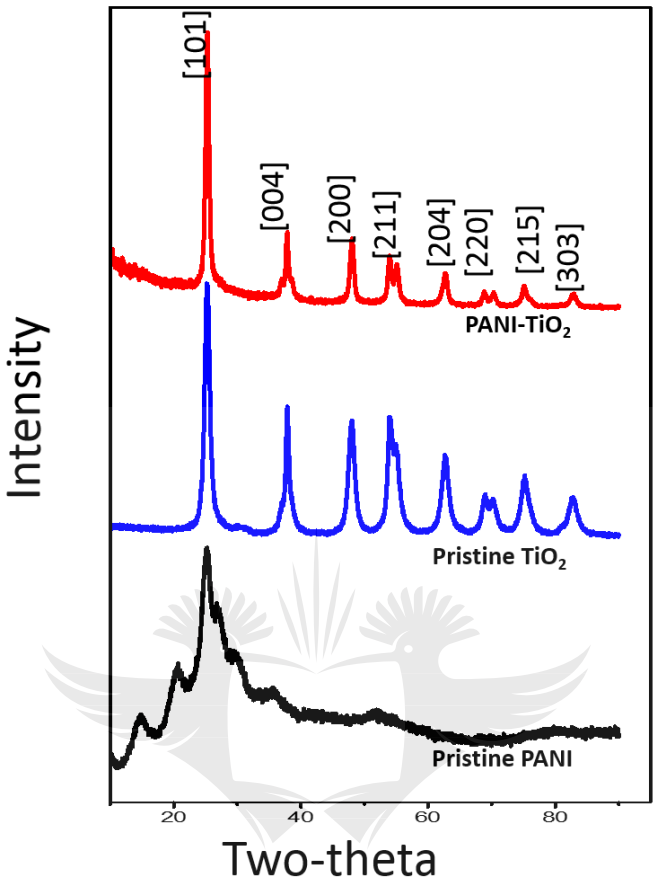

Figure 4. 3: XRD plot of (A) pristine PANI, (B) pristine TiO_2, and (C) PANI-TiO_2 nanocomposite.

These peaks correspond to anatase TiO_2 with hkl crystal planes [101], [004], [200], [105], [211], [204], [116], [220], [215] and [303] respectively [43]. This pattern confirms the formation of pure anatase phase without any other phases with a JCPDS score of 97%. The observed 2θ values were consistent with the standard values and showed the anatase phase of TiO_2 as per Joint Committee on Powder Diffraction Standard (JCPDS) card No. 01-086-1157. The peaks in as-synthesized TiO_2 also appeared in PANI-TiO_2 nanocomposite showing that the TiO_2 did not lose its crystallinity even after incorporation of PANI.

XRD analysis can be used to determine the crystallite size of powdered material by treating the XRD data using the Scherrer equation [44-46]. The particle size of material have been reported to affect the overall performance of the photocatalyst [47]. Small particle sizes have been reported to provide a high surface area to volume ratio, which improves the photocatalytic efficiency by improving the contact between the photocatalysts and the pollutant [47, 48]. In this study, the particle sizes were determined using the Scherrer equation [45]:

$$D = k \lambda / \beta \cos \theta \qquad 4.2$$

Where D is the average size in nanometres, k = 0.89, λ = 0.1540 nm (Cu Kα), β = FWHM x 0.01745 in radians and θ is the peak position.

The results show an average particle size of 16.62 nm. The same peak positions were also observed in a nanocomposite of PANI-TiO_2 with an average particle size of 16.6 nm calculated.

4.4.4 BET analysis of pristine PANI, TiO_2, and PANI-TiO_2

The pore size distribution and specific surface area was determined via nitrogen adsorption-desorption isotherms. Figure 4.4 illustrates that all the as-synthesized photocatalysts can be identified as Type IV isotherm with H4 type hysteresis loop according to the IUPAC-BET classification [49]. This signifies the presence of signifies the presence of mesoporous structure in the photocatalysts [49].

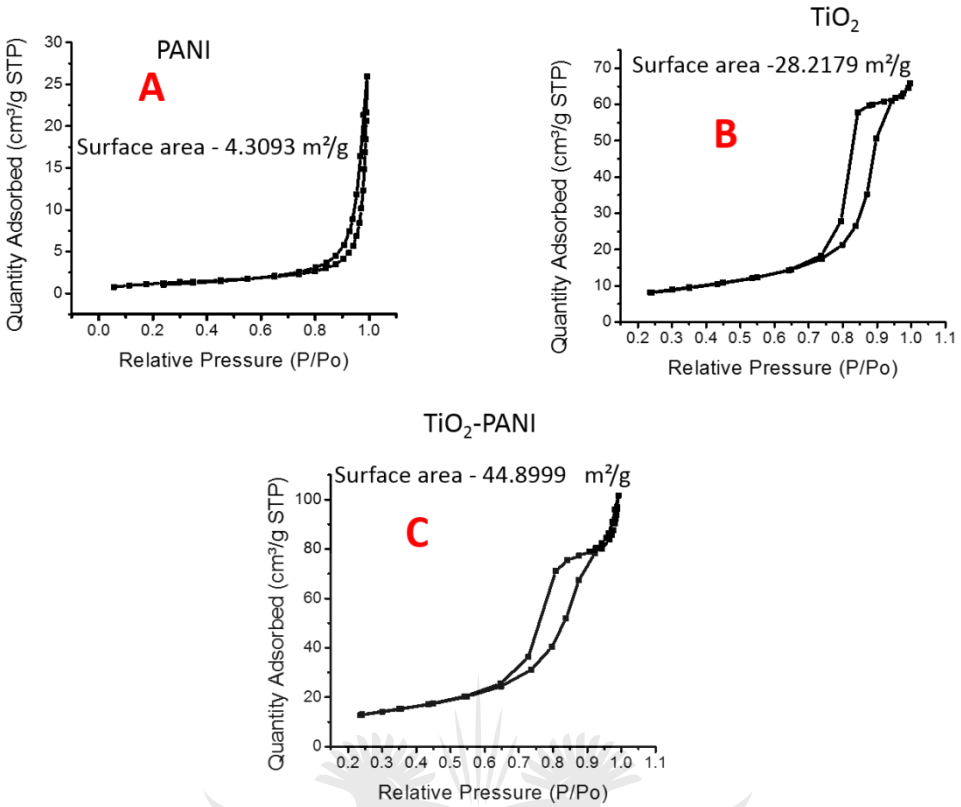

Figure 4. 4: BET surface area of [A], pristine TiO_2 nanorods, [B], PANI-TiO_2.

Table 4.2 summarizes the BET specific surface area, pore volume and pore size of all as-prepared PANI, TiO_2 and PANI-TiO_2 photocatalysts. The BET data showed that the addition of PANI to the calcined TiO_2 resulted in an increase in the surface area from 28.2179 m^2/g of TiO_2 to 44.8999 m^2/g of PANI-TiO_2. A similar trend was observed in the pore volume and pore size due to the incorporation of PANI into the PANI-TiO_2 nanocomposite. The increase in these important parameters may result in high degradation performance of PANI-TiO_2. [44].

Table 4. 2: BET specific surface area, pore volume and pore size of as-prepared PANI, TiO_2 and PANI-TiO_2.

Photocatalyst	S_{BET} (m^2/g)	Pole volume (cm^3/g)	Pore size (nm)
PANI	4.3093	0.033007	30.64
TiO_2	28.2179	0.097520	13.82
PANI-TiO_2	44.8999	0.145248	35.62

4.4.5 SEM analysis of (A) TiO_2 nanorods and (B) PANI-TiO_2

Figure 4.5 shows rod-like TiO_2 photocatalyst (image A). Image B in Figure 4.5 shows a denser rods shaped materials of different sizes.

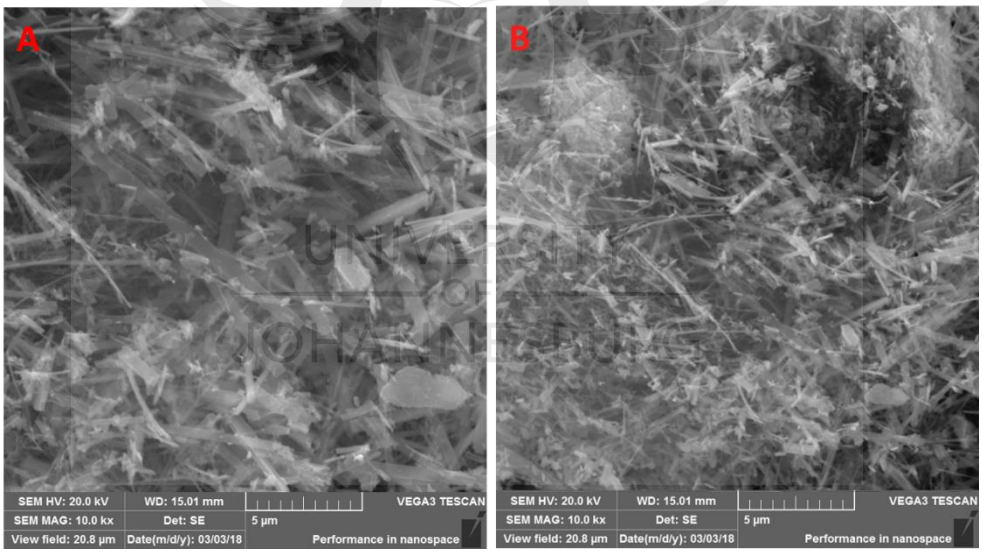

Figure 4. 5: SEM images of pristine TiO_2 (A) and PANI-TiO_2 (B).

4.4.6 TEM analysis of (A) TiO_2 nanorods and (B) SAED analysis TiO_2 nanorods

TEM analysis confirmed that nanorods of TiO_2 were synthesized as shown in Figure 4.6a and Figure 4.6b. These uniformly dispersed TiO_2 nanorods had diameter size range of 40-100 nm. TEM analysis revealed TiO_2 nanorods were wrapped by a thin

layer of PANI forming in the nanocomposite of PANI-TiO_2 (Figure 4.6c and Figure 4.6d).

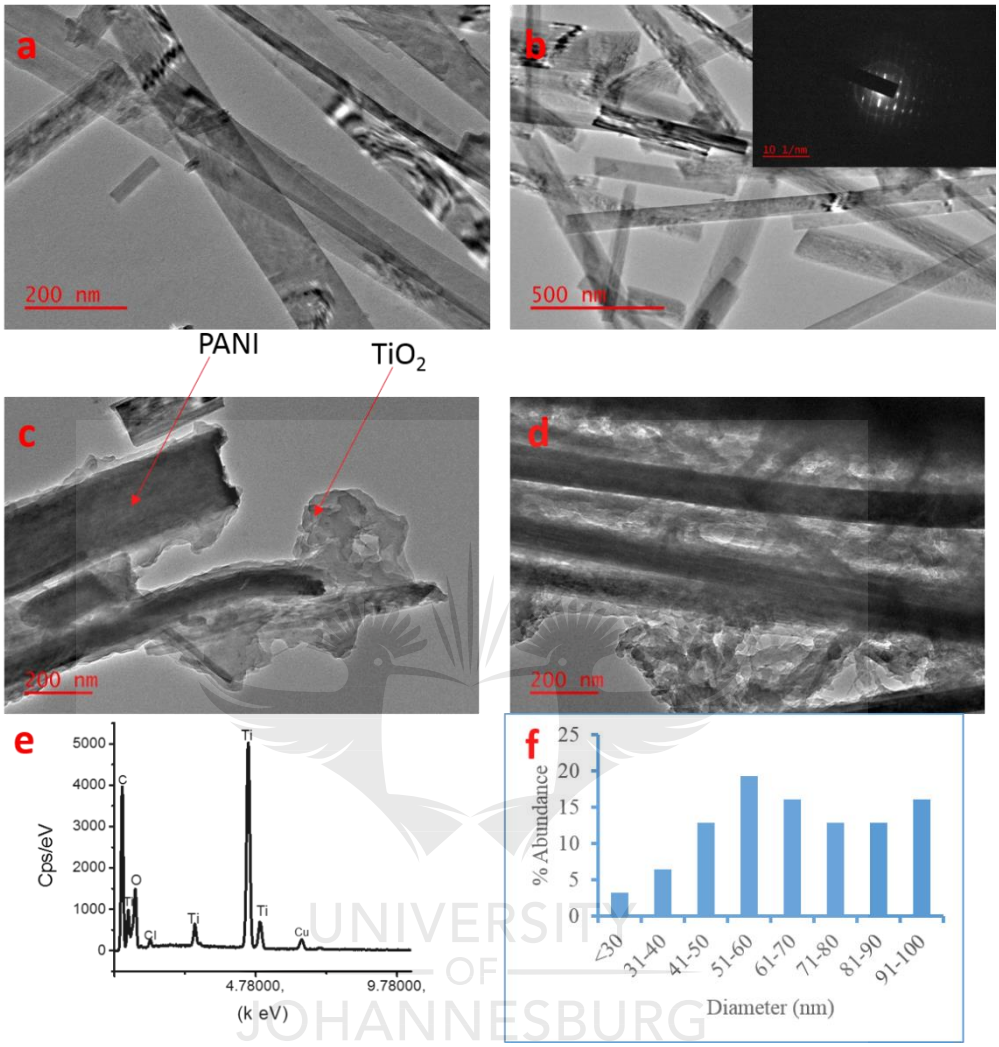

Figure 4. 6: TEM images of (a), (b) pristine TiO_2 (c), (d) PANI-TiO_2, (e) EDS of PANI-TiO_2 and (f) diameter of the TiO_2 nanorods.

EDX elemental analysis in Figure 4.6e showed the nanocomposite was mainly composed of carbon (C), oxygen (O) and titanium (Ti) elements. The chloride ion (Cl-) species and Fe came from the preparation of PANI-TiO_2 nanocomposite. Copper (Cu) atoms shown were due to copper grids used during TEM analysis.

4.4.7 TGA analysis of pristine PANI, TiO_2 nanorods and PANI-TiO_2

TGA was employed to investigate the thermal stability of the TiO_2 and PANI-TiO_2 nanocomposite. TGA profiles of TiO_2 and PANI-TiO_2 nanocomposite are shown in Figure 4.7. TGA results for PANI shows four major weight losses. The weight loss in the first stage, from 50°C to 150°C for the peak of pristine TiO_2 and PANI-TiO_2 nanocomposite is due to the loss of adsorbed and bound water on the nanocomposite [50]. The weight loss at 150°C to 250°C was due to loss of water of crystallization [51]. The weight loss that occurred after 380°C to 500°C was due to the removal of functional groups and breaking of bonds forming the PANI polymers and also due to lose of gaseous emissions *e.g.* carbon monoxide which might have occurred [51]. The final weight loss at 800°C was due to the thermal degradation of the carbonaceous material [52]. TGA for PANI-TiO_2 nanocomposite is shown in Figure 4.7.

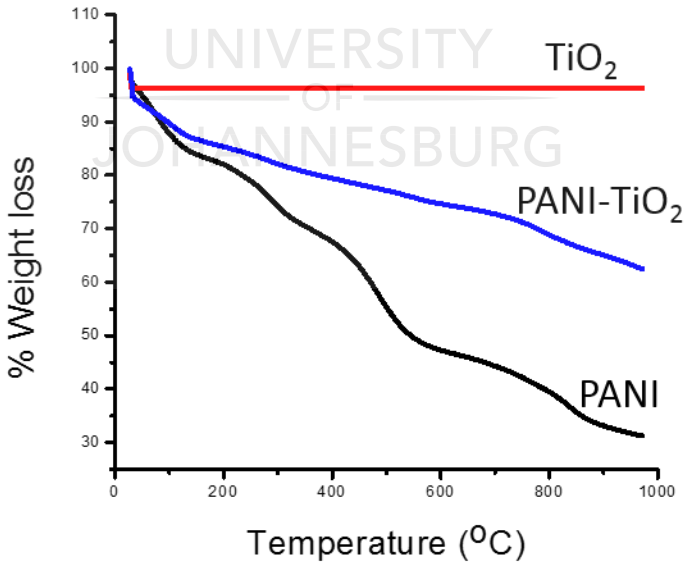

Figure 4. 7: TGA and DTA graphs of pristine PANI, TiO_2, and PANI-TiO_2.

The results indicate three major weight losses. The first weight loss at 25°C – 150°C was due to loss of moisture [53]. Another weight loss observed from 180 - 700°C

was due to loss of low molecular weight oligomers of PANI [26]. After 700°C, there was no weight loss observed for the nanocomposite due to the stability of TiO_2, which was incorporated into PANI to form a nanocomposite. This is in agreement with observations made on pristine TiO_2 [54].

4.4.8 Photoluminescence and UV absorption analysis

Photoluminescence (PL) and UV spectroscopy provide information on the charge separation of materials [52, 55, 56]. PL reveals the migration of charges (electrons and holes) and the formation of defects in the photocatalyst [52]. This helps in understanding the recombination rate of charges at the surface of the photocatalyst. Figure 4.8a shows results of emission of the materials at 530 nm for all sample materials. The intensity of pristine TiO_2 spectra is higher than that of pristine PANI and that of PANI-TiO_2.

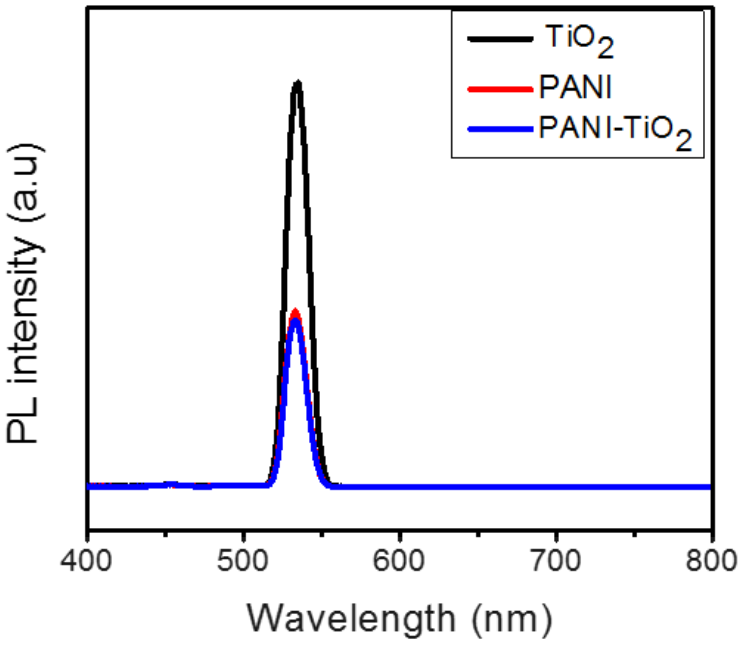

Figure 4. 8a: Luminescence spectra of pristine TiO_2, pristine PANI and PANI-TiO_2.

The results show that the incorporation of PANI can greatly improve the performance of the nanocomposite by reducing the recombination rate of the nanocomposite. This is attributed to the ability of PANI to effect charge separation by transferring electrons to the conduction band of TiO_2 and also trapped holes leading to charge separation [35]. Figure 4.8b shows results of UV analysis of the photocatalysts. The results showed that PANI has a stronger absorption than either PANI-TiO_2 nanocomposite or pristine TiO_2. The wrapping of TiO_2 nanorods with PANI in improved the absorption properties of the PANI-TiO_2 nanocomposite.

Figure 4.8 B shows results of UV analysis of the photocatalysts and their DRS.

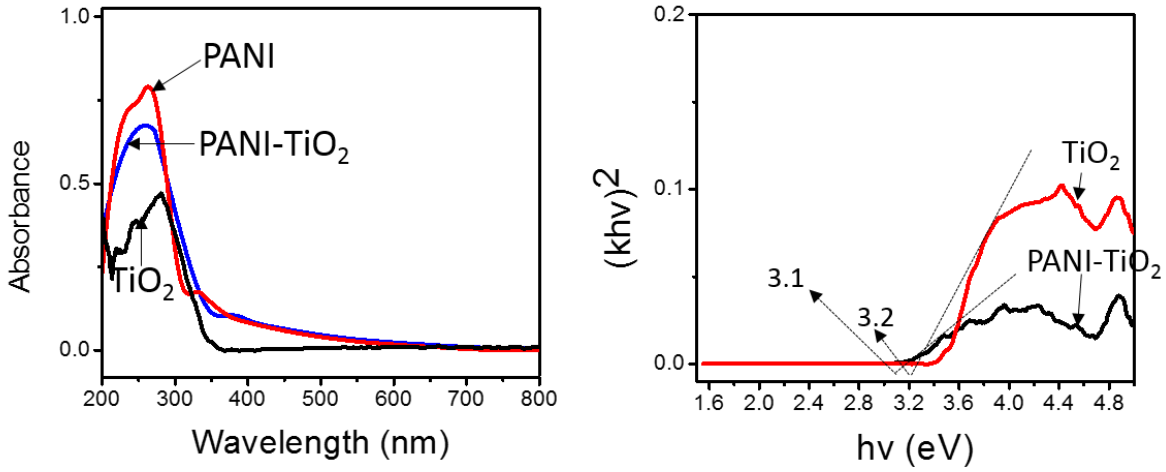

Figure 4.8b: UV absorption spectra of pristine TiO_2, pristine PANI, PANI-TiO_2 and Tauc`s plot of pristine TiO_2 and PANI-TiO_2.

The results showed that PANI has a stronger absorption than either PANI-TiO_2 nanocomposite or pristine TiO_2.The wrapping of TiO_2 nanorods with PANI in improved the absorption properties of the PANI-TiO_2 nanocomposite. This was also reflected in the Tauc`s plot with the band gap estimation of PANI-TiO_2 was at 3.1 eV compared to that of pristine TiO_2 which was at 3.2 eV (Figure 4.8b).

4.4.9 X-Ray Photoelectron Spectroscopy

The surface characterization and chemical states of PANI-TiO_2 nanocomposite was examined by X-ray photoelectron spectroscopy (XPS). Figure 4.9a represents XPS survey scan of PANI-TiO_2 nanocomposite, which revealed the presence of C, O, Ti and N.

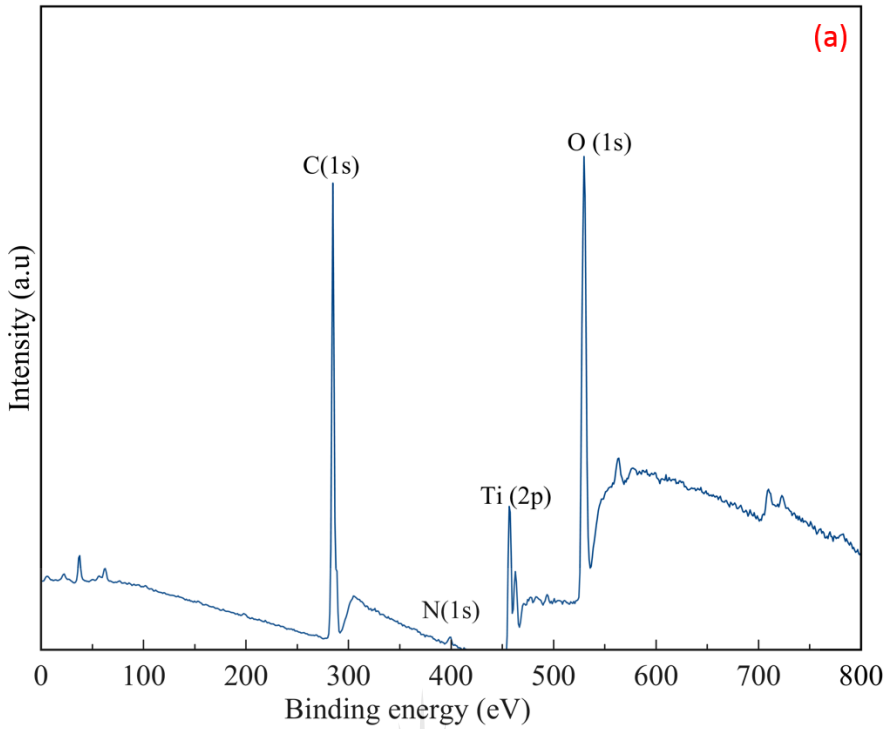

Figure 4. 9 (a): XPS survey scan for TiO_2-PANI.

The XPS results shown in Figure 4.9b reveal a peak at 284.75 eV which was assigned to carbon from the PANI polymer [57]. A small peak was observed at 288.1 eV corresponding to C-O-Ti was observed [58].

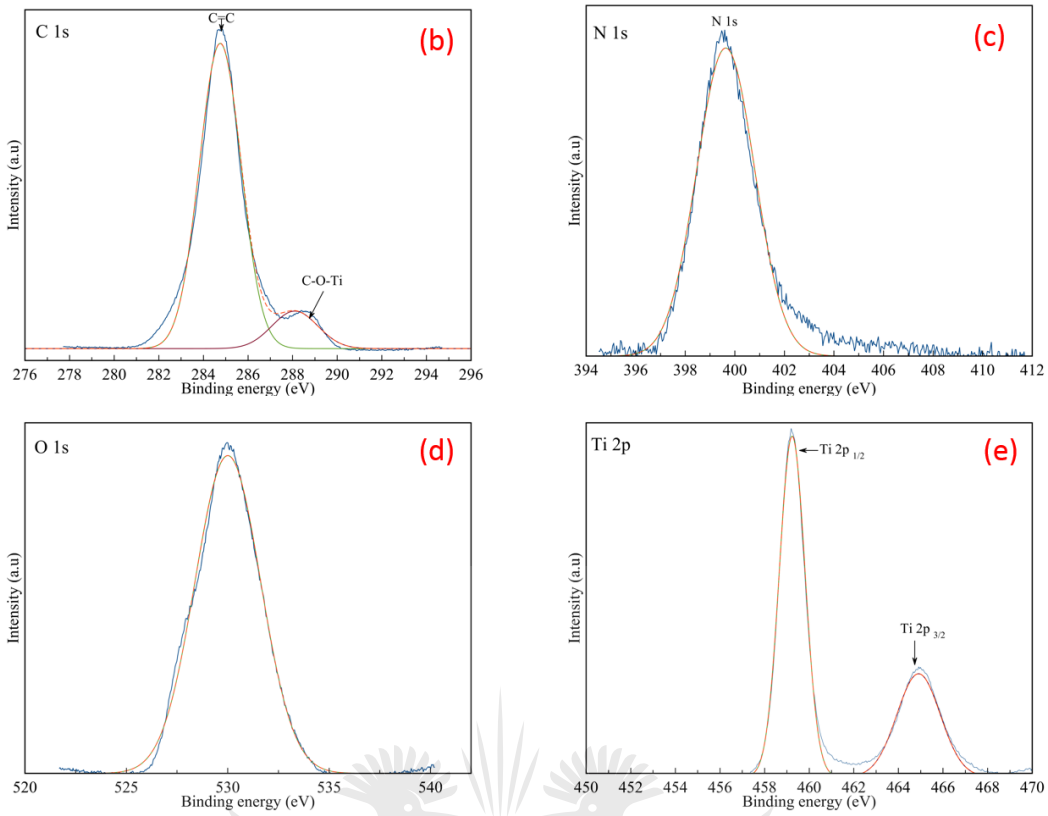

Figure 4.9 (b): Core level XPS spectra for (a) C 1s, (b) N 1s (c) O 1s and Ti 2p of TiO_2-PANI.

A peak in Figure 4.9c at 399.3 eV was due to N 1s peak corroborates positively with quinoid amine and benzenoid amine, which is consistent with the structure of PANI as reported by Golczak *et al* [59]. Figure 4.9d presents the core level O 1s spectra (530 eV) due to O bonds such as Ti−O−Ti and Ti−O−H [57]. Ti 2p core level spectra is presented in Figure 4.9e at 459.2 eV and 464.9 eV due to Ti $2p_{1/2}$ and Ti $2p_{3/2}$ respectively [58, 60].

4.5 APPLICATION RESULTS

4.5.1 Selection of photocatalysts

The photocatalytic action of pristine TiO_2 and PANI-TiO_2 was evaluated using a photocatalyst dosage of 0.2 g/L and 5 mg/L BPA solution at solution pH 6.5. Figure

4.10 shows the photocatalytic degradation of BPA under UV radiation. It is clearly observed that the photocatalytic degradation removal of PANI-TiO_2 was higher than that of pristine TiO_2.

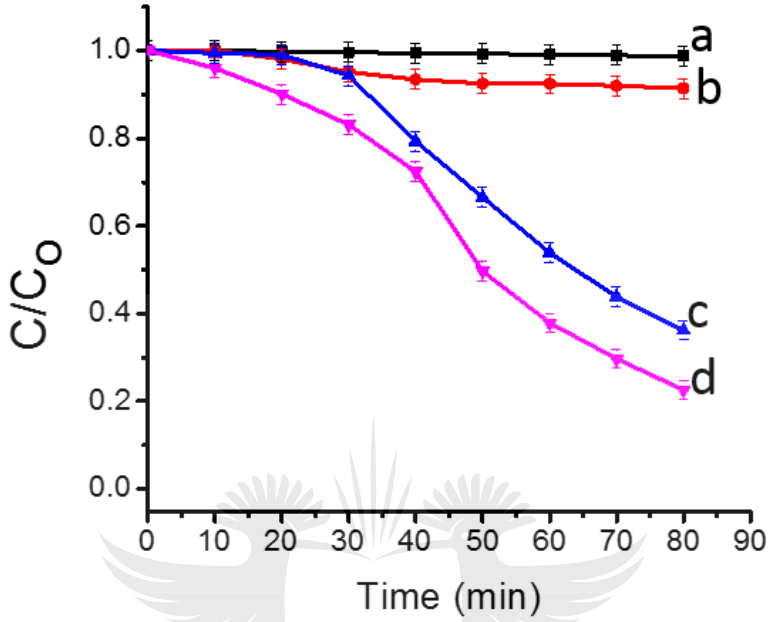

Figure 4. 10: Degradation of BPA on (a) pristine TiO_2 in the dark, (b) PANI-TiO_2 in the dark, photocatalytic degradation on, (c) pristine TiO_2 and (d) PANI-TiO_2.

After 80 mins irradiation, 79.8% degradation of BPA was achieved by PANI-TiO_2 compared to a removal efficiency of 60.7% that was observed for pristine TiO_2. The enhanced photoresponse of PANI-TiO_2 can be attributed to modification of TiO_2 with PANI. This is in agreement with observed results from BET analysis that showed an increase in the surface area of the nanocomposite after modification of TiO_2 with PANI (Figure 4.10). The contribution of PANI to the overall degradation efficiency is further highlighted by the increased removal efficiency of BPA in graph (b) compared to graph (a) under darkness. The removal in graph (b) can be attributed to adsorption via π-π stacking and hydrogen bonding of BPA and PANI [37]. The slight

removal that was observed on graph (a) can be attributed to photolysis. PANI-TiO_2 was chosen for the rest of the experiments.

4.5.2 Effect of pH of BPA solution on its photodegradation

Solution pH plays an important role in determining the efficiency of the photodegradation process. This is because it affects the adsorption-desorption of the organic molecules on the surface of the photocatalyst. In addition, pH influences the generation of hydroxyl radicals as well as active oxygen species that occur on the surface of the photocatalyst [34]. Figure 4.11 shows a comparison of the degradation of BPA (5 ppm) with a dosage of 0.2 g/L at different at different initial BPA solution pH ranging from 4 – 10.

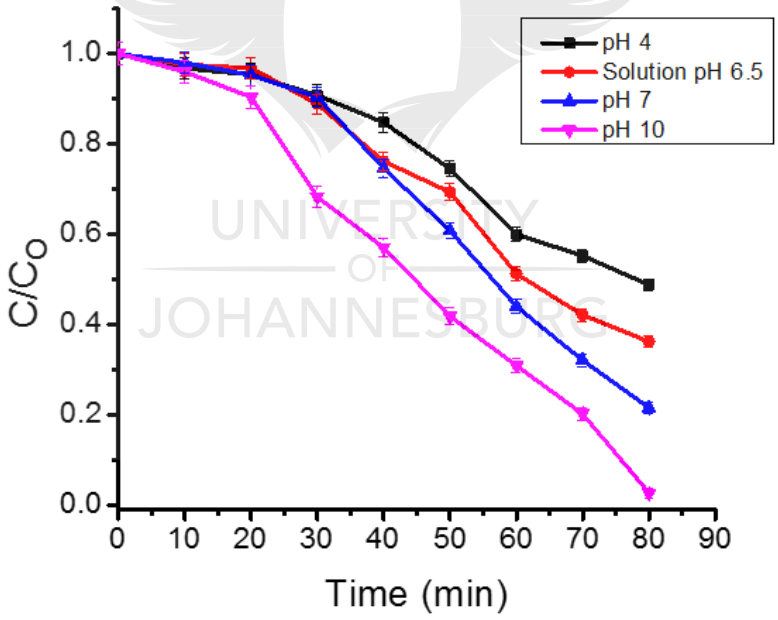

Figure 4. 11: Effects of initial pH on the degradation of BPA using PANI-TiO_2 under UV light.

The results showed that the degradation of BPA depended strongly on the initial solution pH. The reported point of zero charge of TiO_2 from literature is 6.25 whilst

that of PANI is 5.8 [61, 62]. This implies that the surface of the PANI-TiO_2 was negatively charged in alkaline solution and positively charged in acidic solution. On the other hand, BPA had a negative charge due to the hydroxyl molecules in its structure [63]. These surface properties influenced the initial adsorption of BPA on the catalysts. The results in Figure 4.11 show that the BPA removal was 99.8% at pH 10 compared to 79.6% at pH 7 and lowest removal was at pH 4 (50%). The high removal at pH 10 was due to an increase in diffused hydroxyl radicals in the bulk solution that degraded BPA [34, 36, 64]. Therefore, pH of 10 was used as the optimum pH for the rest of the experiments.

4.5.3 Effect of photocatalyst dosage on the photodegradation of BPA

The effect of dosage on the photodegradation of BPA was determined in order to optimize the efficiency of the photodegradation process. Figure 4.12 shows a comparison of the degradation of BPA at different initial photocatalyst dosage.

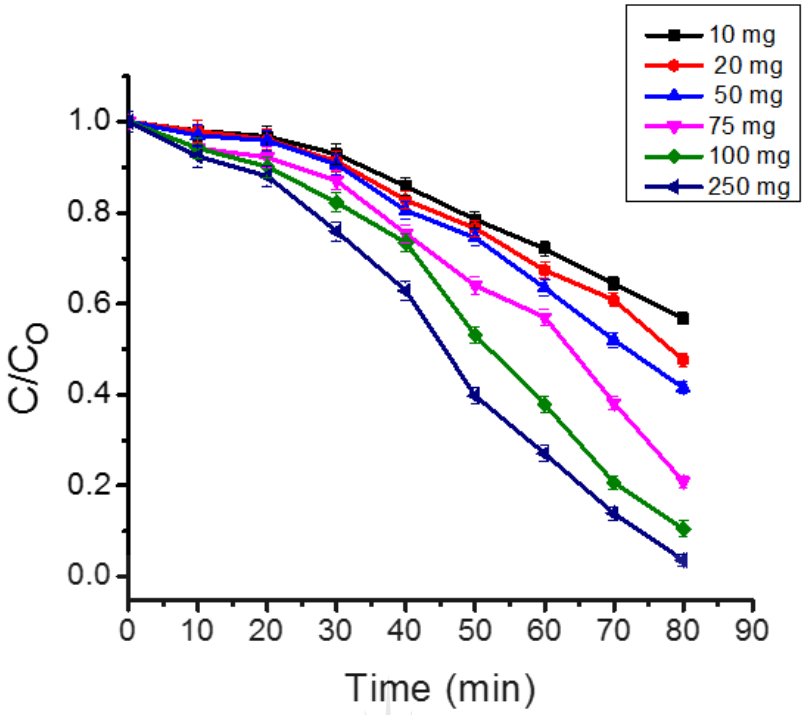

Figure 4. 12: Effect of photocatalyst dosage on the photodegradation of BPA by PANI-TiO_2.

The results show that photodegradation efficiency improved with an increase in the dosage. The increase in dosage increased the number of ·OH radicals which participated in the degradation of BPA [36]. The results shown in Figure 10 show that the highest degradation of 99.9% was attained within 80 mins for dosages of 250 mg. However despite achieving 94.5% degradation efficiency after the same irradiation time, 100 mg dosage in 500 mL BPA was chosen as the optimum dosage for the rest of the study. A high dosage may have reduced the degradation efficiency due to aggregation of the photocatalyst aggregation which may have reduced the surface area of the photocatalyst for light absorption [15]. The BPA solution was degraded up to 40%, 50%, 59.6% and 80.5% by 10 mg, 20 mg, 50 mg, and 75 mg photocatalyst dosages after 80 min of irradiation.

4.5.4 Effect of initial concentration of BPA on photodegradation

The effect of initial BPA concentration on its photodegradation was investigated over a concentration range of 1 ppm - 30 ppm under optimal pH of 10 and a photocatalyst dosage of 0.2 g/L. The photodegradation efficiency was influenced by the initial BPA concentration as shown in Figure 4.13.

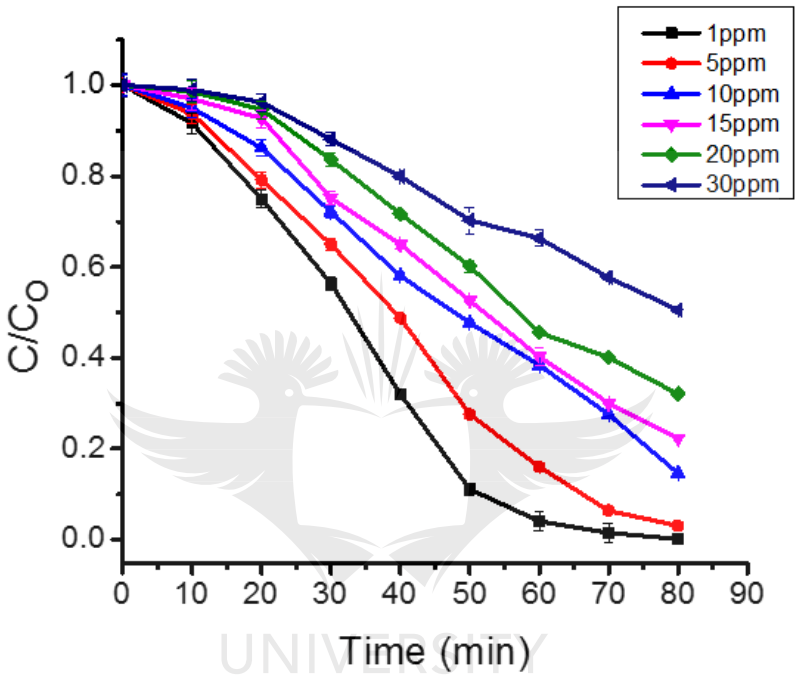

Figure 4. 13: Effect of initial concentration on the photodegradation of BPA by PANI-TiO_2.

Complete degradation of 1-ppm BPA solution was achieved within 80 mins. 99.6% degradation was attained for 5 ppm BPA solution within the same time and only 45.4% was achieved when degrading 30 ppm BPA. After 80 mins of irradiation, 68%, 75.8%, and 85% was degraded for 10 ppm, 15 ppm and 20 ppm BPA solutions respectively. The degradation efficiency decrease with increase in the concentration of BPA. This can be attributed to the increase in the BPA molecules that were adsorbed on the surface of the photocatalyst [35]. This resulted in a reduction in the

photons that were able to reach the surface of the photocatalyst surface and therefore less hydroxyl radicals were generated resulting in reduced photodegradation efficiency [15].

4.5.5 Kinetic studies

A kinetic study on the degradation of BPA by as-synthesized PANI, TiO_2 and PANI-TiO_2. Table 4.3 shows the rate constants for the photodegradation of BPA corresponding to the Langmuir-Hinshelwood kinetics which follows the relationship given below: The rate constant was calculated using the following expression:[65]

$$\ln\left(\frac{C_o}{C}\right) = -kt \qquad (4.4)$$

Where C_o and C is the initial and final concentration respectively, k is the rate constant and t is the irradiation time. The rate constant for the degradation of BPA are shown in Table 4.3. The results show that PANI had the lowest rate constant of 7.04 10^{-4} min^{-1}. Pristine TiO_2 had a rate constant of 2.18 x 10^{-2} min^{-1}. PANI-TiO_2 show a better performance than as-synthesized PANI and TiO_2 with a rate constant of

4.46 x 10^{-2} min^{-1}. The results show a linear agreement with pseudo-first order kinetics with high R^2 values. However, the R^2 value for the degradation of BPA by PANI was 0.6895, which was the lowest suggesting that the removal of BPA did not fit well with the pseudo-first order kinetic model.

Table 4. 3: Rate constants for the degradation of BPA by PANI, TiO_2, and PANI-TiO_2.

Photocatalyst	R^2	Rate constant ($kmin^{-1}$)
PANI	0.6895	7.04×10^{-4}
TiO_2	0.9688	2.18×10^{-2}
PANI-TiO_2	0.9589	4.46×10^{-2}

4.5.6 Effect of nitrate ion on the degradation of BPA

Nitrates have been reported to influence the degradation of organic matter in natural water as it is a source of hydroxide radicals [66]. However, some reports indicate that NO_3^- ions also negatively affect the process of degradation of organics in water as they can scavenge reactive oxygen species [67]. The effects of NO_3^- ion on the degradation of BPA was investigated using environmentally relevant concentrations (0.05 mM, 0.1 mM, 0.5 mM, and 1.0 mM) using 0.2 g/L photocatalyst dosage and 5 mg/L BPA solution with a pH of 6.5. The results in Figure 4.14 showed the presence of nitrate ions in the BPA solution greatly influenced the degradation efficiency.

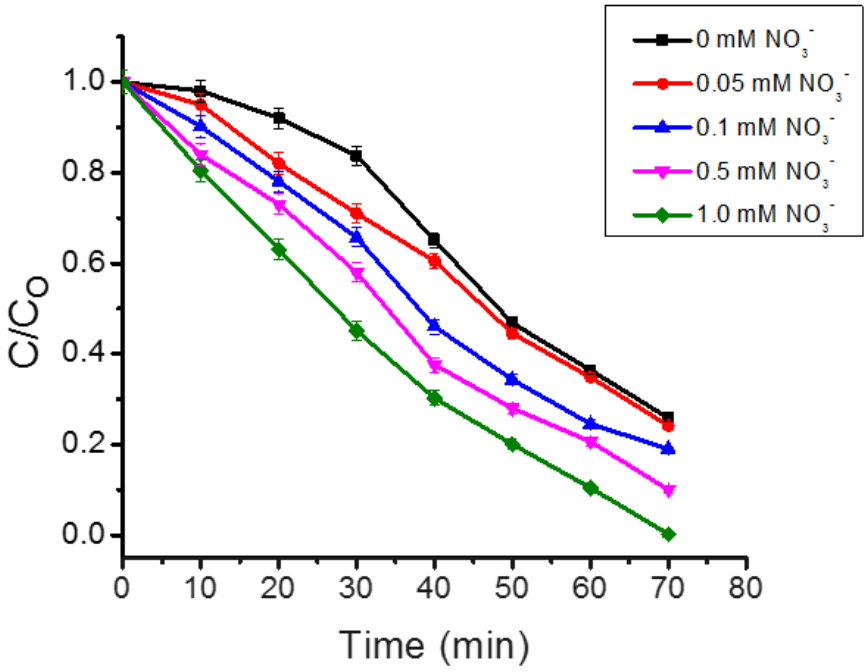

Figure 4. 14: Effect of NO_3^- ion concentration on the photodegradation of BPA by PANI-TiO_2.

The removal efficiency increased with an increase in the concentration of nitrates. The increase in degradation rate was due to the ability of NO_3^- ions to induce the production of OH· radicals according to equations 5-7 [66, 68].

$$NO_3^- + hv \rightarrow [NO_3^-]^* \rightarrow OONO^- \quad 4.5$$

$$[NO_3^-]^* \rightarrow NO_2^- + O(^3P) \quad 4.6$$

$$[NO_3^-]^* \rightarrow NO_2^* + O^* + H_2O \rightarrow NO_2^* + {}^*OH + OH^- \quad 4.7$$

4.5.7 Effect of humic acid on the degradation of BPA

Natural organic matter has been reported to have an influence in the fate of environmental organic contaminants. Guetzloff and Rice reported that the presence of humic acid resulted in an increase in the solubility of polycyclic aromatic hydrocarbon (PAH) [69]. On the other hand, Bo-Ra et al. reported that the presence

of humic acids (5 mg/L) reduced the degradation of BPA by up to 26% [70]. However, some reports also indicated that humic acids had no effect on degradation of organic pollutants [71]. In this study, the effect of humic acids in solution during degradation of BPA (5 mg/L) was investigated by adding 0 mg/L, 1 mg/L, 3 mg/L and 5 mg/L of humic acid. The results shown in Figure 4.15 show that the presence of humic acids in solution at different concentrations consistently inhibited the degradation of BPA.

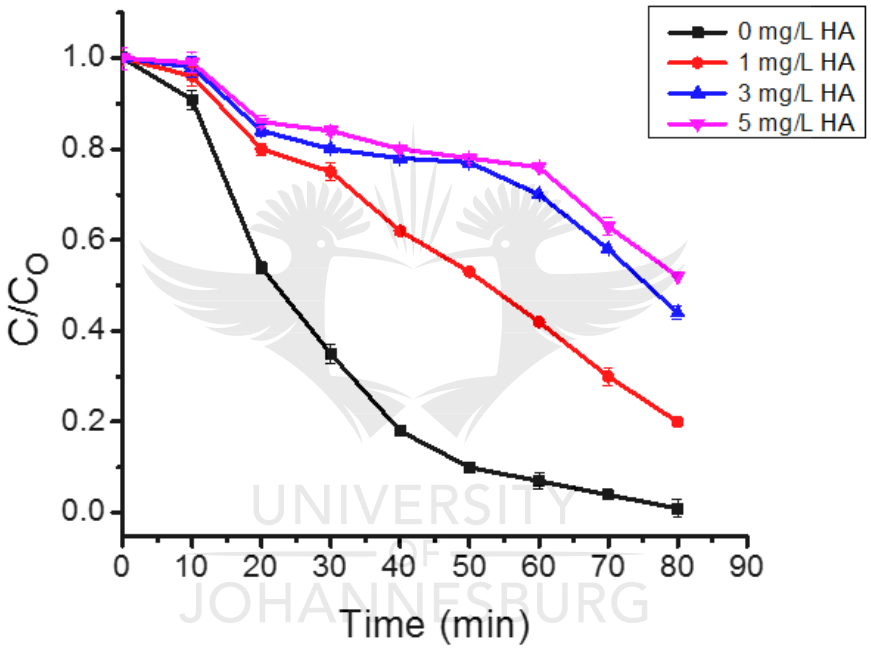

Figure 4. 15: Effect of humic acid concentration on the photodegradation of BPA by PANI-TiO_2.

The highest inhibition was observed with the addition of 5 mg/L. The inhibition was attributed to the blockage of the active sites by adsorbed humic acid on the PANI-TiO_2 photocatalyst [72]. Similarly, Li and Hu reported an inhibition of degradation of tetracycline in the presence of humic acid [73]. They concluded that humic acid quenched $OH^{\cdot}$ radicals that are critical for the degradation process.

4.5.8 By-products identification

BPA was degraded using PANI-TiO_2 and the intermediate products were identified using LC-MS. Samples were collected from the reactor at 0; 20; 60 and 120 mins of irradiation. They were filtered using a 0.45-µm filter discs. The HPLC chromatograms for BPA standard and the degradation products are shown in Figure 16a. The retention time (t_R) of BPA was shown to be at 4.4 mins which was evidenced by the single chromatogram in the samples for BPA standard and that at 0 mins irradiation time. However, after irradiation, the peak due to the parent BPA reduced in size and completely disappeared with irradiation. Subsequently, new peaks appeared in chromatograms with t_R at 1.0; 1.7; and 3.0 that were attributed to degradation products.

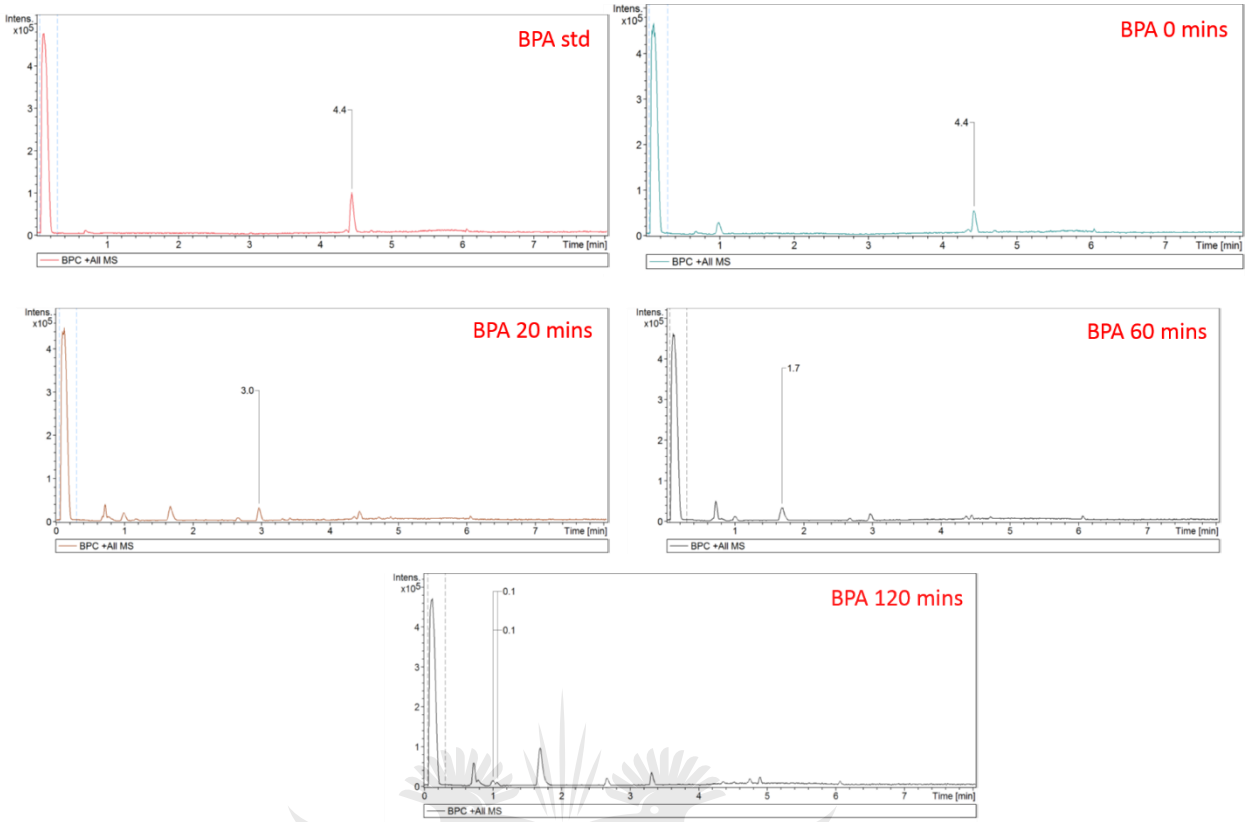

Figure 4. 16a: Chromatograms of BPA standard and samples after 0, 20, 60 and 120 mins of irradiation.

Figure 4.16b show the full mass spectra scans of the samples. The results show that BPA could be ionized in the positive mode producing a molecular ion abundance at m/z 229.1 which corresponded to the protonated BPA, $[M+H]^+$. The results show that a fragment of BPA fragment with m/z of 213.1 was produced after 20 minutes of irradiation [74]. This fragment could be attributed to the loss of a methyl group producing a carbocation, $[C_{14}H_{13}O_2^+]$. Another peak with m/z 135.1 was produced, this was attributed to $[C_9H_{11}O^+]$ which was produced as a result of the cleavage of alkyl-phenyl bond and possible degradation of BPA [74].

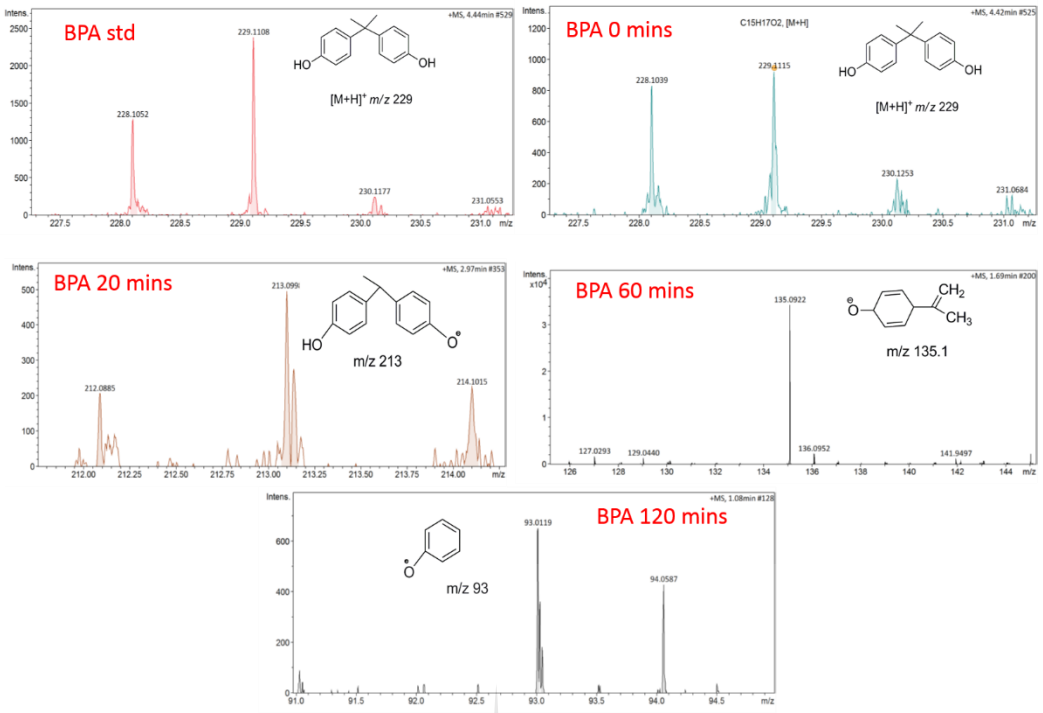

Figure 4.16b. Mass spectra of BPA standard and samples after 0, 20, 60 and 120 mins of irradiation.

A peak observed at m/z 93.1 was attributed to the cleavage of two base phenolic molecules of BPA producing a fragment with formula, C_6H_5O. These degradation products were consistent with those reported in literature [74-76].

From the observed degradation products, a degradation pathway was proposed in Figure 4.17.

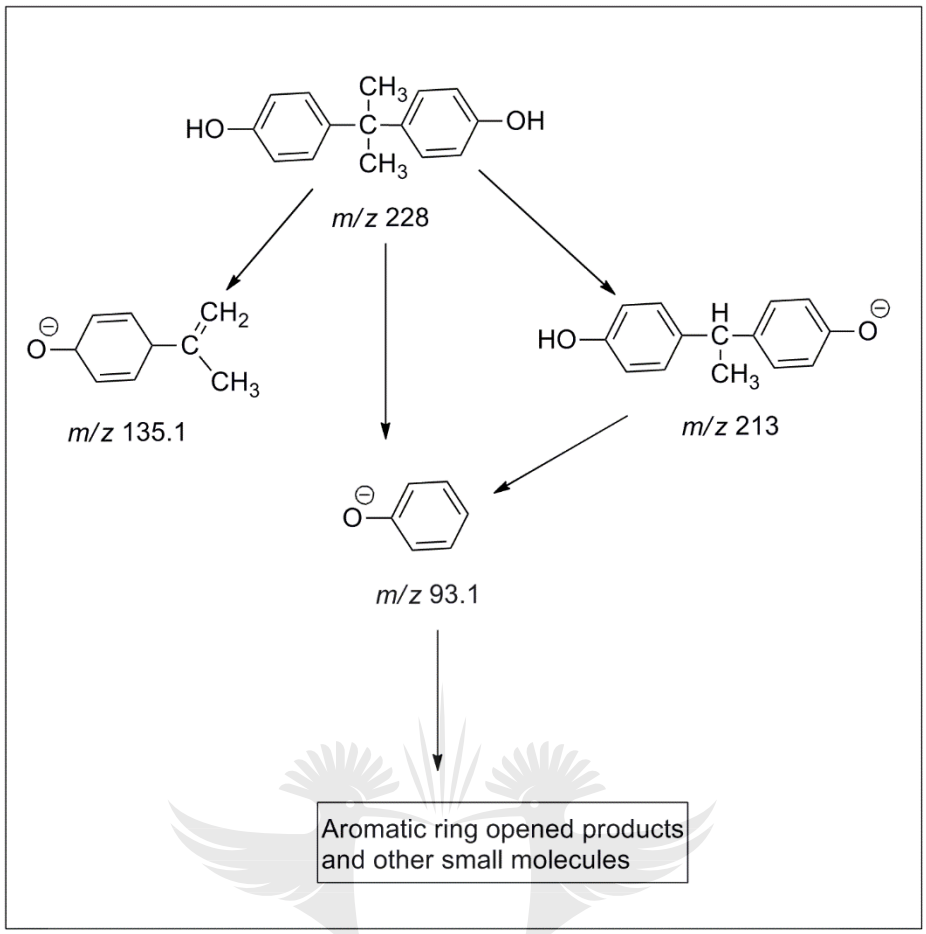

Figure 4. 17: Proposed degradation pathway for BPA using PANI-TiO_2 under UV light.

A fragment of BPA with m/z of 213.1 was formed by a loss of a methyl group from the parent BPA molecule. Another peak with m/z 135.1 was formed as a result of the cleavage of alkyl-phenyl bond. Cleavage of two base phenolic molecules of BPA producing a fragment with m/z 93.1.

4.5.9 Proposed mechanism for BPA degradation

Reactive species such as hydroxyl ($OH\cdot$), superoxide ($\cdot O^{2-}$) and holes (h^+) are responsible for the degradation process [77]. In a study, Brooms et al suggested a mechanism for the degradation of p-cresol by TiO_2/ZnO/PANI [35]. The authors suggested that PANI played an active role in the degradation of p-cresol by

TiO_2/ZnO/PANI by transferring electrons to the conduction band of TiO_2/ZnO and also trapped holes leading to charge separation [35]. In another study, Masid et al suggested the same mechanism when they used PANI-TiO_2 to degrade a dye, reactive blue 4 [77]. However, there is no experimental data to support the suggested degradation mechanisms. In this study, we provide experimental data showing which reactive oxygen species were responsible for the degradation. Different scavengers of reactive species were added to the degradation solution and the degradation performance was evaluated after irradiation at optimized conditions. In this study, potassium iodide (KI) was used to scavenge positive holes [78]. Figure 4.19 shows that only 30% degradation was achieved after the addition of potassium iodide (KI).

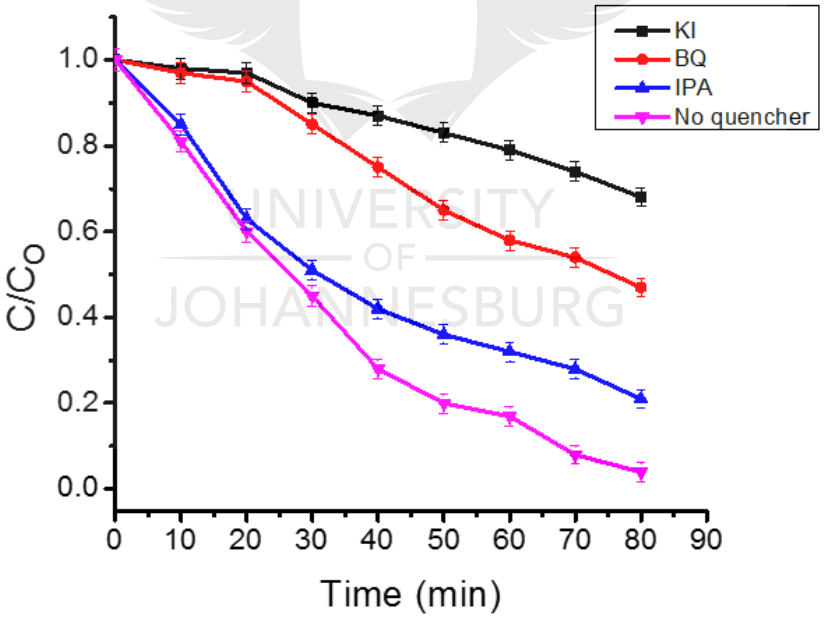

Figure 4. 18: Photodegradation of 5 ppm BPA by PANI-TiO_2 after addition of different reactive species scavengers under UV irradiation.

This suggests that the positively charged holes were actively involved in the degradation of BPA. In the presence of benzoquinone (BQ) which was used as

scavenger for superoxide radicals [79], 48% degradation was achieved which is lower than 99.8% achieved in the absence of quenchers. This suggests that the superoxide radicals were also involved in the degradation of BPA although their involvement was not as dominant as the positive holes. In the presence of 10% volume isopropyl alcohol (IPA) which was used as a scavenger for hydroxyl radicals [76], a slight decrease in the degradation efficiency with an overall degradation of 70% after 80 minutes of irradiation under UV light. This suggests that the hydroxyl radicals were not the dominant reactive species in the degradation of BPA by PANI-TiO_2.

The mechanism for the degradation of BPA was therefore proposed to occur as shown in Figure 4.19.

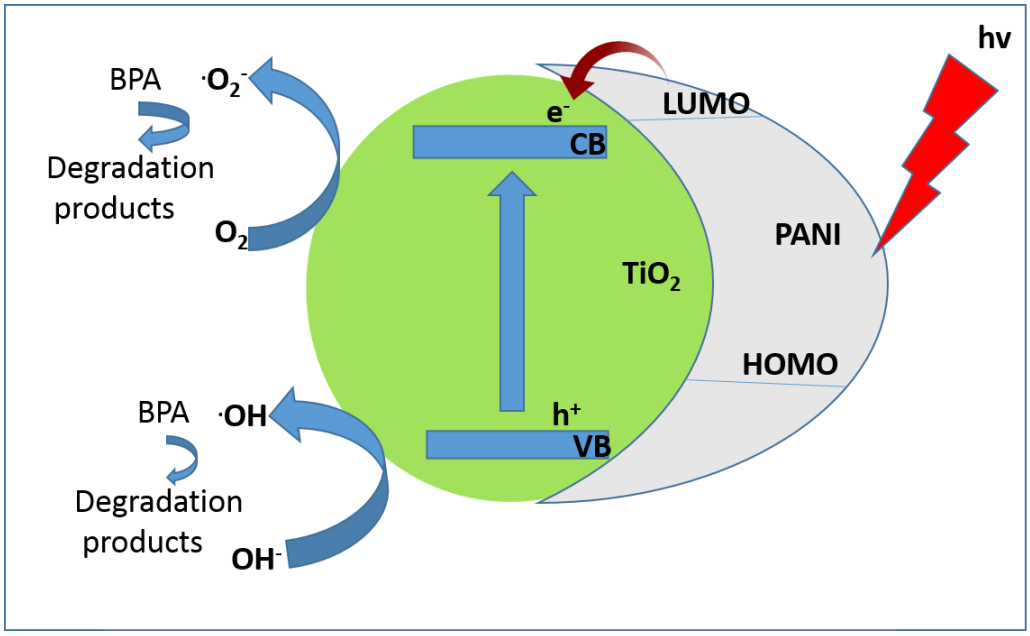

Figure 4. 19: Proposed mechanism for the degradation of BPA using PANI-TiO_2.

After absorbing UV light irradiation PANI can release electrons from the highest energy occupied molecular orbital (HOMO) into the lowest energy unoccupied molecular orbital (LUMO). PANI can transfer the photogenerated electron (e^-) into the conduction band of the TiO_2. The electrons were then scavenged by oxygen molecules forming superoxide that are highly oxidizing and they degraded BPA. Simultaneously, electrons might migrate from the VB of TiO_2 to the HOMO of PANI leaving behind positive charged holes (h+). The positive holes might react with water in the moisture, forming hydroxyl radicals that are also highly oxidizing and they degraded BPA.

4.5.10 Reuse of photocatalyst

The re-use of photocatalysts reduce the cost of the degradation process. In this study, the PANI-TiO_2 photocatalyst was separated from the BPA solution by vacuum filtration and re-used five times. The separated catalyst was washed with distilled

water and then with ethanol and dried in an oven at 60°C for 24 h. The weight loss was determined to be less than 5%. Figure 4.20 shows the degradation performance of the PANI-TiO_2 after four runs. The results show that there was very little loss of efficiency by the catalyst.

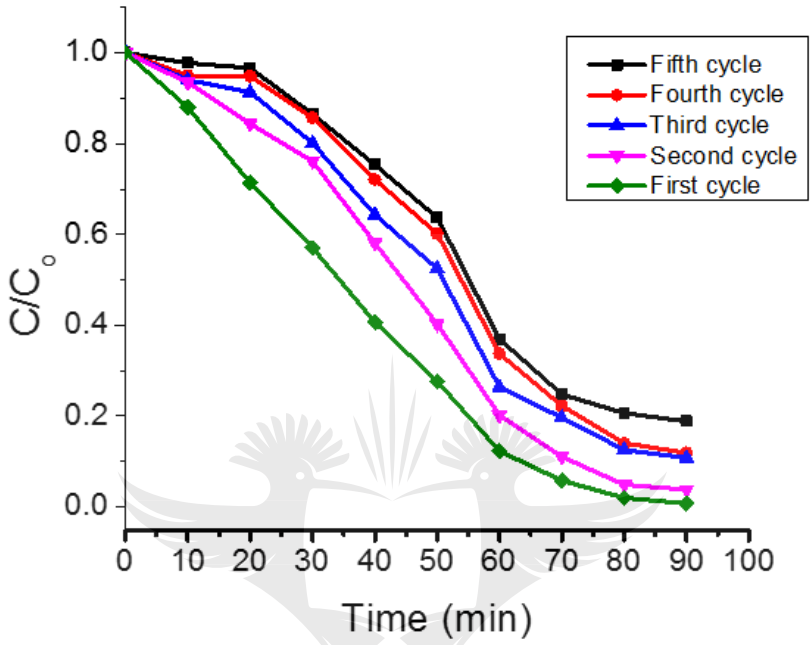

Figure 4. 20: Reuse of PANI-TiO_2 for the degradation of BPA.

PANI-TiO_2 can be re-used at least five times degrading 5 ppm of BPA with a removal efficiency of at least 80% in 90 mins of irradiation under UV light.

4.6 CONCLUSION

PANI wrapped TiO_2 nanorods were successfully synthesized by oxidative polymerization of aniline on hydrothermally pre-synthesized TiO_2 nanorods. The photodegradation of BPA under UV radiation was investigated. The use of nanostructured TiO_2 wrapped in PANI improved the photodegradation efficiency of the photocatalyst due to the synergistic effect of adsorption by PANI and photodegradation by TiO_2. PANI effected charge separation and reduced the rate of

recombination. LC-MS analysis identified degradation products with m/z 213.1, 135.1 and 93.1. In summary, we report, that the degradation of BPA using PANI-TiO_2 nanocomposite has the potential to help alleviate the threat of water contamination by BPA.

4.7 REFERENCES

[1] I. Karaouzas, E. Smeti, A. Vourka, L. Vardakas, A. Mentzafou, E. Tornes, S. Sabater, I. Munoz, N.T. Skoulikidis and E. Kalogianni. Assessing the ecological effects of water stress and pollution in a temporary river - Implications for water management. *Science Total Environment* 618 (2018) 1591-1604.

[2] D.W. Kolpin, E.T. Furlong, M.T. Meyer, E.M. Thurman, S.D. Zaugg, L.B. Barber, and H.T. Buxton. Pharmaceuticals, hormones, and other organic wastewater contaminants in U.S. Streams, 1999−2000: A national reconnaissance. *Environmental Science and Technology* 36 (2002) 1202-1211.

[3] A.M. Paz-Alberto and G.C. Sigua. Phytoremediation: A green technology to remove environmental pollutants. *American Journal of Climate Change* 2 (2013) 71.

[4] L.N. Vandenberg, R. Hauser, M. Marcus, N. Olea, and W.V. Welshons. Human exposure to bisphenol A (BPA). *Reproductive Toxicology* 24 (2007) 139-177.

[5] C. Erler and J. Novak. Bisphenol A exposure: human risk and health policy. *Journal of Pediatric Nursing* 25 (2010) 400-407.

[6] J. Rajasärkkä, M. Pernica, J. Kuta, J. Lašňák, Z. Šimek and L. Bláha. Drinking water contaminants from epoxy resin-coated pipes: A field study. *Water Research* 103 (2016) 133-140.

[7] C.A. Richter, L.S. Birnbaum, F. Farabollini, R.R. Newbold, B.S. Rubin, C.E. Talsness, J.G. Vandenbergh, D.R. Walser-Kuntz and F.S. vom Saal. In vivo effects

of bisphenol A in laboratory rodent studies. *Reproductive Toxicology* 24 (2007) 199-224.

[8] N. Milic, D. Cetojevic-Simin, M. Milanovic, J. Sudji, N. Milosevic, N. Curic, L. Abenavoli, and M. Medic-Stojanoska. Estimation of in vivo and in vitro exposure to bisphenol A as food contaminant. *Food and Chemical Toxicology* 83 (2015) 268-274.

[9] V. Le Fol, S. Ait-Aissa, M. Sonavane, J.M. Porcher, P. Balaguer, J.P. Cravedi, D. Zalko, and F. Brion. In vitro and in vivo estrogenic activity of BPA, BPF, and BPS in zebrafish-specific assays. *Ecotoxicology and Environmental Safety* 142 (2017) 150-156.

[10] F. Acconcia, V. Pallottini, and M. Marino. Molecular mechanisms of action of BPA. *Dose Response* 13 (2015) 15593258-15610582.

[11] R.K. Bhandari, S.L. Deem, D.K. Holliday, C.M. Jandegian, C.D. Kassotis, S.C. Nagel, D.E. Tillitt, F.S. vom Saal and C.S. Rosenfeld. Effects of the environmental estrogenic contaminants bisphenol A and 17α-ethinyl estradiol on sexual development and adult behaviors in aquatic wildlife species. *General and Comparative Endocrinology* 214 (2015) 195-219.

[12] A. Repossi, F. Farabegoli, T. Gazzotti, E. Zironi, and G. Pagliuca. Bisphenol A in edible part of seafood. *Italian Journal of Food Safety* 5 (2016) 5666.

[13] J.R. Koduru, L.P. Lingamdinne, J. Singh and K.-H. Choo. Effective removal of bisphenol A (BPA) from water using a goethite/activated carbon composite. *Process Safety and Environmental Protection* 103 (2016) 87-96.

[14] S. Yüksel, N. Kabay, and M. Yüksel. Removal of bisphenol A (BPA) from water by various nanofiltration (NF) and reverse osmosis (RO) membranes. *Journal of Hazardous Materials* 263 (2013) 307-310.

[15] S. Malato, P. Fernández-Ibáñez, M.I. Maldonado, J. Blanco, and W. Gernjak. Decontamination and disinfection of water by solar photocatalysis: Recent overview and trends. *Catalysis Today* 147 (2009) 1-59.

[16] M. Zielińska, K. Bułkowska, A. Cydzik-Kwiatkowska, K. Bernat and I. Wojnowska-Baryła. Removal of bisphenol A (BPA) from biologically treated wastewater by microfiltration and nanofiltration. *International Journal of Environmental Science and Technology* 13 (2016) 2239-2248.

[17] P. Schröder, J. Navarro-Aviñó, H. Azaizeh, A.G. Goldhirsh, S. DiGregorio, T. Komives, G. Langergraber, A. Lenz, E. Maestri, A.R. Memon, A. Ranalli, L. Sebastiani, S. Smrcek, T. Vanek, S. Vuilleumier, and F. Wissing. Using phytoremediation technologies to upgrade waste water treatment in Europe. *Environmental Science and Pollution Research - International* 14 (2007) 490-497.

[18] R. Reif, S. Suárez, F. Omil, and J.M. Lema. Fate of pharmaceuticals and cosmetic ingredients during the operation of a MBR treating sewage. *Desalination* 221 (2008) 511-517.

[19] M. Wang, J. Ioccozia, L. Sun, C. Lin and Z. Lin. Inorganic-modified semiconductor TiO_2 nanotube arrays for photocatalysis. *Energy and Environmental Science* 7 (2014) 2182-2202.

[20] K. Kalyanasundaram. Photochemical applications of solar energy: photocatalysis and photodecomposition of water. in Photochemistry: Volume 41. *The Royal Society of Chemistry*, (2013) 182-265.

[21] P.A. Zapata, F.M. Rabagliati, I. Lieberwirth, F. Catalina and T. Corrales. Study of the photodegradation of nanocomposites containing TiO_2 nanoparticles dispersed in polyethylene and in poly(ethylene-co-octadecene). *Polymer Degradation and Stability* 109 (2014) 106-114.

[22] O. Bechambi, S. Sayadi, and W. Najjar. Photocatalytic degradation of bisphenol A in the presence of C-doped ZnO: Effect of operational parameters and photodegradation mechanism. *Journal of Industrial and Engineering Chemistry* 32 (2015) 201-210.

[23] E. Bilgin Simsek, B. Kilic, M. Asgin and A. Akan. Graphene oxide based heterojunction TiO_2–ZnO catalysts with outstanding photocatalytic performance for bisphenol-A, ibuprofen, and flurbiprofen. *Journal of Industrial and Engineering Chemistry* 59 (2018) 115-126.

[24] P.V.L. Reddy, K.H. Kim, B. Kavitha, V. Kumar, N. Raza, and S. Kalagara. Photocatalytic degradation of bisphenol A in aqueous media: A review. *Journal of Environmental Management* 213 (2018) 189-205.

[25] W. Wu, G. Shan, S. Wang, L. Zhu, L. Yue, Q. Xiang, Y. Zhang and Z. Li. Environmentally relevant impacts of nano-TiO_2 on abiotic degradation of bisphenol A under sunlight irradiation. *Environmental Pollution* 216 (2016) 166-172.

[26] Y. Li, L. Liu, M. Guo, and M. Zhang. Synthesis of TiO_2 visible light catalysts with controllable crystalline phase and morphology from Ti-bearing electric arc furnace molten slag. *Journal of Environmental Sciences* 47 (2016) 14-22.

[27] W.J. Ong, L.L. Tan, S.P. Chai, S.T. Yong and A.R. Mohamed. Highly reactive {001} facets of TiO_2-based composites: synthesis, formation mechanism and characterization. *Nanoscale* 6 (2014) 1946-2008.

[28] C. Yang, W. Dong, G. Cui, Y. Zhao, X. Shi, X. Xia, B. Tang, and W. Wang. Enhanced photocatalytic activity of PANI/TiO_2 due to their photosensitization-synergetic effect. *Electrochimica Acta* 247 (2017) 486-495.

[29] J. Kavil, S.G. Ullattil, A. Alshahrie, and P. Periyat. Polyaniline as photocatalytic promoter in black anatase TiO_2, *Solar Energy* 158 (2017) 792-796.

[30] X. Tan, J. Wang, X. Pang, L. Liu, Q. Sun, Q. You, F. Tan and N. Li. Indocyanine green-loaded silver nanoparticle@polyaniline core/shell theranostic nanocomposites for photoacoustic/near-infrared fluorescence imaging-guided and single-light-triggered photothermal and photodynamic therapy. *American Chemistry Society Applied Materials and Interfaces* 8 (2016) 34991-35003.

[31] X. Chen, H. Li, H. Wu, Y. Wu, Y. Shang, J. Pan and X. Xiong. Fabrication of TiO_2@PANI nanobelts with the enhanced absorption and photocatalytic performance under visible light. *Materials Letters* 172 (2016) 52-55.

[32] Y. Zheng, C. Chen, Y. Zhan, X. Lin, Q. Zheng, K. Wei, J. Zhu, and Y. Zhu. Luminescence and photocatalytic activity of ZnO nanocrystals: Correlation between structure and property. *Inorganic Chemistry* 46 (2007) 6675-6682.

[33] J. Kavil, S. Ullattil, A. Alshahrie, and P. Periyat. Polyaniline as photocatalytic promoter in black anatase TiO_2 *Solar Energy* 158 (2017) 792-796.

[34] M. Bhaumik, A. Maity, V.V. Srinivasu, and M.S. Onyango. Removal of hexavalent chromium from aqueous solution using polypyrrole-polyaniline nanofibers. *Chemical Engineering Journal* 181-182 (2012) 323-333.

[35] T.J. Brooms, B. Otieno, M.S. Onyango, and A. Ochieng. Photocatalytic degradation of P-cresol using TiO_2/ZnO hybrid surface capped with polyaniline. *Journal of Environmental Science and Health, Part A* 53 (2018) 99-107.

[36] K.P. Sandhya, S. Haridas, and S. Sugunan. Visible light induced photocatalytic activity of polyaniline modified TiO_2 and Clay-TiO_2 composites. 2013 (2013) 9.

[37] M. Sboui, M.F. Nsib, A. Rayes, M. Swaminathan, and A. Houas. TiO_2–PANI/Cork composite: A new floating photocatalyst for the treatment of organic

pollutants under sunlight irradiation. *Journal of Environmental Sciences* 60 (2017) 3-13.

[38] P.R. Deshmukh, S.V. Patil, R.N. Bulakhe, S.N. Pusawale, J.-J. Shim and C.D. Lokhande. Chemical synthesis of PANI–TiO_2 composite thin film for supercapacitor application. *The Royal Society of Chemisty Advances* 5 (2015) 68939-68946.

[39] C.T. Fleaca, M. Scarisoreanu, I. Morjan, C. Luculescu, A.M. Niculescu, A. Badoi, E. Vasile and G. Kovacs. Laser oxidative pyrolysis synthesis and annealing of TiO_2 nanoparticles embedded in carbon–silica shells/matrix. *Applied Surface Science* 336 (2015) 226-233.

[40] T. Ohsaka, F. Izumi and Y. Fujiki. Raman spectrum of anatase, TiO_2, *Journal of Raman Spectroscopy* 7 (1978) 321-324.

[41] J. Cambedouzou, J.L. Sauvajol, A. Rahmani, E. Flahaut, A. Peigney, and C. Laurent. Raman spectroscopy of iodine-doped double-walled carbon nanotubes. *Physical Review B* 69 (2004) 235422.

[42] Y. Haldorai, V.H. Nguyen and J.-J. Shim. Synthesis of polyaniline/Q-CdSe composite via ultrasonically assisted dynamic inverse emulsion polymerization. *Colloid and Polymer Science* 289 (2011) 849-854.

[43] D.A. Erdogan and E. Ozensoy. Hierarchical synthesis of corrugated photocatalytic TiO_2 microsphere architectures on natural pollen surfaces. *Applied Surface Science* 403 (2017) 159-167.

[44] N. Tamura and P.U.P.A. Gilbert. Chapter twenty-one - X-Ray microdiffraction ofbiominerals. in Methods in Enzymology. J.J. De Yoreo Editor. *Academic Press*, (2013) 501-531.

[45] S.A. Speakman. Estimating crystallite size using XRD. MIT Center for Materials Science and Engineering (2014)

[46] Y. Chen, K. Wang and L. Lou. Photodegradation of dye pollutants on silica gel supported TiO_2 particles under visible light irradiation. Journal of *Photochemistry and Photobiology A: Chemistry* 163 (2004) 281-287.

[47] F. Amano, E. Ishinaga and A. Yamakata. Effect of particle size on the photocatalytic activity of WO_3 particles for water oxidation. *The Journal of Physical Chemistry C* 117 (2013) 22584-22590.

[48] H.S.M. Tabaei, M. Kazemeini, and M. Fattahi. Preparation and characterization of visible light sensitive nano titanium dioxide photocatalyst. *Scientia Iranica* 19 (2012) 1626-1631.

[49] H. Ruiz, M. Zambtrano, L. Giraldo, R. Sierra and J.C. Moreno-Pirajan. Production and characterization of activated carbon from oil-palm shell for carboxylic acid adsorption. *Oriental Journal of Chemistry* 31 (2015) 753-762.

[50] S.S. Sambaza, M.L. Masheane, S.P. Malinga, E.N. Nxumalo and S.D. Mhlanga. Polyethyleneimine-carbon nanotube polymeric nanocomposite adsorbents for the removal of Cr^{6+} from water. *Physics and Chemistry of the Earth, Parts A/B/C* 100 (2017) 236-246.

[51] F.-L. Mi, S.-J. Wu and F.-M. Lin. Adsorption of copper(II) ions by a chitosan–oxalate complex biosorbent. *International Journal of Biological Macromolecules* 72 (2015) 136-144.

[52] C. Ravidhas, A.J. Josephine, P. Sudhagar, A. Devadoss, C. Terashima, K. Nakata, A. Fujishima, A.M.E. Raj and C. Sanjeeviraja. Facile synthesis of nanostructured monoclinic bismuth vanadate by a co-precipitation method:

structural, optical and photocatalytic properties. *Materials Science in Semiconductor Processing* 30 (2015) 343-351.

[53] X. Sun, L. Yang, Q. Li, Z. Liu, T. Dong, and H. Liu. Polyethylenimine-functionalized poly(vinyl alcohol) magnetic microspheres as a novel adsorbent for rapid removal of Cr(VI) from aqueous solution. *Chemical Engineering Journal* 262 (2015) 101-108.

[54] M.M. Ba-Abbad, A.A.H. Kadhum, A.B. Mohamad, M.S. Takriff and K. Sopian. Synthesis and catalytic activity of TiO_2 nanoparticles for photochemical oxidation of concentrated chlorophenols under direct solar radiation. *International Journal of Electrochemical Science* 7 (2012) 4871-4888.

[55] K. Gurushantha, L. Renuka, K.S. Anantharaju, Y.S. Vidya, H.P. Nagaswarupa, S.C. Prashantha and H. Nagabhushana. Photocatalytic and photoluminescence studies of ZrO_2 /ZnO nanocomposite for LED and Waste water treatment applications. *Materials Today: Proceedings* 4 (2017) 11747-11755.

[56] R. Ye and A. Barron. Photoluminescence spectroscopy and its applications. Retrieved from the OpenStax-CNX Web site: http://cnx. org/content/m38357/1.2 (2011)

[57] M. Omaish Ansari, M.M. Khan, S. Ansari, K. Raju, J. Lee, and M.H. Cho. Enhanced thermal stability under DC electrical conductivity retention and visible light activity of Ag/TiO_2@polyaniline nanocomposite film, *ACS Applied Materials and Interface* 11 (2014) 8124-8133.

[58] N. Parveen, M.O. Ansari, T.H. Han, and M.H. Cho. Simple and rapid synthesis of ternary polyaniline/titanium oxide/graphene by simultaneous TiO_2 generation and aniline oxidation as hybrid materials for supercapacitor applications. *Journal of Solid State Electrochemistry* 21 (2017) 57-68.

[59] S. Golczak, A. Kanciurzewska, M. Fahlman, K. Langer and J.J. Langer. Comparative XPS surface study of polyaniline thin films. *Solid State Ionics* 179 (2008) 2234-2239.

[60] N.T.T. Linh, P.D. Tuan, and N.V. Dzung. The shifts of band gap and binding energies of titania/hydroxyapatite material. *Journal of Composites* 2014 (2014) 1-5.

[61] U.A. Qureshi, I.H. Gubbuk, M. Ersoz, A.R. Solangi, S.I.H. Taqvi, and S.Q. Memon. Preparation of polyaniline montmorillonite clay composites for the removal of diethyl hexyl phthalate from aqueous solutions. *Separation Science and Technology* 51 (2016) 214-228.

[62] J.-C. Chou and L.P. Liao. Study on pH at the point of zero charge of TiO_2 pH ion-sensitive field effect transistor made by the sputtering method. *Thin Solid Films 476* (2005) 157-161.

[63] Y. Park, Z. Sun, G.A. Ayoko and R.L. Frost. Bisphenol A sorption by organo-montmorillonite: implications for the removal of organic contaminants from water. *Chemosphere* 107 (2014) 249-256.

[64] J. Zhang and Y. Nosaka. Mechanism of the OH radical generation in photocatalysis with TiO_2 of different crystalline types. *The Journal of Physical Chemistry C* 118 (2014) 10824-10832.

[65] K. Porkodi and K.V. Kumar. Comments on" photocatalytic properties of TiO_2 modified with platinum and silver nanoparticles in the degradation of oxalic acid in aqueous solution" Langmuir Hinshelwood kinetics-A theoretical study. *Applied Catalysis B: Environmental* 79 (2008) 108-109.

[66] C.S. Blaszczak-Boxe and A. Saiz-Lopez. Nitrate photolysis in ice and snow: A critical review of its multiphase chemistry. *Atmospheric Environment* 193 (2018) 224-241.

[67] M. Zhan, X. Yang, Q. Xian, and L. Kong. Photosensitized degradation of bisphenol A involving reactive oxygen species in the presence of humic substances. *Chemosphere* 63 (2006) 378-386.

[68] J. Mack and J.R. Bolton. Photochemistry of nitrite and nitrate in aqueous solution: a review. *Journal of Photochemistry and Photobiology A: Chemistry* 128 (1999) 1-13.

[69] T.F. Guetzloff and J.A. Rice. Does humic acid form a micelle? *Science of the Total Environment* 152 (1994) 31-35.

[70] B.R. Lim, S.-H. Do and S.-H. Hong. The impact of humic acid on the removal of bisphenol A by adsorption and ozonation. *Desalination and Water Treatment* 54 (2015) 1226-1232.

[71] Y. Liang, D.W. Britt, J.E. McLean, D.L. Sorensen and R.C. Sims. Humic acid effect on pyrene degradation: finding an optimal range for pyrene solubility and mineralization enhancement. *Applied Microbiology and Biotechnology* 74 (2007) 1368-1375.

[72] S. Li and J. Hu. Photolytic and photocatalytic degradation of tetracycline: Effect of humic acid on degradation kinetics and mechanisms. *Journal of Hazardous Materials* 318 (2016) 134-144.

[73] D. Voutsa. Analytical methods for determination of bisphenol A. in Plastics in Dentistry and Estrogenicity*. Springer*, (2014) 51-77.

[74] S. Majedi and E. Lai. Mass spectrometric analysis of bisphenol A desorption from titania nanoparticles: Ammonium acetate, fluoride, formate, and hydroxide as chemical desorption agents. *Methods and Protocols* 1 (2018) 26.

[75] H. Zhao, L. Xiang, J. Li, Z. Yang, J. Fang, C. Zhao, S. Xu and Z. Cai. Investigation on fragmentation pathways of bisphenols by using electrospray

ionization Orbitrap mass spectrometry. *Rapid Communications in Mass Spectrometry* 30 (2016) 1901-1913.

[76] F. Torki and H. Faghihian. Visible light degradation of naproxen by enhanced photocatalytic activity of NiO and NiS, scavenger study and focus on catalyst support and magnetization. *Photochemistry and Photobiology* 94 (2018) 491-502.

[77] S. Masid, R. Tayade and N. Rao. Efficient visible light active polyaniline/TiO_2 nanocomposite photocatalyst for degradation of Reactive Blue 4. *International Journal of Photocatal Photon* 119 (2014) 190-203.

[78] S. Naraginti, Y. Li, Y. Wu, C. Zhang and A.R. Upreti. Mechanistic study of visible light driven photocatalytic degradation of EDC 17α-ethinyl estradiol and azo dye Acid Black-52: phytotoxicity assessment of intermediates. *The Royal Society of Chemistry Advances* 6 (2016) 87246-87257.

[79] M. Pelaez, P. Falaras, V. Likodimos, K. O'Shea, A. Armah, P.S. Dunlop, J.A. Byrne and D.D. Dionysiou. Use of selected scavengers for the determination of NF-TiO_2 reactive oxygen species during the degradation of microcystin-LR under visible light irradiation. *Journal of Molecular Catalysis A: Chemical* 425 (2016) 183-189.

CHAPTER 5:

VISIBLE LIGHT PHOTODEGRADATION OF IBUPROFEN BY PANI CAPPED WO_3@TiO_2 NANOCOMPOSITE IN WATER

5.0 INTRODUCTION

Water is indispensable for life sustenance. In fact, water is imperative in ensuring food security, good public health, and the generation of energy for industrial growth [1, 2]. Due to the rapid growth in industrial activities and a surge in population growth, pressures on freshwater supply are increasing due to the mounting demands for the sustenance of industrial activities as well as agriculture. Furthermore, freshwater supply is further curbed by increasing pollution [3]. Emerging pollutants are among the key sources of water contamination [4-6]. In recent years, their presence in water sources has increased concerns due to potential adverse ecotoxicological effects [7]. Emerging pollutants are defined as a new class of pollutants without regulatory status and whose impact on the environment and human health is poorly understood [5]. Among the emerging pollutants, pharmaceuticals are of particular concern due to their massive production, usage as well as their biochemical activities [8]. Ibuprofen is one of these emerging pharmaceutical pollutants, which is widely applied as used non-steroidal drugs for the relief of pain and treatment of inflammations. It has since caused concerns due to its negative impacts on living organisms [9]. Its presence and its metabolites in water habitats implies a potential for indirect human exposure via drinking water supplies. Ibuprofen enters water bodies during the manufacturing process as pharmaceutical industrial waste, hospital waste, therapeutic drugs and

via faeces or urine [10, 11]. The reported presence of ibuprofen in the environment has raised alarms due to its reported endocrine disrupting activities.

In order to meet the undeniable need for clean freshwater, water purification has become increasingly important for life. To date, various methods have been reported for the removal of pharmaceuticals from wastewater. These include adsorption, biological treatment, chemical oxidation, and advanced oxidation processes [12-14]. Amongst the advanced oxidation treatment methods, photocatalysis using semiconductor materials has been reported as an effective method for the elimination of pharmaceuticals from aqueous media. Photocatalysis is based on the ability of a semiconductor material to adsorb a photon of energy that is equal to or greater than its band gap energy [15]. This process results in the generation of charges that can be manipulated to degrade organic pollutants such as ibuprofen.

Amongst the several photocatalysts that have been applied to degrade organic contaminants, TiO_2 has shown great potential for water remediation due to its attractive properties such as strong oxidizing power, large surface area, corrosion resistance, non-toxicity, and cost effectiveness [16, 17]. However, its use has been limited due to the high recombination rate of charges. Pairing of TiO_2 with low band gap semiconductors has been reported to greatly improve the separation of charges and improved the overall catalytic performance of the nanocomposites. For example, $BiVO_4/TiO_2$ particles synthesized via a combination of sol gel and hydrothermal techniques showed better performance in degrading gaseous benzene under ultraviolet radiation than pristine $BiVO_4$ and TiO_2 [18]. The improvement was attributed to charge separation due to the heterojunction nanocomposite.

More recently, surface modification of TiO_2 with conducting polymers such as polyaniline (PANI) and polypyrrole (Ppy) has been reported to improve the performance of the photocatalyst by effecting charge separation. In a study, hierarchical 3D flowerlike TiO_2/PANI photocatalysts synthesized via a simple sol−gel method showed improved photocatalytic degradation of methyl orange under UV radiation when compared to pristine TiO_2 [19]. In another study, PPy–TiO_2 nanocomposites showed a better photocatalytic activity for the degradation of methyl orange than that of virgin TiO_2 nanoparticles under sunlight. The authors attributed this improvement to the sensitizing effect of polypyrrole [20]. Hence in this study, the degradation of ibuprofen using a novel PANI capped WO_3/TiO_2 nanocomposite under visible light radiation is reported.

5.0 MATERIALS AND METHODS

5.1.1 Reagents and instrumentation

All chemicals used in present research were of AR grade. Titanium isopropoxide (TTIP), Isopropyl alcohol, acetic acid, sodium hydroxide (NaOH), nitric acid (HNO_3), Iron(III) chloride ($FeCl_3$), aniline, Ibuprofen, Methanol (HPLC Grade), Acetonitrile (HPLC Grade), Sodium tungstate dihydate ($Na_2WO_4.2H_2O$), ethylene glycol (E.G), hydrochloric acid, ethanol and acetone were acquired from Sigma Aldrich and used without further purification. Ultrapure water was obtained from a Merck water system (MiliQ).

A Physical Electronics (PHI) Quantum 200 XPS spectrophotometer with Al Kα as the excitation source was used to measure the surface characterization and chemical states of materials. X-ray diffraction was carried out using a Philips, X"Pert PRO MPD X-ray diffractometer. The surface area, pore volume, and pore size were

determined using a Micromeritics ASAP 2020, Brunauer-Emmett-Teller analyzer (Norcross, USA). Raman spectra were taken using a WITec Confocal Raman Microscope. Ultraviolet−visible diffuse absorbance and reflectance spectra (DRS) were measured using a Shimadzu 1700 UV spectrophotometer. The morphology and elemental composition of materials was done by a VEGA3 TESCAN (Bruno, Czech Republic) scanning electron microscope. In-depth analysis of the morphology of materials was done using a JEOL JEM-2100 transmission electron microscopy (TEM) electron microscope (Peabody, Massachusetts, USA) and the images were collected by Gaitan Digital Imaging software. Thermogravimetric analysis (TGA), was conducted using a STA 7200RV HITACHI thermogravimetric analyzer. Photoluminescence measurements were performed using a Perkin Elmer LS45 Fluorescence Spectrometer. The concentration of ibuprofen was measured using a 1260 Infinity Agilent Technologies high performance liquid chromatography.

5.1.2 Synthesis of WO_3 nanocomposites

WO_3 nanosphere-like structures were synthesized using a solvothermal method. Typically, 0.05 mmol of sodium tungstate dihydrate was dissolved in a mixture of E.G and water in the ratio (1:2.5) under vigorous stirring at 75°C. 5 mL of HCl (12.0 M) was slowly added to the solution under stirring resulting in a yellow precipitate. After aging for an hour at 75°C, the mixture was transferred to a teflon vessel and heated in an autoclave at 180°C for 12 hrs. After cooling, the yellow precipitate was washed with distilled water until ~pH 7. It was washed with ethanol, distilled and then dried in an oven at 60°C and then calcined at 450°C in a muffle furnace in air.

5.1.3 Synthesis of TiO_2 nanorods

TiO_2 nanorods were synthesized using a hydrothermal method. Typically, 5 mL of TTIP was dissolved in a mixture of Isopropyl alcohol and water (5:3). The solution was poured into a 100 ml beaker and stirred. Concentrated acetic acid (6 mL) was added to the solution whilst stirring. The solution was stirred for 3 h. and heated to 180°C in an autoclave for 24 hr. The solution was then cooled at room temperature and then washed with excess ethanol to yield a white precipitate. The precipitate was washed with distilled water until ~pH 7. The precipitate was then dried in an oven at 60°C and then calcined at 500°C in a muffle furnace in air producing TiO_2 nanoparticles. TiO_2 nanoparticles were then dispersed in 10 M NaOH solution and stirred until homogeneity was achieved. The mixture was placed in a teflon lined autoclave and then heated to 180°C in an autoclave for 24 hr. The solution was then cooled at room temperature and then washed with dilute HNO_3 and then with distilled water until ~ pH 7. The precipitate was then dried in an oven at 60°C and calcined at 500°C in a muffle furnace in air producing TiO_2 nanorods.

5.1.4 Synthesis of WO_3@TiO_2 nanocomposite

WO_3 nanosphere-like structures were grown on TiO_2 nanorods following a two-step process. Typically, TiO_2 nanorods (1 g) were dispersed in a 30 mL mixture of E.G and water in the ratio (1:2.5) under vigorous stirring at 75°C. Sodium tungstate dehydrate (0.3 g) was added to the beaker and 5 mL of HCl (12.0 M) was slowly added to the solution under stirring resulting in a yellow precipitate. After aging for an hour at 75°C, the mixture was transferred to a Teflon vessel and heated in an autoclave at 180°C for 12 h. After cooling, the yellowish white precipitate was washed with distilled water until ~pH 7. It was then washed with ethanol, distilled

and dried in an oven at 60°C and calcined at 450°C in a muffle furnace in air producing WO_3/TiO_2.

5.1.5 Synthesis of PANI/WO_3@TiO_2 nanocomposite

PANI/WO_3@TiO_2 nanocomposite was synthesized by dispersing the WO_3@TiO_2 nanocomposite in 80 mL of water and 0.2 mL of aniline monomer was added followed by 6 g of $FeCl_3$. The mixture was stirred for 5 min and aged for 24 hr without stirring. The mixture was then washed with acetone to remove unreacted oligomers followed by washing with distilled water until a ~pH 7. The product was then dried in an oven at 60°C for 24 hrs.

5.2 CHARACTERIZATION TECHNIQUES

A Shimadzu UV spectrophotometer was used to record the diffuse reflectance spectra (DRS) in the range of 190–900 nm. In the analysis potassium bromide (KBr) powder was used a reference. The functional groups of the materials were analyzed by Fourier transform infrared (FTIR) spectra were recorded from 400–4000 cm^{-1} using KBr pellets. Surface area and porosity of the nanocomposites were analyzed using a Brunauer Emmett Teller (BET) surface area analyzer (ASAP 2020, Micromeritics Instruments, USA) using N_2 adsorption and desorption isotherms. The structural properties were analyzed by X-ray diffraction (XRD) (Philips, X'Pert PRO MPD, mineral powder diffraction) analysis that was carried to investigate the crystallinity of the nanocomposite. The instrument uses an X-Ray source of Cu α-radiation beam with excitation wavelength of 0.15406 nm for the analysis. Raman spectra were collected from a Perkin Elmer Raman Microscope 200. The morphology of the materials were analyzed using a JEOL JEM-2100 transmission electron microscopy (TEM) and a scanning electron microscopy (SEM).

5.3 PHOTOCATALYTIC DEGRADATION STUDIES

The photodegradation studies were carried out by dispersing 0.1 g of photocatalyst in 500 mL of 5 mg/L ibuprofen solution. The photodegradation activity was investigated as a function of time. The photocatalytic experiments were conducted in a reactor in which the samples were kept under agitation. In the experiments to determine the effect of the initial solution pH on the degradation of Ibuprofen, 0.1 M HCl or 0.1 M NaOH solutions were used to adjust the pH. The suspension was magnetically stirred in the dark for 30 min to ensure the adsorption equilibrium of Ibuprofen on the catalyst. The mixture was irradiated with a 250 W Xenon lamp. At varied time intervals, aliquots (10 mL) were removed from the sample and filtered through 0.45 µm membranes filter discs.

Ibuprofen analysis was conducted using an Agilent high-performance liquid chromatography (HPLC). The mobile phase was composed of a mixture of water adjusted to pH 2.5 with phosphoric acid and acetonitrile (40/60, v/v). A C18 reversed-phase column (4.6 nm × 150 nm) was used for chromatographic analysis and elution time of 15 min, and a detector wavelength of 220 nm. All measurements of the ibuprofen degradation at different irradiation times were performed three times to confirm their reproducibility. The effect of pH was determined at pH 3.5, solution pH 5.8 and pH 9 using 0.1 g photocatalyst in 500 mL of 5 mg/L ibuprofen solution. Similarly, the effect of photocatalyst dosage was investigated for the photodegradation of ibuprofen by varying the mass of the photocatalyst from 10 mg to 250 mg in a 500 mL of 5 mg/L ibuprofen solution. The effect of initial ibuprofen concentration was investigated at different initial ibuprofen concentration from 1 ppm to 30 ppm. The presented data points are mean values. The removal efficiency of ibuprofen was calculated as follows:

$$\% \, Removal = \frac{C_i - C_f}{C_i} x \, 100 \qquad 5.1$$

where C_i (mg/L) is initial concentration of adsorbate in solution, C_f (mg/L) is the final concentration of adsorbate in the filtrate.

5.4 CHARACTERIZATION OF THE PHOTOCATALYSTS

5.4.1 FTIR analysis

In the FTIR spectrum of pristine TiO_2 (Figure 5.1) the broad absorption peak at 700 cm^{-1} corresponds to Ti-O-Ti vibrational frequencies [21].

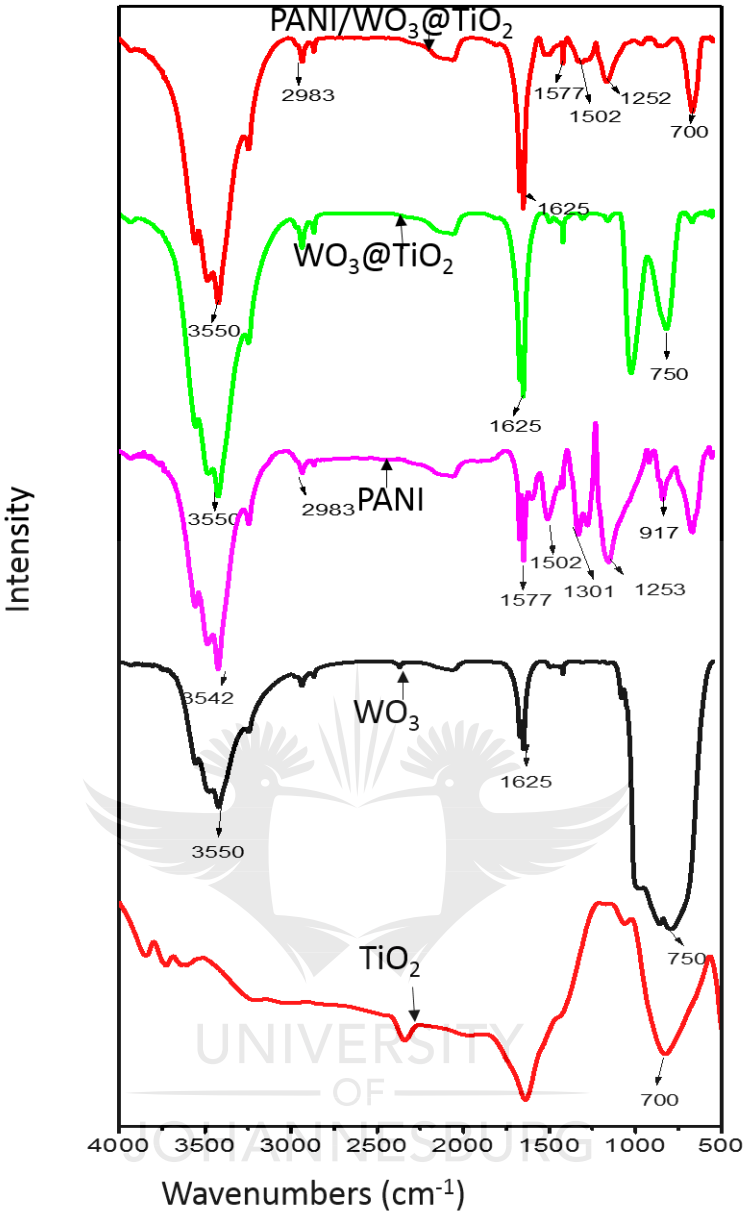

Figure 5. 1: FTIR spectra of pristine TiO_2, pristine WO_3, pristine PANI, WO_3@TiO_2, and PANI/WO_3@TiO_2.

The strong absorption peak for pristine WO_3 in the range 650–950 cm^{-1} is due to the stretching modes of O-W-O bonds. The peak at 1625 cm^{-1} is due to the W-O bending mode. The wide band in the region of 3200–3600 cm^{-1} is ascribed to the W-OH stretching [22]. FTIR spectroscopy analysis confirmed the incorporation of PANI into a nanocomposite of PANI/WO_3@TiO_2 as shown by the functional groups

of PANI that are present in the PANI/WO_3@TiO_2 nanocomposite. The main peaks of PANI were all confirmed in the spectra (b) with peaks appearing at 3662 cm^{-1}, 2955 cm^{-1}, 1577 cm^{-1}, 1502 cm^{-1}, 1250 cm^{-1} and 827 cm^{-1} [23-25]. The band at 3662 cm^{-1} corresponds to the N-H stretching mode and the peak around 2955 cm^{-1} correspond to the aromatic C-H vibration [26]. The peaks appearing at 1577 cm^{-1} and 1502 cm^{-1} are due the C=C and C=N stretch of the benzoid and quinoid respectively (Figure 5.1).

5.4.2 Raman analysis

The Raman spectrum revealed that the anatase phase of TiO_2 was synthesized as shown by the typical peaks of anatase TiO_2 that appeared at 637 cm^{-1}, 514 cm^{-1}, 396 cm^{-1} and 195 cm^{-1} [27, 28] as shown in Figure 5.2.

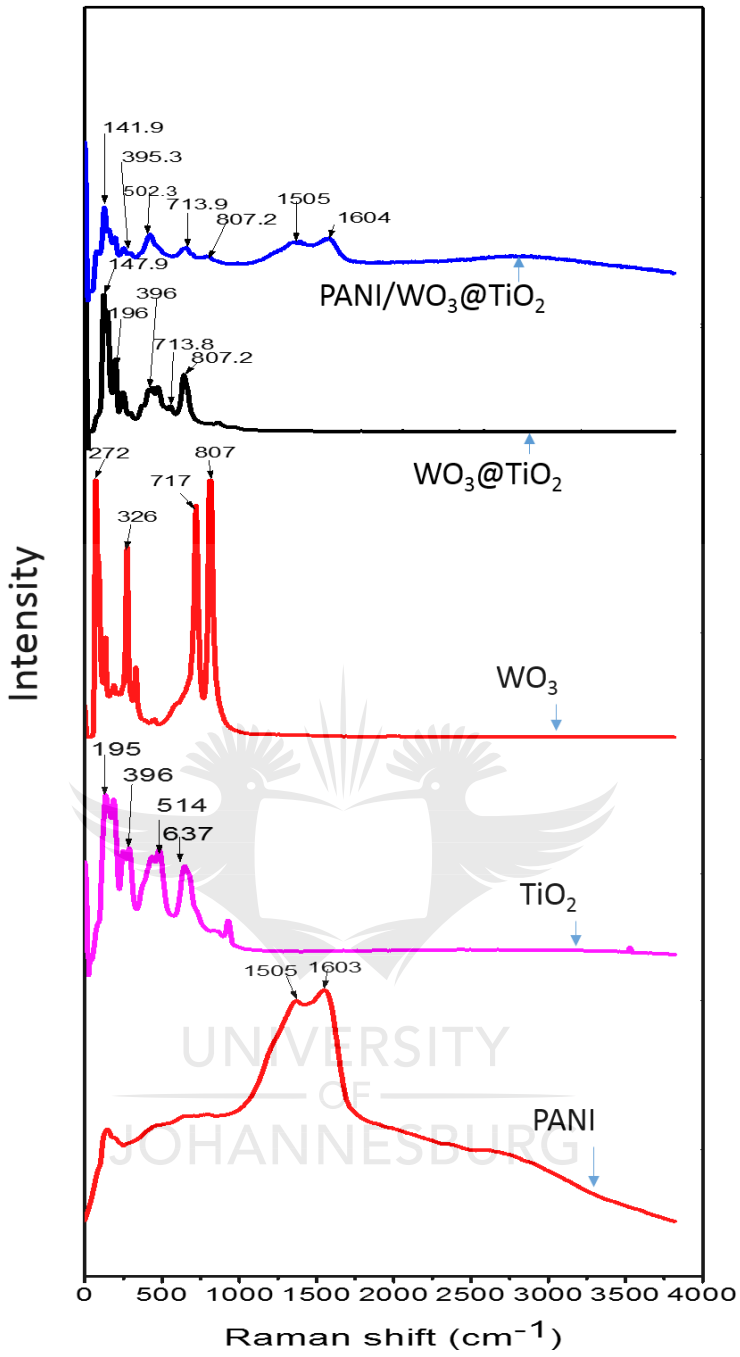

Figure 5. 2: Raman spectra of pristine WO_3, pristine TiO_2, pristine PANI, WO_3@TiO_2, and PANI/WO_3@TiO_2.

In the pristine WO_3, the peaks at 272 cm^{-1} and 326 cm^{-1} relate to the bending vibration of W-O-W bond [22, 29]. The peak at wave number of 717 cm^{-1} correspond to O-W-O vibration, whilst the one at 807 cm^{-1} corresponds to the crystalline WO_3 stretching vibration of the bending oxygen of W-O-W [22]. These peaks are typical

vibrational modes of monoclinic WO_3 that typically appear at 717 cm^{-1} and 807 cm^{-1} [30]. Raman spectroscopic analysis also confirmed that the TiO_2 anatase phase and the monoclinic WO_3 were not compromised by the incorporation of PANI polymer. In addition, it confirmed the incorporation of PANI polymer in the PANI/WO_3@TiO_2 nanocomposite as evidenced by the appearance of the D band and the G band at 1603 cm^{-1} and 1505 cm^{-1} respectively that are typically associated with carbon based materials [31].

5.4.3 XRD analysis

The photocatalysts were analyzed by powder XRD using Cu Kα radiation and identified based on diffraction patterns. XRD diffraction plots of the photocatalyst are shown in Figure 5.3.

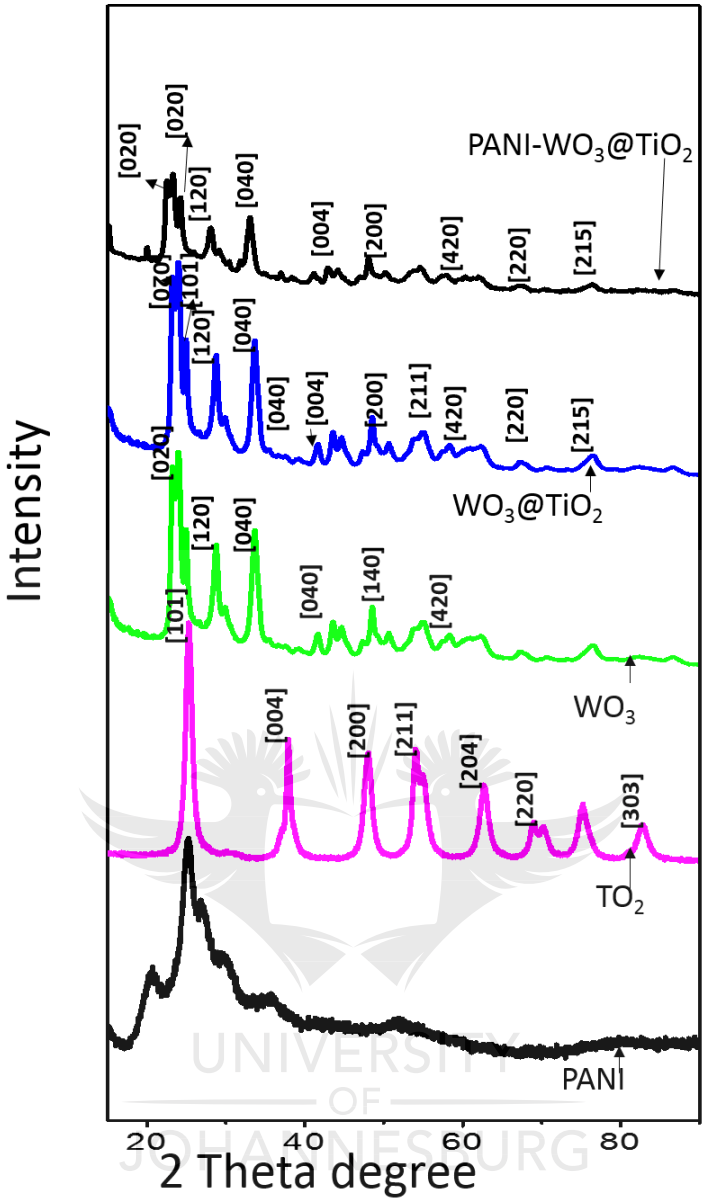

Figure 5. 3: XRD diffraction plots of pristine TiO_2, pristine PANI, pristine WO_3, WO_3@TiO_2, and PANI/WO_3@TiO_2.

The as-synthesized TiO_2 photocatalyst showed the anatase phase according to JCPDS card No. 01-086-1157. The spectra of TiO_2 had peaks at 2θ values of 25.22°, 37.78°, 47.94°, 54.15°, 54.96°, and 62.69°, which were indexed to the (101), (004), (200), (211), (105), and (204) planes of TiO_2. The diffraction peaks obtained from the as-synthesized WO_3 were indexed to the monoclinic phase of WO_3 according to JCPDS card No. 04-005-4487. No peaks arising from other tungsten

compounds or other phases of WO_3 were observed in the diffraction pattern of as-synthesized WO_3. This suggests a pure phase of WO_3 was obtained after calcination. The overlapped 2θ = 26.75° can be indexed to the (020) plane of WO_3 and (101) plane of TiO_2 and this represents successful incorporation of WO_3 in TiO_2. The crystallite size (D) for both TiO_2 and WO_3 were calculated using Debye–Scherrer Equation (see Equation 5.2) with the values obtained to be 17.41 and 15.30 nm, respectively.

$$D = \frac{0.9\lambda}{\beta \cos\theta} \qquad 5.2$$

However, the crystallite size for the nanocomposite could not be ascertained as these were two distinct phases. XRD analysis of as-synthesized PANI showed two broad peaks at 2θ=20.5° and 25.3°, This suggested an amorphous structure of the PANI and the results are in agreement with results that were obtained by Haldari et al [32].

5.4.4 BET analysis

The specific surface area the pore volume and pore size of the materials were determined by BET analysis. The N_2 adsorption-desorption isotherms of the materials. BET results are shown in Figure 5.4.

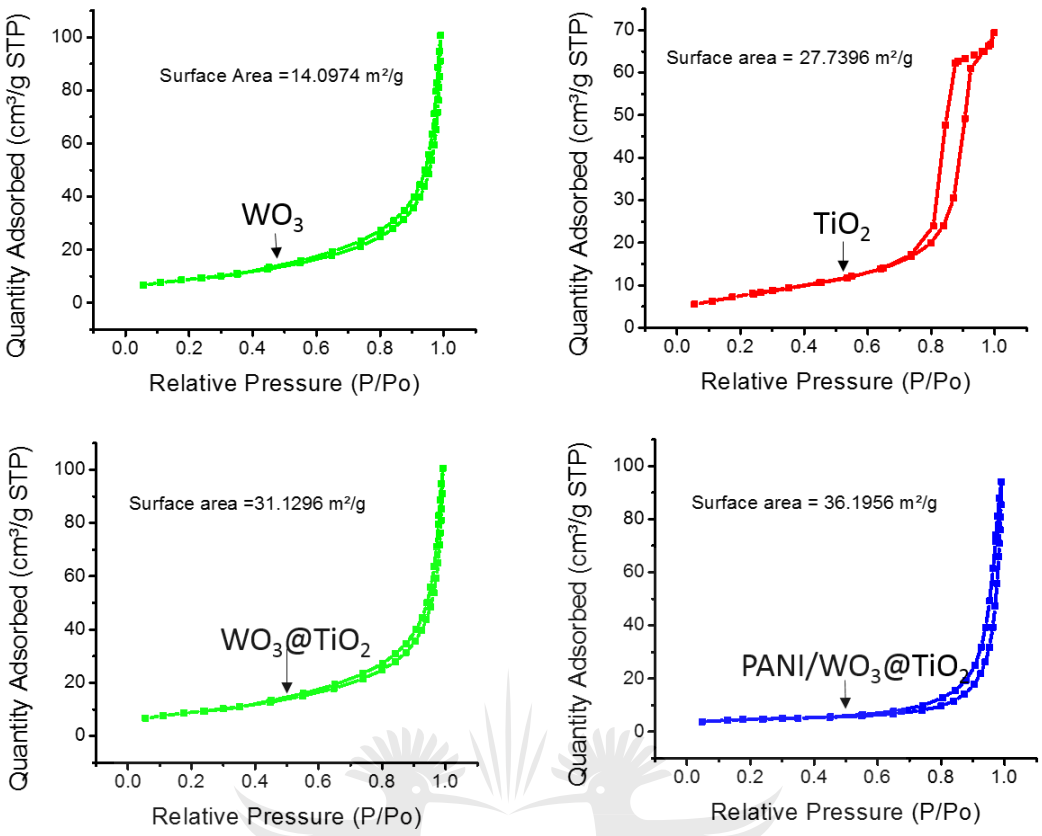

Figure 5. 4: BET analysis plot for TiO_2, WO_3, WO_3@TiO_2, and WO_3@TiO_2-PANI.

The surface area of the pristine WO_3 and TiO_2 samples were 14.0974 m^2/g and 27.7396 m^2/g respectively compared to 31.1296 m^2/g of WO_3@TiO_2 nanocomposite. The results show that pairing up TiO_2 and WO_3 resulted in an improvement in the surface area of the resultant nanocomposite. Further improvement of the surface area was noted in the PANI/WO_3@TiO_2 nanocomposite. This improvement is attributed to the effect of PANI. However, the results show that the pore volume did not change much after incorporation of WO_3 to TiO_2 although there was a slight increase in the pore volume. There was no marked difference in pore volume after incorporation of PANI on the WO_3@TiO_2 nanocomposite. All the as-synthesized photocatalysts can be identified as Type IV isotherm with H4 type hysteresis loop according to the IUPAC-BET classification [33].

5.4.5 Thermal gravimetric analysis

Thermogravimetric analysis was carried out on materials to investigate their thermal stability. TGA profiles of TiO_2, WO_3, WO_3@TiO_2, and PANI/WO_3@TiO_2 nanocomposite are shown in Figure 5.5.

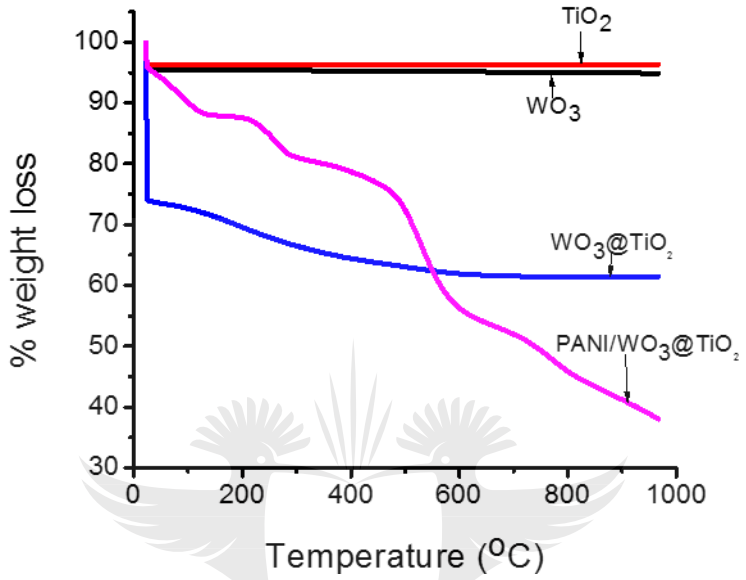

Figure 5. 5: Thermal profile for TiO_2, WO_3, WO_3@TiO_2, and WO_3@TiO_2-PANI.

The TGA curve of pristine TiO_2 and pristine WO_3 samples only showed mass losses at 100°C, which was due to the release of absorbed water and another weight loss at around 320°C due to loss of crystalline water and formation of a WO_3 phase [34]. The TGA curves of as WO_3@TiO_2 sample also showed mass losses around 100°C, which was attributed to loss of water [35]. Pristine TiO_2, WO_3 and WO_3@TiO_2 photocatalyst samples showed remarkable thermal stability up to a 1000°C. PANI/WO_3@TiO_2 nanocomposite showed three weight losses. The first weight loss weight observed from 30°C to 200°C for the nanocomposite was due to the evaporation of adsorbed and bound water on the nanocomposite [36]. The weight loss observed between 200°C and 300°C was due to the breaking of polymer bonds whilst the weight loss up to 500°C was due to the degradation of the PANI polymer

composite [37, 38]. After 600°C, 35% weight residue were not decomposed. This residue may be due to oxides of WO_3 and TiO_2.

5.4.6 SEM and EDS analysis

SEM analysis showed that TiO_2 rods of different sizes were formed as well as nano sphere-like WO_3 (Figure 5.6).

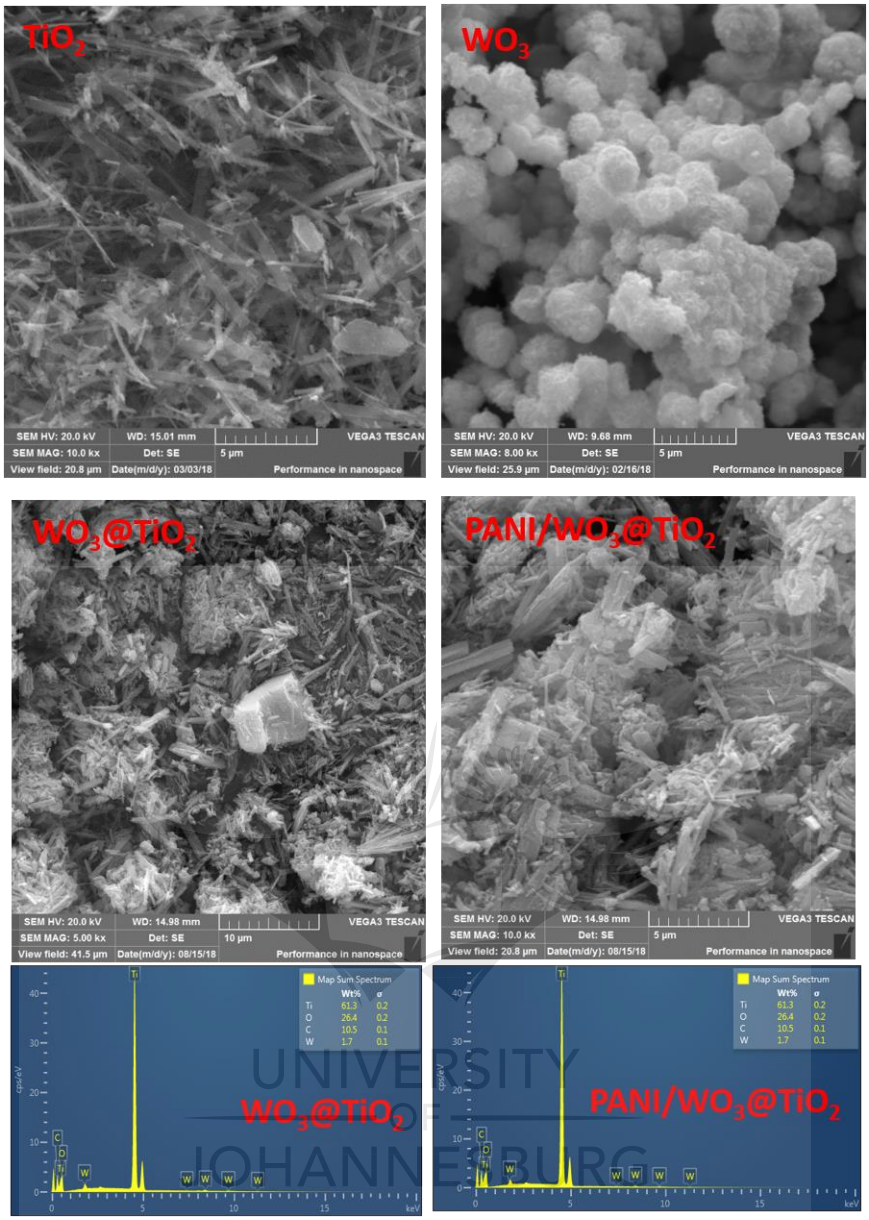

Figure 5. 6: SEM images for (A) pristine TiO_2 nanorods, B) pristine WO_3 nano spheres, (C) WO_3@TiO_2 and EDS for PANI/WO_3@TiO_2.

SEM micrograph of the WO_3@TiO_2 nanocomposite show nano sphere-like structures dispersed in rods. EDS analysis confirmed the elemental composition of the nanocomposite to consist of Ti, O, W and C.

5.4.7 TEM analysis

TEM analysis of as-synthesized WO_3 photocatalyst showed that the nano sphere-like structures disintegrated in ethanol during preparation for TEM analysis.

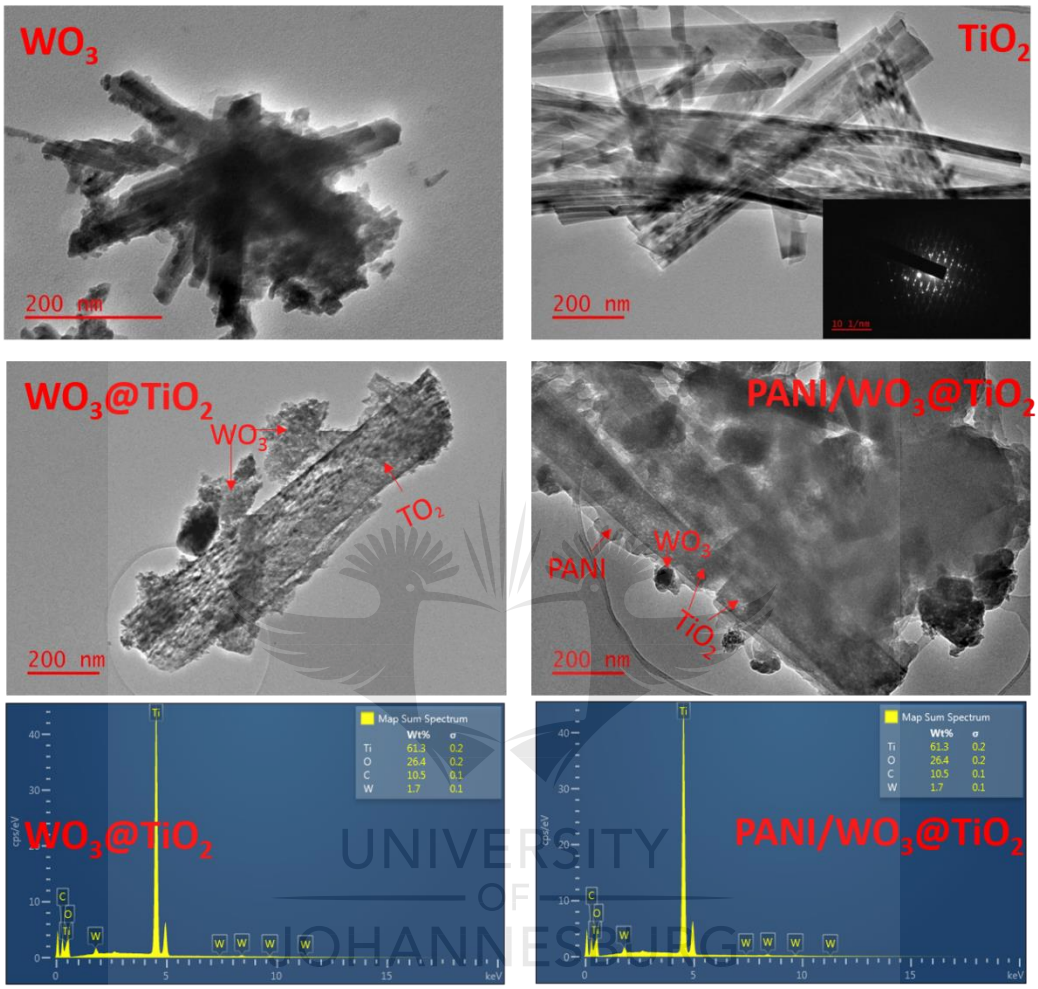

Figure 5. 7: TEM images for pristine WO_3 nanoflowers, pristine TiO_2 nanorods, WO_3@TiO_2, PANI/WO_3@TiO_2 and EDS of WO_3@TiO_2, PANI/WO_3@TiO_2.

TEM images of as-synthesized TiO_2 showed rods of different size with diameters of between 30-100 nm. The analysis of WO_3@TiO_2 showed that a heterojunction was formed with WO_3 sitting on TiO_2. TEM analysis of as-synthesized PANI/WO_3@TiO_2 photocatalyst showed nano sphere-like structures of WO_3 sitting on TiO_2 nanorods and a layer of PANI covering them (Figure 5.7). EDS analysis confirmed the elemental composition of the nanocomposite to consist of Ti, O, W and C.

5.4.8 UV-Vis -DRS

The optical properties of the as–prepared photocatalysts and nanocomposites was evaluated using the UV–Vis spectrophotometer. Figure 5.8a show that UV absorbance of PANI has two absorption peaks at 268 and 395 nm which were ascribed to a π−π transition of the benzenoid rings and charge transfer from the benzenoid to the quinoid, respectively [39]. The spectra of pristine TiO_2 was also measured and showed an absorbance band edge at 385 nm.

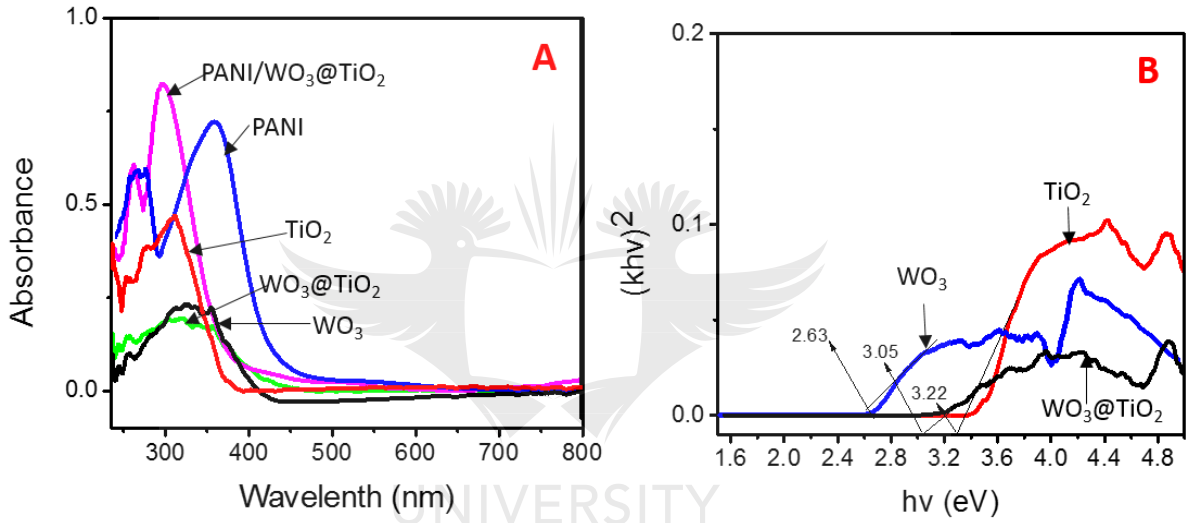

Figure 5. 8: (A) UV-Vis DRS and (B) Tauc`s plot of pristine TiO_2, pristine WO_3 and WO_3@TiO_2.

The absorption edge of the as synthesized WO_3 was observed around 455 nm A noticeable shift in the absorption edge towards the visible-light region (λ > 400 nm) was observed for the WO_3@TiO_2 nanocomposite. The shift in the band edge of WO_3@TiO_2nanocomposite was attributed to the effect of WO_3, which has its absorption band edge at a high wavelength. The absorption edges of WO_3@$TiO_2$was around 460 nm, which is in agreement with as-synthesized WO_3. The absorption of as-synthesized PANI was higher than that of as-synthesized TiO_2

and WO_3. The wrapping of the WO_3@TiO_2 nanocomposite with PANI improved the absorption properties of the nanocomposite as shown in the absorption spectra of PANI/WO_3@TiO_2. However, the absorption edge of PANI/WO_3@TiO_2 was reduced to 420 nm after incorporation of PANI. Figure 5.8 shows a band gap of WO_3@TiO_2 nanocomposite to be estimated at 3.05 eV that is lower than the optical band gap of TiO_2 (3.22 eV). The reduction in the band gap of the TiO_2 based nanocomposite was attributed to be due to the effect of WO_3 photocatalyst that has an estimated band gap of 2.63 eV. The estimated band gap of as-synthesized WO_3 is in agreement with what has been reported in literature [40].

5.4.9 Photoluminescence analysis

The charge separation transfer of the photocatalyst samples were investigated using photoluminescence spectroscopy (PL). PL analysis reveals the migration of charges (electrons and holes) and the formation of defects in the photocatalyst [41]. This helps in understanding the recombination behavior of charges at the surface of the photocatalyst. Figure 5.9 shows results of emission of the materials at 530 nm for all photocatalyst materials.

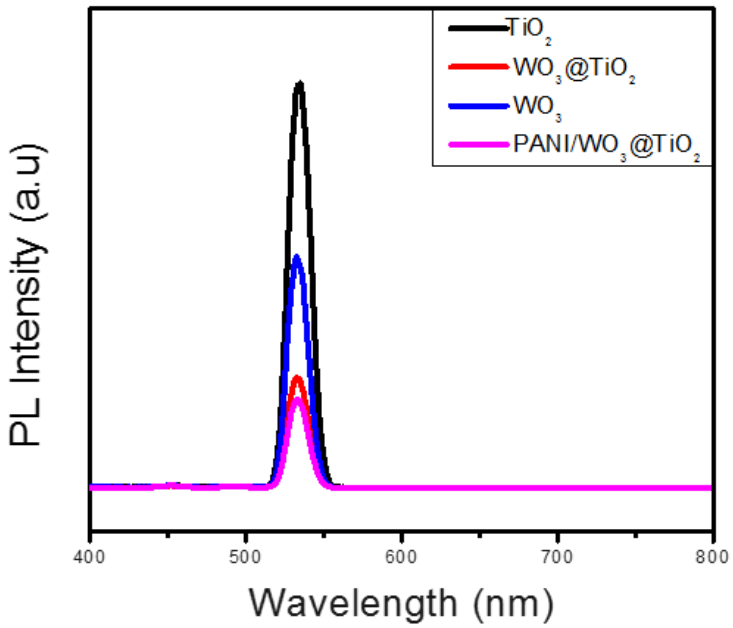

Figure 5. 9: PL emission spectra of pristine TiO_2, pristine WO_3, WO_3@TiO_2, and PANI/WO_3@TiO_2.

The charge separation at the surface of a semiconductor material influences the performance of the photocatalyst. The results show that the intensities of both pristine TiO_2 and WO_3 is higher than of the nanocomposite of WO_3@TiO_2 and WO_3@TiO_2/PANI. The results show that the incorporation of PANI greatly improved the performance of the nanocomposite by reducing the recombination rate of the nanocomposite. This is attributed to the ability of PANI to effect charge separation due to its conductivity property [26]. The results are in agreement with the absorption analysis, which showed that PANI has a stronger absorption than either TiO_2 or WO_3.

5.4.10 X-Ray Photoelectron Spectroscopy

To investigate the surface composition and chemical states of the elements in the sample, XPS spectra of PANI/WO_3@TiO_2 nanocomposite was examined by X-ray

photoelectron spectroscopy (XPS). Figure 5.10 a represents XPS survey scan of PANI/WO_3@TiO_2 nanocomposite which revealed the presence of W, C, O, Ti, and N. Their corresponding photo electron peaks were found to be W4f, W4d, C1s, N1s, O 1s, and Ti 2p.

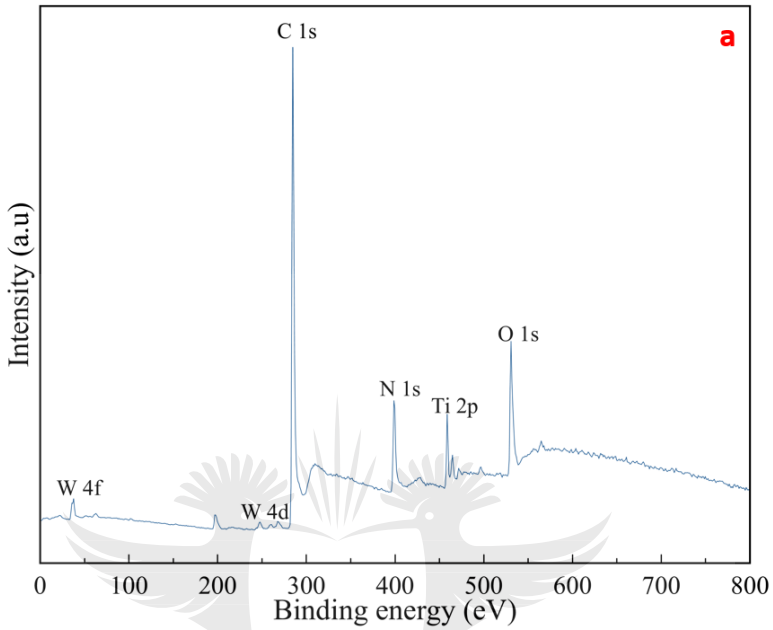

Figure 5. 10 (a): XPS survey scan for PANI/WO_3@TiO_2.

Figure 5.10b show peaks at 36.2 eV and 38.2 eV corresponding to the typical binding energies of W^{6+} oxidation (W $4f_{7/2}$ and W $4f_{5/2}$ respectively) [42, 43] .There are two peaks at 248.06 eV and 260.57 eV are shown in Figure 5.10c and were ascribed to W $4d_{5/2}$ and W $d_{3/2}$ respectively [44].

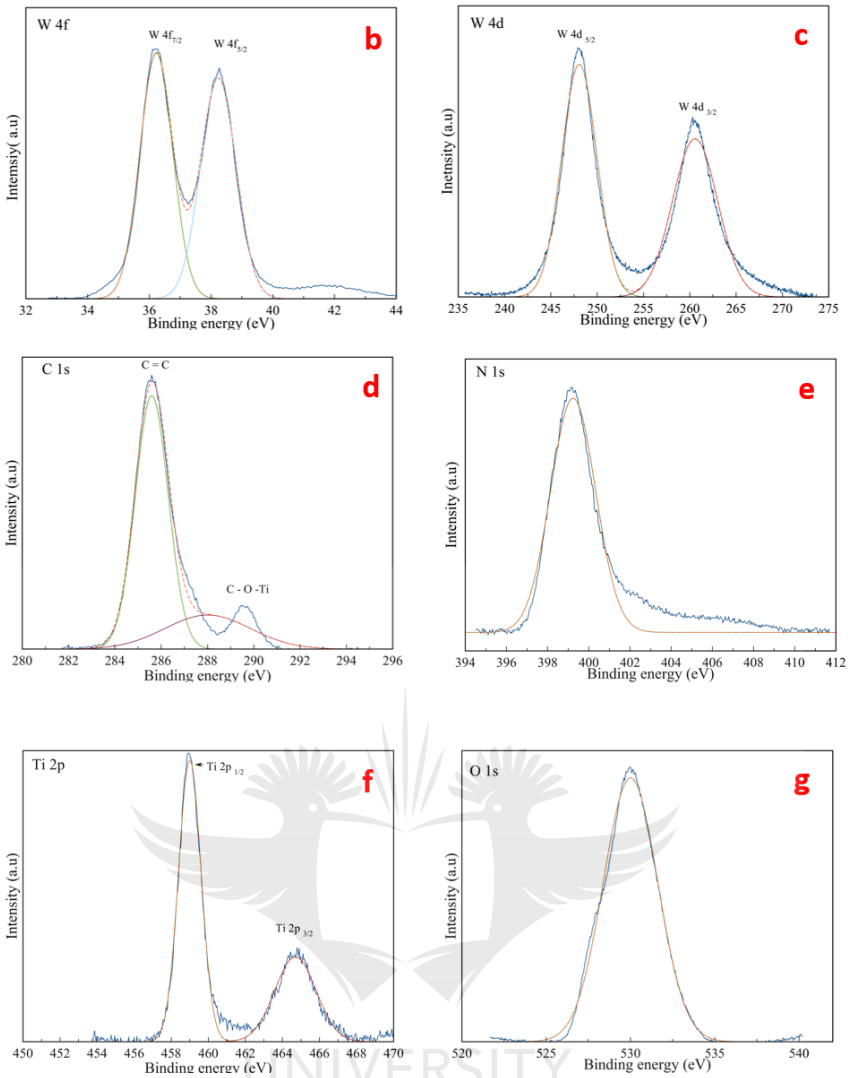

Figure 5.10 b: Core level XPS spectra for (b) W 4f, (c) W 4d, (d) C 1s, (e) N 1s, (f) Ti 2p and (g) O 1s of PANI/WO_3@TiO_2.

Figure 5.10d reveal a peak at 284.75 eV which was assigned to carbon from the PANI polymer [45]. Figure 5.10e shows a peak at 399.6 eV which was ascribed to N 1s from PANI [45].Core level spectra of Ti 2p is shown in Figure 5.10 f at 459.2 eV and 464.9 eV due to Ti $2p_{1/2}$ and Ti $2p_{3/2}$ respectively [46, 47]. A peak due to the core level O 1s spectra of O bonds such as O-W-O, Ti−O−Ti, and Ti−O−H appeared at 530 eV [39] [48] (Figure 5.10).

5.5 APPLICATION

5.5.1 Catalyst selection

The photocatalytic degradation of ibuprofen was investigated using as-synthesized TiO_2, WO_3, WO_3@TiO_2, and PANI/ WO_3@TiO_2 catalysts at solution pH 5.8 and the results are shown in Figure 5.11.

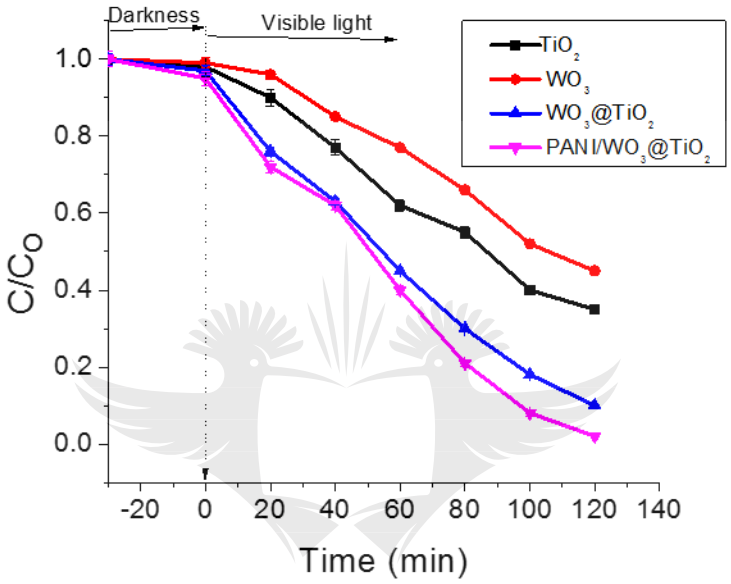

Figure 5. 11: Degradation performance of pristine TiO_2, pristine WO_3, WO_3@TiO_2 and PANI/ WO_3@TiO_2 on ibuprofen.

The results show that PANI/WO_3@TiO_2 had the best degradation performance with a degradation of 99.8% after 120 mins of visible light irradiation. The results revealed that WO_3@TiO_2 had 90% degradation efficiency compared to 50% and 46.5% for pristine TiO_2 and WO_3 respectively. The improvement was attributed to charge separation in the WO_3@TiO_2 heterojunction. Yan et al. also reported similar improvements. The authors reported an enhanced degradation by a CdS/$CoWO_4$ heterojunction photocatalyst when they degraded methylene blue (MB) under visible light irradiation compared to pristine CdS and $CoWO_4$ [49].

The results show that 99.8% degradation was achieved by PANI/WO_3@TiO_2 after irradiation for the same time. This was a higher degradation percentage compared to the 90% attained by WO_3@TiO_2. This improvement was attributed to the adsorption by PANI, which has been reported to be adsorptive towards organics [50]. Furthermore, PANI has an ability to effect charge separation that can improve the performance of a photocatalyst. The results show that ~ 10% ibuprofen was removed in the dark and this was attributed to adsorption on the surface of PANI/WO_3@TiO_2 that was mainly covered by PANI. This was in agreement with findings by Kavil et al when polyaniline-black anatase titania (PANI-BAT) nanocomposite was used to degrade methyl orange [51]. The authors suggested that the high degradation by PANI-BAT was due to the ability of PANI to effect charge separation in the nanocomposite. PANI/WO_3@TiO_2 was used as a catalyst of choice for the rest of the experiments to investigate other parameters.

5.5.2 Effect of pH on the degradation of ibuprofen

The degradation of ibuprofen at pH 3.5, 5.8 and 9 was investigated. The effects of these respective pH conditions were studied using a dosage of 0.2 g/L and ibuprofen concentration of 5 mg/L. Figure 5.12 shows the effect of pH on the degradation of ibuprofen by PANI/WO_3@TiO_2 nanocomposite at pH values, 3.5; solution pH 5.8 and 9. The degradation of ibuprofen was greatly influenced by pH as shown in Figure 5. 12.

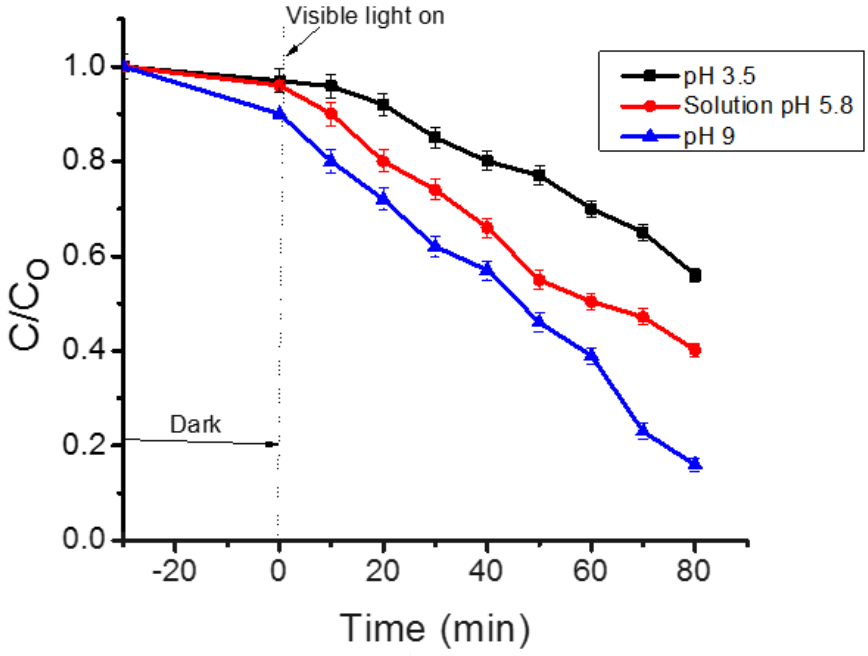

Figure 5. 12: Effect of pH on the degradation of ibuprofen.

The reported point of zero charge for WO_3, TiO_2, and PANI are 4.7, 6.2 and 5.8 respectively [52-54]. This implies that the surface of PANI/WO_3@TiO_2 was negatively charged in alkaline environment and positively charged in acidic solutions. On the other hand ibuprofen molecule, the substrate has a negative charge due to the hydroxyl molecules in its structure [55]. These surface properties influence the initial adsorption of ibuprofen on the photocatalysts. The results show that the higher the initial solution pH the higher the degradation with the highest degradation observed at initial solution pH of 9. The highest degradation was observed at initial solution pH 9 after 80 mins irradiation with a removal efficiency of up to 85.6% whilst the highest for initial solution pH 5.8 and 3.5 was 58.9% and 41.4% respectively after the same time of irradiation. In solution, ibuprofen exists in ionic form and molecular form and the lower degradation efficiency at low pH i.e. 3.5 was due to the fact that the molecular form of ibuprofen was dominant in solution [56]. This implies that the pH was lower than the pKa [57]. At higher pH of 9,

ibuprofen existed in anionic form and this was more susceptible to degradation. These results are in agreement to a study carried out by Choina et al who observed a similar trend when degrading ibuprofen with TiO_2 at pH 3, 7 and 9 [58]. They observed the highest degradation at ibuprofen solution pH 9 and the lowest at solution pH 3. They concluded that the lower degradation at low pH was due to the protonation of TiO_2 and the carboxyl group of ibuprofen and this resulted in electrostatic repulsion between the substrate and the catalyst surface [58]. In this study pH, 9 was used as the optimum pH for all the other experiments.

5.5.3 Effect of photocatalyst dosage on the degradation of ibuprofen

The degradation of ibuprofen was carried out using 10 mg, 20 mg, 50 mg, 100 mg and 250 mg at 5 mg/L ibuprofen solution pH 9. The results shown in Figure 5.13 shows that the degradation increased greatly with an increase in the photocatalyst dosage from 10 mg-50 mg.

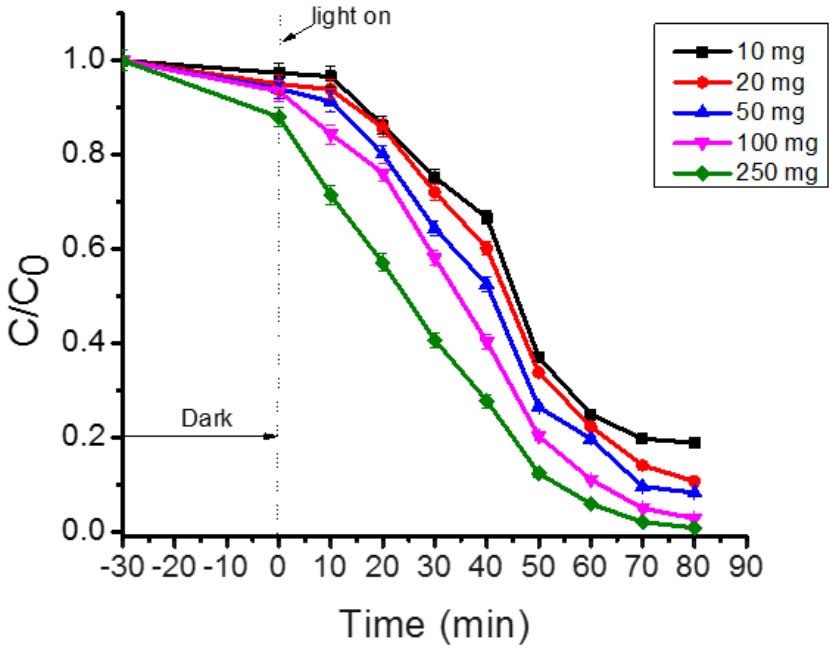

Figure 5. 13: Effect of photocatalyst dosage on the degradation of ibuprofen.

The increase is attributed to an increase in the hydroxyl radicals that was produced due to an increase in the photocatalyst [59]. However, the results show that the degradation efficiency increased marginally with increase in photocatalyst dosage of 100 mg to 250 mg after 80 mins of irradiation. Therefore, a photocatalyst dosage of 100 mg was used for the rest of the experiments. The reduction in performance of the photocatalyst was attributed to light scattering due to aggregation of the photocatalyst particles [60, 61].

5.5.4 Effect of bicarbonate ion concentration on degradation of ibuprofen

Bicarbonate anions may naturally exist in water sources as a result of the dissolution of carbon dioxide in water [62]. Their presence in water samples has been reported to influence the degradation of organics during the advanced oxidation processes due to their ability to quench radicals that are used in degradation processes [61, 62]. However, various reports in literature indicate beneficial results due to their

presence in water during advanced oxidation processes [64, 65]. In this study, the effect of bicarbonate during degradation of ibuprofen were investigated. The results of this study show that bicarbonate ions greatly influence the degradation of ibuprofen (Figure 5.14).

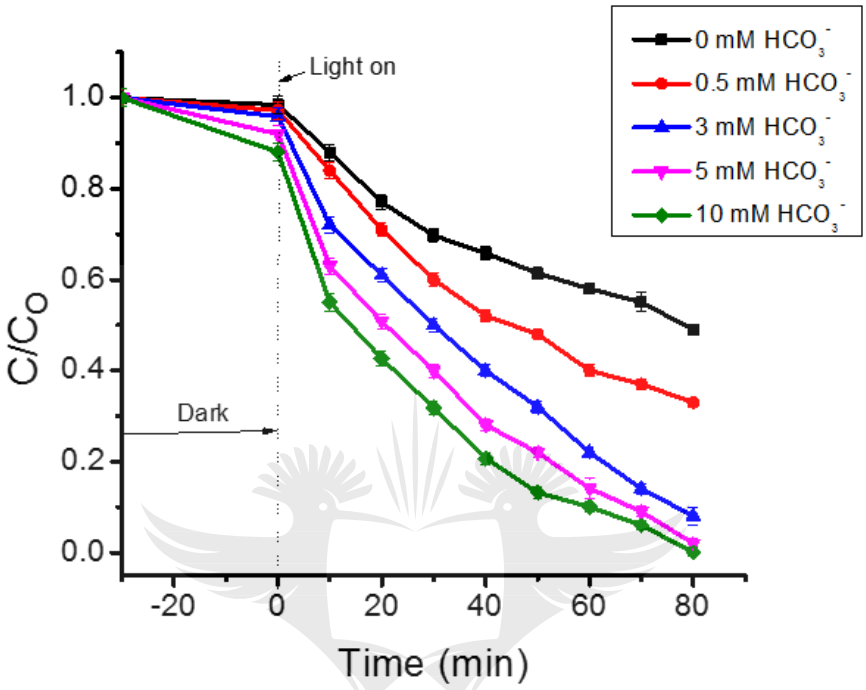

Figure 5. 14: Effect of bicarbonate ions concentration on the degradation of 5 mg/L ibuprofen solution using 0.1 g/L PANI/WO_3@TiO_2 photocatalyst.

The degradation rate was accelerated with an increase in concentration from 0.5 mM to 5 mM. Interestingly, a further increase in $NaHCO_3$ concentration to 10 mM, resulted in little effect on the degradation process. However, there was a slight increase in the degradation maximum up to 99.3% compared to the sample with 5 mM $NaHCO_3$ (98.4%).

5.5.5 Effect of persulfate ions concentrations on the degradation of ibuprofen

Persulfate anions are well known oxidising agents for the degradation of organic pollutants using their reactive sulfate radicals. The redox potential of persulfate radical ($SO_4^{-\cdot}$) is 2.6 V and can be utilized to oxidize organics. The sulfate radicals were generated according to Equation 5.3 [66]:

$$S_2\ O_8^{2-} + \ h\nu \rightarrow 2\ SO_4^{\cdot -} \qquad 5.3$$

In this study, different concentrations (0.5 mM-10 mM) were added to the degradation reaction and evaluated for the degradation of 5 mg/L ibuprofen solution. The results show that adding persulfate anions to the reaction mixture resulted in acceleration of the degradation rate of ibuprofen due to an increase in oxidation rate due to the $SO_4^{\cdot}$ (Figure 5.15).

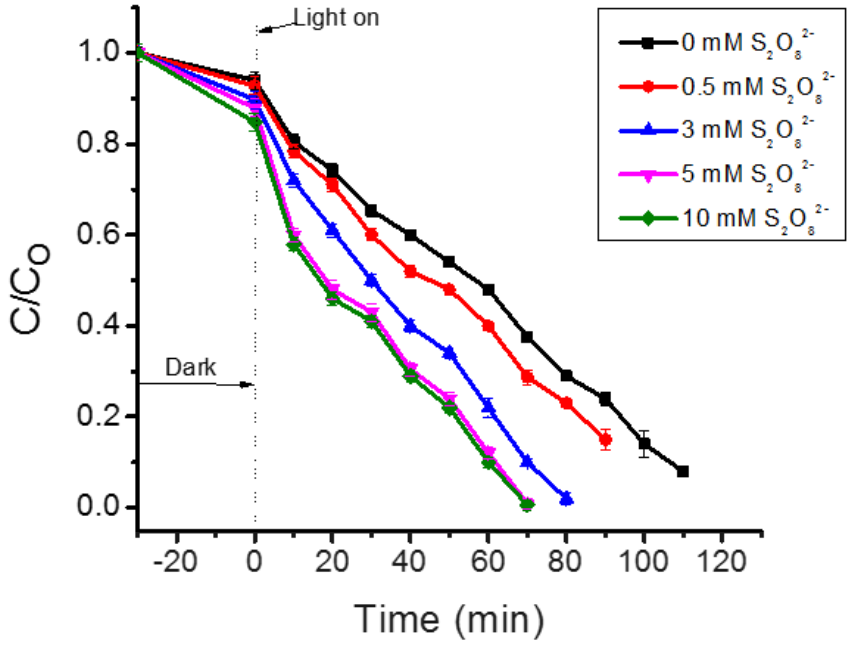

Figure 5. 15: Effect of bicarbonate ions concentration on the degradation of 5 mg/L ibuprofen solution using 0.1 g/L PANI/WO_3@TiO_2 photocatalyst.

However, the rate of degradation reduced slightly at 10 mM persulfate concentration. This may be due to consumption of $SO_4^{-\cdot}$ radicals according to Equation 5.4 [67].

$$SO_4^{-\cdot} + S_2O_8^{2-} \rightarrow SO_2^{2-} + S_2O_8^{-\cdot} \qquad 5.4$$

The slight reduction in the rate of reduction at 10 mM $S_2O_8^{2-}$ concentration was also due to the quenching of $OH^{\cdot}$ radicals by the excess $S_2O_8^{2-}$ according to Equation 5.5 [68].

$$S_2O_8^{2-} + OH^{\cdot} \rightarrow SO_4^{-\cdot} + SO_4^{2-} + OH^{-} \qquad 5.5$$

5.5.6 Kinetics studies

The kinetics of ibuprofen degradation by PANI/WO_3@TiO_2 was investigated using Langmuir-Hinshelwood (L-H), which is expressed by the pseudo-first order model Equation 5.6: [69- 70]

$$\ln\left(\frac{C_o}{C_t}\right) = K_r K_{ad} t = K_{app} t \qquad 5\,6$$

Where K_{app} is the apparent rate constant of the pseudo-first order reaction (min^{-1}), C_o is the equilibrium of ibuprofen in the dark, C_t is the remaining concentration of ibuprofen at a certain irradiation time. Figure 5.16 shows the plot of $\ln\left(\frac{C_o}{C}\right)$ vs irradiation time for the photodegradation of ibuprofen over a concentration range of 1 mg/L - 20 mg/L under optimal pH of 9 and a photocatalyst dosage of 0.1 g/L. In this study, the degradation rate for ibuprofen conformity to the L-H kinetic model as linearity of the plot of K_{app} vs the initial concentration of ibuprofen had a linear relationship [71]. All the graphs showed good linear correlation ($R^2 > 0.98$).

Similar trend was observed when the kinetics of the degradation by as-synthesized TiO_2, WO_3, WO_3@TiO_2, and PANI/WO_3@TiO_2. The value of K_{app} for the degradation of ibuprofen by WO_3@TiO_2 and PANI/WO_3@TiO_2 was 2.59 x 10^{-2} and 3.5 x 10^{-2} respectively that were significantly higher than that of pristine TiO_2 and WO_3, which were 1.92 x10^{-2} and 1.78 x10^{-2} respectively.

5.5.7 By-products identification

Ibuprofen was degraded by PANI/WO_3@TiO_2 under visible light irradiation and the intermediates were identified using LC-MS. Samples were collected before irradiation, 20 min, 40 min and 60 min of irradiation with visible light. The samples were filtered using 0.45 µm filter discs. The chromatograms of ibuprofen standard and samples are shown in Figure 5.16a. These results show a clear peak due to ibuprofen in the standard sample and the sample before irradiation with a retention time (t_R) of 5.2 mins (Figure 5.16a). However, after irradiation, the ibuprofen peak

reduced in size and new peaks were observed in the chromatograms with t_R at 4.9; 4.3, and 3.5.

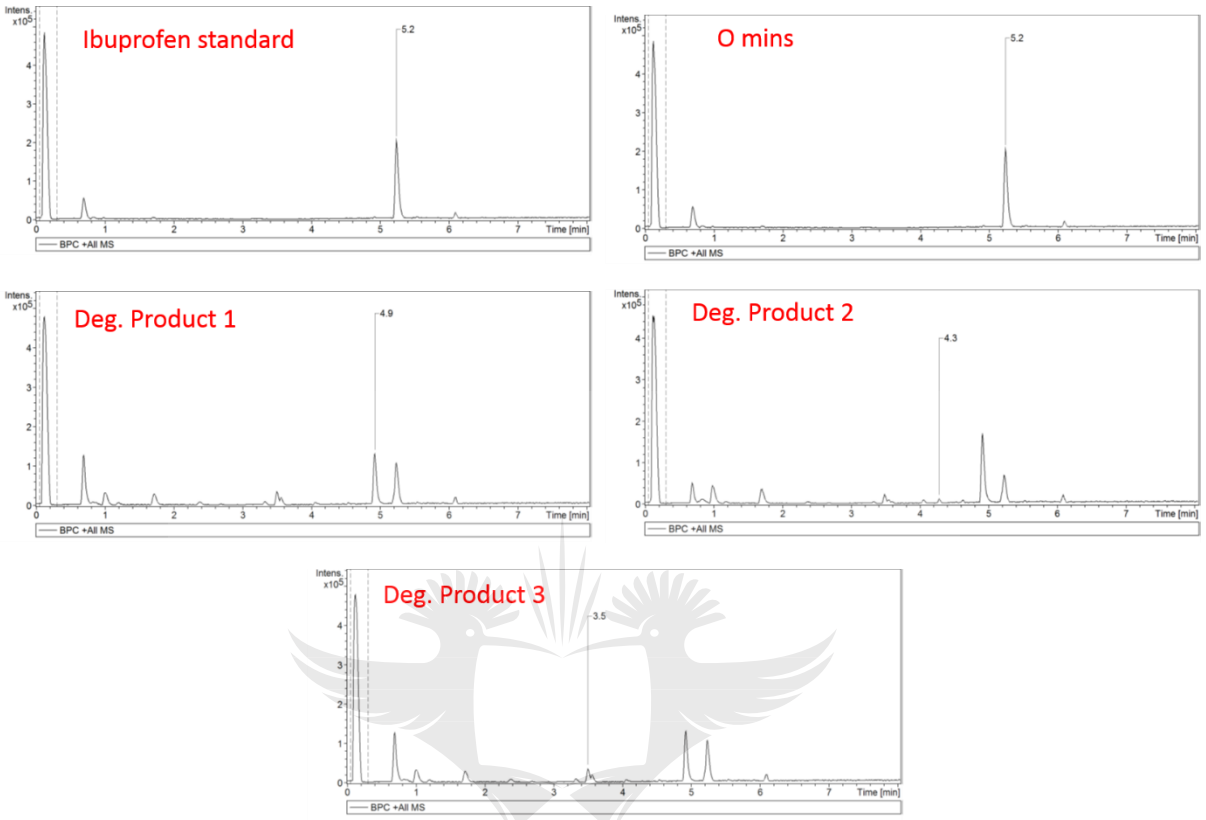

Figure 5. 16a: Chromatograms of ibuprofen standard and samples after irradiation with visible light.

The corresponding mass spectra are show in Figure 5.16b.

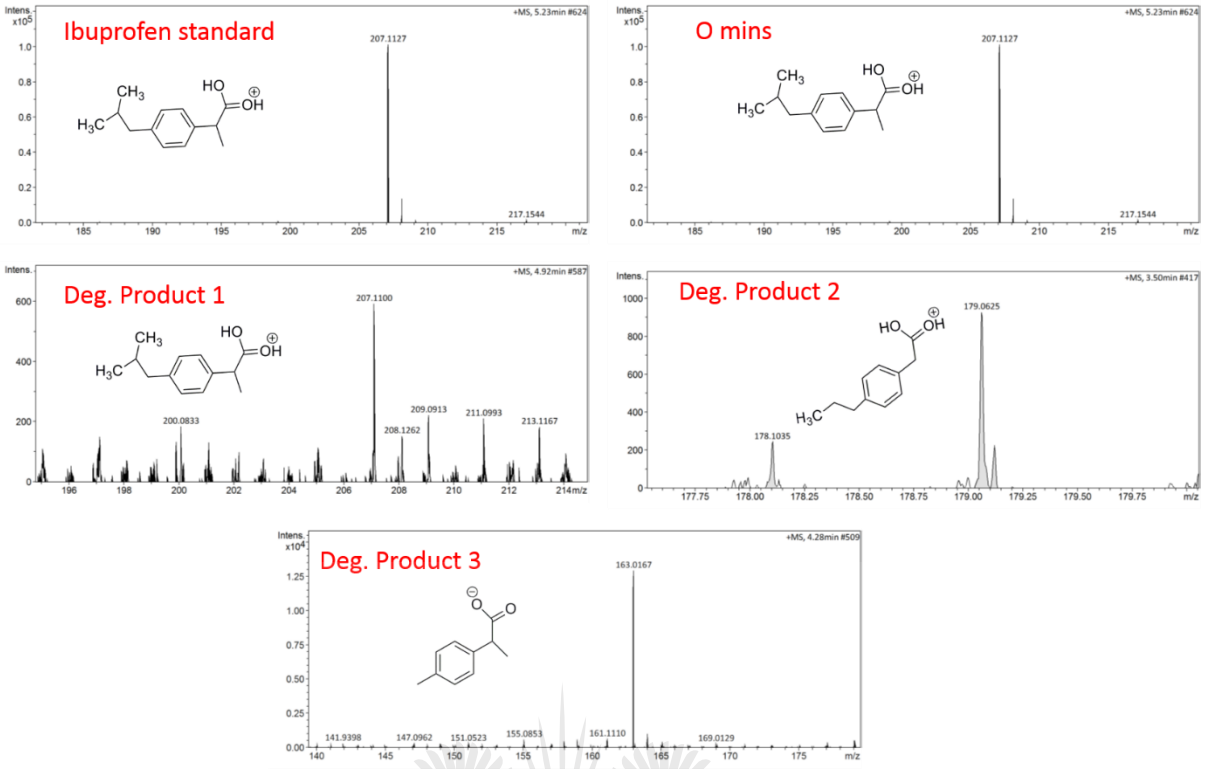

Figure 5.16b: Mass spectra of ibuprofen standard and samples after irradiation with visible light.

The parent ibuprofen (MW 206) was ionized and gave a fragment with m/z 207 which was ascribed to ibuprofen positive ion $[M + H]^+$. Product with m/z 179 was formed by loss of C_2H_5 after attack by reactive oxidative species (ROS). Product with m/z 163 was formed after loss of C_3H_5. Alternatively, product with m/z 163 was formed from the decarboxylation of the product with m/z 179. Similarly, product with m/z 150 was formed from the decarboxylation of product with m/z 164. Therefore, direct decarboxylation was the main degradation pathway of ibuprofen.

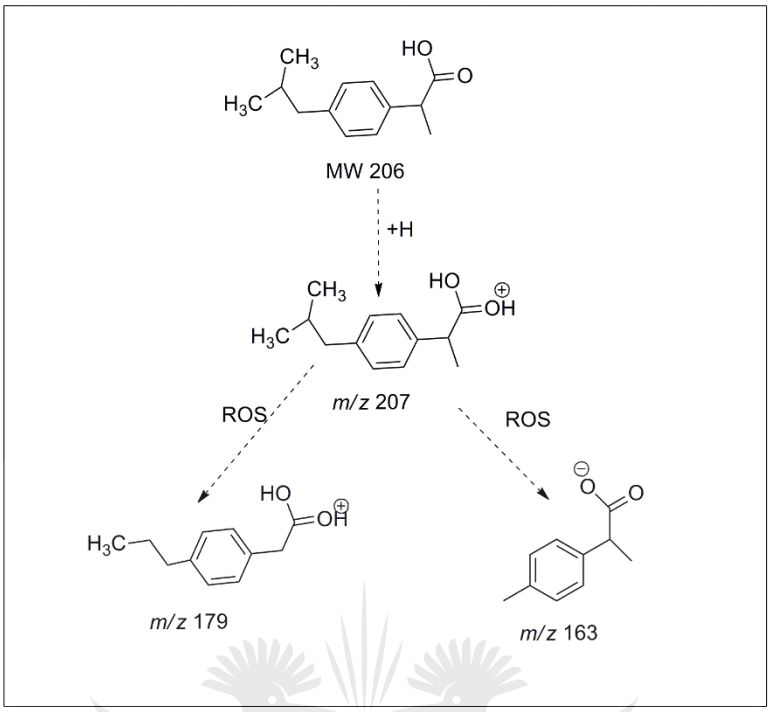

Figure 5.17: Proposed degradation pathway for ibuprofen using PANI/ WO_3@TiO_2 under visible light.

5.5.8 REUSABILITY OF PANI/ WO_3@TIO_2

The recycling of photocatalysts reduce the cost of the degradation process. In this study, the reused PANI/WO_3@TiO_2 photocatalyst was separated from the ibuprofen solution by vacuum filtration. The separated catalyst was washed with distilled water and then with ethanol and dried in an oven at 60°C for 24 h. The PANI/WO_3@TiO_2 was recycled four times after which the weight loss was determined and in our study it was ~ 5%. Figure 5.18 shows the degradation performance of the photocatalyst after four runs. The results show that there was very little loss of efficiency by the catalyst.

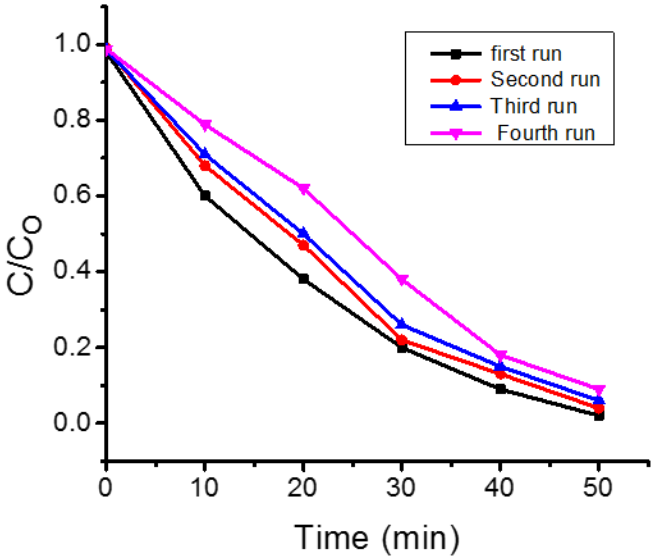

Figure 5. 18: Reusability of PANI/WO_3@TiO_2 for the degradation of ibuprofen.

Therefore, the catalyst can be reused up to four cycles without losing much degradation ability.

5.6 Conclusion

A novel PANI capped WO_3@TiO_2 was successfully synthesized and applied for degradation of ibuprofen. The results of the study show that the rate of degradation is greatly influenced by higher pH and photocatalyst dosage of up to 50 mg. Pairing TiO_2 with a lower bandgap semiconductor, WO_3 extended the use of the nanocomposite into the visible light region of the solar spectrum. In addition, the performance of the photocatalyst was also improved due to improved charge separation provided by the heterojunction as shown in photoluminescence studies. The incorporation of PANI further improved the charge separation and the absorption ability of the photocatalyst. Bicarbonate and persulfate ions also had an influence in the degradation of ibuprofen. Degradation products with m/z 179 and 163 were identified by LC-MS analysis. The PANI capped heterojunction of WO_3@TiO_2 can be reused up to four cycles without loss of degradation ability.

5.7 References

[1] J. Zhao, W. Ren, H.-M. Cheng, Graphene sponge for efficient and repeatable adsorption and desorption of water contaminations, *Journal of Materials Chemistry,* 22 (2012) 20197-20202.

[2] M. McGuinness, What are the real implications on public health of water contamination events? water contamination emergencies: Managing the threats, Water Contamination Emergencies: Managing the Threats, *The Royal Society of Chemistry* 2013, pp. 156-160.

[3] S. Giannakis, S. Rtimi, C. Pulgarin, Light-assisted advanced oxidation processes for the elimination of chemical and microbiological pollution of wastewaters in developed and developing countries, *Molecules*, 22 (2017)1070 -1091.

[4] A.B.A. Boxall, New and emerging water pollutants arising from agriculture, (2012).

[5] T. Deblonde, C. Cossu-Leguille, P. Hartemann, Emerging pollutants in wastewater: A review of the literature, *International Journal of Hygiene and Environmental Health*, 214 (2011) 442-448.

[6] D.J. Lapworth, N. Baran, M.E. Stuart, R.S. Ward, Emerging organic contaminants in groundwater: A review of sources, fate, and occurrence, *Environmental Pollution,* 163 (2012) 287-303.

[7] J. Rivera-Utrilla, M. Sanchez-Polo, M.A. Ferro-Garcia, G. Prados-Joya, R. Ocampo-Perez, Pharmaceuticals as emerging contaminants and their removal from water. A review, *Chemosphere*, 93 (2013) 1268-1287.

[8] R.L. Oulton, T. Kohn, D.M. Cwiertny, Pharmaceuticals and personal care products in effluent matrices: A survey of transformation and removal during

wastewater treatment and implications for wastewater management, *Journal of Environmental Monitoring,* 12 (2010) 1956-1978.

[9] F.T. Mathias, D.H. Fockink, G.R. Disner, V. Prodocimo, J.L.C. Ribas, L.P. Ramos, M.M. Cestari, H.C. Silva de Assis, Effects of low concentrations of ibuprofen on freshwater fish Rhamdia quelen, *Environmental Toxicology and Pharmacology,* 59 (2018) 105-113.

[10] E. Archer, B. Petrie, B. Kasprzyk-Hordern, G.M. Wolfaardt, The fate of pharmaceuticals and personal care products (PPCPs), endocrine disrupting contaminants (EDCs), metabolites and illicit drugs in a WWTW and environmental waters, *Chemosphere*, 174 (2017) 437-446.

[11] M. Starling, C.C. Amorim, M.M.D. Leao, Occurrence, control and fate of contaminants of emerging concern in environmental compartments in Brazil, *Journal of Hazardous Materials*, 18 (2018) 30275-3894.

[12] E. Villar-Navarro, R.M. Baena-Nogueras, M. Paniw, J.A. Perales, P.A. Lara-Martín, Removal of pharmaceuticals in urban wastewater: High rate algae pond (HRAP) based technologies as an alternative to activated sludge based processes, *Water Research,* 139 (2018) 19-29.

[13] S. Patibandla, J.-Q. Jiang, X. Shu, Toxicity assessment of four pharmaceuticals in aquatic environment before and after ferrate(VI) treatment, *Journal of Environmental Chemical Engineering*, 6 (2018) 3787-3797.

[14] D. Kanakaraju, B.D. Glass, M. Oelgemöller, Advanced oxidation process-mediated removal of pharmaceuticals from water: A review, *Journal of Environmental Management*, 219 (2018) 189-207.

[15] C. Byrne, G. Subramanian, S.C. Pillai, Recent advances in photocatalysis for environmental applications, *Journal of Environmental Chemical Engineering*, 6 (2018) 3531-3555.

[16] A. Manassero, M.L. Satuf, O.M. Alfano, Photocatalytic degradation of an emerging pollutant by TiO_2-coated glass rings: a kinetic study, *Environmental Science Pollution Research International,* 24 (2017) 6031-6039.

[17] A.T. Kuvarega, R.W.M. Krause, B.B. Mamba, Nitrogen/palladium-codoped TiO_2 for efficient visible light photocatalytic dye degradation, *The Journal of Physical Chemistry C*, 115 (2011) 22110-22120.

[18] Y. Hu, W. Chen, J. Fu, M. Ba, F. Sun, P. Zhang, J. Zou, Hydrothermal synthesis of $BiVO_4$/TiO_2 composites and their application for degradation of gaseous benzene under visible light irradiation, *Applied Surface Science*, 436 (2018) 319-326.

[19] N. Guo, Y. Liang, S. Lan, L. Liu, J. Zhang, G. Ji, S. Gan, Microscale hierarchical three-dimensional flowerlike TiO_2/PANI composite: synthesis, characterization, and its remarkable photocatalytic activity on organic dyes under UV-light and sunlight irradiation, *The Journal of Physical Chemistry C*, 118 (2014) 18343-18355.

[20] D. Wang, Y. Wang, X. Li, Q. Luo, J. An, J. Yue, Sunlight photocatalytic activity of polypyrrole–TiO_2 nanocomposites prepared by 'in situ' method, *Catalysis Communications,* 9 (2008) 1162-1166.

[21] C.T. Fleaca, M. Scarisoreanu, I. Morjan, C. Luculescu, A.M. Niculescu, A. Badoi, E. Vasile, G. Kovacs, Laser oxidative pyrolysis synthesis and annealing of TiO_2 nanoparticles embedded in carbon–silica shells/matrix, *Applied Surface Science,* 336 (2015) 226-233.

[22] M.F. Daniel, B. Desbat, J.C. Lassegues, B. Gerand, M. Figlarz, Infrared and Raman study of WO_3 tungsten trioxides and WO_3, xH_2O tungsten trioxide tydrates, *Journal of Solid State Chemistry*, 67 (1987) 235-247.

[23] K.P. Sandhya, S. Haridas, S. Sugunan, Visible light induced photocatalytic activity of polyaniline modified TiO_2 and Clay-TiO_2 composites, [213] K.P. Sandhya, S. Haridas, S. Sugunan, Visible light induced photocatalytic activity of polyaniline modified TiO_2 and Clay-TiO_2 composites, *Bulletin of Chemical Reaction Engineering and Catalysis* 8 (2013): 145-159.

[24] P.R. Deshmukh, S.V. Patil, R.N. Bulakhe, S.N. Pusawale, J.-J. Shim, C.D. Lokhande, Chemical synthesis of PANI–TiO_2 composite thin film for supercapacitor application, *The Royal Society of Chemistry Advances,* 5 (2015) 68939-68946.

[25] M. Sboui, M.F. Nsib, A. Rayes, M. Swaminathan, A. Houas, TiO_2–PANI/Cork composite: A new floating photocatalyst for the treatment of organic pollutants under sunlight irradiation, *Journal of Environmental Sciences,* 60 (2017) 3-13.

[26] T.J. Brooms, B. Otieno, M.S. Onyango, A. Ochieng, Photocatalytic degradation of P-cresol using TiO_2/ZnO hybrid surface capped with polyaniline, *Journal of Environmental Science and Health, Part A,* 53 (2018) 99-107.

[27] J. Dhanalakshmi, S. Iyyapushpam, S.T. Nishanthi, M. Malligavathy, D.P. Padiyan, Investigation of oxygen vacancies in Ce coupled TiO_2 nanocomposites by Raman and PL spectra, *Advances in Natural Sciences: Nanoscience and Nanotechnology,* 8 (2017) 015015.

[28] T. Ohsaka, F. Izumi, Y. Fujiki, Raman spectrum of anatase, TiO_2, *Journal of Raman Spectroscopy,* 7 (1978) 321-324.

[29] C.Y. Ng, K. Abdul Razak, Z. Lockman, WO_3 nanorods prepared by low-temperature seeded growth hydrothermal reaction, *Journal of Alloys and Compounds*, 588 (2014) 585-591.

[30] M. S, M.M. Margoni, K. Ramamurthi, R.R. Babu, G. V, Hydrothermal assisted growth of vertically aligned platelet like structures of WO_3 films on transparent conducting FTO substrate for electrochromic performance, *Applied Surface Science*, 449 (2018) 77-91.

[31] J.-B. Wu, M.-L. Lin, X. Cong, H.-N. Liu, P.-H. Tan, Raman spectroscopy of graphene-based materials and its applications in related devices, *Chemical Society Reviews,* 47 (2018) 1822-1873.

[32] Y. Haldorai, V.H. Nguyen, J.J. Shim, Synthesis of polyaniline/Q-CdSe composite via ultrasonically assisted dynamic inverse emulsion polymerization, *Colloid and Polymer Science* 289 (2011) 849-854.

[33] H. Ruiz, M. Zambtrano, L. Giraldo, R. Sierra, J.C. Moreno-Pirajan, Production and characterization of activated carbon from oil-palm shell for carboxylic acid adsorption, *Oriental Journal of Chemistry*, 31 (2015) 753-762.

[34] M. Gotić, M. Ivanda, S. Popović, S. Musić, Synthesis of tungsten trioxide hydrates and their structural properties, *Materials Science and Engineering: B*, 77 (2000) 193-201.

[35] M.M. Ba-Abbad, A.A.H. Kadhum, A.B. Mohamad, M.S. Takriff, K. Sopian, Synthesis and catalytic activity of TiO_2 nanoparticles for photochemical oxidation of concentrated chlorophenols under direct solar radiation, *International Journal of Electrochemical Science,* 7 (2012) 4871-4888.

[36] M. Abbate, L. D'Orazio, Water diffusion through a titanium dioxide/poly(carbonate urethane) nanocomposite for protecting cultural heritage: Interactions and viscoelastic behavior, *Nanomaterials*, 7 (2017) 271.

[37] V.G. Kulkarni, L.D. Campbell, W.R. Mathew, Thermal stability of polyaniline, *Synthetic Metals*, 30 (1989) 321-325.

[38] S.S. Sambaza, M.L. Masheane, S.P. Malinga, E.N. Nxumalo, S.D. Mhlanga, Polyethyleneimine-carbon nanotube polymeric nanocomposite adsorbents for the removal of Cr^{6+} from water, *Physics and Chemistry of the Earth, Parts A/B/C,* 100 (2017) 236-246.

[39] M. Omaish Ansari, M.M. Khan, S. Ansari, K. Raju, J. Lee, M.H. Cho, Enhanced thermal stability under DC electrical conductivity retention and visible light activity of Ag/TiO_2@polyaniline nanocomposite film, *American Chemical Society Applied Materials and Interface* 11 (2014) 8124-8133.

[40] P.P. González-Borrero, F. Sato, A. Medina, M. Baesso, A. Bento, G. Baldissera, C. Persson, G. Niklasson, C. Granqvist, A. Ferreira da Silva, Optical band-gap determination of nanostructured WO_3 film, *Applied Physics Letters* 96 (2010) 061909-061910.

[41] C. Ravidhas, A.J. Josephine, P. Sudhagar, A. Devadoss, C. Terashima, K. Nakata, A. Fujishima, A.M.E. Raj, C. Sanjeeviraja, Facile synthesis of nanostructured monoclinic bismuth vanadate by a co-precipitation method: structural, optical and photocatalytic properties, *Materials Science in Semiconductor Processing*, 30 (2015) 343-351.

[42] S. Rahimnejad, J. He, F. Pan, X.e. Lee, W. Chen, K. Wu, G. Qin Xu, Enhancement of the photocatalytic efficiency of WO_3 nanoparticles via hydrogen plasma treatment, *Materials Research Express* 1 (4) 2014.

[43] C. Navío, S. Vallejos, T. Stoycheva, E. Llobet, X. Correig, R. Snyders, C. Blackman, P. Umek, X. Ke, G. Van Tendeloo, C. Bittencourt, Gold clusters on WO_3 nanoneedles grown via AACVD: XPS and TEM studies, *Materials Chemistry and Physics,* 134 (2012) 809-813.

[44] F. Mehmood, J. Iqbal, M. Ismail, A. Mehmood, Ni doped WO_3 nanoplates: An excellent photocatalyst and novel nanomaterial for enhanced anticancer activities, *Journal of Alloys and Compounds,* 746 (2018) 729-738.

[45] S. Golczak, A. Kanciurzewska, M. Fahlman, K. Langer, J.J. Langer, Comparative XPS surface study of polyaniline thin films, *Solid State Ionics*, 179 (2008) 2234-2239.

[46] N. Parveen, M.O. Ansari, T.H. Han, M.H. Cho, Simple and rapid synthesis of ternary polyaniline/titanium oxide/graphene by simultaneous TiO_2 generation and aniline oxidation as hybrid materials for supercapacitor applications, *Journal of Solid State Electrochemistry* 21 (2017) 57-68.

[47] N.T.T. Linh, P.D. Tuan, N.V. Dzung, The shifts of band gap and binding energies of titania/hydroxyapatite material, *Journal of Composites*, 2014 (2014) 5.

[48] S. Adhikari, S. Mandal, D. Sarkar, D.-H. Kim, G. Madras, Kinetics and mechanism of dye adsorption on WO_3 nanoparticles, *Applied Surface Science* 420 (2017) 472-482.

[49] X. Yan, Z. Wu, C. Huang, K. Liu, W. Shi, Hydrothermal synthesis of CdS/$CoWO_4$ heterojunctions with enhanced visible light properties toward organic pollutants degradation*, Ceramics International,* 43 (2017) 5388-5395.

[50] S. Zarrin, F. Heshmatpour, Photocatalytic activity of TiO_2/Nb_2O_5/PANI and TiO_2/Nb_2O_5/RGO as new nanocomposites for degradation of organic pollutants, *Journal of Hazardous Materials*, 351 (2018) 147-159.

[51] J. Kavil, S. Ullattil, A. Alshahrie, P. Periyat, Polyaniline as photocatalytic promoter in black anatase TiO_2, *Solar Energy* 158 (2017) 792-796.

[52] U.A. Qureshi, I.H. Gubbuk, M. Ersoz, A.R. Solangi, S.I.H. Taqvi, S.Q. Memon, Preparation of polyaniline montmorillonite clay composites for the removal of diethyl hexyl phthalate from aqueous solutions, *Separation Science and Technology,* 51 (2016) 214-228.

[53] J.-C. Chou, L.P. Liao, Study on pH at the point of zero charge of TiO_2 pH ion-sensitive field effect transistor made by the sputtering method, *Thin Solid Films*, 476 (2005) 157-161.

[54] L. Manceriu, R.A. Carcel, Prediction of TiO_2 and WO_3 nanopowders surface charge by the evaluation of point of zero charge (PZC), *Environmental Engineering and Management Journal* 10 (2011) 1021-1026.

[55] Y. Park, Z. Sun, G.A. Ayoko, R.L. Frost, Bisphenol A sorption by organo-montmorillonite: implications for the removal of organic contaminants from water, *Chemosphere*, 107 (2014) 249-256.

[56] S. Canonica, L. Meunier, U. von Gunten, Phototransformation of selected pharmaceuticals during UV treatment of drinking water, *Water Research,* 42 (2008) 121-128.

[57] U. Domańska, A. Pobudkowska, A. Pelczarska, P. Gierycz, pKa and solubility of drugs in water, ethanol, and 1-octanol, *The Journal of Physical Chemistry B*, 113 (2009) 8941-8947.

[58] J. Choina, C. Fischer, G.U. Flechsig, H. Kosslick, V.A. Tuan, N.D. Tuyen, N.A. Tuyen, A. Schulz, Photocatalytic properties of Zr-doped titania in the degradation of the pharmaceutical ibuprofen, *Journal of Photochemistry and Photobiology A: Chemistry*, 274 (2014) 108-116.

[59] J.M. Doña, C. Garriga, J. Araña, J. Pérez, G. Colon, M. Macías, J.A. Navio, The effect of dosage on the photocatalytic degradation of organic pollutants, *Research on Chemical Intermediates*, 33 (2007) 351-358.

[60] N. Jallouli, L.M. Pastrana-Martinez, A.R. Ribeiro, N.F. Moreira, J.L. Faria, O. Hentati, A.M. Silva, M. Ksibi, Heterogeneous photocatalytic degradation of ibuprofen in ultrapure water, municipal and pharmaceutical industry wastewaters using a TiO_2/UV-LED system, *Chemical Engineering Journal,* 334 (2018) 976-984.

[61] S. Malato, P. Fernández-Ibáñez, M.I. Maldonado, J. Blanco, W. Gernjak, Decontamination and disinfection of water by solar photocatalysis: Recent overview and trends, *Catalysis Today*, 147 (2009) 1-59.

[62] D. Poulton, H. Baldwin, Oxygen exchange between carbonate and bicarbonate ions and water. I. Exchange in the absence of added catalysts, *Canadian Journal of Chemistry*, 45 (1967) 1045-1050.

[63] C.-H. Liao, S.-F. Kang, F.-A. Wu, Hydroxyl radical scavenging role of chloride and bicarbonate ions in the H_2O_2/UV process, *Chemosphere*, 44 (2001) 1193-1200.

[64] L. Cheng, M. Wei, L. Huang, F. Pan, D. Xia, X. Li, A. Xu, Efficient H_2O_2 oxidation of organic dyes catalyzed by simple copper(II) ions in bicarbonate aqueous solution, *Industrial and Engineering Chemistry Research*, 53 (2014) 3478-3485.

[65] C. Pétrier, R. Torres-Palma, E. Combet, G. Sarantakos, S. Baup, C. Pulgarin, Enhanced sonochemical degradation of bisphenol-A by bicarbonate ions, *Ultrasonics Sonochemistry,* 17 (2010) 111-115.

[66] S.Y. Oh, D.S. Shin, Degradation of spent caustic by Fenton and persulfate oxidation with zero-valent iron, *Journal of Chemical Technology and Biotechnology,* 88 (2013) 145-152.

[67] S. Norzaee, E. Bazrafshan, B. Djahed, F. Kord Mostafapour, R. Khaksefidi, UV activation of persulfate for removal of penicillin G antibiotics in aqueous solution, *The Scientific World Journal*, 2017 (2017) 1-6.

[68] H. Yang, S. Zhuang, Q. Hu, L. Hu, L. Yang, C. Au, B. Yi, Competitive reactions of hydroxyl and sulfate radicals with sulfonamides in Fe^{2+}/S_2O8^{2-} system: Reaction kinetics, degradation mechanism, and acute toxicity, *Chemical Engineering Journal*, 339 (2018) 32-41.

[69] K.V. Kumar, K. Porkodi, F. Rocha, Langmuir–Hinshelwood kinetics – A theoretical study, *Catalysis Communications*, 9 (2008) 82-84.

[70] K. Porkodi, K.V. Kumar, Comments on" photocatalytic properties of TiO_2 modified with platinum and silver nanoparticles in the degradation of oxalic acid in aqueous solution" Langmuir Hinshelwood kinetics-A theoretical study*, Applied Catalysis B: Environmental,* 79 (2008) 108-109.

[71] M.J.N. Gotostos, C.C. Su, M.D.G. De Luna, M.c. Lu, Kinetic study of acetaminophen degradation by visible light photocatalysis, *Journal of Environmental Science and Health, Part A*, 49 (2014) 892-899.

CHAPTER 6:

ENHANCED DEGRADATION OF BPA IN WATER BY PANI SUPPORTED Ag/TiO_2 NANOCOMPOSITE UNDER UV AND VISIBLE LIGHT

6.0 INTRODUCTION

The growth in human population and industrial activities has led to an increase in the presence of synthetic organic chemicals in water sources [1]. These synthetic compounds form part of a new class of contaminants commonly referred to as emerging pollutants [2]. Emerging pollutants are chemical substances that have no regulation, and are suspected to affect the environment or whose effects are unknown [3]. The presence of these emerging contaminants in surface and groundwater resources that are relied upon for drinking water presents a serious problem due to challenges in their removal during treatment processes. Among the emerging pollutants, Bisphenol A, a synthetic organic compound has been reported to be an endocrine disrupting compound that is responsible for a plethora of negative effects on human and animal health [4].

In order to remove emerging pollutants from water habitats, different water treatment technologies have been applied. Among these technologies, advanced technologies have been utilized to a varying success to remove BPA from water sources. However, the use of these advanced processes has been met with challenges that have limited their use. For example, reverse osmosis is an efficient treatment technology for the removal of BPA and other emerging organic pollutants but its use has been limited because of the high cost of operation [5]. On the other hand, adsorption, a technology which has been shown to be effective in removing BPA from water has recently been raising concerns due to secondary pollution from the

spent adsorbents [6]. Recently, advanced oxidation technologies, have consistently been reported to be an effective method to eliminate emerging organic contaminants from water [7-11]. Among the advanced oxidation processes, photocatalysis especially under solar radiation has been reported to be a cheap, efficient and green technology for environmental remediation [12, 13]. However, despite the success of photocatalysis as a 'green' technology, there have been challenges in expanding the optical absorption of semiconductors to the visible range of the solar spectrum and minimizing the recombination rate of photogenerated charges [14, 15]. Amongst the semiconductors, TiO_2 has been widely applied due to its strong oxidizing power, large surface area, corrosion resistance, non-toxicity, and cost effectiveness [14, 16].

The use of TiO_2 photocatalysts for industrial applications has been limited due to high recombination rate and the fact that these are only photo responsive in the ultra-violet region [17, 18]. Different strategies toward improving these intrinsic limitations of TiO_2 include doping with inorganic or metallic species or photosensitizing TiO_2 with organic dyes [19-21]. Among the different techniques, doping with metals has been the most commonly applied method for reducing the recombination of charges and achieving visible light-driven photocatalysis by TiO_2 [22, 23]. Metal doping has largely been popular due to its simplicity, high efficiency, and easy synthetic route [22, 24]. Metal dopants have been reported to act as sinks for trapping electrons and holes thereby reducing the rate of recombination [23]. For example, Bi-doped TiO_2 and Ni-TiO_2 nanocomposites were reported to have better photo-catalytic performance in the degradation of ibuprofen compared to Degussa TiO_2 due to charge separation effected by Bi and Ni respectively [25].

Recently, surface modification of TiO_2 with conducting polymers has attracted great attention [26-28]. This has been reported to greatly enhance the degradation performance due to improved charge separation. For example, TiO_2/Nb_2O_5/PANI nanocomposite synthesized by a hydrothermal process and in-situ polymerization of PANI was shown to have better degradation properties than TiO_2/Nb_2O_5 due to improved charge separation effected by PANI [29]. In another study, 3D porous PANI/TiO_2–graphene hydrogel showed enhanced degradation of BPA under UV radiation due to improved photoresponse by PANI. PANI was chosen as a polymer because of its stability, facile synthesis in addition to its absorption properties for organics via π-π stacking [30]. Due to these desirable properties of PANI, TiO_2, and nano Ag, we envision an enhanced degradation performance from the nanocomposite.

Although there have been reports of Ag doped TiO_2 nanocomposite as photocatalysts for organics, there are no reports on PANI supported Ag@TiO_2 for the degradation of Bisphenol A under UV and visible light [31-33].

Based on the above consideration, in the present work, Ag@TiO_2-PANI nanocomposite was prepared and applied for the degradation of BPA under UV radiation and visible irradiation.

6.1 MATERIALS AND METHODS

6.1.1 Reagents and instrumentation

Aniline, silver nitrate ($AgNO_3$,99%), titanium isopropoxide (TTIP), isopropyl alcohol, acetic acid, sodium hydroxide (NaOH), nitric acid (HNO_3), iron(III) chloride ($FeCl_3$), Isopropyl alcohol, methanol (HPLC Grade), acetonitrile (HPLC Grade), hydrochloric

acid, potassium iodide, benzoquinone, ethanol and acetone were purchase from Sigma Aldrich and used without further purification. Ultrapure water was obtained from a Merck water system (MiliQ).

UV−visible diffuse absorbance and reflectance spectra (DRS) were measured using a Shimadzu 1700 UV spectrophotometer. Raman spectra were recorded using a WITec Confocal Raman Microscope. X-ray diffraction was conducted using a Philips, X"Pert PRO MPD X-ray diffractometer. A Micromeritics ASAP 2020 surface area and porosity analyzer (Norcross, USA) was used for analysis of samples Brunauer-Emmett-Teller (BET). A VEGA3 TESCAN (Bruno, Czech Republic) scanning electron microscope was used for SEM and electron dispersive x-ray spectroscopy analysis. In-depth analysis of the morphology of materials was performed by a JEOL JEM-2100 transmission electron microscopy (TEM) electron microscope (Peabody, Massachusetts, USA). The images were collected on Gaitan Digital Imaging software.

X-ray photoelectron spectroscopy (XPS) analysis was performed using a Physical Electronics (PHI) Quantum 200 XPS spectrophotometer with Al Kα as the excitation source. Thermogravimetric analysis (TGA), was conducted using a STA 7200RV HITACHI thermogravimetric analyzer. Photoluminescence measurements were performed using a Perkin Elmer LS45 Fluorescence Spectrometer.

6.1.2 Synthesis of PANI

PANI was synthesized following a method reported in literature with slight modification [34]. In a typical synthesis, an oxidant, $FeCl_3$ (6 g) was dissolved in 40 mL of distilled water and 0.8 mL of aniline monomer was rapidly added to the oxidant solution under stirring. Distilled water (40 mL) was slowly added to the solution while

stirring for about five minutes and then left to stand for 12 hr producing a green product. The green product was washed with acetone to remove unreacted aniline monomers and then further washed with distilled water ~pH 7. The green product was filtered under vacuum and dried in an oven at 60°C.

6.1.3 Synthesis of TiO_2 nanofibers

The synthesis of TiO_2 nanofibers was carried out using a microwave method. In a typical synthesis, TTIP (3 mL) was dissolved in a mixture of Isopropyl alcohol and water (5:3). The solution was poured into a 100 mL beaker and stirred. Concentrated acetic acid (6 mL) was added to the solution whilst stirring. The solution was stirred until homogeneous (~ 2hrs). NaOH pellets (6 g) were then added to the mixture slowly and stirred until they completely dissolved. The mixture in a beaker was covered with a watch glass and quickly transferred to a microwave at a power of 200 W for 20 min. The white powder obtained was washed with deionised water and ethanol dried in air at 80°C for 24 h to remove water and excess ethanol. The powders were then calcined at 500°C in a muffle furnace in air producing TiO_2 nanofibers.

6.1.4 Synthesis of Ag@TiO_2 nanocomposite

Ag@TiO_2 nanocomposite was synthesized in two steps. Typically 1 g TiO_2 nanofibers synthesized in section 6.1.3 were dispersed in 30 mL of ethanol solution. $AgNO_3$ salt (10 mg) was added to the suspension and stirred for an hour in the dark. The mixture was then irradiated with a UV lamp for 10 min under stirring to photo-reduce the Ag ions on the TiO_2 nanofibers. The mixture was centrifuged and dried in an oven at 60°C whilst covered in a perforated aluminum foil.

6.1.5 Synthesis of Ag@TiO_2-PANI nanocomposite

Ag@TiO_2-PANI nanocomposite was synthesized by dispersing a sample synthesized following the procedure outlined in section 2.4 in water and adding an aniline monomer and 3 g of $FeCl_3$. The mixture was then irradiated with a UV lamp for 10 min under stirring. This was followed by washing with acetone to remove the unreacted aniline monomers. The greenish precipitate was then dried in an oven at 60°C whilst covered in a perforated aluminum foil.

6.2 PHOTOCATALYTIC DEGRADATION STUDIES

The photodegradation activity of the as-synthesized catalysts was evaluated using 5 mg/L BPA solution in a reactor under simulated solar and ultraviolet light. In the experiments, the mixture of the catalyst and BPA was magnetically stirred in the dark for 30 min to ensure the adsorption equilibrium of BPA on the catalyst. To investigate the performance of the catalyst under UV light a mercury lamp (400 W) was used. For performance evaluation under visible light, a halogen (500 W) lamp, was used at room temperature. In order to maintain constant temperature, cooled water was continuously circulated through the double-walled jacket of photo reactor.

In a typical test, 0.2 g/L of the photocatalyst was dispersed in BPA solutions (5 mg/L). At varied time intervals, aliquots (10 mL) were removed from the sample and filtered through 0.45 µm membranes filter discs. BPA analysis was conducted using an Agilent high-performance liquid chromatography (HPLC) using acetonitrile/water (40/60, v/v) as the mobile phase, an elution time of 15 min, and a detector wave-length of 275 nm. A C18 reversed-phase column (4.6 nm × 150 nm) was used for chromatographic analysis. All measurements of the BPA degradation at different irradiation times were performed three times to confirm their reproducibility. The

presented data points are mean values. The removal efficiency of BPA was calculated as follows:

$$\% \, Removal = \frac{C_i - C_f}{C_i} x \, 100 \qquad 6.1$$

where C_i (mg/L) is initial concentration of adsorbate in solution, C_f (mg/L) is the final concentration of adsorbate in the filtrate.

6.3 CHARACTERIZATION OF THE PHOTOCATALYSTS

6.3.1 Raman spectra analysis

Figure 6.1 shows Raman spectra of as-prepared, PANI, TiO_2, 2% Ag@TiO_2 and 2% Ag@TiO_2-PANI samples.

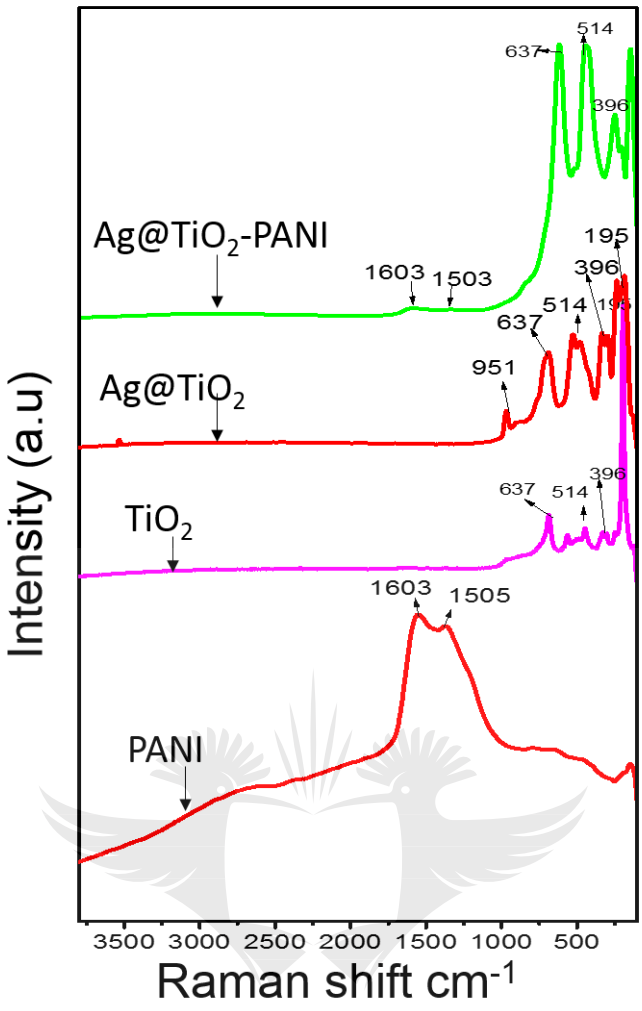

Figure 6.1: Raman spectra of pristine PANI, pristine TiO_2, 2% Ag@TiO_2 and 2% Ag@TiO_2-PANI.

The Raman spectra of PANI showed, two characteristic bands: D-band and G-band, which are observed at 1505 cm^{-1} and 1603 cm^{-1} respectively. The D-band and G-band are found in carbonaceous materials [35]. The Raman scattering spectra of pristine TiO_2 showed typical anatase peaks at 195, 396, 514 and 637 cm^{-1} [36]. This in agreement with XRD results (Figure 6.2). Raman spectra of Ag@TiO_2 showed all peaks that appeared in pristine TiO_2 and this showed that the incorporation of Ag did not alter the phase of the TiO_2. A peak at 951 cm^{-1} in the Ag@TiO_2 sample was

due to the presence of Ag_2O [37]. The spectra for Ag@TiO_2-PANI nanocomposites showed both peaks corresponding to PANI as well as of anatase TiO_2.

6.3.2 XRD analysis

Figure 6.2 shows results for XRD analysis carried out on photocatalysts. The XRD patterns revealed that the Ag nanoparticles, TiO_2, Ag@TiO_2, and Ag@TiO_2-PANI nanocomposite were crystalline.

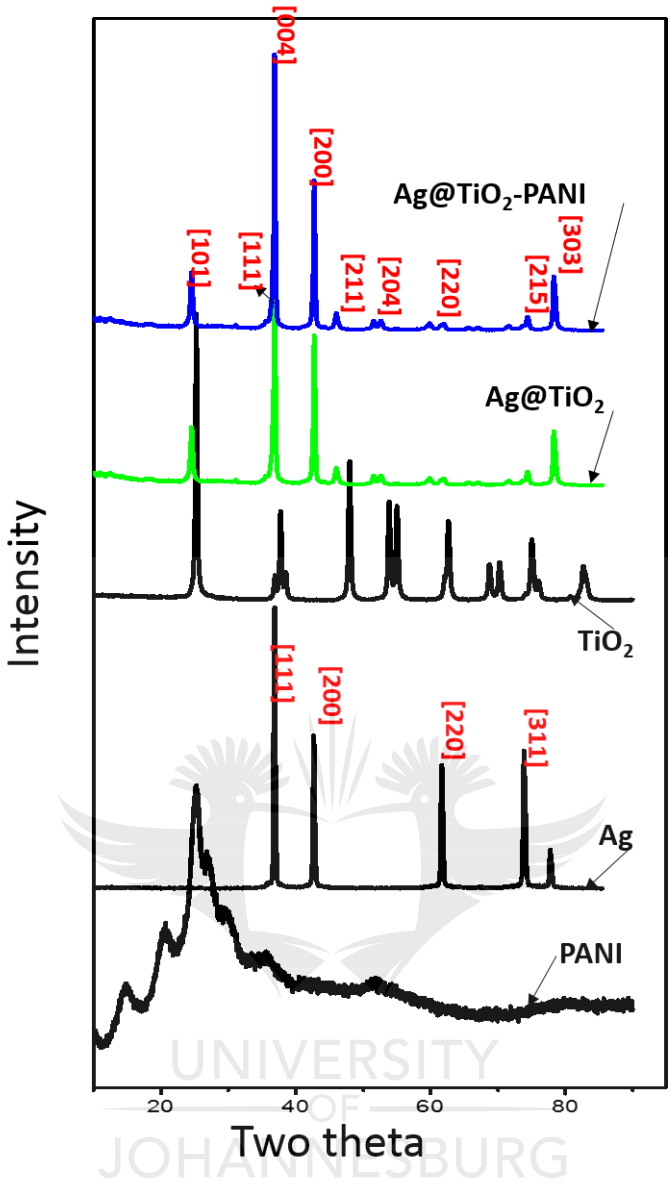

Figure 6.2: XRD plot of pristine PANI, pristine Ag, pristine TiO_2, and Ag@TiO_2-PANI.

The XRD analysis of PANI showed two broad peaks at 2θ=20.5° and 25.3° suggesting that PANI was amorphous [38]. This is in agreement with the XRD results that Mostafaei et al. reported for PANI. XRD patterns of nano Ag showed characteristic diffraction peaks at 2θ values of 38.45°, 46.35°, 64.75° and 78.05° which corresponds to the planes of [1 1 1], [2 0 0], [2 2 0] and [3 1 1] respectively [39]. Analysis of TiO_2 resulted in peaks corresponding to the 2θ values

of 25.22°, 37.78°, 47.94°, 54.15°, 54.96°, and 62.69° which were indexed to the [101], [004], [200], [211], [105], and [204] planes of TiO_2, which corresponded to the standard pattern of the anatase phase (JCPDS card No. 01-086-1157) [40]. From the XRD patterns, a slight shift of the plane 101 peak in the Ag@TiO_2 and Ag@TiO_2-PANI samples was observed. This shift to lower 2θ values indicate that the Ag doped samples were in a state of uniform compressive stress as explained by Parangusan et al.[41]. In addition, the intensity of the diffraction peaks decreased. This may be attributed to the lattice disorder of TiO_2 by Ag ions similarly observed by Roy et al. when they doped SnO_2 nanocrystals with Co [41, 42].

The crystallite sizes were estimated using Debye–Scherrer equation (see Equation 6.2) and estimated by using the full width at half maxima of the XRD peaks [43].

$$D = \frac{0.89\lambda}{t\cos\theta} \qquad 6.2$$

where K is the grain shape factor (0.89 for spherical),

λ is the wavelength of CuKα (1.5406 Å) and

t is the thickness of the crystal and θ is the Bragg`s angle.

The average crystallite size of anatase TiO_2 and Ag were calculated to be 17.5 nm and 8.23 nm.

6.3.4 BET analysis

Figure 6.3 shows the nitrogen adsorption isotherm (BET) of as-synthesized photocatalysts.

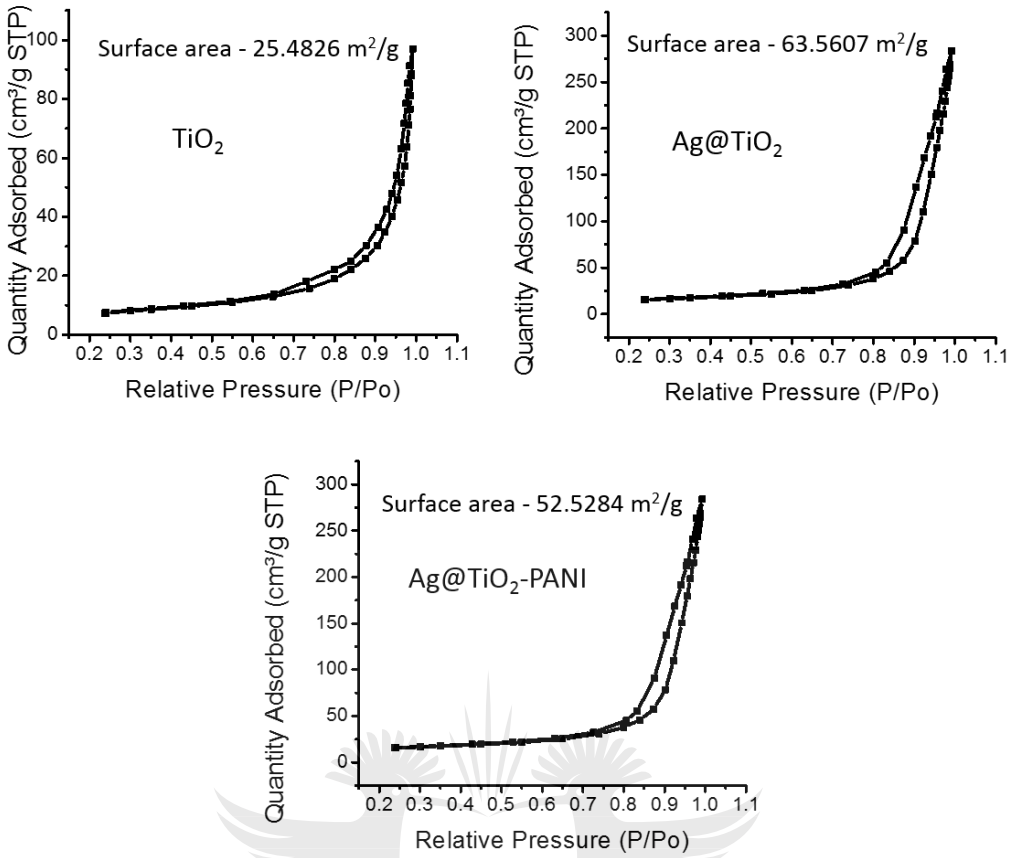

Figure 6.3: BET plot of pristine TiO_2 and 2% $Ag@TiO_2$ and 2% $Ag@TiO_2$-PANI.

BET analysis showed that doping TiO_2 with Ag greatly increased the surface area from 24.5 m^2/g for pristine TiO_2 to 63.5 m^2/g of the nanocomposite. However, the surface area of 2% $Ag@TiO_2$ reduced to 52.5 m^2/g after wrapping the 2% $Ag@TiO_2$ nanocomposite in PANI. This is understandable as the polymer compacted the nanofibers and Ag nanoparticles, which resulted in a dense nanocomposite. The results shown in Figure 6.3 illustrates that all the as-synthesized photocatalysts can be identified as Type IV isotherms with H4 type hysteresis loop according to the IUPAC-BET classification [44]. This signifies the presence of mesoporous structure in the photocatalysts [44].

6.3.5 SEM analysis

SEM micrographs showed that nanofibers of TiO_2 were prepared with different diameters. The morphology of the nanofibers did not change on attaching Ag nanoparticles on them. However, the TiO_2 nanofibers agglomerated together on wrapping them with PANI as shown in Figure 6.4a.

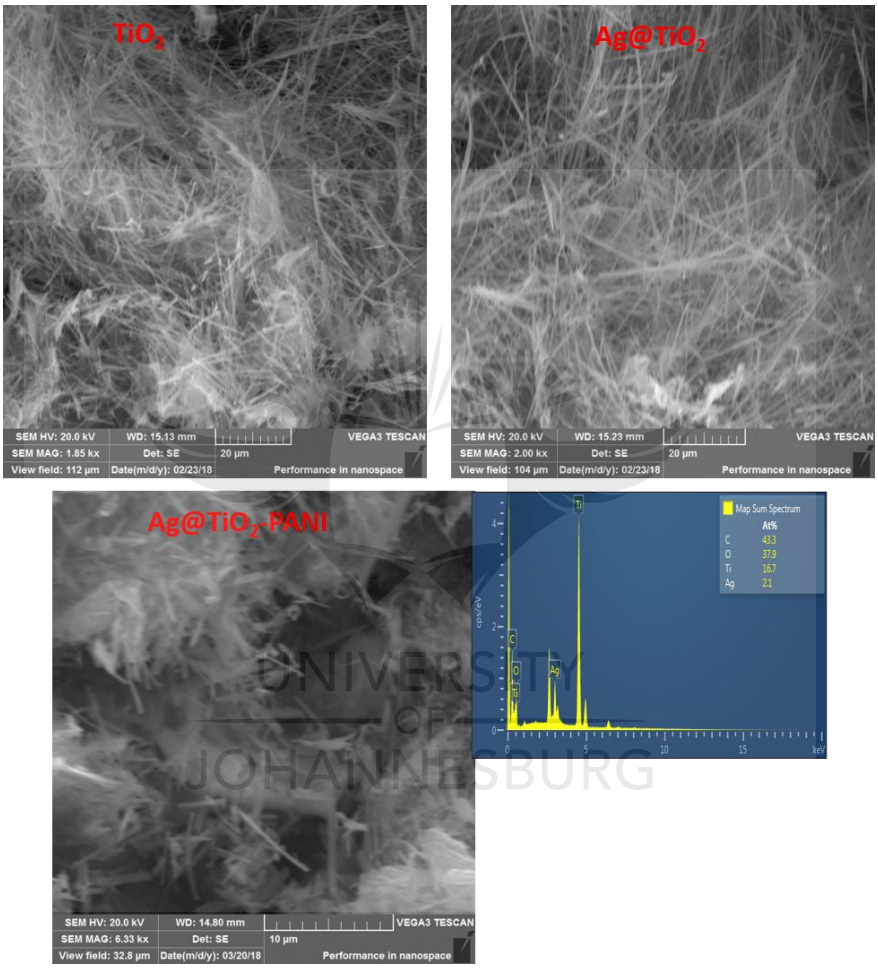

Figure 6.4a: SEM images of pristine TiO_2 and 2% Ag@TiO_2 and EDS of 2% Ag@TiO_2-PANI.

As seen in the mapping images (Figure 6.4b) the nanocomposites was predominantly composed of Ti, C, O, and Ag that were homogeneously distributed in the nanocomposite.

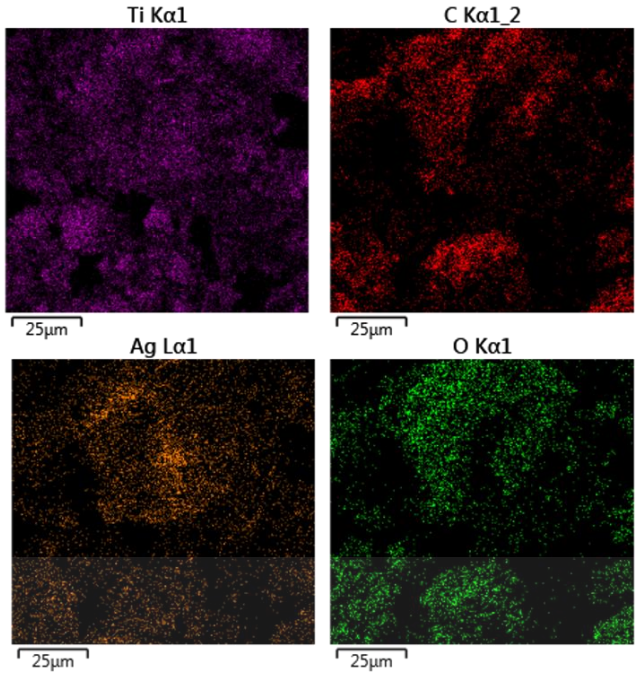

Figure 6.4b: Mapping image area of 2% Ag@TiO_2-PANI.

These results corroborated with results obtained for EDS analysis shown in Figure 6.4a.

6.3.6 TEM analysis

TEM images of pristine TiO_2 nanorods, Ag@TiO_2 and Ag@TiO_2-PANI were shown in Figure 6.5.

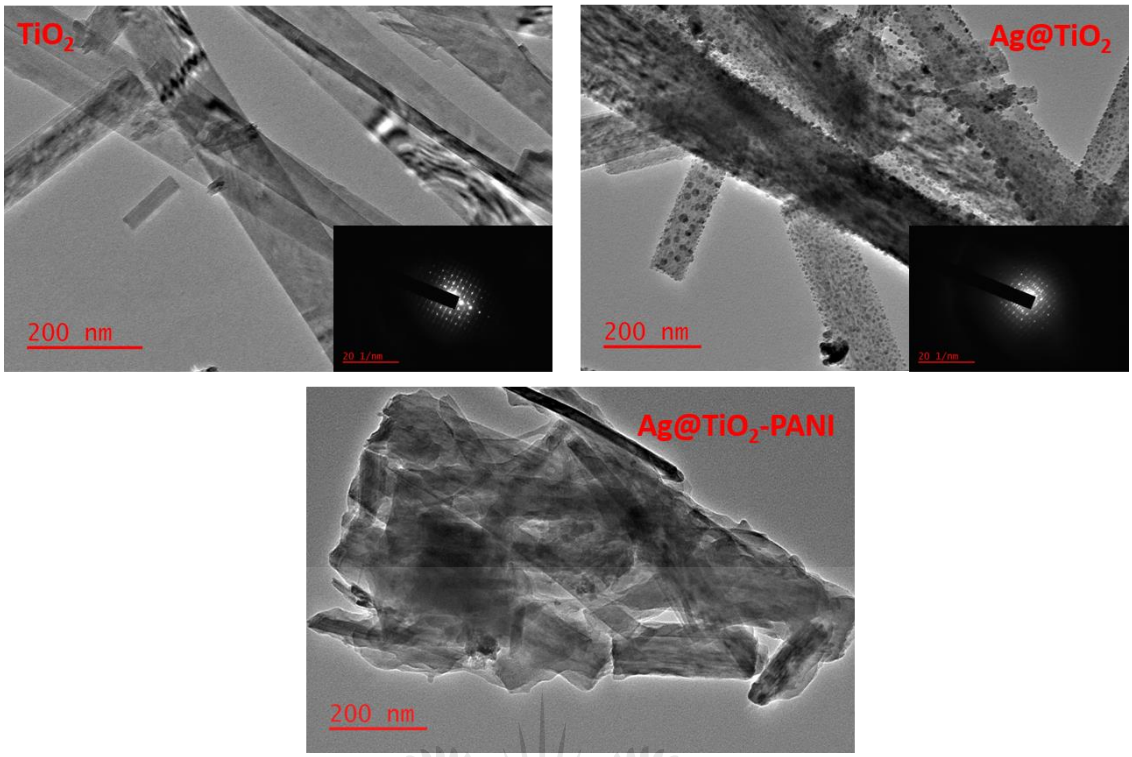

Figure 6.5: TEM images of pristine TiO_2, Ag@TiO_2, and Ag@TiO_2-PANI.

The results showed that the pristine TiO_2 nanorods were successfully synthesized. The TEM images showed uniformly dispersed TiO_2 nanorods of different sizes. The TEM images also showed minimal agglomeration of the TiO_2 nanoparticles. Agglomeration is not ideal in a photocatalyst as it will affect the absorption of light and hence the photodegradation efficiency in the nanocomposite or the photocatalyst. TEM image of Ag@TiO_2 show Ag nanoparticles of different sizes on the surface of TiO_2 nanorods. A layer of PANI covered the TiO_2 nanorods as revealed by the TEM images shown in Figure 6.5.

6.3.7 Band gap estimation for pristine TiO_2 nanorods and Ag doped TiO_2

Figure 6.6a shows the UV absorbance of PANI with two absorption peaks at 268 and 395 nm which were ascribed to a π−π transition of the benzenoid rings and charge transfer from the benzenoid to the quinoid, respectively [45].

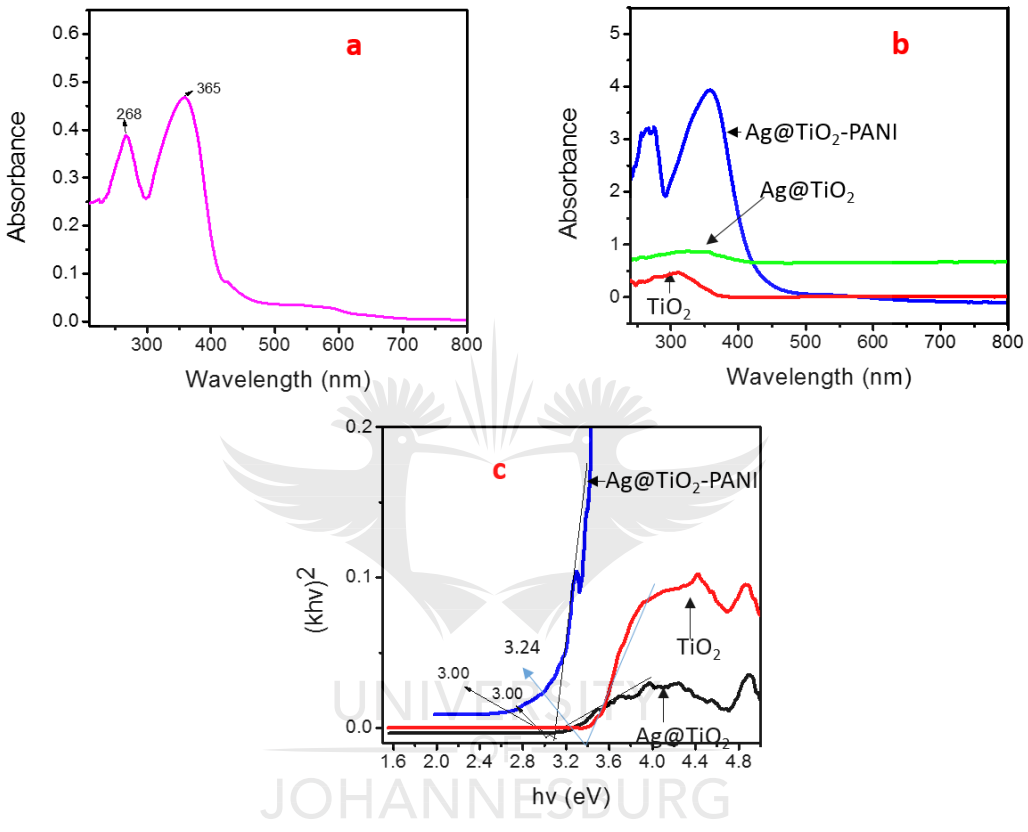

Figure 6.6: (a) UV DRS of pristine PANI, (b) UV DRS of TiO_2, 2% Ag@TO_2, 2% Ag@TO_2-PANI and (c) Tauc`s plot of pristine.

Figure 6.6b shows that the incorporation of Ag on the TiO_2 surface greatly influenced the surface properties of the nanocomposite with changes in the optical properties in the region of 400–500 nm that can be attributed to the surface plasmon resonance effect [46]. The band gap of pristine TiO_2 nanorods was shown to be about 3.2 e.V. This is in agreement with reported band gap for anatase TiO_2 [47]. This is in perfect sync with XRD results that were reported earlier. The results shown in Figure 6b

show that the band gap decreased to 3.0 e.V after loading Ag on the surface of TiO_2. The modification of band gap is essentially due to the interaction between the Ag and TiO_2 nanoparticles. Ag nanoparticles influence the band gap of the nanocomposite by creating of trap levels for electrons between the conduction bands and valence bands of TiO_2. The loading of Ag nanoparticles on TiO_2 results in the synergetic interaction of the Ag nanoparticles on the TiO_2 surface, surface plasmon resonance effect, reduction of the band gap, and enhancement of the charge transfer process [48]. This is in agreement with the findings of other researchers [49].

6.3.8 Thermogravimetric analysis

TGA was used to study the thermal stability of the photocatalysts. The results of the thermal profiles of as-synthesized photocatalysts are shown in Figure 6.7.

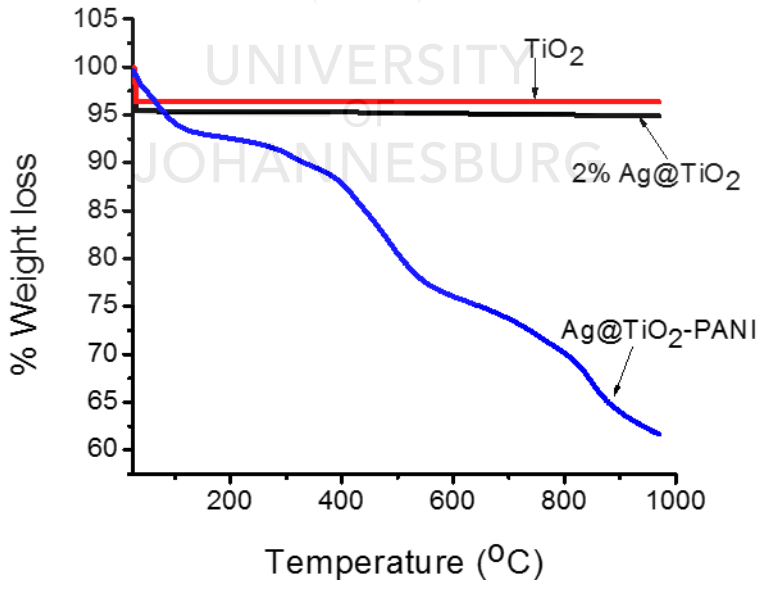

Figure 6.7: Thermal profile for TiO_2, 2% Ag@TiO_2, and 2% Ag@TiO_2-PANI.

The results showed similar weight loss up to 100°C in TiO_2 and Ag@TiO_2. This weight loss was due to loss of water molecules in the catalysts [45]. Ag@TiO_2-PANI

nanocomposite had three major stages of weight losses. The first weight loss until ~150°C was due to the loss of water and other volatile impurities in the nanocomposite. The weight loss at 400°C is due to structural decomposition of the PANI whilst above 450°C there was degradation of oligomers in the nanocomposite [50]. The third loss above 500°C was due to the loss of PANI. The residue that remained above 550°C was due to Ag@TiO_2.

6.3.9 X-Ray Photoelectron spectrometry

XPS was used to investigate the surface composition and the chemical states of the elements of Ag@TiO_2-PANI nanocomposite. Figure 6.8a shows the X-ray survey scan of Ag@TiO_2-PANI which showed that the nanocomposite was composed of Ag, C, N, Ti and O elements with photo-electron peaks Ag 3d, C 1s, N 1s, Ti 2p, and O 1s respectively.

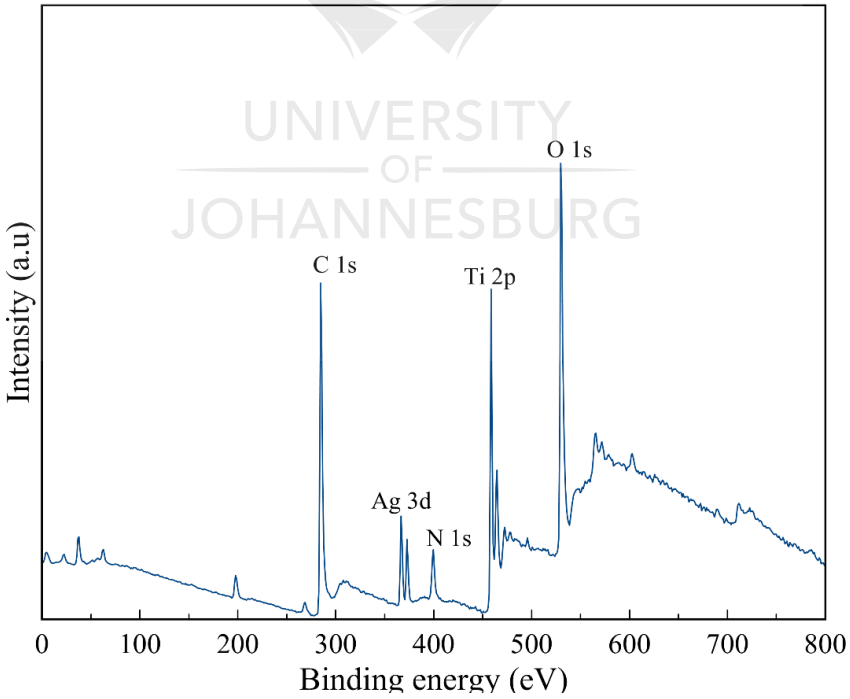

Figure 6.8 (a) XPS survey scan for Ag@TiO_2-PANI nanocomposite.

A peak at 284.75 eV shown in Figure 6.8b was assigned to carbon from the PANI polymer [51]. Figure 6.8c shows a peak at 367.1 eV and 373.1 eV that were assigned to 3d5/2 and 3d3/2 respectively [52]. Figure 6.8d shows a peak at 399.6 eV which was ascribed to N 1s from PANI [51]. Core level spectra of Ti 2p is shown in Figure 6.8e at 459.2 eV and 464.9 eV due to Ti 2p1/2 and Ti 2p3/2 respectively [53].

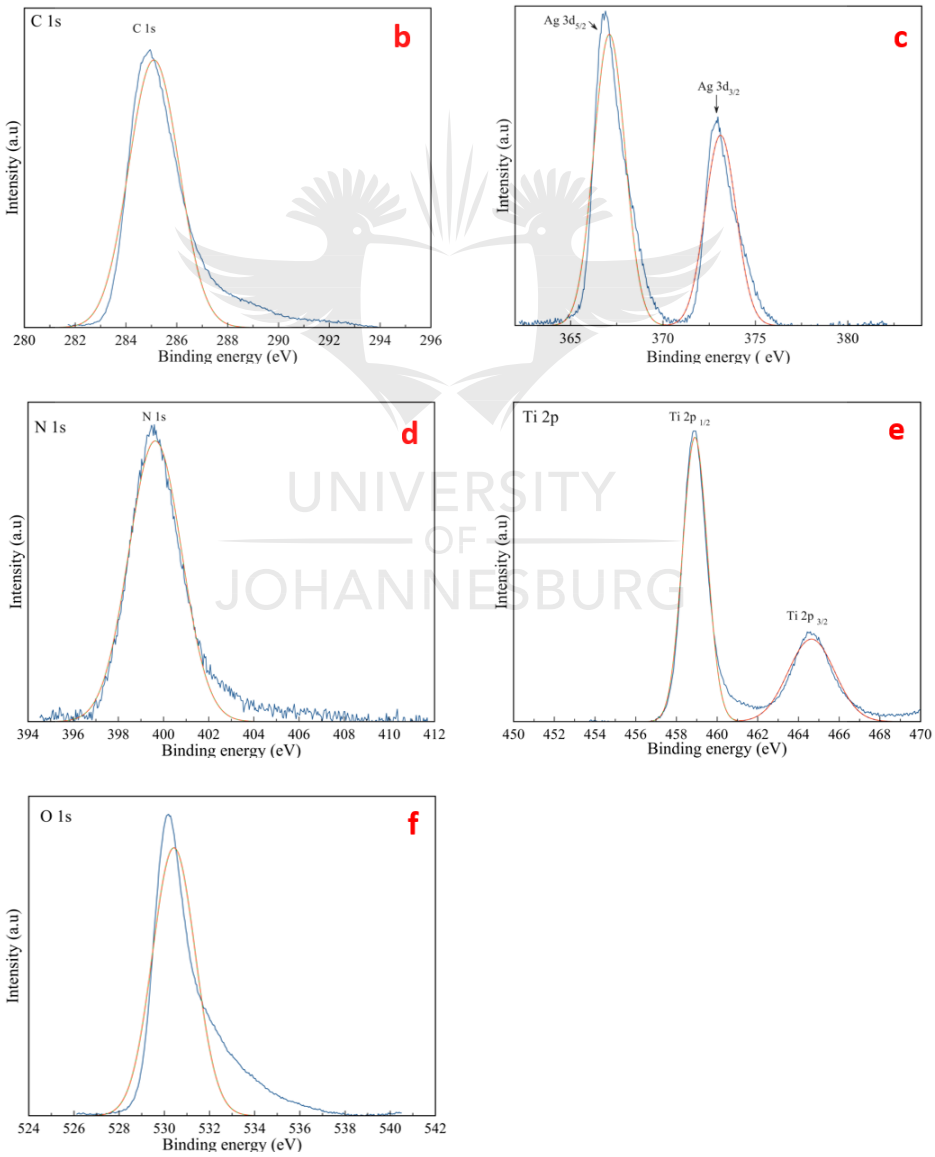

Figure 6.8: Core level XPS spectra for (b) C 1s, (c) Ag 3d, (d) N 1s (e) Ti 2p and (f) O 1s of 2%Ag@TiO_2-PANI nanocomposite.

6.3.10 Photoluminescence

Photoluminescence (PL) intensity is widely reported to indicate the recombination of charges in a semiconductor material [54]. Low PL intensity indicates low recombination rate of electron and holes. This presents a better chance of charge transfer by charge carriers. PL intensity can be manipulated by doping of semiconductor materials [55]. In this study, the PL spectra of materials was measured at excitation wavelength of 351.8 nm. As shown in Figure 6.9, 2% Ag@TiO_2-PANI nanocomposite has the lowest PL intensity compared to TiO_2, PANI and 2% Ag@TiO_2. Furthermore, the results revealed that modification of TiO_2 with PANI and Ag nanoparticles reduced the intensity of the PL.

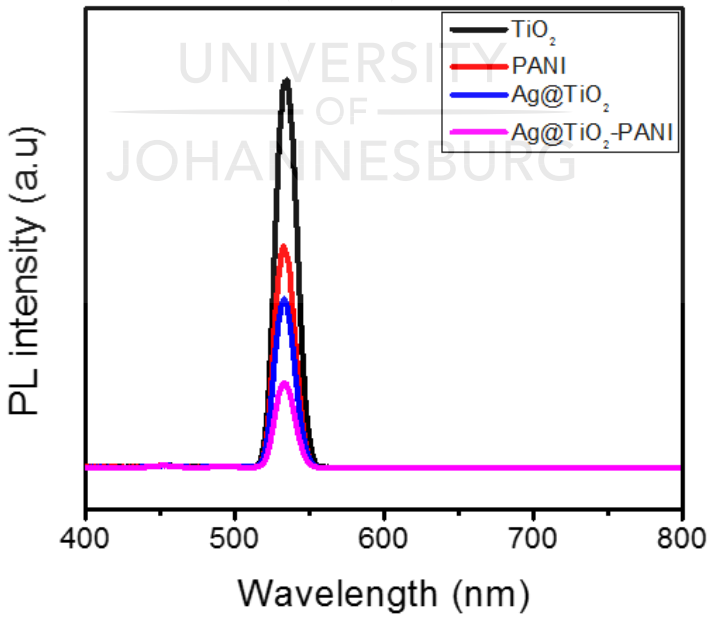

Figure 6.9: PL spectra of TiO_2, PANI, 2% Ag@TiO_2, and 2% Ag@TiO_2-PANI at an excitation wavelength of 351.8 nm.

This indicates that 2% Ag@TiO_2-PANI has the lowest recombination rate of charges. Therefore, it presents a better efficiency as a photocatalyst. The incorporation of PANI resulted in charge separation which occurred by transfer of electrons to the conduction band of TiO_2 and trapping of holes by PANI.

6.4 PHOTODEGRADATION OF BPA

6.4.1 Catalyst selection

The photocatalytic degradation of BPA was investigated using different catalysts at solution pH 6.5. The results are shown in Figure 6.10.

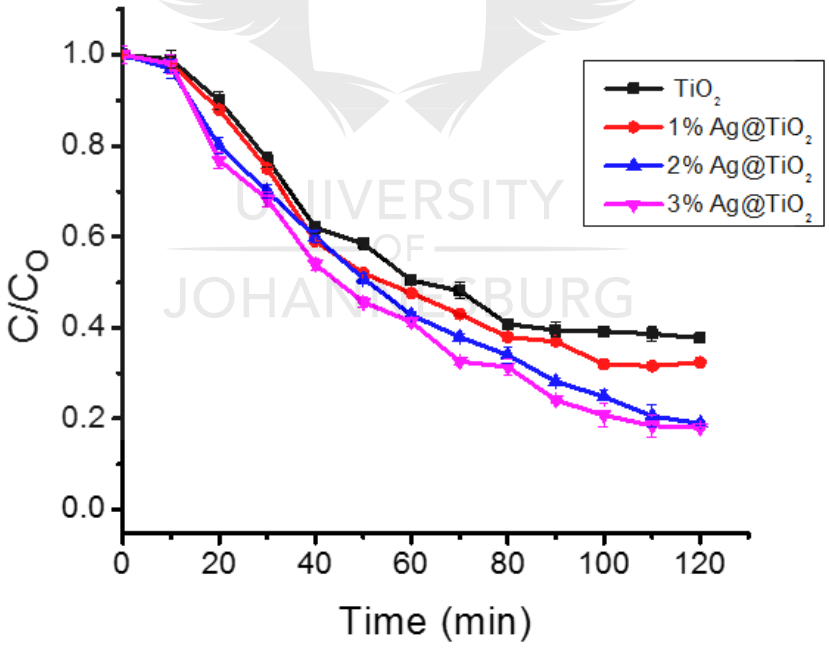

Figure 6.10: Degradation performance of Ag-loaded TiO_2 catalysts on BPA.

The photocatalytic degradation of 5 mg/L of BPA was investigated using different catalysts at solution pH 6.5. The results are shown in Figure 6.10. The results show an improvement in catalyst performance with Ag loading. The highest BPA removal

percentage was achieved with 3% Ag@TiO_2 which removed 81.4% compared to 62.2% by pristine TiO_2 and 67.6% by 1% Ag@TiO_2 after 120 mins of visible light irradiation. The improvement in removal was attributed to the ability of Ag nanometals to effect charge separation by scavenging electron in the conduction band of TiO_2 thereby improving its photocalytic properties [56]. However, there was little difference in the removal percentage between 3% Ag@TiO_2 and 2% Ag@TiO_2 which had a removal of 82.5%. Therefore, a 2% Ag@TiO_2 was chosen for further modification with PANI.

Figure 6.11 show results of the performance of different Ag loaded TiO_2 photocatalyst and 2% Ag@TiO_2-PANI nanocomposite in the removal of 5 mg/L BPA.

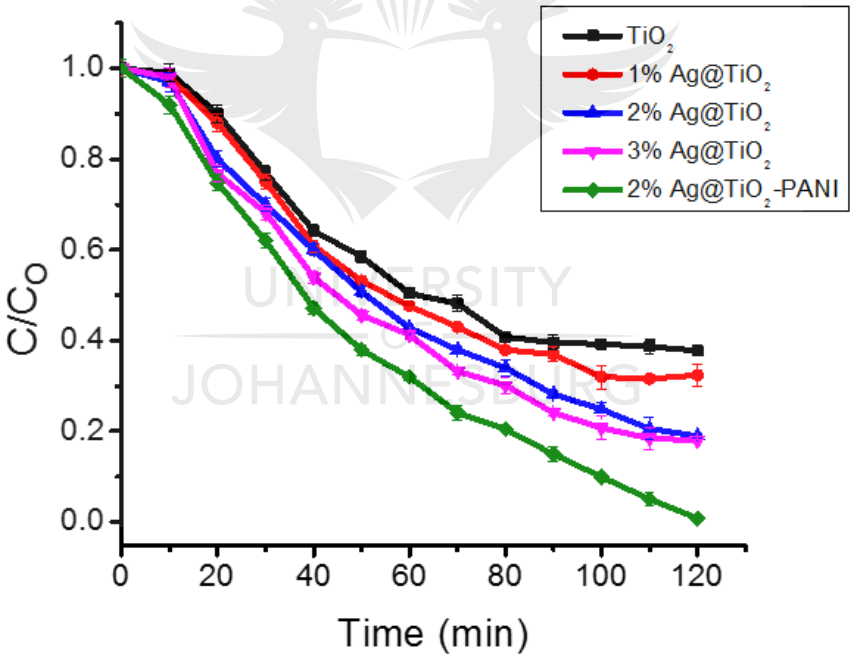

Figure 6.11: Degradation performance of different catalyst on BPA.

The results showed that incorporation of PANI in the 2% Ag@TiO_2 nanocomposite enhanced the degradation performance further with removal of up to 99.7% under visible light irradiation. The improvement was attributed to PANI`s ability to effect

charge separation in addition to its ability to adsorb organics and facilitate their degradation by a semiconductor such as TiO_2 [26, 28, 29].

6.4.2 Comparison of BPA degradation under UV and solar light source

The photodegradation of BPA solution by as-synthesized TiO_2, 2% $Ag@TiO_2$ and 2% $Ag@TiO_2$-PANI was carried out under UV and visible light at room temperature. Figure 6.12 (a) shows the degradation performance of TiO_2, $Ag@TiO_2$, $Ag@TiO_2$-PANI, and photolysis. Pristine TiO_2 degraded 60% BPA in 70 mins under UV light irradiation. The addition of Ag nanoparticles to TiO_2 resulted in a 99.4% degradation efficiency within 60 mins by the 2% $Ag@TiO_2$ nanocomposite. The enhanced degradation by $Ag@TiO_2$ can be attributed to the plasmonic effect of Ag nanoparticles [57, 58]. The incorporation of PANI to 2% $Ag@TiO_2$ further resulted in slight acceleration of the degradation of BPA with 99.5% attained within 55 mins of UV irradiation. This was ascribed to improved charge separation effected by PANI in addition to the plasmonic effect of Ag [58, 59].

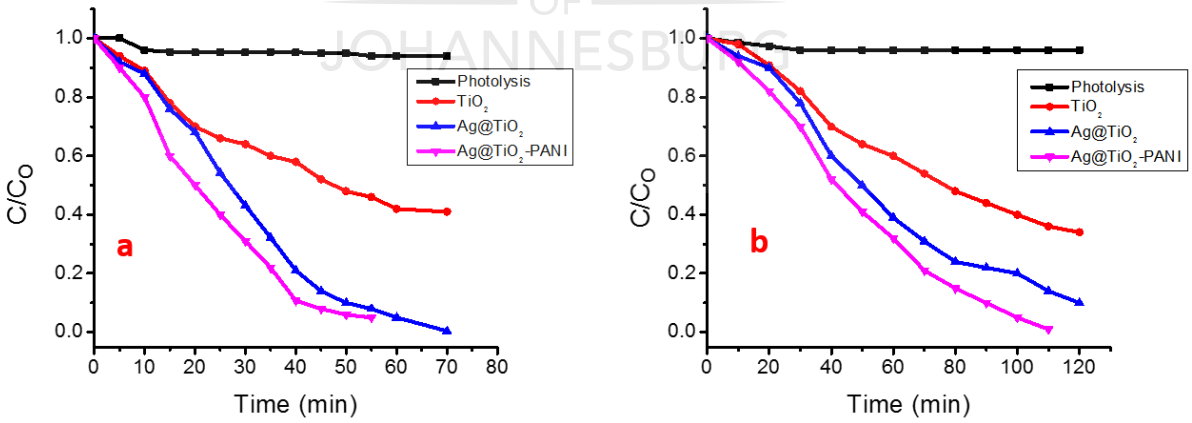

Figure 6.12: Degradation of BPA under (a) UV and (b) visible light.

Figure 6.12 (b) shows the degradation performance of the catalysts under visible light irradiation. The results show that the degradation of BPA took longer to achieve maximum degradation under visible light than under UV light. As-synthesized TiO_2

photocatalyst had the lowest removal efficiency of the catalysts used with a removal percentage of 60% over 110 mins of visible light irradiation. There was a marked removal performance by 2% Ag@TiO_2 nanocomposite with a removal of 95.8% in the same time under visible light irradiation. The improvement was due to the plasmonic influence of Ag nanoparticles. Likewise, an improvement in the performance of 2% Ag@TiO_2-PANI nanocomposite was noted under visible light irradiation with a removal percentage of 99.7% attained in 110 mins. The improvement was attributed to a combined effect of plasmonic effect of Ag nanoparticles, the charge separation effected by PANI [26, 59]. In addition, PANI adsorbs organics such as BPA allowing them more contact time with TiO_2 for degradation.

6.4.3 Kinetics

For a better understanding of the photocatalytic efficiency of the as-synthesized photocatalysts, the kinetic analysis of BPA degradation was investigated under ultra-visible light and visible light irradiation. The pseudo-first kinetic model can be used to describe the degradation of BPA and is by the expressed by Langmuir-Hinshelwood relation shown in Equation 6.3: [60]

$$\frac{-dc}{dt} = kr\frac{Kc}{1+Kc} \qquad 6.3$$

where (−dC/dt) is the rate of degradation of BPA, C is the concentration of BPA, t is the reaction time, kr is a reaction rate constant, and K is the adsorption coefficient of the reactants. The results of the Langmuir-Hinshelwood kinetic model are shown in Figure 6.13. Figure 6.13(a) shows the kinetics under UV radiation and Figure 6.13(b) shows the kinetics under visible radiation.

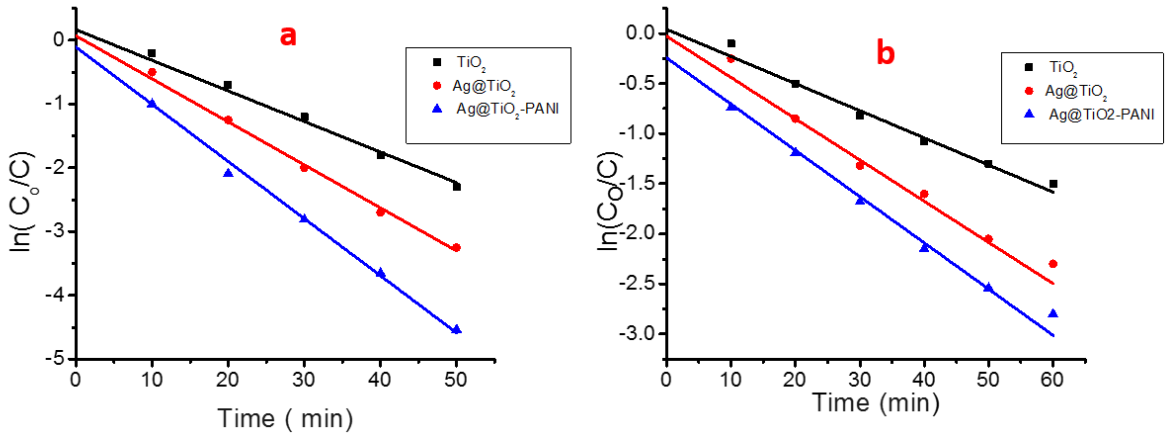

Figure 6.13: ln (C/C_o) vs time under (a) UV and (b) visible irradiation.

The results in Figure 6.13 suggests that the degradation of BPA follow the L-H kinetic model with good linear relationship (R^2> 0.99). The value of kr for the degradation of BPA under UV light irradiation by 2% Ag@TiO_2 and 2% Ag@TiO_2-PANI was 2.8 X 10^{-2} min^{-1} and 3.4 X 10^{-2} min^{-1} respectively compared to 1.96 X 10^{-2} min^{-1} by pristine TiO_2. The values of kr were slightly lower under visible radiation but still showed the same increase after modification of TiO_2 with values of 2.3 X 10^{-2} min^{-1} and 2.85 X10^{-2} min^{-1} for 2% Ag@TiO_2 and 2% Ag@TiO_2-PANI compared to 1.78 X 10^{-2} min^{-1} of pristine TiO_2.

Table 6.1 shows a brief comparison of the degradation of BPA by different catalyst. It can be noted that the removal of BPA by 2% Ag@TiO_2-PANI is higher than the catalyst reported in literature. In addition, 2% Ag@TiO_2-PANI can be utilized under both UV and visible light with a degradation of at least 99.5%.

Table 6.1: Comparative results obtained for BPA degradation

Degradation system	Reaction conditions	Observations	Reference
2% N,B-TiO_2	1 µM 50 mL 0.5 g/L catalyst Visible light	79% degradation after 120 min	[61]
Vanadium-Titanate-Magnetite (VTM)	50 mg/L 12g/L catalyst Visible light	90% degradation, 120 min	[62]
Co_3O_4/Mxene	20 mg/L 0.1g/L catalyst Visible light	95% degradation, 20 min	[63]
$Mn_{1.8}Fe_{1.2}O_4$	10 mg/L 0.1g/L catalyst Visible light	95% degradation, 30 mins	[63]
Pulsed discharged plasma activated carbon	4 g 4 /min gas flow rate 100 mL/min BPA flow rate	95.3%, 60 mins	[64]
Ag@TiO_2-PANI	5 mg/L 0.2g/L 500 mL Visible light and UV light	99.7%(Visible light), 120 mins 99.5% (UV light, 60 mins)	In this study

6.4.4 Possible mechanism for BPA degradation

Reactive species such as hydroxyl ($OH^{\cdot}$), superoxide ($\cdot O^{2-}$) and holes (h^{+}) are strong oxidizing agents that have been widely reported to degrade organic pollutants [65,

66]. In this study, the investigation of the reactive species that were involved in the degradation of BPA by 2% Ag@TiO_2-PANI was carried out by using different scavengers for specific reactive species under visible light. The study was conducted by adding 1 mL of either 10 mM potassium iodide (KI), 10 mM of benzoquinone (BQ) or 10% isopropyl alcohol (IPA) to 500 mL reaction solution. Figure 6.14 show that very little degradation was achieved after the addition of KI that was used as a holes scavenger. This suggests that the positively charged holes were actively involved in the degradation of BPA.

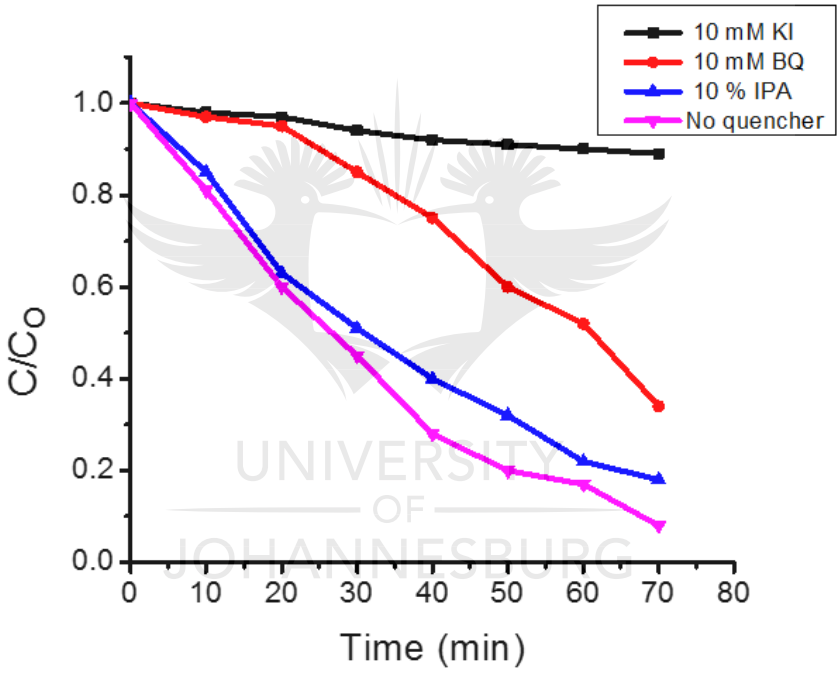

Figure 6.14: Photodegradation of BPA by 2% Ag@TiO_2-PANI after addition of different reactive species scavengers under visible irradiation.

In the presence of BQ, which was used as scavenger for superoxide radicals, degradation was reduced to 70 %. This suggests that the superoxide radicals were also involved in the degradation of BPA although their involvement was not as dominant as the positive holes. In the presence of 10%, IPA which was used as a scavenger for hydroxyl radicals, a slight decrease in the degradation efficiency was

observed suggesting that the hydroxyl radicals were not the dominant reactive species in the degradation of BPA by 2% Ag@TiO_2-PANI.

6.4.5 Mineralization of BPA

To test the activity of the 2% Ag@TiO_2-PANI, BPA mineralization was investigated by measuring the total organic carbon (TOC) variation during the degradation process. An initial BPA concentration of 5 mg/L was used. The results are shown in Figure 6.15.

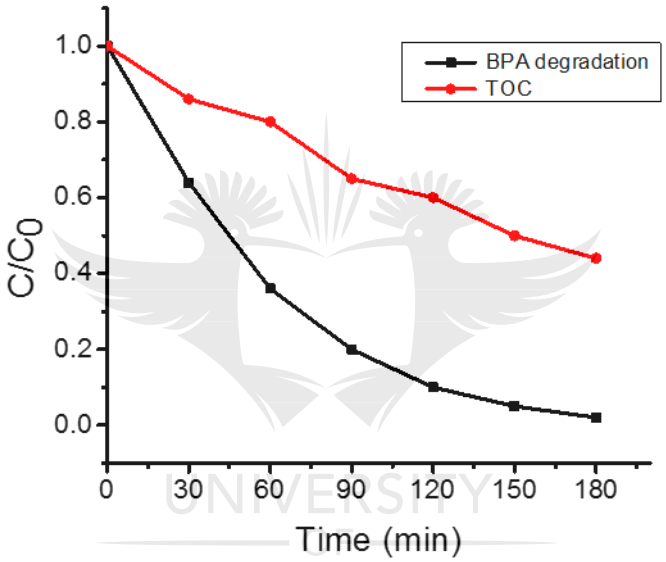

Figure 6.15: Removal of TOC during BPA degradation by Ag@TiO_2-PANI under visible light irradiation.

The results show that the photodegradation of BPA by Ag@TiO_2-PANI was effective under visible light irradiation. The results show that 56% of TOC was removed when 98% of BPA was degraded.

6.4.6 Reusability of Ag@TiO_2-PANI

The reusability of photocatalysts reduce the cost of the degradation process. To evaluate the performance of 2% Ag@TiO_2-PANI over reuse, the catalyst was collected by vacuum filtration after the degradation of 5 mg/L BPA, washed with

Milli-Q water and dried at 60°C in an oven. The weight loss of the catalyst was determined after which the dried catalyst was used for the degradation of a 5 mg/L BPA fresh solution in each of the cycles it was reused (four). The weight loss was determined and in our study, it was ~ 5%. Figure 6.16 shows the degradation performance of the photocatalyst after four runs. The results show that there was very little loss of efficiency by the catalyst with a degradation of at least 90% in the fourth cycle.

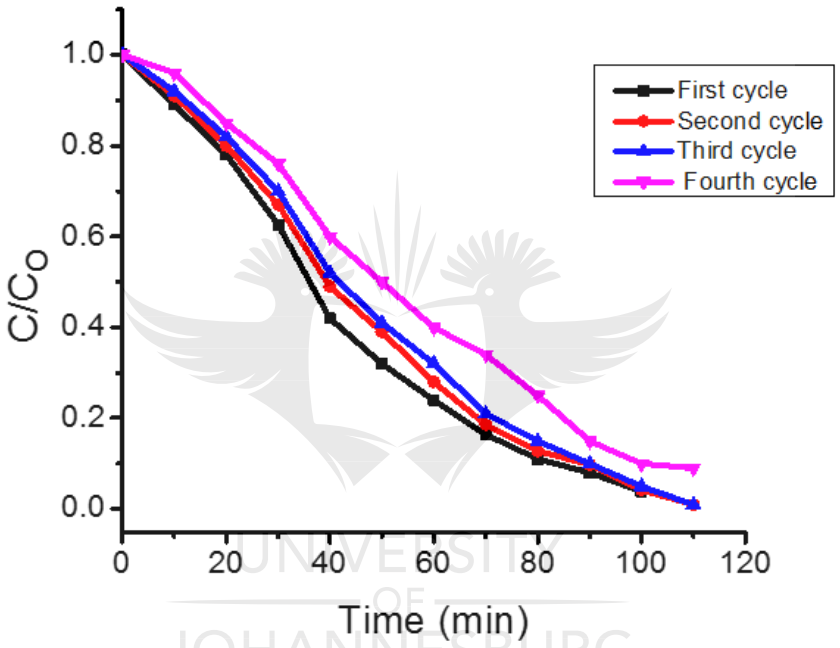

Figure 6.16: Reusability of 2% Ag@TiO_2-PANI for the degradation of BPA.

6.5 CONCLUSION

A PANI anchored 2% Ag@TiO_2 nanocomposite was successfully synthesized and applied for the degradation of BPA under UV and visible light radiation. TEM images showed successful deposition of Ag nanoparticles on TiO_2 nanofibers. TEM images also showed the successful wrapping of the 2% Ag@TiO_2 in a PANI polymer matrix. The Tauc`s plot showed that the band gap of the TiO_2 was reduced by the addition of Ag nanoparticles from 3.24 eV to 3.0 eV. The degradation experiments

highlighted that the incorporation of Ag and PANI improved the performance of the nanocomposites under UV and visible light irradiation with a removal of up to 99.8% attained in 110 mins under visible light. In addition, the degradation experiments showed that the reactive species that were dominant in the degradation of BPA were h^+ and $\cdot O_2^-$. The PANI supported 2% Ag@TiO_2 nanocomposite can be reused at least four times to degrade 5 mg/L BPA solution.

6.6 REFERENCES

[1] C. Sophia A, E.C. Lima, Removal of emerging contaminants from the environment by adsorption, *Ecotoxicology and. Environmental Safety*, 150 (2018) 1-17.

[2] V. Geissen, H. Mol, E. Klumpp, G. Umlauf, M. Nadal, M. van der Ploeg, S.E. van de Zee, C.J. Ritsema, Emerging pollutants in the environment: a challenge for water resource management, *International Soil and Water conservation Research*, 3 (2015) 57-65.

[3] B.-V. Chang, S.-N. Fan, Y.-C. Tsai, Y.-L. Chung, P.-X. Tu, C.-W. Yang, Removal of emerging contaminants using spent mushroom compost, *Science of The Total Environment,* 634 (2018) 922-933.

[4] R.K. Bhandari, S.L. Deem, D.K. Holliday, C.M. Jandegian, C.D. Kassotis, S.C. Nagel, D.E. Tillitt, F.S. Vom Saal, C.S. Rosenfeld, Effects of the environmental estrogenic contaminants bisphenol A and 17alpha-ethinyl estradiol on sexual development and adult behaviors in aquatic wildlife species, *General and Comparative Endocrinology,* 214 (2015) 195-219.

[5] S. Yüksel, N. Kabay, M. Yüksel, Removal of bisphenol A (BPA) from water by various nanofiltration (NF) and reverse osmosis (RO) membranes, *Journal of Hazardous Materials,* 263 (2013) 307-310.

[6] J.R. Koduru, L.P. Lingamdinne, J. Singh, K.-H. Choo, Effective removal of bisphenol A (BPA) from water using a goethite/activated carbon composite, *Process Safety and Environmental Protection*, 103 (2016) 87-96.

[7] M. Starling, C.C. Amorim, M.M.D. Leao, Occurrence, control and fate of contaminants of emerging concern in environmental compartments in Brazil, *Journal of Hazardous Materials*, 18 (2018) 30275-3894.

[8] C. Pétrier, R. Torres-Palma, E. Combet, G. Sarantakos, S. Baup, C. Pulgarin, Enhanced sonochemical degradation of bisphenol-A by bicarbonate ions, *Ultrasonics Sonochemistry,* 17 (2010) 111-115.

[9] K. Gandhi, S. Lari, D. Tripathi, G. Kanade, Advanced oxidation processes for the treatment of chlorpyrifos, dimethoate, and phorate in aqueous solution, *Journal of Water Reuse and Desalination*, 6 (2016) 195-203.

[10] P. Bansal, A. Verma, S. Talwar, Detoxification of real pharmaceutical wastewater by integrating photocatalysis and photo-Fenton in fixed-mode, *Chemical Engineering Journal*, 349 (2018) 838-848.

[11] D. Kanakaraju, B.D. Glass, M. Oelgemöller, Advanced oxidation process-mediated removal of pharmaceuticals from water: A review, *Journal of Environmental Management,* 219 (2018) 189-207.

[12] M.M. Ba-Abbad, A.A.H. Kadhum, A.B. Mohamad, M.S. Takriff, K. Sopian, Synthesis and catalytic activity of TiO_2 nanoparticles for photochemical oxidation of concentrated chlorophenols under direct solar radiation, *International Journal of Electrochemical Science*, 7 (2012) 4871-4888.

[13] D.A. Erdogan, E. Ozensoy, Hierarchical synthesis of corrugated photocatalytic TiO_2 microsphere architectures on natural pollen surfaces, *Applied Surface Science*, 403 (2017) 159-167.

[14] W.J. Ong, L.L. Tan, S.P. Chai, S.T. Yong, A.R. Mohamed, Highly reactive {001} facets of TiO_2-based composites: synthesis, formation mechanism and characterization, *Nanoscale,* 6 (2014) 1946-2008.

[15] Z. Dargahi, H. Asgharzadeh, H. Maleki-Ghaleh, Synthesis of Mo-doped TiO_2/reduced graphene oxide nanocomposite for photoelectrocatalytic applications, *Ceramics International*, 44 (2018) 13015-13023.

[16] P.M. Álvarez, J. Jaramillo, F. López-Piñero, P.K. Plucinski, Preparation and characterization of magnetic TiO_2 nanoparticles and their utilization for the degradation of emerging pollutants in water, *Applied Catalysis B: Environmental,* 100 (2010) 338-345.

[17] S.A. Bakar, C. Ribeiro, Rapid, and morphology controlled synthesis of anionic S-doped TiO_2 photocatalysts for the visible-light-driven photodegradation of organic pollutants, *The Royal Society of Chemistry Advances,* 6 (2016) 36516-36527.

[18] N.O. Balayeva, M. Fleisch, D.W. Bahnemann, Surface-grafted WO_3/TiO_2 photocatalysts: Enhanced visible-light activity towards indoor air purification, *Catalysis Today*, 313 (2018) 63-71.

[19] E. Bae, W. Choi, Highly enhanced photoreductive degradation of perchlorinated compounds on dye-sensitized metal/TiO_2 under visible light, *Environmental Science and Technology*, 37 (2003) 147-152.

[20] M. Aliabadi, One-step synthesis of highly efficient TiO_2-CdS-Ag nanocomposite for remove organic pollution, *Separation and Purification Technology,* 174 (2017) 145-149.

[21] T. Boningari, S.N.R. Inturi, M. Suidan, P.G. Smirniotis, Novel one-step synthesis of nitrogen-doped TiO_2 by flame aerosol technique for visible-light photocatalysis:

Effect of synthesis parameters and secondary nitrogen (N) source, *Chemical Engineering Journal*, 350 (2018) 324-334.

[22] B. Ünlü, S. Çakar, M. Özacar, The effects of metal doped TiO_2 and dithizone-metal complexes on DSSCs performance, *Solar Energy*, 166 (2018) 441-449.

[23] M. Crişan, D. Mardare, A. Ianculescu, N. Drăgan, I. Niţoi, D. Crişan, M. Voicescu, L. Todan, P. Oancea, C. Adomniţei, M. Dobromir, M. Gabrovska, B. Vasile, Iron doped TiO_2 films and their photoactivity in nitrobenzene removal from water, *Applied Surface Science*, 455 (2018) 201-215.

[24] J. Vargas Hernández, S. Coste, A. García Murillo, F. Carrillo Romo, A. Kassiba, Effects of metal doping (Cu, Ag, Eu) on the electronic and optical behavior of nanostructured TiO_2, *Journal of Alloys and Compounds*, 710 (2017) 355-363.

[25] V. Bhatia, A. Dhir, Transition metal doped TiO_2 mediated photocatalytic degradation of anti-inflammatory drug under solar irradiations, J*ournal of Environmental Chemical Engineering,* 4 (2016) 1267-1273.

[26] X. Chen, H. Li, H. Wu, Y. Wu, Y. Shang, J. Pan, X. Xiong, Fabrication of TiO_2@PANI nanobelts with the enhanced absorption and photocatalytic performance under visible light, *Materials Letters*, 172 (2016) 52-55.

[27] M. Sboui, M.F. Nsib, A. Rayes, M. Swaminathan, A. Houas, TiO_2–PANI/Cork composite: A new floating photocatalyst for the treatment of organic pollutants under sunlight irradiation, *Journal of Environmental Sciences*, 60 (2017) 3-13.

[28] C. Yang, W. Dong, G. Cui, Y. Zhao, X. Shi, X. Xia, B. Tang, W. Wang, Enhanced photocatalytic activity of PANI/TiO_2 due to their photosensitization-synergetic effect, *Electrochimica Acta,* 247 (2017) 486-495.

[29] S. Zarrin, F. Heshmatpour, Photocatalytic activity of TiO_2/Nb_2O_5/PANI and TiO_2/Nb_2O_5/RGO as new nanocomposites for degradation of organic pollutants, *Journal of Hazardous Materials*, 351 (2018) 147-159.

[30] S.K. Sharma, Green Chemistry for dyes removal from waste water: research trends and applications, John Wiley and Sons, 2015.

[31] R. Fang, M. He, H. Huang, Q. Feng, J. Ji, Y. Zhan, D.Y.C. Leung, W. Zhao, Effect of redox state of Ag on indoor formaldehyde degradation over Ag/TiO_2 catalyst at room temperature, *Chemosphere*, 213 (2018) 235-243.

[32] L. Elsellami, F. Dappozze, A. Houas, C. Guillard, Effect of Ag+ reduction on the photocatalytic activity of Ag-doped TiO_2, *Superlattices and Microstructures*, 109 (2017) 511-518.

[33] W. Liang, J. Li, Y. Jin, Photo-catalytic degradation of gaseous formaldehyde by TiO_2/UV, Ag/TiO_2/UV and Ce/TiO_2/UV, *Building and Environment*, 51 (2012) 345-350.

[34] M. Bhaumik, A. Maity, V.V. Srinivasu, M.S. Onyango, Removal of hexavalent chromium from aqueous solution using polypyrrole-polyaniline nanofibers, *Chemical Engineering Journal,* 181-182 (2012) 323-333.

[35] J.-B. Wu, M.-L. Lin, X. Cong, H.-N. Liu, P.-H. Tan, Raman spectroscopy of graphene-based materials and its applications in related devices, *Chemical Society Reviews*, 47 (2018) 1822-1873.

[36] T. Ohsaka, F. Izumi, Y. Fujiki, Raman spectrum of anatase, TiO_2, *Journal of Raman Spectroscopy,* 7 (1978) 321-324.

[37] G.I.N. Waterhouse, G.A. Bowmaker, J.B. Metson, The thermal decomposition of silver (I, III) oxide: A combined XRD, FT-IR and Raman spectroscopic study, *Physical Chemistry Chemical Physics,* 3 (2001) 3838-3845.

[38] A. Mostafaei, A. Zolriasatein, Synthesis, and characterization of conducting polyaniline nanocomposites containing ZnO nanorods, Progress in Natural Science: *Materials International,* 22 (2012) 273-280.

[39] K. Jyoti, M. Baunthiyal, A. Singh, Characterization of silver nanoparticles synthesized using Urtica dioica Linn. leaves and their synergistic effects with antibiotics, *Journal of Radiation Research and Applied Sciences*, 9 (2016) 217-227.

[40] D. Chaudhary, N. Khare, V. Vankar, Ag nanoparticles loaded TiO_2/MWCNT ternary nanocomposite: a visible-light-driven photocatalyst with enhanced photocatalytic performance and stability, *Ceramics International,* 42 (2016) 15861-15867.

[41] H. Parangusan, D. Ponnamma, M. Al Ali AlMaadeed, Flexible tri-layer piezoelectric nanogenerator based on PVDF-HFP/Ni-doped ZnO nanocomposites, *The Royal Society of Chemistry Advances*, 7 (2017) 50156-50165.

[42] S. Roy, A.G. Joshi, S. Chatterjee, A.K. Ghosh, Local symmetry breaking in SnO_2 nanocrystals with cobalt doping and its effect on optical properties, *Nanoscale*, 10 (2018) 10664-10682.

[43] N. Tamura, P.U.P.A. Gilbert, Chapter Twenty-one-X-Ray microdiffraction ofbiominerals, in J.J. De Yoreo (Ed.) Methods in Enzymology, *Academic Press*, 2013, pp. 501-531.

[44] H. Ruiz, M. Zambtrano, L. Giraldo, R. Sierra, J.C. Moreno-Pirajan, Production and characterization of activated carbon from oil-palm shell for carboxylic acid adsorption, *Oriental Journal of Chemistry*, 31 (2015) 753-762.

[45] M. Omaish Ansari, M.M. Khan, S. Ansari, K. Raju, J. Lee, M.H. Cho, Enhanced thermal stability under DC electrical conductivity retention and visible light activity of

Ag/TiO_2@polyaniline nanocomposite film, *ACS Applied Materials and Interface* 11 (2014) 8124-8133.

[46] S.P. Lim, A. Pandikumar, N.M. Huang, H.N. Lim, Enhanced photovoltaic performance of silver@ titania plasmonic photoanode in dye-sensitized solar cells, *The Royal Society of Chemistry Advances*, 4 (2014) 38111-38118.

[47] S.M. El-Sheikh, T.M. Khedr, A. Hakki, A.A. Ismail, W.A. Badawy, D.W. Bahnemann, Visible light activated carbon and nitrogen co-doped mesoporous TiO_2 as efficient photocatalyst for degradation of ibuprofen, *Separation and Purification Technology*, 173 (2017) 258-268.

[48] K. Mondal, A. Sharma, Recent advances in the synthesis and application of photocatalytic metal–metal oxide core–shell nanoparticles for environmental remediation and their recycling process, *The Royal Society of Chemistry Advances,* 6 (2016) 83589-83612.

[49] J. Taing, M.H. Cheng, J.C. Hemminger, Photodeposition of Ag or Pt onto TiO_2 nanoparticles decorated on step edges of HOPG, *American Chemistry Society Nano*, 5 (2011) 6325-6333.

[50] N. Chandrakanthi, M.A. Careem, Thermal stability of polyaniline, *Polymer Bulletin*, 44 (2000) 101-108.

[51] S. Golczak, A. Kanciurzewska, M. Fahlman, K. Langer, J.J. Langer, Comparative XPS surface study of polyaniline thin films, *Solid State Ionics*, 179 (2008) 2234-2239.

[52] C.-C. Shen, Q. Zhu, Z.-W. Zhao, T. Wen, X. Wang, A.-W. Xu, Plasmon enhanced visible light photocatalytic activity of ternary $Ag_2Mo_2O_7$@AgBr–Ag rod-like heterostructures, *Journal of Material Chemistry* 3 (2015) 14661-14668.

[53] B. Bharti, S. Kumar, H.-N. Lee, R. Kumar, Formation of oxygen vacancies and Ti^{3+} state in TiO_2 thin film and enhanced optical properties by air plasma treatment, *Scientific Reports* 6 (2016) 32355.

[54] K. Gurushantha, L. Renuka, K. Anantharaju, Y. Vidya, H. Nagaswarupa, S. Prashantha, H. Nagabhushana, Photocatalytic and photoluminescence studies of ZrO_2/ZnO nanocomposite for LED and waste water treatment applications, *Materials Today: Proceedings,* 4 (2017) 11747-11755.

[55] F. Mehmood, J. Iqbal, M. Ismail, A. Mehmood, Ni doped WO_3 nanoplates: An excellent photocatalyst and novel nanomaterial for enhanced anticancer activities, *Journal of Alloys and Compounds*, 746 (2018) 729-738.

[56] A.T. Kuvarega, R.W. Krause, B.B. Mamba, Nitrogen/palladium-codoped TiO_2 for efficient visible light photocatalytic dye degradation, *The Journal of Physical Chemistry C,* 115 (2011) 22110-22120.

[57] W. He, J. Cai, X. Jiang, J.J. Yin, Q. Meng, Generation of reactive oxygen species and charge carriers in plasmonic photocatalytic Au@TiO_2 nanostructures with enhanced activity*, Phys Chem Chem Phys,* 20 (2018) 16117-16125.

[58] B. Luo, D. Xu, D. Li, G. Wu, M. Wu, W. Shi, M. Chen, Fabrication of a Ag/Bi_3TaO_7 plasmonic photocatalyst with enhanced photocatalytic activity for degradation of tetracycline, A*merican Chemistry Society Applied Materials and Interfaces*, 7 (2015) 17061-17069.

[59] J. Kavil, S. Ullattil, A. Alshahrie, P. Periyat, Polyaniline as photocatalytic promoter in black anatase TiO_2, *Solar Energy* 158 (2017) 792-796.

[60] J.P. Valente, P.M. Padilha, A.O. Florentino, Studies on the adsorption and kinetics of photodegradation of a model compound for heterogeneous photocatalysis onto TiO_2, *Chemosphere*, 64 (2006) 1128-1133.

[61] W.H.M. Abdelraheem, M.K. Patil, M.N. Nadagouda, D.D. Dionysiou, Hydrothermal synthesis of photoactive nitrogen- and boron- codoped TiO_2 nanoparticles for the treatment of bisphenol A in wastewater: Synthesis, photocatalytic activity, degradation byproducts, and reaction pathways, *Applied Catalysis B: Environmental*, 241 (2019) 598-611.

[62] L. Lai, H. Zhou, B. Lai, Heterogeneous degradation of bisphenol A by peroxymonosulfate activated with vanadium-titanium magnetite: Performance, transformation pathways, and mechanism, *Chemical Engineering Journal*, 349 (2018) 633-645.

[63] Y. Liu, R. Luo, Y. Li, J. Qi, C. Wang, J. Li, X. Sun, L. Wang, Sandwich-like Co_3O_4/MXene composite with enhanced catalytic performance for Bisphenol A degradation, *Chemical Engineering Journal,* 347 (2018) 731-740.

[64] H. Guo, H. Wang, Q. Wu, J. Li, Degradation and mechanism analysis of bisphenol A in aqueous solutions by pulsed discharge plasma combined with activated carbon, *Separation and Purification Technology,* 190 (2018) 288-296.

[65] L.V.C. Lima, M. Rodriguez, V.A.A. Freitas, T.E. Souza, A.E.H. Machado, A.O.T. Patrocínio, J.D. Fabris, L.C.A. Oliveira, M.C. Pereira, Synergism between n-type WO_3 and p-type δ-FeOOH semiconductors: High interfacial contacts and enhanced photocatalysis, *Applied Catalysis B: Environmental*, 165 (2015) 579-588.

[66] P. Li, C. Liu, G. Wu, Y. Heng, S. Lin, A. Ren, K. Lv, L. Xiao, W. Shi, Solvothermal synthesis and visible light-driven photocatalytic degradation for tetracycline of Fe-doped $SrTiO_3$, *The Royal Society of Chemistry Advances*, 4 (2014) 47615-47624.

CHAPTER 7:

CONCLUSION AND RECOMMENDATION

7.1 INTRODUCTION

This chapter aims at providing a concise summary of the findings of this study. The extent of fulfilling the objectives is shown in this chapter. Finally, recommendations for future work are given in this chapter.

7.2 GENERAL CONCLUSIONS

The main thrust of this Ph.D. research project was to prepare nanostructured titanium dioxide composites and use them in the removal of selected emerging organic pollutants. These as-synthesized nanostructures were prepared *via* wet chemical methods. This study revealed that the band gap of TiO_2 can be reduced by modification of its surface by introducing metal dopants. The study also revealed the charge separation in a TiO_2 based nanostructure can be achieved by doping with metal dopants such as Ag and pairing TiO_2 with other semiconductor materials such as WO_3. The charge separation in metal-doped TiO_2 was due to the scavenging of electrons in the conduction band by the metal centers. In addition, the study also revealed that charge separation can be effected by anchoring TiO_2 based nanostructures on a conducting support such as PANI. Surface modification of TiO_2 with PANI resulted in enhanced performance in the degradation of BPA. The improvement was brought about by the absorption property effected by PANI in addition to change separation.

The study revealed that the band gap of TiO_2 can be reduced by forming a heterojunction with another semiconductor. WO_3@TiO_2 nanocomposite had an

estimated band gap of 3.05 eV compared to the 3.22 eV of the virgin TiO_2. The pairing of the semiconductors resulted in shifting of the band edge of the semiconductor to a higher wavelength allowing its use under visible irradiation.

Anchoring of TiO_2 based nanocomposites on PANI resulted in an enhanced performance in the removal of BPA and ibuprofen. This was ascribed to the ability of PANI to adsorb the organics via π-π stacking and hydrogen bonding on its surface resulting in maximum degradation by the semiconductor.

The synthesis of TiO_2 using a microwave synthesis approach resulted in a change in morphology to nanofibers compared to nanorods that were produced under hydrothermal synthesis. Microwave synthesis proved to be a faster method that also produced more uniform nanostructures compared to the hydrothermal synthetic route.

One of the major findings of this study was that the presence of humic acids in solution at different concentrations inhibited the degradation of BPA. This was because humic acid quenched $OH^{\cdot}$ radicals that are critical for the degradation process. In the degradation of ibuprofen, HCO_3^- and $S_2O_8^{2-}$ ions influenced the degradation process. The HCO_3^- increased the degradation of ibuprofen at a concentration of 0.5 mM to 5 mM. A further increase in HCO_3^- concentration to 10 mM, resulted in little effect on the degradation process. On the other hand, the addition of $S_2O_8^{2-}$ ions upto 10 mM resulted in acceleration of the degradation rate of ibuprofen.

7.2 RECOMMENDATIONS

This research has led to further questions in need of further investigation. The following recommendations could be considered for future study.

- Different synthetic techniques need to be explored to investigate the different morphologies that could result and the influence of these different morphologies on degradation of emerging organic pollutants.
- Different supports for TiO_2 nanocomposites should be investigated and their influence on degradation of BPA and ibuprofen determined.
- More studies could be investigated on the degradation of BPA and ibuprofen using different semiconductors.
- Utilization of non-metal modifications especially phosphorous and graphitic carbon nitride for degradation of BPA and ibuprofen.
- Theoretical study using density functional theory (DFT) need to be explored to investigate the surface-adsorbed species in order to have a better understanding of the reactivity of the species and the surface of the semiconductors. This will go a long way in assisting in future design of materials for degradation of emerging organic pollutants.
- There is need to come up with better designs for catalysts that can be recovered after use in addition to their regeneration to reduce the overall cost of the degradation process in large scale applications.
- The as-synthesized nanostructures in this study can be explored further in hydrogen production, supercapacitors, batteries, and gas sensing applications.
- The TiO_2- based nanocomposites open up opportunities in reduction of CO_2 that maybe explored in the future.

- The Ag doped photocatalyst can be investigated for antimicrobial activity to solve another water problem.

APPENDIX 1

Appendix 1.1: Summary of adsorption and degradation of BPA.

Catalyst	UV radiation		Visible light radiation	
	% BPA adsorption (30 min)	% BPA degradation after (80 min)	% BPA adsorption (30 min)	% BPA degradation after (120 min)
TiO_2	4	60	2	62
$Ag@TiO_2$	5.6	99.5	7.2	95.8
$Ag@TiO_2$-PANI	10	99.8	9.9	99.8

Appendix 1.2: Summary of adsorption and degradation of ibuprofen adsorption.

Catalyst	% Ibuprofen adsorption (30 min)	% Ibuprofen degradation after (120 min)
TiO_2	1	58.5
WO_3	0.5	50.0
$WO_3@TiO_2$	3	90.0
$PANI/WO_3@TiO_2$	10	99.8

APPENDIX 2

Appendix 1.3: Photodegradation rate constants for the degradation of BPA under UV and visible radiation.

Sample	Rate constant $kmin^{-1}$ under UV radiation	Rate constant $kmin^{-1}$ under visible radiation
TiO_2	1.96 X 10^{-2}	1.78 X 10^{-2}
$Ag@TiO_2$	2.8 X 10^{-2}	2.3 X 10^{-2}
$Ag@TiO_2$-PANI	3.4 X 10^{-2}	2.85 X 10^{-2}